INFORMATION TO USERS

This manuscript has been reproduced from the microfilm master. UMI films the text directly from the original or copy submitted. Thus, some thesis and dissertation copies are in typewriter face, while others may be from any type of computer printer.

The quality of this reproduction is dependent upon the quality of the copy submitted. Broken or indistinct print, colored or poor quality illustrations and photographs, print bleedthrough, substandard margins, and improper alignment can adversely affect reproduction.

In the unlikely event that the author did not send UMI a complete manuscript and there are missing pages, these will be noted. Also, if unauthorized copyright material had to be removed, a note will indicate the deletion.

Oversize materials (e.g., maps, drawings, charts) are reproduced by sectioning the original, beginning at the upper left-hand corner and continuing from left to right in equal sections with small overlaps. Each original is also photographed in one exposure and is included in reduced form at the back of the book.

Photographs included in the original manuscript have been reproduced xerographically in this copy. Higher quality 6" x 9" black and white photographic prints are available for any photographs or illustrations appearing in this copy for an additional charge. Contact UMI directly to order.
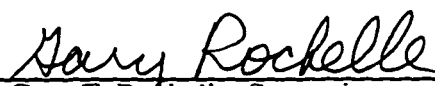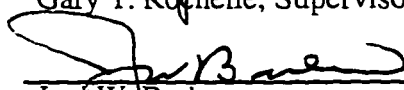
Thermodynamic Model for Acid Gas Loaded

Aqueous Alkanolamine Solutions
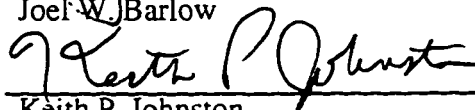
Approved by
Dissertation Committee:

_____
Gary T. Rochelle, Supervisor
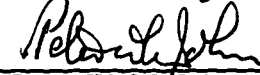
_____
Joel W. Barlow

_____
Keith P. Johnston

_____
Isaac C. Sanchez

_____
Peter W. M. John

Thermodynamic Model for Acid Gas Loaded
Aqueous Alkanolamine Solutions

by

Mark Leon Posey, B.S.

Dissertation

Presented to the Faculty of the Graduate School of

The University of Texas at Austin

in Partial Fulfillment

of the Requirements

for the Degree of

Doctor of Philosophy

The University of Texas at Austin
December, 1996

UMI Number: 9719459

Dedication

This dissertation is dedicated to my wife, Kimberly. Her constant support, enthusiasm and love kept me going through the long hours and late nights.

Acknowledgements

I would like to thank the members and instructor of my Taekwon Do class for two years of fun and personal enrichment. The exercise and interaction were a welcome break from the rigors of graduate study.

I have also been fortunate to work with many fine and knowledgeable individuals. Discussions on gas treating with Msafiri Mshewa, Manuel Pacheco and Shoichi Kaganoi were enjoyable and fruitful. Interaction with other gas treating researchers and industrial sponsors of our research has also been a positive experience. I want to thank my research group for four years of fun and camaraderie. It has been a pleasure knowing and working with you all.

Last, but not least, I want to thank my supervising professor, Dr. Gary T. Rochelle. His comments and suggestions are always constructive and invariably improve the quality of the work. He always strives to achieve a deeper understanding of things and instills that quest for knowledge in his students. I have learned a lot from Dr. Rochelle during the process of researching and writing this dissertation. It has been both a challenging and rewarding experience.

Thermodynamic Model for Acid Gas Loaded
Aqueous Alkanolamine Solutions

Mark Leon Posey, Ph.D.

The University of Texas at Austin, 1996

Supervisor: Gary T. Rochelle

Natural gas and refinery gas streams usually contain acid gases such as carbon dioxide and hydrogen sulfide that must be removed. The prevailing method for removing these gases is by chemical absorption into aqueous alkanolamine solutions. The common amines used are methyldiethanolamine (MDEA), diethanolamine (DEA), monoethanolamine (MEA) and their mixtures. To better design and operate these absorption systems, a good vapor-liquid equilibrium model of the chemical thermodynamics is needed.

It is difficult to measure vapor-liquid equilibrium (VLE) data accurately at low acid gas concentrations. However, good predictions at these conditions are crucial to determining system performance and economics. Therefore, a primary goal of this work was to improve existing model predictions and understanding of low loading behavior. As acid gas approaches a loading of zero, the solution

becomes a binary amine-water system. Freezing point data from the literature and heat of mixing data measured in this work have been regressed along with total pressure data to significantly improve modeling of the binary amine-water systems.

Abundant VLE data exists at moderate to high loadings, but very little exists at low loading, and even then, discrepancies are seen between data sources. Therefore, pH and conductivity data have been measured to supplement the VLE data and improve confidence in model predictions at low acid gas loadings. The electrolyte-nonrandom two-liquid model has been used to represent thermodynamics in these solutions. The Data Regression System™ (DRS) of Aspen Plus™ was utilized to regress model parameters to the experimental data. DRS reports not only the regressed parameters, but calculates error in the parameter values and provides a parameter correlation matrix. These tools made it possible to critically analyze model sensitivity to the parameters. The important parameters and interactions are identified and provide the key to obtaining better model predictions. By comparing analogous parameters from MDEA and DEA systems, intelligent choices were made for mixed amine parameters in the MDEA-DEA-H_2S-CO_2 system. With the knowledge gained, reasonably accurate predictions can made for other mixed amine systems for which experimental data does not exist.

Table of Contents

List of Tables

xvii

List of Figures

xxiv

xxv

Chapter 1: Introduction to Acid Gas Treating

1.1 GAS TREATING BY CHEMICAL ABSORPTION

Natural gas streams and refinery process streams often contain hydrogen sulfide (H_2S) and carbon dioxide (CO_2) gases that must be removed. The traditional treating method is an absorption/stripping system using aqueous solutions of alkanolamines. For natural gas production, typical pipeline specifications call for less than 4 ppmv H_2S due to possible corrosion and the health and environmental concerns of H_2S. CO_2 specifications are more flexible and vary from 10 ppmv for ammonia or liquefied natural gas plants to a few percent for pipeline natural gas (Astarita et al., 1983). Light hydrocarbons such as methane and ethane have a very low solubility in these aqueous alkanolamine solutions.

The gas stream containing the H_2S and CO_2 is contacted countercurrently with the amine solution at approximately 40°C and 1000 psia, see figure 1.1. The amine solution which now contains the acid gases, called rich amine, is sent through a heat recovery exchanger and then to the top of the stripper. A steam heated reboiler maintains 120°C in the stripper to reverse the absorption reactions. The desorbed gases are then either sent to a Claus plant for conversion of the H_2S to elemental sulfur, or to an incinerator depending on the H_2S concentration. The now "lean amine" is recycled back through the heat exchanger to the top of the absorber.
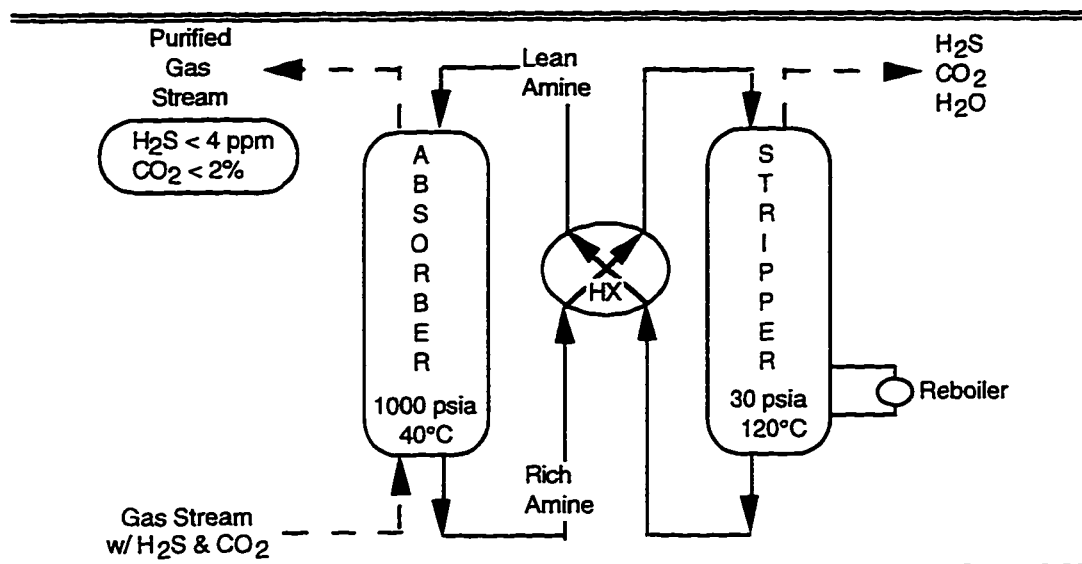
Figure 1.1   Simplified schematic of an absorption / stripping system for removal
of H_2S and CO_2 from natural gas streams using aqueous
alkanolamine solutions.

The common amines used are monoethanolamine (MEA), diethanolamine

(DEA), methyldiethanolamine (MDEA) and 2-(2-aminoethoxy) ethanol, known

more commonly by its Huntsman Chemical trade name, Diglycolamine®

(DGA®). MDEA and its mixtures with MEA or DEA began receiving attention

in the early eighties. MDEA blends can combine the favorable properties of fast

CO_2 reactions for MEA and DEA with the low heats of reaction for MDEA to

achieve a "tuned" process with the desired H_2S / CO_2 selectivity.

2

HO —CH2 — CH2 — N⟨H / H

Monoethanolamine - MEA

HO —CH2—CH2 —O—CH2 —CH2—N⟨H / H

Diglycolamine® - DGA®

HO —CH2 — CH2 ⟩N—H
HO —CH2 — CH2 ⟋

Diethanolamine - DEA

HO —CH2 — CH2 ⟩N —CH3
HO —CH2 — CH2 ⟋

Methyldiethanolamine - MDEA
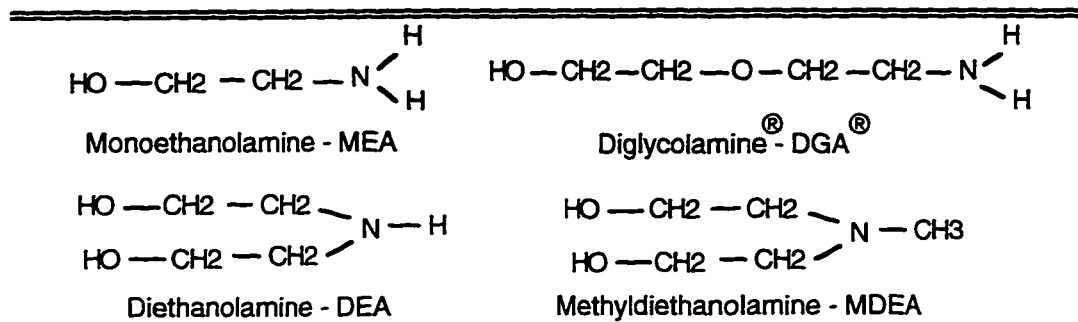
Figure 1.2 Commonly used alkanolamines for natural gas treating.

Although the basics of this process are very old, new alkanolamines and new mixtures of alkanolamines keep the industry continually improving its processes. The development of faster computers and simulation programs, such as Aspen Plus™, give us the ability to create more sophisticated and accurate models that would have been unreasonably slow ten years ago. A good model of the absorption/stripping system can be useful to both the designer and operator. The designer can use the model to predict the number of stages required, what amine recirculation rate to use, and what the utility requirements are for a specified separation. The operator can use a model that has been fine tuned to match the system operating conditions to troubleshoot possible problems, such as inefficient trays that occur later in the life of a gas treating system.

1.2 PREVIOUS EQUILIBRIUM MODELS

1.2.1 Kent-Eisenberg

Kent and Eisenberg (1976) created the first equilibrium model that received widespread use. Their model was based on pseudo-equilibrium constants and Henry's Law. They regressed the pseudo-equilibrium constants for

3

the amine protonation and carbamate reversion reactions for MEA and DEA systems to fit experimental vapor-liquid equilibria (VLE) data. This resulted in a model which has only two parameters per acid gas to account for the ionic strength dependencies of the acid gas partial pressure. The model was reasonably accurate at loadings greater than 0.1, but was inaccurate at lower loadings due to the manipulations of the amine equilibrium constants. Another drawback of this model was that it could not be used to find ionic species concentrations. By regressing the equilibrium constants they have effectively combined the activity coefficients with species mole fractions making independent determinations of either impossible. Only MEA and DEA systems were studied in their paper and they report a reasonable predictive agreement with mixed acid gas data.

1.2.2 Edwards et al.

Edwards et al. (1975, 1978) developed a model for aqueous solutions of ammonia with carbon dioxide, hydrogen sulfide, sulfur dioxide and hydrogen cyanide. These chemical systems are similar to the typical gas treating chemical system, alkanolamine-H_2O-CO_2-H_2S. They also compiled chemical equilibrium and Henry's constants in water for the various compounds as a function of temperature. Austgen (1989) based many of his constants on this compilation. Their equation for activity coefficients, eq. 1.1, is the basis for the Deshmukh-Mather model.

1.2.3 Deshmukh-Mather

Deshmukh and Mather (1981) produced a more thermodynamically rigorous model based on extended Debye-Hückel theory and the work of Edwards

4

et al. (1975, 1978) and Beutier and Renon (1978). Their activity coefficient equation had one term to account for electrostatic forces by the Debye-Hückel law and a second term with adjustable parameters to account for short range interactions.

$$\ln \gamma_k = \frac{-A z_k^2 I^{0.5}}{1 + b_k I^{0.5}} + 2 \sum \beta_{kj} m_j \qquad (1.1)$$

The Peng-Robinson equation of state was used to determine vapor phase fugacity coefficients. One important thing to note is that they have assumed the activity coefficient of water to be 1.0. Our work shows that the water activity coefficient can be different from 1.0 and is highly correlated with the amine activity coefficient. A 5% change in water activity coefficient can result in a large change in the amine activity coefficient.

To simplify their regressions, species having small concentrations were removed from the mass balances and their parameters were set to zero so that they had no effect on the model. As an example, for the MEA-CO_2-H_2S-H_2O system, CO_2, H_2S, OH^-, H^+, $S^=$, and $CO_3^=$ would be neglected. These assumptions leave questions about the validity of the model in the low loading ranges where the above neglected species are important. Deshmukh and Mather neglect any mixed acid gas parameters and state that combining the single acid gas systems sufficiently predicts mixed acid gas equilibrium. Weiland et al. (1993 & 1995) used the Deshmukh-Mather model to predict CO_2 and H_2S equilibrium for MEA, DEA, DGA® and MDEA.

5

1.2.4 Lee Model

Lee (1992 & 1994) has been developing a modified group contribution model for equilibrium predictions for gas treating systems. His model is modified from previous group contribution methods in that it can account for gas molecules such as CO_2 and H_2S that can not be broken into groups. The possible benefits of his model when completed would be the ability to predict the behavior of new proposed alkanolamine molecules for which there is no data. A drawback of group contribution methods is that they require accurate data for a series of chemically similar compounds to generate the group constants. Accurate data is often hard to find for the amines of interest, such as MDEA, and data for the other amines in a series, which have no industrial use, are non-existent. Since the parameters of his model are also regressed on acid gas VLE data, it has the same data discrepancy problems to contend with as do other models.

1.2.5 Electrolyte-NRTL Model

Austgen (1989) utilized the electrolyte-Nonrandom Two-Liquid (NRTL) theory developed by Chen and coworkers in a series of articles; Chen et al. (1979, 1982), Chen and Evans (1986) and Mock et al. (1986) to model acid gas VLE. This model reduces to the NRTL model of Renon and Prausnitz (1968) when no acid gases are present.

To model the limiting case of amine-water, Austgen found as much total pressure data from the literature as he could and regressed it. Unfortunately, activity coefficients for amine and water are not very sensitive to total pressure data at industrially important conditions. This resulted in a set of parameters for

the binary amine-water systems with questionable accuracy and temperature dependence. Chang (1992) improved amine-water modeling by measuring and regressing binary freezing point depression data. However, the enthalpy predictions of his amine-water models were still not correct.

Austgen also collected all the data he could find for acid gas vapor-liquid equilibrium in MDEA, MEA, DEA and DGA® and regressed parameters for these data. He provides sets of parameters for the above amines with CO_2 and H_2S separately. He states in his dissertation that no additional parameters are needed to predict VLE in the amine-H_2S-CO_2-H_2O systems and provides model comparisons for these systems.

Very little mixed amine data existed when Austgen was preparing his model. Therefore, Austgen measured VLE data for MDEA-MEA-CO_2 and MDEA-DEA-CO_2 systems at 40°C and 80°C. He then successfully regressed this mixed amine data using two additional parameters that did not exist for the single amine systems.

Because of the lack of confidence in the MDEA-H_2O binary parameters, Austgen set them to zero. This means his MDEA-Acid Gas models asymptote to an ideal solution as the acid gas concentrations go to zero. We know from several sources that the MDEA-H_2O system is highly non-ideal. The accuracy of the other amine-water binary models is also in question due to the model's low sensitivity to the total pressure data he used. Errant amine-water models effect predictions at acid gas loadings below approximately 0.01. Unfortunately, VLE data is sparse below 0.01 putting greater emphasis on an accurate model structure.

1.3 Model Selection

For this work we have selected the electrolyte-NRTL model for representation of equilibrium in these systems. It has the added feature of being completely flexible in choice of the chemical system. Calculations can be made for systems as simple as amine-water and as complex as mixed amine, mixed acid gas systems such as $MDEA-DEA-H_2O-H_2S-CO_2$. The electrolyte-NRTL model can also predict more complex systems from parameters for the subset systems. For example, parameters from $MDEA-H_2S$ and $MDEA-CO_2$ can be combined to make predictions for the $MDEA-H_2S-CO_2$ without regressing additional parameters. In some cases, predictions for mixed acid gas or mixed amine systems would benefit from regression of additional parameters, but this is not always necessary.

This model is available as a property package in Aspen Plus™. This in itself was a positive factor in selecting this model. Aspen is widely used in the process industries and parameter sets that are obtained here can be immediately utilized by practicing engineers. If some new model structure were created, a FORTRAN code for equilibrium calculations would have to be provided. Even then, the end user would still have to have FORTRAN code to model heat and mass transfer in the absorber and stripper units. This added effort on the part of the end user would greatly reduce the use and reference to our work. Aspen Plus™ also has a built in data regression algorithm called the Data Regression System™ (DRS). DRS allows simultaneous regression of many types of data such as VLE, heat of mixing, freezing point, and pH which aids our

8

thermodynamic method of using all of the data to create a well rounded model. The DRS also allowed the concentration on issues of the data quality, model structure and low loading behavior rather than fighting with convergence routines and creation of a regression algorithm.

A final reason for choosing this model is its applicability. Its structure specifically allows the inclusion of two solvents in the system, whereas other electrolyte models only allow water as a solvent. In acid gas treating, both the amine and the water are considered solvents. The model has also been shown to work for highly concentrated electrolyte solutions. Chen and coworkers have shown the electrolyte-NRTL model to predict well for numerous concentrated electrolyte systems. Austgen has also successfully applied this model to acid gas treating systems, with some deficiencies as noted above. Based on these successes, it was determined that we could use this model framework to improve our understanding of acid gas treating thermodynamics with an emphasis at low loading conditions.

1.4 SCOPE

Absorption of the acid gases into the alkanolamine solutions is governed by the mechanism of mass transfer with chemical reaction. Other researchers are currently investigating rates of mass transfer and chemical reaction kinetics in these systems and that effort is beyond the current scope. However, all of the rate models contain a term for the equilibrium solubility of the acid gases to establish a driving force for mass transfer. Accurate speciation of the solution is an integral part of the equilibrium calculations required by rate based models. Therefore, a

9

good model for predicting the solution thermodynamics at all possible combinations of temperature, amine concentration, and acid gas loading is needed.

One goal of this work is to obtain a set of parameters for the electrolyte-NRTL model for the MDEA-DEA-H_2O-CO_2-H_2S system. MDEA is receiving increased use in gas treating compared to the other amines due to its lower heat of absorption with acid gases, lower corrosivity, and lower vapor pressure. MDEA also has a much slower rate of reaction with CO_2 than the primary or secondary amines. This is a desirable trait because the CO_2 inlet partial pressure is often already below output specifications and unfavorably hinders the ability of the solution to absorb H_2S into the ppm range. There are situations where an MDEA solution will achieve the desired H_2S removal, but cannot meet the CO_2 removal specifications due to its slow reaction. In these cases, rather than using a different amine, the amine solution is "tuned" to the inlet gas by adding DEA to the MDEA solution. By adding the faster reacting DEA in the exact amount needed, the CO_2 outlet specification can be met without losing all the benefits that MDEA offers over the other amines. To decide exactly how much DEA is needed and what effects this has on operating parameters, an accurate VLE model is needed. It is for these reasons the MDEA-DEA-H_2O-CO_2-H_2S system was chosen for modeling.

One problem that is encountered in modeling acid gas treating is that experimenters report statistically different partial pressures of the acid gases at the exact same conditions. Usually, differences between the data sets cannot be easily attributed to errors in procedures or methods. This leads to the unfortunate

situation where VLE data is uncertain at crucial design conditions, such as at the top of the absorber. In fact, accurate experimental data in the very low acid gas loading ranges is nearly impossible to collect. However, using an accurate and valid thermodynamic model we can determine with certainty which data set is correct and make VLE predictions with confidence at acid gas loadings well below where any data currently exist. This is accomplished by careful selection of the constants and parameters used and by performing model driven experiments. At experimental conditions where the accuracy or quantity of VLE data is lacking, thermodynamically related data can be used to fill in the void. Data such as heat of acid gas absorption, pH, freezing point depression and heat of mixing can be regressed along with VLE data to create a complete model for thermodynamic equilibrium in acid gas treating systems that is more accurate than a model based upon VLE data alone.

Chapter 2: Solution Thermodynamics

Removal of acid gases from natural gas streams is typically accomplished by physico-chemical absorption into aqueous alkanolamine solutions. Mass transfer is carried out in a trayed absorber or stripper where the liquid and vapor phases are brought into contact. To predict equilibrium compositions and therefore the outlet concentrations, we must understand the solution thermodynamics involved. The reader is assumed to have a basic familiarity with thermodynamics and no attempt is made to present the entire thermodynamic framework here.

Discussion of equilibrium thermodynamics is broken into two parts in this chapter. The first part covers the physical vapor-liquid equilibrium (VLE) of molecular species. The second part discusses the chemical reactions that typically occur in aqueous alkanolamine gas treating systems. Most of the basic thermodynamic theory presented here is taken from the book <u>Molecular Thermodynamics of Fluid-Phase Equilibria</u> by Prausnitz, Lichtenthaler and Azevedo (Prausnitz et al., 1986).

2.1 CONCENTRATION UNIT CONVERSIONS

Before we can begin modeling the alkanolamine-acid gas system, a concentration basis must be chosen. The electrolyte-NRTL model that is used here was developed using mole fraction concentrations. One difficulty that is encountered in modeling these systems is that experimental data exists in three different concentration units, mole fractions, molalities and molarities. In order to

keep a consistent model we must use a single concentration system for all equations and experimental data. Therefore, relationships are needed to convert between the different concentration bases.

2.1.1 Molality to mole fraction

Molality, m_i, is defined as moles of substance i per kg of solvent. Molality units are typically used for dilute solutions in water where mole fractions would require many decimal places to maintain accuracy. To convert to the mole fraction scale, kg solvent in the denominator needs to be converted to total moles of solution. The conversion is performed as follows, where MW_{solv} is the molecular weight of the solvent in grams per gram mole.

$$x_i = m_i * MW_{solv} * \frac{1\,kg}{1000\,g} \tag{2.1}$$

Assuming that the solvent is water, equation 2.1 becomes

$$x_i = m_i * \frac{18}{1000} \tag{2.2}$$

2.1.2 Molarity to mole fraction

Molarity units require more information for conversion to mole fractions than does molality. Molarity is defined as moles of the substance of interest per liter of solution. A liter of solution is not well defined since the density of alkanolamine solutions change with concentration and temperature. Therefore, the density of the solution (g soln / L soln) must be known in order to convert to mole fractions. First, the weight fraction, w_i, of the amine is calculated from equation 2.3.

$$w_i = \frac{M_i * MW_i}{\rho_{soln} * 1000} \tag{2.3}$$

where w_i is the weight fraction of i, grams i / total grams soln

13

M_i is the Molarity of component i, mol i / L soln

MW_i is the molecular weight of component i, grams i / gmol i

ρ_{soln} is the density of the solution, grams soln / mL soln

To convert from weight fraction to mole fraction one has to assume that amine and water are the only important species. This is usually possible since experimental data is reported as a function of the unloaded amine-water concentration even at very high acid gas loadings. Equation 2.4 is then used to convert weight fraction to mole fraction.

$$x_i = \frac{\dfrac{w_i}{MW_i}}{\dfrac{w_i}{MW_i} + \dfrac{1-w_i}{MW_{H2O}}} \tag{2.4}$$

2.2 VAPOR-LIQUID PHASE EQUILIBRIA

Absorption of acid gases proceeds in two "steps". Figure 2.1 illustrates, in a simplified manner, the two step process of acid gas absorption or desorption. For the first step, gas phase species must be dissolved into the aqueous phase. This equilibrium will sometimes be written in a form resembling a chemical reaction as shown below, where "(g)" refers to a molecule in the gas phase and "(aq)" refers to a gas molecule dissolved in an aqueous solution.

$$H_2S \ (g) \Leftrightarrow H_2S \ (aq) \tag{2.5}$$

The second step shown in figure 2.1 is the chemical reactions. Chemical reactions serve to convert the aqueous gas species into ions and keep reaction 2.5 continuing to the right. It is these acid-base reactions which give alkanolamine solutions their high acid gas capacities. Chemical reactions are discussed in detail in section 2.3.

14
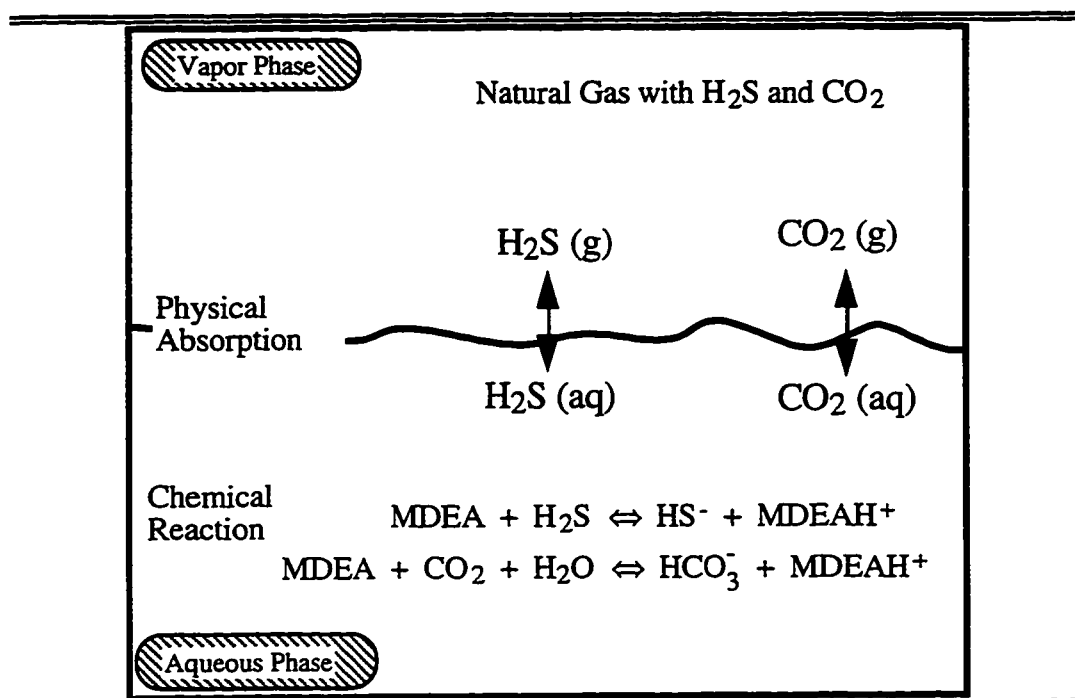
Figure 2.1 Simplified illustration of the equilibrium processes involved in acid gas absorption or desorption into aqueous alkanolamine solutions.

2.2.1 Chemical potential and fugacity

Equilibrium between two phases, labeled here α and β, was described using chemical potentials by Gibbs. He states that at equilibrium, the chemical potential of a species must be the same in both phases.

$$\mu_i^\alpha = \mu_i^\beta \tag{2.6}$$

While this forms the backbone of equilibrium thermodynamics, it is not directly useful itself. A way was needed to relate this abstract concept to measurable quantities such as temperature and compositions. G. N. Lewis took the Gibbs-Duhem equation for a pure substance i. He then substituted the ideal gas law for the partial volume term and equation 2.7 resulted.

$$\mu_i - \mu_i^o = RT \ln \frac{P}{Po} \qquad (2.7)$$

Since the assumptions on equation 2.7 are too limiting for practical use, Lewis recast the equation, replacing pressures with fugacities. The only requirement of equation 2.8 is an isothermal change in the chemical potential, and allows prediction for multiple non-ideal phases. He further defined this fugacity ratio as an activity shown in equation 2.9.

$$\mu_i - \mu_i^o = RT \ln \frac{f_i}{f_i^o} \qquad (2.8)$$

$$\frac{f_i}{f_i^o} \equiv \text{activity} = a_i \qquad (2.9)$$

We can apply the above definitions to equation 2.6 and obtain a new, completely general, expression of equilibrium. It is from equation 2.10 that our equations for vapor-liquid equilibrium are derived.

$$f_i^\alpha = f_i^\beta \qquad (2.10)$$

2.2.2 Vapor Phase non-idealities

A fugacity coefficient is defined as the ratio of the fugacity of component i in the vapor phase with its ideal gas partial pressure. Fugacity coefficients are further defined that in the limit of zero pressure, the gas partial pressure equals the fugacity, i.e. ϕ_i goes to one.

$$f_i^v = \phi_i \, y_i \, P \qquad (2.11)$$

The fugacity coefficient can be related to known measurable variables with an empirical equation of state. One example is the modification of the Redlich-Kwong equation by Soave (Soave, 1972). Whichever equation of state is used, it

16

must be written in terms of the gaseous molar volume of the component of interest. Then the integration on equation 2.12 can be applied to relate the equation of state to the fugacity coefficient.

$$RT \ln \varphi_i = \int_0^P [\upsilon_i - \frac{RT}{P}] \, dP \tag{2.12}$$

2.2.3 Liquid phase non-idealities

Beginning with the definition of activity in equation 2.9, activity coefficient is defined as given below in equation 2.13.

$$\gamma_i \equiv \frac{a_i}{x_i} = \frac{f_i^L}{f_i^o \, x_i} \tag{2.13}$$

Rearranging equation 2.13 gives us a starting form for the liquid phase fugacity shown in equation 2.14.

$$f_i^L = \gamma_i \, x_i \, f_i^o \tag{2.14}$$

f_i^o is the standard state fugacity for pure liquid component i. For compounds which are liquids at standard conditions, like alkanolamines and water, the standard state fugacity coefficient is defined as the pure component vapor pressure, P_i^o, at the temperature of the system.

$$f_i^L = \gamma_i \, x_i \, P_i^o \, \exp\left(\int_{Pi^o}^P \frac{\upsilon_i \, dP}{RT} \right) \tag{2.15}$$

The integral term added to equation 2.15 is known as the Poynting correction and accounts for system pressures that are different from the saturation pressure. When the liquid phase is assumed incompressible the integral is easily determined and equation 2.16 results for non-supercritical components. At the relatively low pressures in acid gas vapor-liquid equilibrium the Poynting correction is usually very close to 1 and can be neglected.

17

$$f_i^L = \gamma_i \, x_i \, P_i^{\,o} \exp\!\left(\frac{\upsilon_i \,(P-Pi^{\,o})}{RT}\right)$$ (2.16)

The vapor-liquid equilibrium relationship for regular components is then the combination of equations 2.16 and 2.11.

$$\phi_i \, y_i \, P = \gamma_i \, x_i \, P_i^{\,o} \exp\!\left(\frac{\upsilon_i \,(P-Pi^{\,o})}{RT}\right)$$ (2.17)

Supercritical components such as CO_2 and H_2S will not exist as pure species in alkanolamine gas treating systems and therefore require a different reference state. The infinite dilution reference state is used for supercritical components. As the mole fraction approaches zero, γ_i^* approaches 1 and f_i^o approaches H_i^o. Activity coefficient reference states are discussed in detail in section 2.2.4 below.

$$f_i = \gamma_i^* \, x_i \, H_i^o \exp\!\left(\int_{Pi^o}^{P} \frac{\upsilon_i^\infty \, dP}{RT}\right)$$ (2.18)

H_i^o is Henry's constant and defined to be $\frac{f_i}{x_i}$. Equation 2.19 is then the VLE relationship for supercritical components.

$$\phi_i \, y_i \, P = \gamma_i^* \, x_i \, H_i^o \exp\!\left(\int_{Pi^o}^{P} \frac{\upsilon_i^\infty \, dP}{RT}\right)$$ (2.19)

2.2.4 Activity Coefficient Normalization

To maintain consistency with the fugacity reference states limits for the activity coefficients must be defined. In this work, solvent activity coefficients are defined to approach one as the solvent mole fraction approaches one. Solute and ionic activity coefficients are defined to approach one as the mole fraction approaches zero in pure water. Note that γ^* does not necessarily approach one as its concentration approaches zero in a mixed solvent.

Solutes, ions: $\gamma_i^* \rightarrow 1.0$ as $x_i \rightarrow 0.0$ in water (2.20)

18

Solvents: $\qquad \gamma_{solv} \to 1.0$ as $x_{solv} \to 1.0 \qquad$ (2.21)

Since solutes and ions are normalized differently than water, their activity coefficients are said to be unsymmetrically normalized. An asterisk is used to indicate that an activity coefficient is unsymmetrically normalized. The electrolyte-NRTL model defines the alkanolamines as a second solvent subject to the limit in equation 2.21 above. This convention is know as symmetrically normalized since both the water and the amine approach activity coefficients of one as they approach their pure liquid states.

This convention for the alkanolamines requires a conversion of the amine protonation equilibrium constant since all equilibrium constants are determined based on the asymmetric activity coefficient convention. Section 2.3 provides the details on making the conversion of alkanolamine protonation equilibrium constants.

2.2.5 Activity Coefficient Relationships

Most of the variables on the right side of equations 2.17 and 2.19 are known a priori. In fact, if there were no chemical reactions occurring and activity coefficients could be assumed close to one, equation 2.17 reduces to Raoult's Law and calculations can be made without having to fit experimental data. Unfortunately, acid gas treating solutions are highly non-ideal and activity coefficients are far from one. Therefore, a method must be devised for calculation of activity coefficients as a function of solution composition and temperature. One can develop an empirical, direct expression for activity coefficients and fit experimental data with the expression. Another method is to create a model for

excess Gibbs energy which is related to activity coefficients through equation 2.22. Experimental data is then regressed upon parameters in the excess Gibbs energy model. Details of the Nonrandom Two-Liquid (NRTL) and electrolyte-NRTL model are given in Chapters 3 and 5, respectively.

$$g_{ex} = RT \sum_i x_i \ln \gamma_i \tag{2.22}$$

The NRTL model (Renon and Prausnitz, 1968) is an excess Gibbs energy model. It is preferable to empirical relationships since it inherently provides the proper behavior as mole fractions approach one or zero. A model based on excess Gibbs energy is also desirable due to its direct relationships with excess enthalpy given in equation 2.23. Excess enthalpy is related to heat of mixing and heat of absorption data. Therefore, having this direct relationship between excess Gibbs energy and excess enthalpy allows the combined regression of pressure and enthalpy data. This is tremendously useful where VLE data is of poor quality or non-existent. In addition, excess enthalpy is directly related to the temperature dependence of the activity coefficients and greatly improves modeling of temperature dependent variables.

$$\frac{d\left(\frac{g_{ex}}{RT}\right)}{d(1/T)} = -\frac{h_{ex}}{R} \tag{2.23}$$

2.3 CHEMICAL EQUILIBRIA

Discussion so far has concerned the thermodynamics of molecules between two phases. However, all of the species considered in this work also undergo chemical reactions. Acid gas removal by absorption into alkanolamine solutions is the preferred method of acid gas removal due to the high capacity of

20

these solutions. This capacity for acid gases is a result of the weak basicity of the amines which react with the acid gases to convert them into ions thereby trapping them in the liquid phase. These reversible acid-base reactions provide a large capacity enhancement over simple physical absorption. Some physical absorption processes are being used in industry, but usually for limited, specific applications. One example where physical absorption is preferred is the removal of carbonyl sulfide (COS) from natural gas. COS reacts irreversibly with some amines and would quickly neutralize the alkanolamine solution requiring expensive replacement of the entire solution inventory. For these cases, a non-reactive physical solvent would be used. Further discussion of physical solvents will not be carried out here since CO_2 and H_2S both undergo reversible reactions with alkanolamines.

Equilibrium constants are required for each of the reactions occurring in solution. Chemical equilibrium constants are related to the activities of each of the species as shown in equations 2.24 through 2.26. The lower case letters are the stoichiometric coefficients, v_i, and the capital letters are labels for the chemical species.

$$K = \prod_i a_i^{v_i} \qquad (2.24)$$

$$bB + cC = dD + eE \qquad (2.25)$$

$$K = \frac{a_D^d \, a_E^e}{a_B^b \, a_C^c} \qquad (2.26)$$

Equilibrium constants can usually be determined from titration experiments which are extrapolated to zero concentrations. This is necessary since only concentrations can be determined experimentally. Since activity

21

contains both activity coefficient and mole fractions as given in equation 2.13, to determine K from equation 2.26 all of the activity coefficients must approach one. It is convenient then that activity coefficients for ions and water are defined to approach one as the solution approaches pure water. Alkanolamine activity coefficients are an exception to this rule and equilibrium constants taken from the literature must be converted to the convention used in this work. Section 2.3.2.2 discusses the conversion of the amine protonation equilibrium constants in more detail.

Equilibrium constants are a function of temperature however, and the typical form is given in equation 2.27.

$$\ln K = A + \frac{B}{T} + C * \ln T + D*T \tag{2.27}$$

Equilibrium constants are related to the change in Gibbs energy due to the reaction as shown in equation 2.28. From the definition of G we also obtain an expression directly relating the temperature dependence of the equilibrium constants with the heat of the reaction, eq. 2.29.

$$\ln K = \frac{\Delta G_{rxn}}{RT} \tag{2.28}$$

$$\frac{d \ln K}{d(1/T)} = -\frac{\Delta H_{rxn}}{R} \tag{2.29}$$

2.3.1 Acid Gas Treating Reactions

The following set of chemical reactions are unique to acid gas treating systems. Equilibrium constants reported in this work are calculated based on the directions the following reactions are written. Details on the temperature dependent parameters of equation 2.27 for these reactions are given in chapter 5.

$$2 H_2O \Leftrightarrow OH^- + H_3O^+ \tag{2.30}$$

$$CO_2 + 2\,H_2O \Leftrightarrow HCO_3^- + H_3O^+ \qquad (2.31)$$

$$HCO_3^- + H_2O \Leftrightarrow CO_3^= + H_3O^+ \qquad (2.32)$$

$$H_2S + H_2O \Leftrightarrow HS^- + H_3O^+ \qquad (2.33)$$

$$HS^- + H_2O \Leftrightarrow S^= + H_3O^+ \qquad (2.34)$$

$$MDEAH^+ + H_2O \Leftrightarrow MDEA + H_3O^+ \qquad (2.35)$$

$$DEAH^+ + H_2O \Leftrightarrow DEA + H_3O^+ \qquad (2.36)$$

$$DEACOO^- + H_2O \Leftrightarrow DEA + HCO_3^- \qquad (2.37)$$
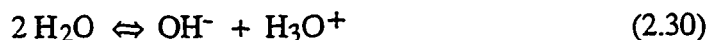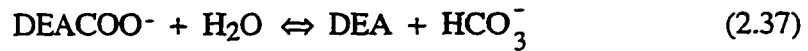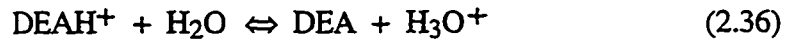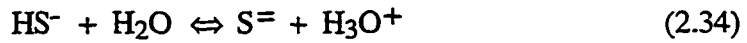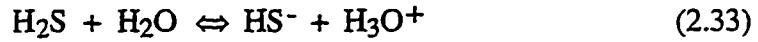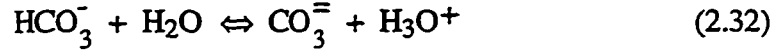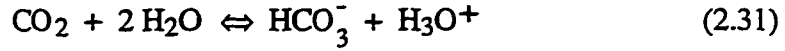
Primary and secondary alkanolamines are known to react directly with CO_2 to form a carbamate ionic species. Reaction 2.37 gives the carbamate reversion reaction for DEA which is a secondary amine. MDEA is a tertiary amine and does not form a carbamate species. Unfortunately, since carbamate, carbonate and bicarbonate all exist simultaneously when absorbing CO_2 into primary or secondary amines, the equilibrium constant for equation 2.37 is difficult to isolate. Very little independent experimental determinations exist for the DEA carbamate equilibrium constant and it is usually determined by regression of VLE data.

2.3.2 Equilibrium Constant Conversion

Typically, equilibrium constants reported in the literature are reported at infinite dilution in water and with concentrations on a molality basis. In this work mole fraction units are used, therefore all of the equilibrium constants have to be converted. The following section provides a description of the process. In addition, our convention for alkanolamines states that their activity coefficients approach γ_{am}^{∞} and not 1 as their concentration approaches zero in water.

23

Therefore, to use literature values of alkanolamine reactions we normalize them by the infinitely dilute activity coefficient. This procedure is detailed below in section 2.3.2.2.

2.3.2.1 Converting Molality to Mole Fraction Basis

Equilibrium constants as given in the experimental literature are typically reported on a molality basis. Molality units, $\frac{\text{moles solute}}{\text{kg water}}$, are more convenient for use in dilute wet chemistry where the solution density can be assumed to equal one and be mostly water. However, our model is based on the mole fraction concentration scale so these constants must be converted.

Equilibrium constants are written in terms of activities as given in equation 2.24. Using the water reaction as an example, equation 2.30, we write the molality based equilibrium constant as

$$K_{mw} = \frac{a_{OH^-}\, a_{H3O^+}}{a_{H_2O}\, a_{H_2O}}$$ (2.38)

Since the solution is assumed to be infinitely dilute in water, the activity of water equals 1 and all solute activity coefficients also approach one, resulting in equation 2.39.

$$K_{mw} = m_{OH^-}\, m_{H3O^+}$$ (2.39)

Both species molal concentrations are converted to mole fractions as given below in 2.40. It is assumed that moles of water approximately equals the total moles of solution.

$$x_i = m_i * \frac{18\,\text{g}\,H_2O}{\text{mole}\,H_2O} * \frac{1\,\text{kg}\,H_2O}{1000\,\text{g}\,H_2O}$$ (2.40)

In our example then, $K_{xw} = K_{mw} \left(\frac{18}{1000}\right)^2$ and

$$\ln K_{xw} = \ln K_{mw} + 2\ln\frac{18}{1000} = \ln K_{mw} + 2(-4.0174)$$ (2.41)

So it is shown that the natural log of the molality based equilibrium constant has 4.0174 subtracted from it for each additional compound in the numerator, neglecting water. Therefore, all of the reactions except for water ionization have 4.0174 subtracted from it only once in converting from the molality to mole fraction basis. Note also that the conversion in 2.41 is not affected by temperature and therefore the conversion can be applied to only the "A" parameter in equation 2.27.

2.3.2.2 Amine Protonation reaction conversion

Our model assumes that amine activity coefficients approach one as pure amine is approached. However, equilibrium constants are typically measured by extrapolating pH data to infinite dilution in water. The equilibrium constant based on unsymmetric activity coefficients is given in equation 2.42. When the limit of infinite dilution in water is applied, equation 2.43 results. $K_x^{*\infty}$ is the constant normally reported in the literature as a function of temperature.

$$K_x^* = \frac{X_{am} X_{H3O+}}{X_{amH+} X_{H_2O}} \frac{\gamma^*_{am} \gamma^*_{H3O+}}{\gamma^*_{amH+} \gamma^*_{H_2O}} \tag{2.42}$$

$$K_x^{*\infty} = \frac{X_{am} X_{H3O+}}{X_{amH+} X_{H_2O}} \tag{2.43}$$

Applying the conventions used in this work for activity coefficients at infinite dilution in water results in equation 2.44 which does not match equation 2.43.

$$K_x^\infty = \frac{X_{am} X_{H3O+}}{X_{amH+} X_{H_2O}} \gamma^\infty_{am} \tag{2.44}$$

Therefore, to use these constants consistently in our model, the equilibrium constants must be divided by the infinitely dilute amine activity

coefficient, γ_{am}^{∞}, over the temperature range of interest. γ_{am}^{∞} is calculated from a VLE model of the binary amine-water system which is described in detail in chapter 3. The resulting values were then re-fit to the standard temperature dependent form for equilibrium constants. It is this modified amine protonation equilibrium constant that is utilized in the electrolyte-NRTL model. Note also that the DEA carbamate equilibrium constant will contain a symmetrically normalized DEA activity coefficient. Therefore, comparisons of K_{carb} with other literature values may also require normalization by γ_{DEA}^{∞}.

2.4 CONCLUSIONS

In this chapter the basic concepts of vapor-liquid equilibria calculations were discussed. Equations and equilibrium relationships that are utilized in this work were presented to give the reader a better understanding of how abstract thermodynamic concepts relate to concrete experimental data. With the theory presented here the reader should have a better understanding of the relationships of the variables and how they can be related to experimentally measured quantities. It was assumed that the reader has a basic understanding of chemical thermodynamics and no attempt was made to derive relationships from their origin. For more details on thermodynamics the reader is referred to the following books which are a current representation of thermodynamic theory: Molecular Thermodynamics of Fluid-Phase Equilibria (Prausnitz et al., 1986), Computer Calculations for Multicomponent Vapor-Liquid and Liquid-Liquid Equilibria (Prausnitz et al., 1980), Introduction to Chemical Engineering

<u>Thermodynamics</u> (Smith and Van Ness, 1975), <u>Perry's Chemical Engineers'</u> <u>Handbook</u>, 6th ed., pp 4-52 to 4-89.

In VLE calculations the quantities that are typically unknown are the activity coefficients and concentrations of all of the chemical species. Henry's constants and pure component vapor pressures are known from independent experiments. Equilibrium constants for all of the reactions, except the carbamate reversion, are also known from independent experiments and are used to relate the activities of the species. Then, with a consistent activity coefficient model and the requirements of overall charge and mass balances, the VLE problem can be solved.

Chapter 3: Binary Alkanolamine-Water Systems

To model the thermodynamics of the acid gas-alkanolamine-water systems, we first must understand the binary alkanolamine-water systems. As the acid gas loading approaches zero in these solutions, a binary amine-water system results. By improving our knowledge of the thermodynamics in this binary system, we increase our faith in the extrapolations of the model to very low acid gas loadings.

3.1 MODEL STRUCTURE

Early in this project it was decided to use the electrolyte-NRTL model (Chen et al., 1979) as the structure of the equilibrium model. As the concentration of ions approaches zero, this model reduces to the Nonrandom Two-Liquid (NRTL) Model of Renon and Prausnitz (1968). It was therefore logical to model the binary systems using the NRTL model. The resulting binary parameters are then included in the complete acid gas-alkanolamine-water system and their values are not further regressed.

The NRTL model is an excess Gibbs energy model which has the following form for a binary system:

$$\frac{g^{ex}}{RT} = x_1 x_2 \left(\frac{\tau_{21} G_{21}}{x_1 + x_2 G_{21}} + \frac{\tau_{12} G_{12}}{x_2 + x_1 G_{12}} \right) \tag{3.1}$$

with $\qquad \tau_{12} = a_{12} + \dfrac{b_{12}}{T} \qquad\qquad \tau_{21} = a_{21} + \dfrac{b_{21}}{T}$

$\qquad\qquad\quad G_{12} = \exp(-\alpha_{12}\tau_{12}) \qquad\quad G_{21} = \exp(-\alpha_{21}\tau_{21})$

$\qquad\qquad\quad x_1 = $ liquid mole fraction of component 1

Renon and Prausnitz (1968) state that the nonrandomness parameter, α, can roughly be related to the inverse of the coordination number. Coordination numbers are on the order of 6-12, therefore α loses its physical significance for values outside the range of 0.1 to 0.3. Based on these statements by Renon and Prausnitz, α was kept constant at 0.2 for all of the binary systems. The subscripts 1 and 2 denote liquid components amine and water, respectively. Note that the parameters are not reversible, i.e. τ_{12} does not necessarily equal τ_{21}. So, for a binary system the four parameters are a_{12}, b_{12}, a_{21} and b_{21}, where the b terms represent temperature dependence. From thermodynamics we get the equation (3.2) for amine activity coefficient:

$$\ln \gamma_1 = x_2^2 \left(\tau_{21} \left(\frac{G_{21}}{x_1 + x_2 G_{21}} \right)^2 + \frac{\tau_{12} G_{12}}{(x_2 + x_1 G_{12})^2} \right) \qquad (3.2)$$

For the activity coefficient of component 2 we need only to replace all the subscript 1's with 2's and vice versa. By taking the limit as the mole fraction of amine approaches zero, we get an explicit form of equation (3.2) for the infinitely dilute amine activity coefficient. This equation is given because the infinitely dilute amine activity coefficients are needed for normalization of the equilibrium constant of amines with water, as described in Chapter 2.

$$\ln \gamma_{amine}^{\infty} = \tau_{H2O\text{-}amine} + \tau_{amine\text{-}H2O} * \exp(-\alpha * \tau_{amine\text{-}H2O}) \qquad (3.3)$$

3.2 TYPES OF EXPERIMENTAL DATA

We can see from equations 3.1 and 3.2 how excess Gibbs energy and activity coefficients are related to the model parameters. But how do we relate the

.

model parameters to experimental data? The relationship between each data type and the parameters is different and they are described separately below.

3.2.1 Total Pressure Data

For our binary systems the following equation can be used to represent equilibrium for total pressure data. For this type of data, mixtures of various mole fraction ratios of alkanolamine to water are prepared and the total solution vapor pressure is measured as a function of temperature. Pressures for amine-water data are usually low enough to neglect gas phase non-idealities.

$$P = \gamma_i P_i^o x_i + \gamma_j P_j^o x_j \qquad (3.4)$$

where   P is the total solution vapor pressure

P_i^o is the Antoine pure vapor pressure of component i

x_i is the mole fraction of component i

γ_i is the symmetric activity coefficient of component i

For total pressure data, the missing values in equation 3.4 are the activity coefficients. Therefore, the model parameters are varied to change the calculated activity coefficients in order to fit the total pressure data. Since the vapor pressures of the amines are very low compared to water, 90% or more of the total pressure is due to water. This leads to the unfortunate situation where a 10% error in the total pressure can completely hide the amine contribution to the total pressure. As a result, activity coefficients cannot be very accurately determined from this data.

3.2.2 Vapor-Liquid Equilibrium (VLE) Data

Occasionally, in addition to total pressure, the concentrations of amine and water in the vapor phase are measured. Equation (3.4) then expands to include this information and the activity coefficients can now be independently determined.

$$P \, y_i + P \, y_j = \gamma_i \, P_i^0 \, x_i + \gamma_j \, P_j^0 \, x_j \qquad (3.5)$$

where y_i is the vapor phase mole fraction of component i

Usually a gas chromatograph was used to analyze the vapor phase compositions. However, even with this sensitive instrument, the very low amine vapor concentrations are hard to determine. In fact, VLE data was only found for the most volatile amine, monoethanolamine.

3.2.3 Freezing Point Depression Data

From freezing point theory (Harned and Owen, 1950), we can relate the activity of water directly to the freezing point depression of water. Equation (3.6) is usually truncated to the first term since it contributes almost all of the value of the activity. It can then be rearranged using the mole fraction definition of activity coefficient to obtain equation (3.7).

$$-\ln(a_w) = \frac{\Delta H_f}{RT_o^2} \Delta T_f + \{\frac{\Delta H_f}{RT_o} - \frac{\Delta C_p}{2R}\}\frac{\Delta T_f^2}{T_o^2} \qquad (3.6)$$

where R is the universal gas constant, 8.314 J/gmol-K
T_o is the normal freezing point of water, 273.15 K
ΔT_f is the change in freezing point of water, $T-T_o$, K
ΔH_f is the heat of fusion of water, -6.008 kJ/gmol
ΔC_p is the heat capacity difference between water and ice, 37.6 J/gmol-°C

31

$$\gamma_w = \frac{\exp\left(\frac{-0.018*\Delta T_f}{1.858}\right)}{x_w} \qquad (3.7)$$

Chang et al. (1993) measured freezing point depression for the most common alkanolamines. They then used this data along with total pressure data to obtain a reasonable set of NRTL parameters for several alkanolamine-water systems. This work also utilizes this data. Freezing point data does have the drawback of being at temperatures far from the area of interest. The freezing point data ranged from -40°C to 0°C, whereas absorption/stripping systems operate between 40°C and 120°C.

3.2.4 Excess Enthalpy Data

Excess enthalpy is defined here as the isothermal enthalpy change per mole of solution when mixing two pure liquids without a chemical reaction. When defined in this way, the calorimetrically measured heat of mixing is identical to the excess enthalpy, h_{ex}, of the solution. Excess enthalpy data is beneficial to modeling because it is directly related to the temperature dependence of excess Gibbs energy.

$$\frac{d\left(\frac{g_{ex}}{RT}\right)}{d(1/T)} = -\frac{h_{ex}}{R} \qquad (3.8)$$

Therefore, in an excess Gibbs energy model for activity coefficients excess enthalpy measurements will provide a more accurate temperature dependence for the model. Applying the derivative in equation 3.8 to the binary NRTL form (equation 3.1), results in equation 3.9 which illustrates the relationship of excess enthalpy to the parameters of the model. The b terms have

32

moved out to the front of the equation signifying their importance to the calculation of h_{ex} and the temperature dependence of the model.

$$-\frac{h_{ex}}{R} = \frac{x_1 x_2 b_{21} G_{21}[x_1(\alpha\tau_{21}-1)-x_2 G_{21}]}{(x_1+x_2 G_{21})^2} + \frac{x_1 x_2 b_{12} G_{12}[x_2(\alpha\tau_{12}-1)-x_1 G_{12}]}{(x_2+x_1 G_{12})^2} \qquad (3.9)$$

Several researchers have investigated the use of excess enthalpy data for calculating vapor-liquid equilibria (VLE). Gow (1993) showed that partial molar excess enthalpy data, ΔH_{ex}^{∞}, alone could be used with the Wilson or NRTL models to predict VLE. Hanks et al. (1971) showed that by using excess enthalpy data alone VLE could be predicted with the NRTL model. Hanks et al. (1978b) also showed that higher temperature VLE can be predicted from lower temperature heat of mixing data. Hanks et al. (1978a) address the method of simultaneous regression of h_{ex} and g_{ex}. They note that above some limit, the higher the nonideality, the higher the error in simultaneous prediction of the data. The data we have used fall well below their upper limit on g_{ex} of l3450l J/gmol soln at $\alpha=0.2$.

Unfortunately, very little excess enthalpy data was found in the open literature. It was determined that this data would be greatly beneficial to proper modeling of the binary alkanolamine-water systems. Therefore, experiments were undertaken to measure the excess enthalpy for MEA, MDEA and DEA solutions. Details on these experiments are given below in section 3.3.

3.3 EXCESS ENTHALPY EXPERIMENTS

3.3.1 Chemicals Used

The DEA used is from Texaco Chemical, lot # 7H-1184/ODS-92-0232, and is listed as 100% pure. The MDEA is Texaco "Textreat® M", lot# ODS92-0179, and is listed as 95-99.99% pure. The MEA is from Fisher, lot# 851955, listed as purified grade. The stock amines were vacuum degassed at approximately 80°C before being transferred into smaller containers for use, but no other purifications were made. The 0.1 mol/L NaOH was prepared from vacuum distilled DI water. NaOH pellets were tared into a 250 mL volumetric flask and the DI water was then added in stages to allow for the volume of mixing. The exact concentration is not critical since the NaOH only serves to prevent the amine protonation reaction which can cause a ΔH_{rxn} error.

3.3.2 Experimental Method

A SETARAM model C80 batch calorimeter was used for the experiments. Details on the calorimeter procedures and calibration are given in Ziaee (1995). The temperature was controlled by the computer to ±0.2°C. The calorimeter has a sample cell and a reference cell, each with upper and lower compartments. Samples of approximately 2.0 grams total weight were prepared gravimetrically on an analytical balance accurate to ±0.0001 g. In the reference cell, the amine and water were premixed to their final desired composition, separated into equal volumes and placed in the two compartments separated by an aluminum foil membrane. The reference cell serves to cancel out the heat supplied to maintain isothermal conditions and the negligible heat of stirring.

34

In the sample cell the two fluids were placed into the separate, sealed compartments on either side of the membrane and were not mixed until the experiment began. The two cells were lowered into the calorimeter block to heat up to the temperature of the experiment. Once both vessels have reached the test temperature, both membranes were broken and the solutions were stirred lightly for one minute. Heat flux detectors measured the difference in heat flow between the vessels and the calorimetric block. The calorimetric block had sufficient thermal mass to supply or receive heat to the vessels without changing temperature. A curve was generated of differential heat flow versus time. The area under this curve was then integrated by the computer to calculate the total heat of mixing of the sample solution.

3.3.3 Sources of Error

The mostly likely cause of error in these experiments is alkanolamine sticking to the walls of the cell and never mixing with the total solution. Another possible error is the heat of reaction of CO_2 that might be dissolved in either solution. Some CO_2 absorption is possible in the process of weighing out the samples, but atmospheric contact has been minimized as much as possible. For the 70°C data the pure chemicals were kept in septum sealed bottles and withdrawn with syringes to minimize air contact and maintain a vacuum over the liquids.

3.3.4 Experimental Results and Data Confirmation

The average error in the heat of mixing data is 5% or better as evidenced in the repeat measurements. Some outliers exist for various reasons and have

been flagged in Table 3.1. The heat of mixing curves follow an expected third order behavior. Figure 3.1 shows excess enthalpy data for MEA with water by Touhara et al. (1982) and Buslaeva et al. (1983) at 25°C, and the data collected in this work at 25°C and 70°C. The one point collected at 25°C is within 2% of Touhara's data and serves to confirm the analytical procedure used here. The curves are the regressed predictions using the Nonrandom Two-Liquid (NRTL) model which are discussed later. The Buslaeva data was not included in the regressions, but serves to confirm the other experimental data at 25°C.

Figures 3.2 and 3.3 display the heat of mixing data for MDEA and DEA, respectively. The heat of mixing data is not fit perfectly due to the influence of other data used in the regressions. It is interesting to note that MDEA and MEA have a significant change in heat of mixing between 25°C and 70°C compared to DEA.

Table 3.1. Experimentally measured heats of mixing of pure amines into 0.1N NaOH at 25°C and 70°C

Amine	Temp °C	Final Conc. X amine	Heat of mixing J/gmol soln.		Amine	Temp °C	Final Conc. X amine	Heat of mixing J/gmol soln.	
DEA	25	0.0186	-233		MDEA	25	0.0159	-265	
DEA	25	0.0215	-391	*	MDEA	25	0.0362	-699	
DEA	25	0.0405	-515		MDEA	25	0.0912	-1401	
DEA	25	0.0680	-823		MDEA	25	0.1472	-1912	
DEA	25	0.0683	-801		MDEA	25	0.2043	-2170	
DEA	25	0.1461	-1406		MDEA	25	0.2942	-2207	*
DEA	25	0.1488	-1491	*	MDEA	25	0.3016	-2413	
DEA	25	0.2836	-1887		MDEA	25	0.3426	-2348	
DEA	25	0.3882	-2016		MDEA	25	0.4455	-2230	
DEA	25	0.3896	-1900		MDEA	25	0.4956	-2021	
DEA	25	0.4805	-1771		MDEA	25	0.4986	-1998	
DEA	25	0.6037	-1512		MDEA	25	0.4994	-2184	*
DEA	25	0.7488	-1013		MDEA	25	0.6480	-1691	
					MDEA	25	0.7383	-1212	
DEA	69.3	0.0187	-356	*					
DEA	69.4	0.0693	-793		MDEA	69.3	0.0987	-1029	
DEA	69.4	0.2029	-1595		MDEA	69.4	0.2009	-1793	
DEA	69.4	0.3941	-1791		MDEA	69.5	0.2928	-1915	
DEA	69.2	0.5705	-1635	*	MDEA	69.4	0.4785	-1772	
DEA	69.3	0.8015	-812		MDEA	69.8	0.6522	-1382	
MEA	25	0.4925	-2269						
MEA	69.3	0.1541	-1391						
MEA	69.3	0.3085	-1988						
MEA	69.4	0.4090	-2171						
MEA	69.7	0.4948	-2105						
MEA	69.4	0.6720	-1690						

* Questionable or outlying data point.

37
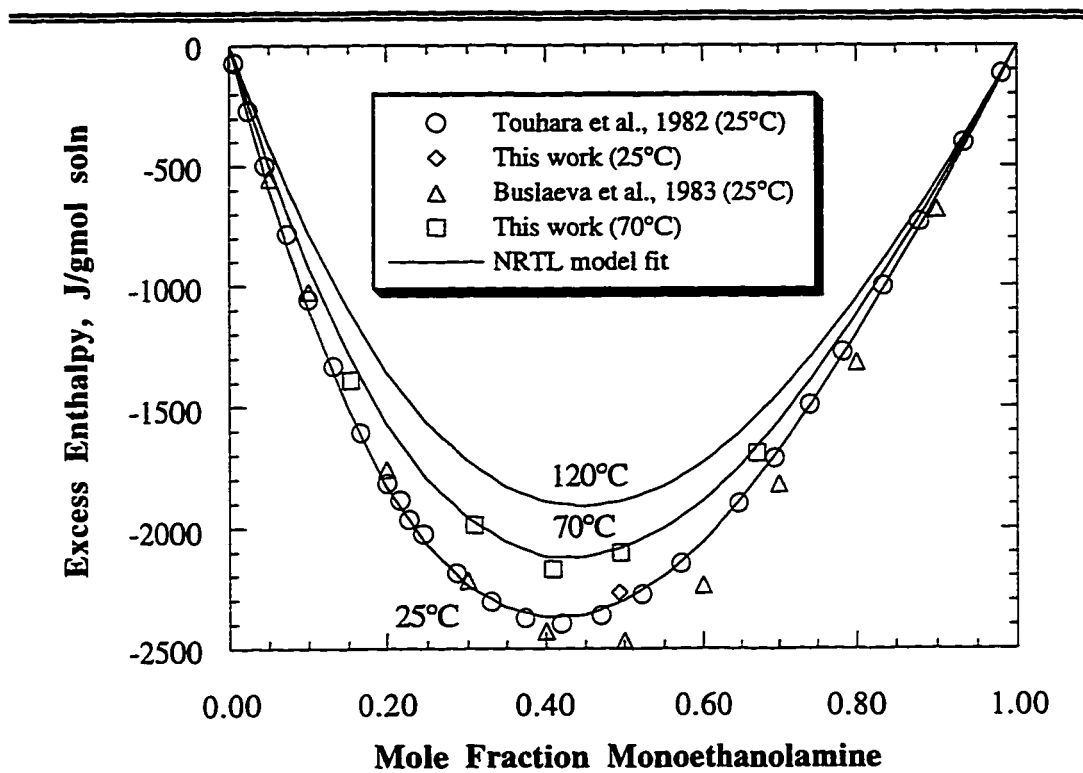
Figure 3.1. Heat of mixing experimental data for monoethanolamine into water. Curves predicted by NRTL regression of total pressure, freezing point, heat of mixing and vapor-liquid equilibrium data.

38
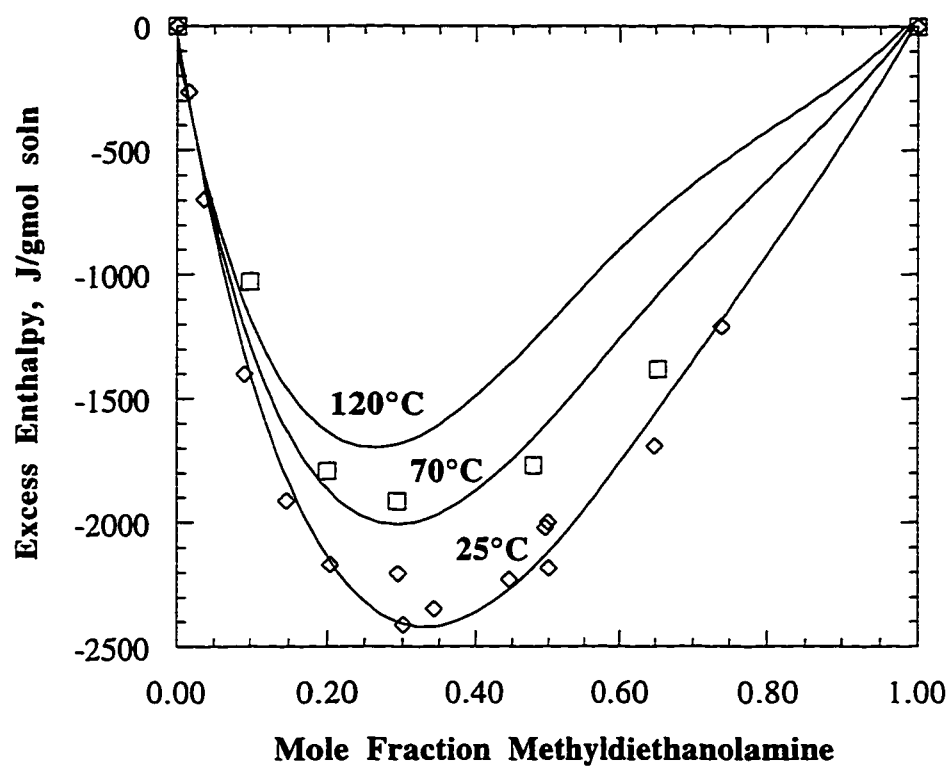
Figure 3.2. Heat of mixing of pure MDEA into 0.1 mol/L NaOH. Curves predicted by NRTL regression of total pressure, freezing point and heat of mixing data.
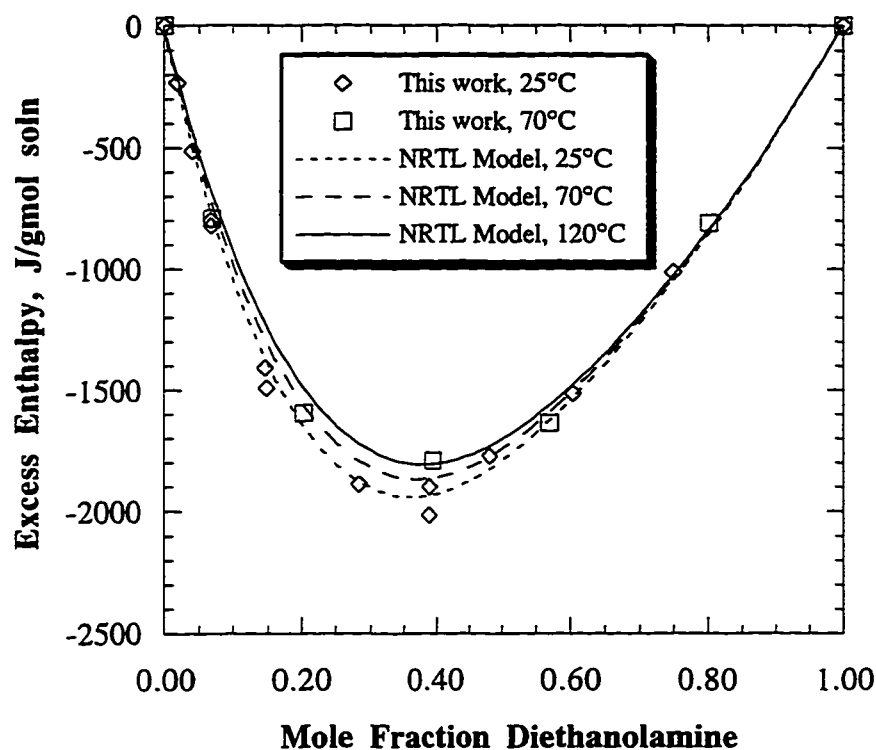
Figure 3.3. Heat of mixing of pure DEA into 0.1 mol/L NaOH. Curves predicted by NRTL regression of total pressure, freezing point and heat of mixing data.

Kim et al. (1987) have measured the slopes of the heat of mixing curves for MEA, MDEA and DEA at zero amine concentration and 25°C. These slopes along with their confidence limits are compared in Table 3.2. All of the slopes from figures 3.1 to 3.3 compare favorably with those of Kim.

Table 3.2. Comparison of heat of mixing at infinite dilution

Alkanolamine	This work ΔH_{ex}^{∞} @ 25°C (kJ/gmol)	Kim et al., 1987 ΔH_{ex}^{∞} @ 25°C (kJ/gmol)	This work ΔH_{ex}^{∞} @ 70°C (kJ/gmol)
Monoethanolamine	-12.61±0.12 (Touhara, 1982)	-11.43±0.09	-11.82±0.82
Diethanolamine	-14.16±0.77	-14.50±0.06	-13.01±2.07
Triethanolamine	—	-14.38±0.08	—
Diisopropanolamine	—	-4.5±0.14	—
Methyldiethanolamine	-19.16±1.44	-20.5±0.2	-14.40±1.88

3.3.5 BYU Heat of Mixing Data

Researchers at Brigham Young University (Sue Gillespie and John Oscarson) have also measured heats of mixing of amines with water. However, their data is for amines already diluted with water. For example, they measured the heat of mixing of 50 wt% MDEA with pure water. Unfortunately, these experiments are not directly related to excess enthalpy, making them slightly more difficult to use. Also, at the time of writing, this data was not published in any public journal. Although their data seemed to corroborate our own, a comparison will not be made herein because their data is not publicly available.

3.4 OTHER REQUIRED INFORMATION

3.4.1 Antoine equations

Antoine equations for water, monoethanolamine and diethanolamine were obtained from the DIPPR data banks (Daubert, 1985) and are given in Table 3.3. The Antoine equations are given with pressure in Pascals and temperature in

Kelvin. The equation for water was found to be accurate within 0.5 mmHg throughout the whole temperature range utilized here as compared to literature tables (Perry, 1984). No plot is given for water because the data sets available are too numerous. A plot of the MEA and DEA vapor pressure curves compared to experimental data are shown in figures 3.4 and 3.5, respectively. The Antoine equation for MDEA is derived from data by Dow Chemical and Union Carbide and is shown compared to data from Daubert (1990) in figure 3.6. The temperature ranges indicate at which temperatures data exist and shows that DEA and MDEA pressures are extrapolated at absorber conditions.

Table 3.3 Pure component Antoine equations with pressure in Pascals and temperature in Kelvin.

H_2O : $\ln P^o_{H_2O} = 72.55 - 7206.7 / T - 7.1385 * \ln T + 4.046E\text{-}6*T^2$	: 273-650 K
MEA : $\ln P^o_{MEA} = 172.78 - 13492 / T - 21.914 * \ln T + 1.3779E\text{-}5*T^2$	: 283-452 K
DEA : $\ln P^o_{DEA} = 286.01 - 20360 / T - 40.422 * \ln(T) + 3.2378e\text{-}2*T$	:323-473 K
MDEA : $\ln P^o_{MDEA} = 26.13691 - 7588.516 / T$	:413-513 K
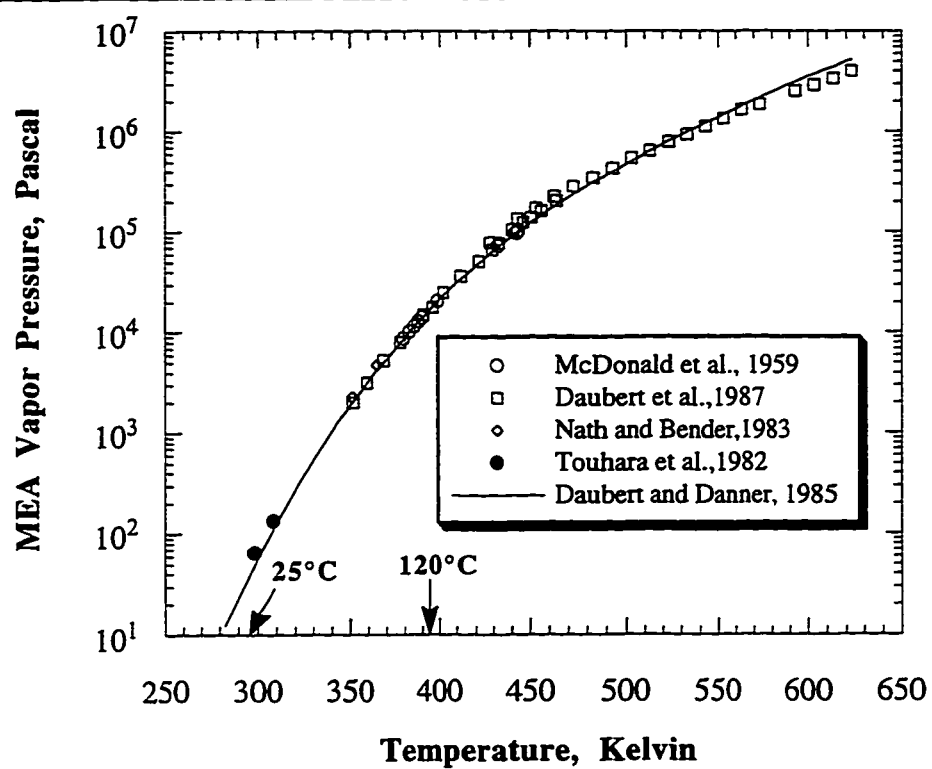
Figure 3.4 Vapor pressure of pure monoethanolamine in Pascals as a function of temperature.

43
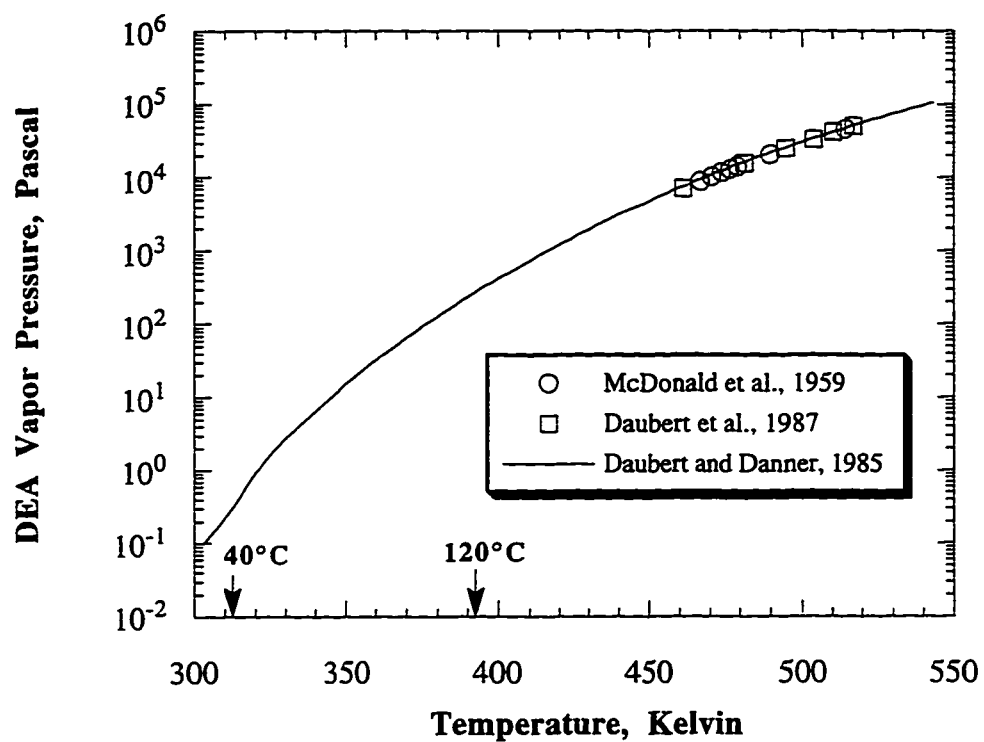
Figure 3.5 Vapor pressure of pure diethanolamine in Pascals as a function of temperature.
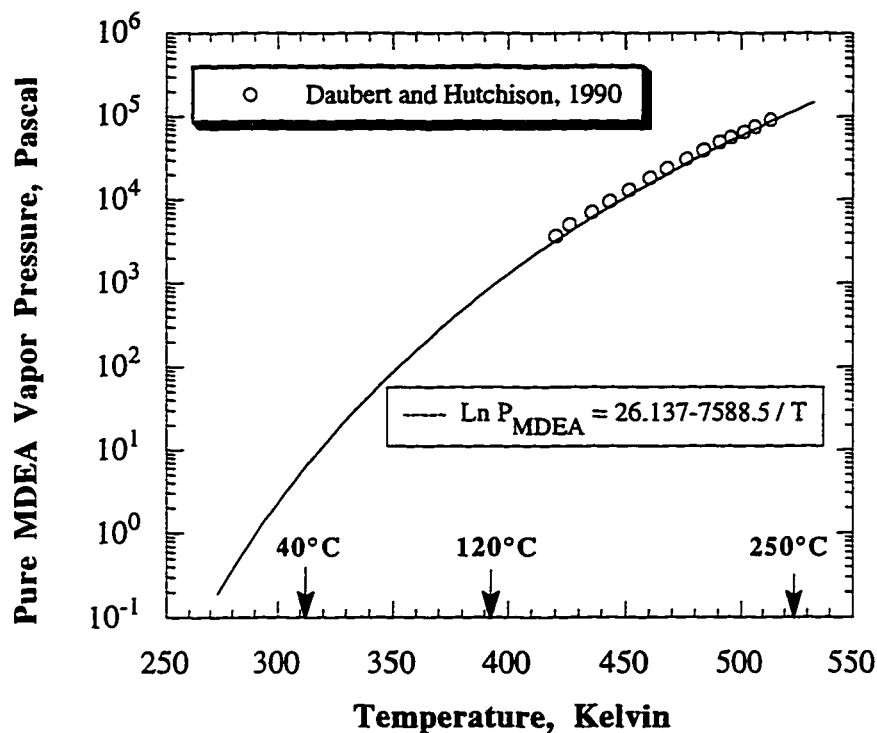
Figure 3.6 Vapor pressure of pure methyldiethanolamine in Pascals as a function of temperature.

3.5 REGRESSION RESULTS

The Data Regression System™ of Aspen Plus™ was used to regress the data to the NRTL model. Aspen performs a non-linear optimization by varying the parameters to minimize Q in the following objective function.

$$Q = \sum_k \left(\sum_j \left(\sum_i \left(\frac{Z_{exp} - Z_{pred}}{\sigma_Z} \right)^2 \right)_i \right)_j \right)_k \qquad (3.10)$$

The objective function is summed over all i variables (Z) for each j data point and all k data sets. The standard deviations serve to equally weigh the variables so

that, for example, pressure in Pascals is not more important than composition in mole fractions.

3.5.1 MEA-H₂O

To demonstrate the benefit of heat of mixing data on alkanolamine modeling we have performed five regression cases. The data sets used in these regression cases for MEA-H$_2$O are given in Table 3.4 and the resulting parameters are given in Table 3.5. For all cases, α was constant at 0.2 and the standard deviations for the minor variables were set to zero so that they would not be fit by Aspen. The first case is a regression of only total pressure data (Nath and Bender, 1983; Touhara et al., 1982). We obtained four NRTL parameters in contrast to the identical regression by Austgen (1989) which set two parameters to zero. The second case uses the above total pressure data and adds the freezing point regression data from Chang et al. (1993). Case three regresses the above total pressure, freezing point and heat of mixing data. Case four adds the Texaco in-house total pressure and vapor-liquid equilibrium data to the regression. The parameters for case four are considered the best set for complete modeling of monoethanolamine-water systems. Even though the "a" parameters are near zero they are still important to the model. To demonstrate this, both "a" parameters were set to zero and only the "b" parameters were regressed (this is case five) on the same data set as in case four. Even though some pressure data are actually fit a little better, the temperature dependence breaks down and the sum of squares error is twice that of case four.

The first benefit of using the heat of mixing data is the dramatic decrease in parameter standard deviations. For example, the $b_{H_2O\text{-}MEA}$ parameter standard deviation decreases from 2421 to 579 as freezing point depression is added. It then decreases to 34 when heat of mixing and VLE data are added. All of the parameter standard deviations decrease approximately 98% when going from case one to case four. When the parameters are known with more confidence the chances of being at a local minimum, which is not the best global answer, are reduced.

Table 3.4. Experimental data used for regression of the binary amine-water systems

Amine	Data type	Pressure kPa	Amine Conc. range	Temp. range °C	Reference/source	
MEA	Total Pressure	1.3 - 75	0 - 0.93	60, 78, 91.7	Nath, 1983	
	Total Pressure	0.065 - 5.5	0.03 - 0.89	25, 35	Touhara, 1982	
	Total Pressure	6.8 - 88.5	0.27 - 0.81	55 - 140	Texaco, 1989	
	Freezing point	n/a	0.004 - 0.14	0 to -20	Chang, 1993	
	Heat of mixing	n/a	0.006 - 0.98	25	Touhara, 1982	
	Heat of mixing	n/a	0.15 - 0.67	25, 70	This work	
	VLE	6.6 - 69	0.23 - 0.96	44 - 95	Texaco, 1989	
MDEA	Total Pressure	20 - 100	0.05 - 0.78	60 - 160	Texaco, 1989	
	Total Pressure	1.4 - 41	0 - 50 wt%	20,40,60,80	GRI - Sandall	
	Total Pressure	6.9 - 540	0.02, 0.0447	45 - 156	Kuwairi, 1983	
	Freezing point	n/a	0.0 - 0.09	0 to -13	Chang, 1993	
	Heat of mixing	n/a	0 - 1.0	25, 70	This report	
DEA	Total Pressure	6.9 - 100	0.2 - 0.8	40 - 180	Texaco, 1989	
	Freezing point	n/a	0.005 - 0.08	0 to -11	Chang, 1993	
	Heat of mixing	n/a	0 - 1.0	25, 70	This report	
	Total Pressure	100 - 1900	0 - 30 wt%	100 - 210	Kennard, 1984	*
	Total Pressure	1.4 - 48	0 - 30 wt%	20,40,60,80	Sandall, 1993	*
	Total Pressure	1.4 - 100	40,60,80,90, 92,96,98 wt%	40 - 120	Dow, 1988	*

* This data set was not used to regress the binary NRTL DEA-H_2O parameters.

Table 3.5. NRTL parameter results for all MEA-H$_2$O regression cases

Data Included	TP	TPFP	TPFPHmix	TPFPHmixVLE	b's only
Total Pressure	X	X	X	X	X
Freezing Point		X	X	X	X
ΔHmix			X	X	X
VLE				X	X
Parameters			(Best case)		
a H$_2$O-MEA	-1.767	-7.333	1.215	1.194	0.000
std-dev	7.607	1.948	0.125	0.122	0.000
b H$_2$O-MEA	1502.4	3115.5	823.5	879.3	1272.4
std-dev	2421.3	579.5	37.6	33.8	9.16
a MEA-H$_2$O	0.174	3.157	0.100	-0.035	0.000
std-dev	2.782	0.886	0.079	0.064	0.000
b MEA-H$_2$O	-810.0	-1698.3	-870.4	-859.0	-912.4
std-dev	871.4	258.6	11.9	10.6	1.59

Table 3.6 provides a condensed, quantitative measure of the fit using the average absolute percent deviation. This aids in comparing the data fits by the respective modeling cases. It shows that for case four the pressure data is fit approximately as well as in case one, but with a better fit of the heat of mixing data. Even though the pressure data covers a reasonable range of temperatures, its regression does not provide the correct temperature dependence. Table 3.6 also compares the predicted slope of the heat of mixing curves at zero mole fraction MEA and 25°C for the first four cases. Notice that case one does not predict the proper excess enthalpy as measured by Touhara et al. (1982). The freezing point data improves the prediction, but the regressions containing the Touhara data are closest to predicting the proper behavior. Proper excess enthalpy predictions are important for liquid mixture enthalpy calculations and temperature extrapolations of the model.

48

Addition of the heat of mixing data also decreases the correlation coefficients between the parameters (Table 3.7). The covariance of b_{H_2O-MEA} with a_{MEA-H_2O} decreased from 0.97 to 0.003. Correlations for all of the parameter pairs are shown to decrease significantly, therefore every parameter is less dependent on the values of the other parameters and takes on more significance of its own.

Table 3.6. Comparison of data fits for different regression cases for the MEA-water system

| Data set | Variable | Regression cases | | | | |
		Tot. Pres	TP FP	TP FP Hmix	TPFP Hmix VLE	b's only
		average absolute percent deviation				
Nath 60°C	P_{tot}	5.52	6.74	6.92	5.76	5.50
Nath 78°C	P_{tot}	4.66	4.79	8.22	6.25	4.67
Nath 91.7°C	P_{tot}	3.86	3.30	9.59	7.20	4.53
Touhara 25°C	P_{tot}	7.65	6.28	7.13	6.51	5.45
Touhara 35°C	P_{tot}	7.00	6.52	6.58	5.99	4.69
Beckmann	γ		0.213	0.195	0.206	0.258
Osmometer	γ		0.047	0.030	0.028	0.042
Hmix 25°C	ΔHmix			2.60	2.43	2.73
Hmix 70°C	ΔHmix			1.89	2.11	6.68
Texaco TP	P_{tot}				10.86	7.25
Texaco VLE	Y_{MEA}				14.38	11.03
NRTL Model Prediction, 25°C	ΔH_{ex}^{∞} (kJ/gmol)	-4.42	-9.47	-12.86	-12.76	

* Touhara et al. (1982) gives $\Delta H_{ex}^{\infty} = -12.5$ kJ/gmol at 25°C.

Table 3.7. Parameter correlation coefficient matrix for four regression cases

Parameter	a H_2O-MEA	b H_2O-MEA	a MEA-H_2O
b H_2O-MEA	-0.997	1. Total Pressure Only	
	-0.993	2. Tot. Pres. + Frz. Pt.	
	-0.680	3. TP + FP + Hmix	
	-0.765	4. TP FP Hmix VLE	
a MEA-H_2O	-0.979	0.966	
	-0.986	0.973	
	-0.565	-0.186	
	-0.619	0.003	
b MEA-H_2O	0.984	-0.977	-0.997
	0.987	-0.988	-0.993
	0.853	-0.234	-0.904
	0.875	-0.395	-0.911

Since we have determined case four to be the best set of parameters for the MEA-H_2O system, we only show the detailed data fits for this case. Figure 3.7 compares the total pressure data from Touhara et al. (1982) and Nath and Bender (1983) to the NRTL model predictions. The model fit is relatively close, but tends to overpredict the data due to the influence of the other data sets in the regression. Figure 3.8 shows that the freezing point data was fit quite well. Chang et al. (1993) measured freezing points by two different methods, Beckmann and osmometry, which reflects the two different data sets. Figure 3.9 shows that the model overpredicts the in-house total pressure of Texaco Chemical by as much as 20% and underpredicts gas phase MEA mole fractions by as much as 30% with a wide scatter. Of course, since this experimental data is not publicly available its accuracy has not been confirmed through a peer review process.
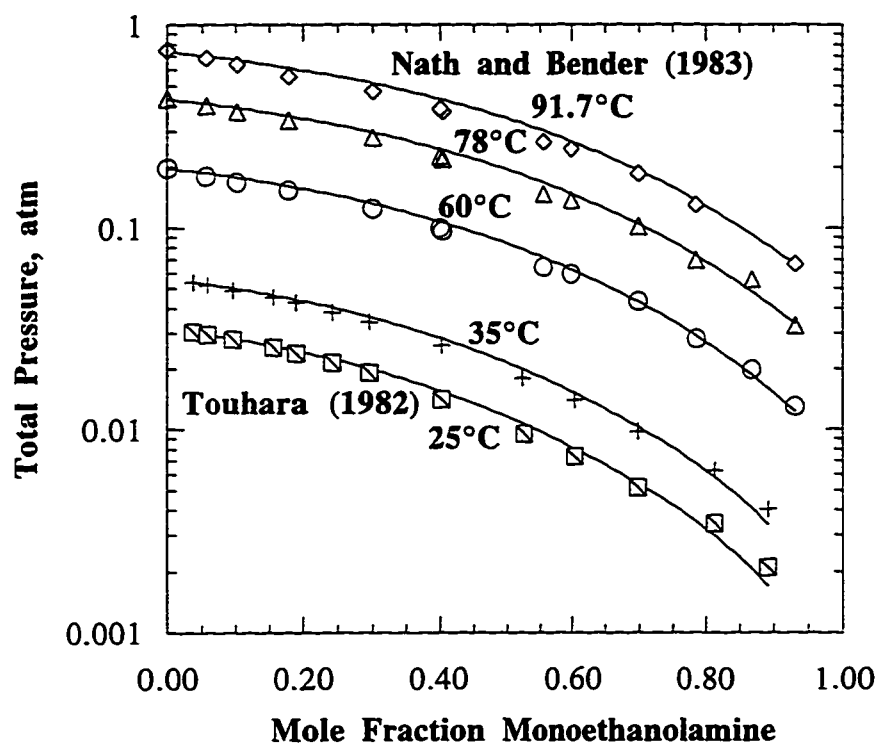
Figure 3.7. Total vapor pressure of MEA-H_2O solutions. Curves predicted by the combined regression of total pressure, freezing point, heat of mixing and vapor-liquid equilibrium data.
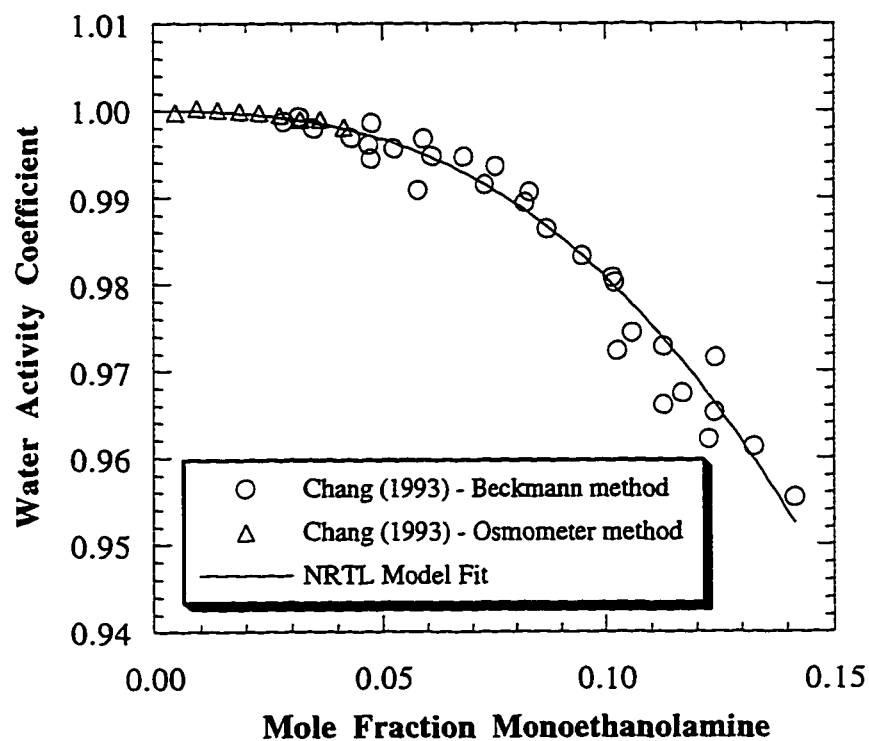
Figure 3.8. Experimental freezing point data given as water activity coefficient for MEA-H_2O with the NRTL model fit from the combined regression of total pressure, freezing point, heat of mixing and vapor-liquid equilibrium data.
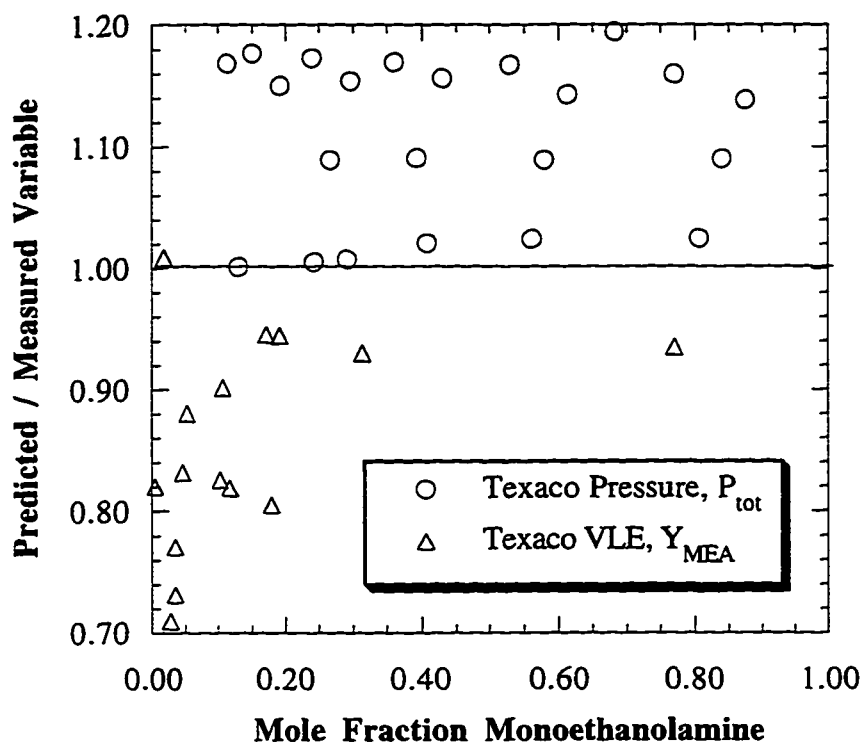
Figure 3.9. Ratio of predicted and measured total pressure data and vapor mole fraction monoethanolamine measured by Texaco Chemical in-house as predicted from a regression of total pressure, freezing point, heat of mixing and vapor-liquid equilibrium data.
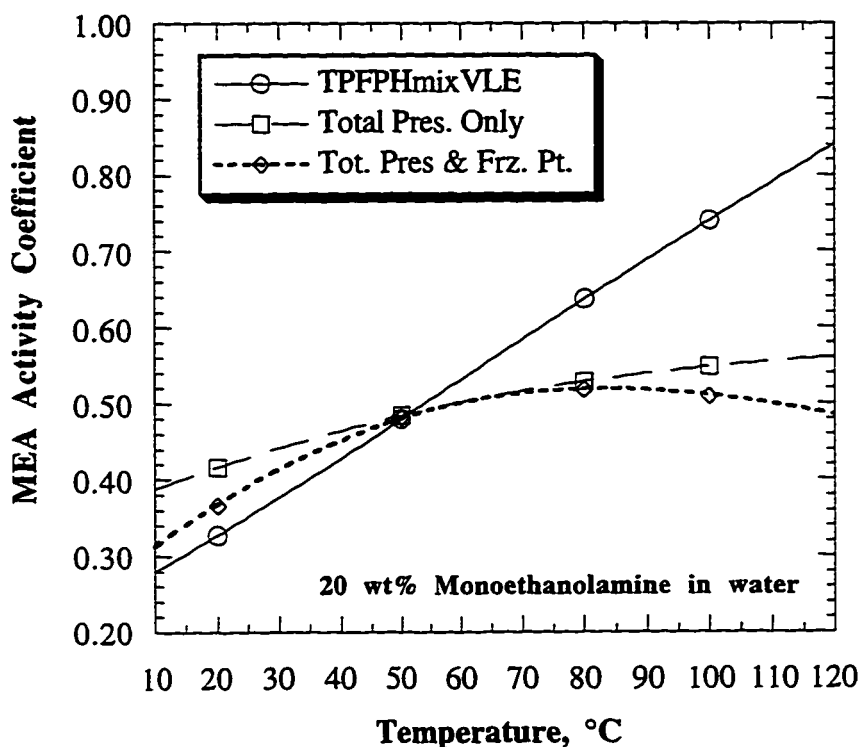
Figure 3.10. Model predictions for three different regression cases of monoethanolamine activity coefficients in 20 wt% aqueous solution between 10°C and 120°C.

A final analysis confirms that a model using heat of mixing data is quite different from one that does not. Figure 3.10 shows the predictions of MEA activity coefficient in a 20 wt% aqueous MEA solution over a range of temperatures for three of the regression cases. Interestingly, all three models predict the same at about 50°C, however the difference at 120°C is significant. Whether or not heat of mixing data is used in the regression of the NRTL parameters can make a 50% difference in the prediction of amine vapor pressure, and therefore amine losses, at 120°C. Even for predictions of acid gas vapor-

liquid equilibrium the value of the amine activity coefficient is important due to its presence in the equilibrium constant. Chang (1992) showed that at infinite dilution the amine-water parameters affect acid gas equilibrium predictions. Therefore, the prediction of H_2S VLE at 120°C and low loadings could be as much as 50% different based on the different predictions of amine activity coefficients.

3.5.2 MDEA-H_2O

Modeling of MDEA-H_2O has been improved by use of freezing point and heat of mixing data. Since the benefits of using the above data has already been discussed for MEA-water, only the final results are given for the MDEA and DEA systems. Table 3.4 lists the data sets upon which the parameters are regressed. Using only the Texaco data, Austgen (1989) was not able to determine the b parameters. By using the Texaco total pressure and freezing point data, Chang et al. (1993) were able to determine all four NRTL parameters, but the standard deviations on their parameters were larger than the values reported below in Table 3.8. Table 3.9 gives the parameter correlation matrix which shows reduced, but still high correlation between the parameters. The relatively high standard deviation of the parameters are due to the high correlation and not from a "lack of fit" of the model.

55

Table 3.8. NRTL parameters for MDEA and DEA with $\alpha=0.2$

Parameter	Value	Std. Deviation
A H_2O-MDEA	9.473	0.531
B H_2O-MDEA	-1902.4	196.1
A MDEA-H_2O	-2.173	0.193
B MDEA-H_2O	-147.4	77.8
A H_2O-DEA	4.172	0.471
B H_2O-DEA	175.1	133.7
A DEA-H_2O	-1.579	0.091
B DEA-H_2O	-546.4	25.7

Table 3.9. MDEA-H_2O parameter correlation matrix

	A H_2O-MDEA	B H_2O-MDEA	A MDEA-H_2O	B MDEA-H_2O
A H_2O-MDEA	1.000			
B H_2O-MDEA	-0.953	1.000		
A MDEA-H_2O	-0.860	0.958	1.000	
B MDEA-H_2O	0.788	-0.930	-0.983	1.000

The nonrandomness parameter, α, was also set constant to 0.2 for the MDEA-water system. For the three data sets used the predicted to measured ratio of the total solution pressure is plotted against temperature in figure 3.11. Most of the Texaco total pressure data was fit within ±5%. The Sandall (1993) data has a stated fixed pressure error of ±0.03 psi which explains why the data has a higher percent error at low temperatures. The fact that this data is evenly distributed around one and predicts the 60°C and 80°C within 2% confirms that the model is consistent with the Sandall data. The heat of mixing data at 25°C was fit well and the 70°C data fit sufficiently considering that there were only five data points to force the fit (see figure 3.2).
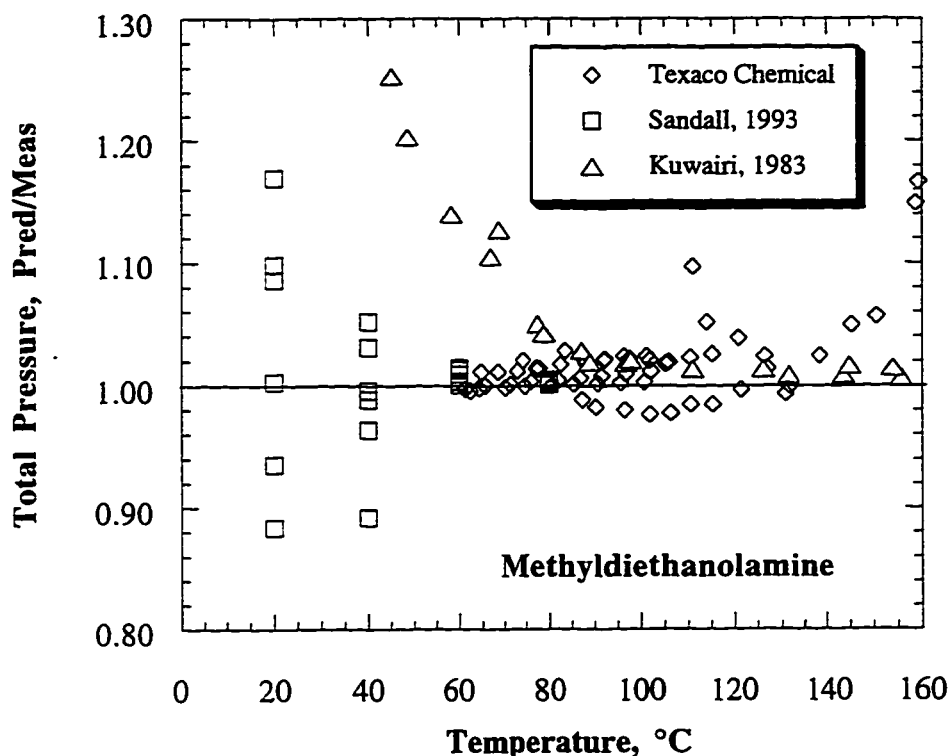
Figure 3.11. Ratio of predicted and measured total solution vapor pressure versus temperature for the three listed data sets from the NRTL regression for the MDEA-H₂O system.

The offset fit of the two different methods of freezing point determinations, figure 3.12, suggests that the model has balanced different temperature dependencies imposed by different data sets. Figures 3.13 and 3.14 give the predictions of the model for the binary MDEA-H₂O system at 40°C, 70°C and 120°C, for activity coefficients and excess Gibbs energy, respectively. Figure 3.13 illustrates that at industrial conditions, the amine activity coefficient changes significantly with temperature. Although this does not significantly affect solution total pressure, γ_{MDEA} is an important part of several acid gas

equilibrium equations and therefore is very important to acid gas vapor-liquid equilibrium predictions. Figure 3.2 demonstrates that for heat of mixing data to be useful for amine-water modeling, it needs to be collected over the full mole fraction range and not just at industrial conditions. Some equilibrium models assume that MDEA activity coefficient goes to 1 as its concentration goes to zero. Figure 3.15 gives the activity coefficient of MDEA by this asymmetric convention. Note the strong temperature dependence of the activity coefficient at industrial compositions.
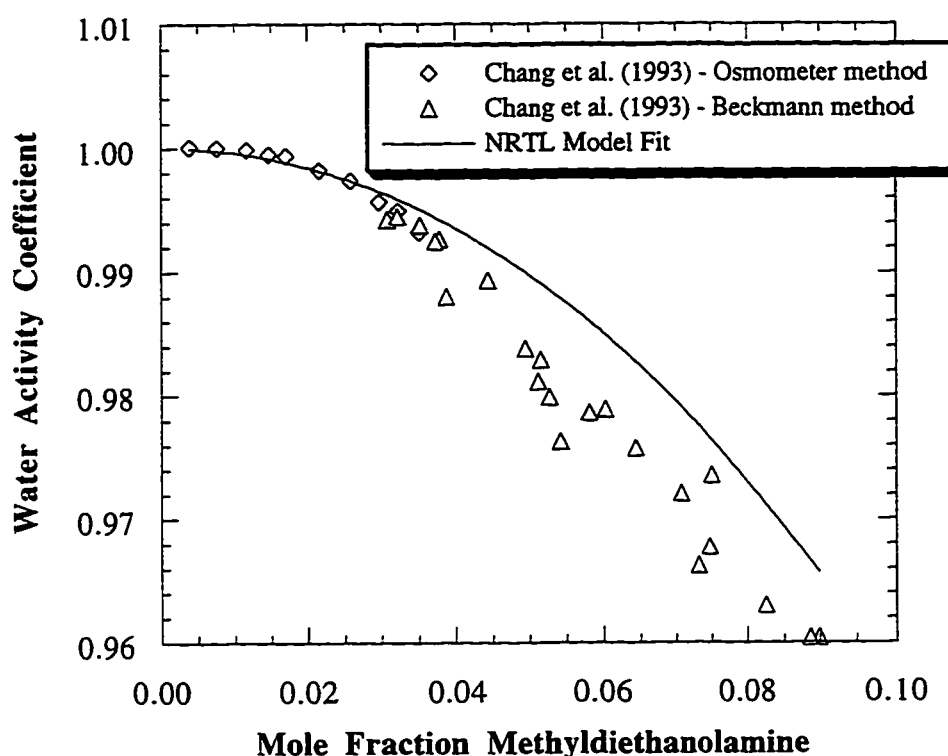
Figure 3.12. Experimental freezing point data for the MDEA-H_2O system, given as water activity coefficient, is shown compared to its prediction from the NRTL regression.
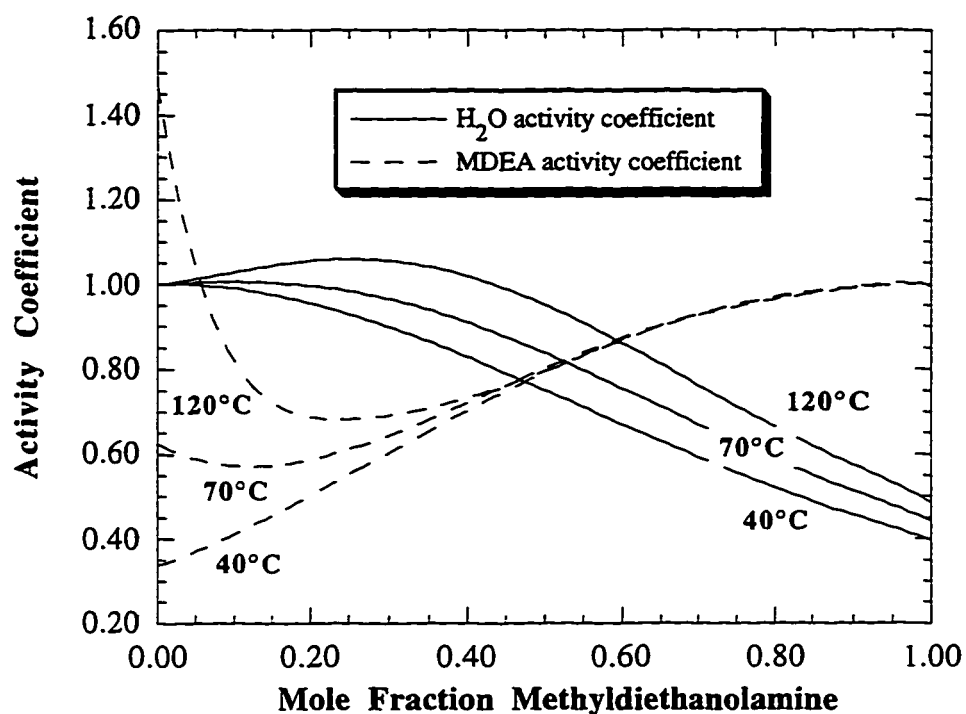
Figure 3.13. NRTL model predictions of water and methyldiethanolamine activity coefficients at 40°C, 70°C and 120°C over the entire mole fraction range using the symmetric convention of activity coefficients.
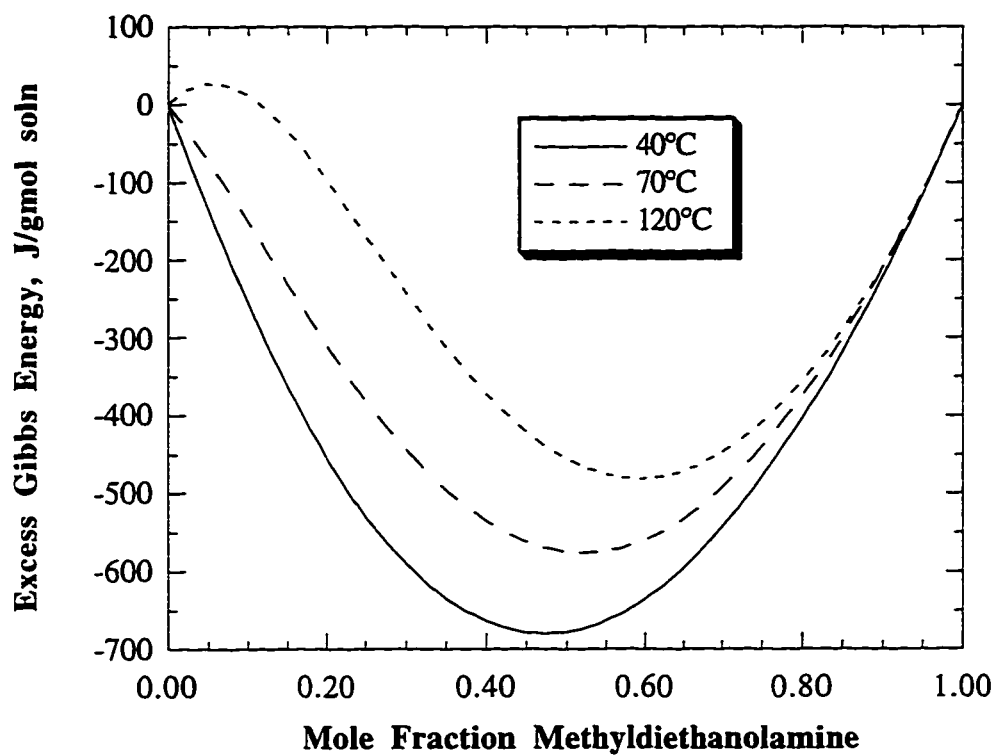
Figure 3.14. NRTL model predictions of excess Gibbs energy for MDEA-H_2O
mixtures at 40°C, 70°C and 120°C.
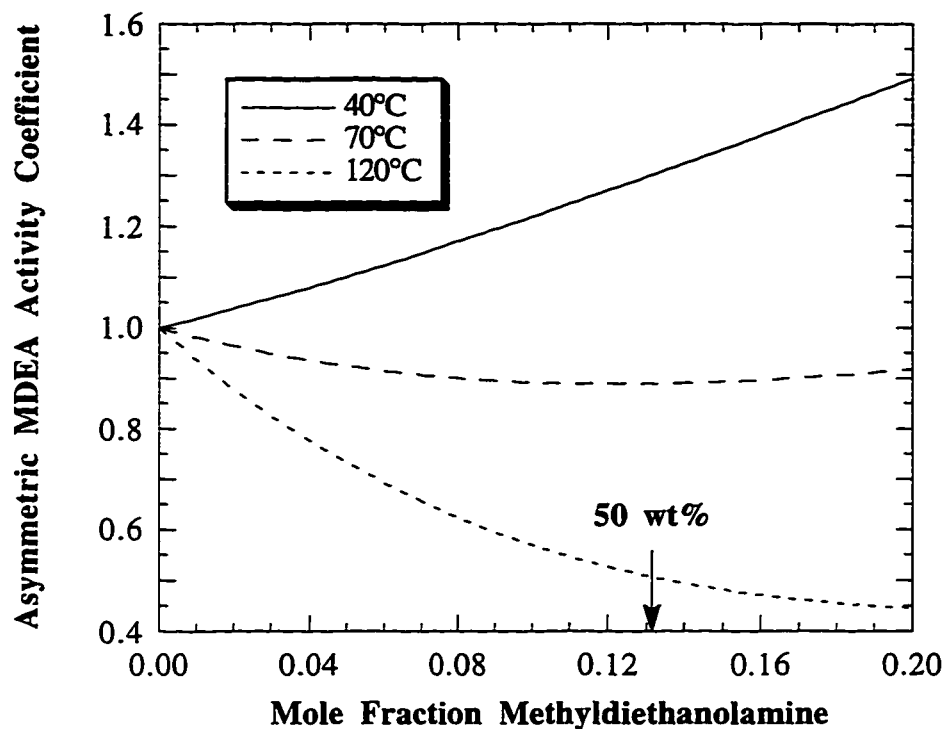
Figure 3.15. NRTL model prediction of MDEA activity coefficients at 40°C,
70°C and 120°C by the asymmetric convention.

Another total pressure data set (Xu et al., 1991) was found after we had completed the above regression. Therefore, we have used the model parameters to predict the total pressure data at the same MDEA concentrations and temperatures. Figure 3.16 shows that our model fits this unregressed data within experimental error.

61
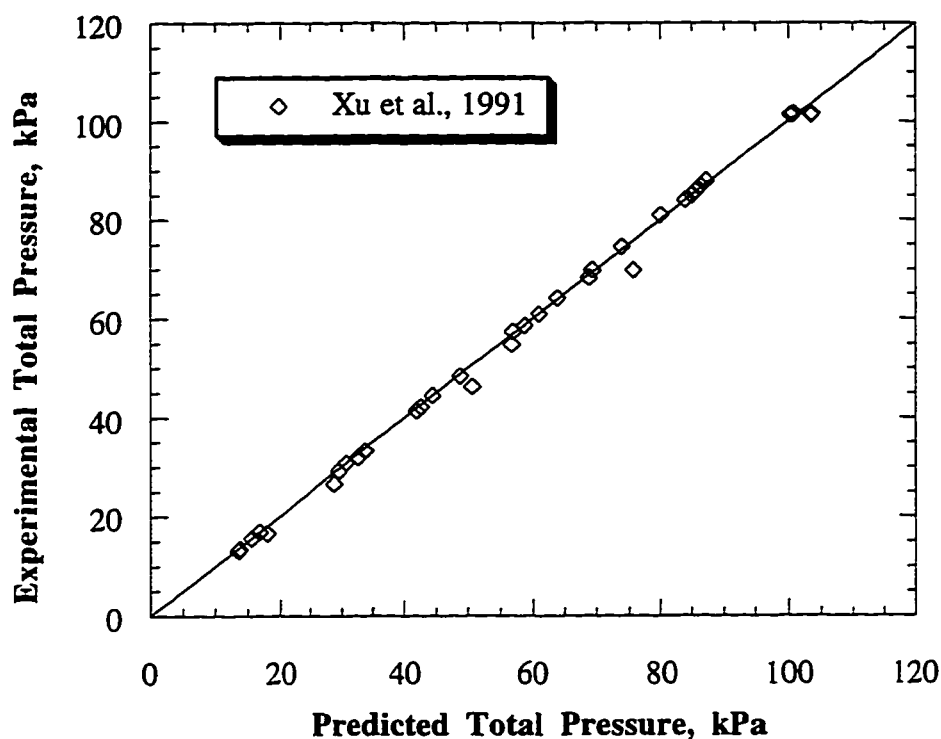
Figure 3.16 Comparison of model predictions to experimentally measured solution total pressure data for the MDEA-H_2O system at various temperatures and MDEA concentrations.

3.5.3 DEA-H_2O

For DEA-H_2O we chose to regress only the Texaco total pressure data with freezing point and heat of mixing data. However, with the parameters obtained we have predicted the remaining three total pressure data sets given in Table 3.4. The Kennard and Sandall data were excluded because they are not at a high enough mole fraction to deviate significantly from Raoult's law. The Dow data was not included because it was read from a graph and the high mole fraction, high temperature pressure data is significantly higher than the Texaco

data. Table 3.8 gives the resulting parameters and Table 3.10 gives the parameter correlation matrix.

Table 3.10. DEA-H$_2$O parameter correlation matrix

	A H$_2$O-DEA	B H$_2$O-DEA	A DEA-H$_2$O	B DEA-H$_2$O
A H$_2$O-DEA	1.000			
B H$_2$O-DEA	-0.950	1.000		
A DEA-H$_2$O	-0.861	0.755	1.000	
B DEA-H$_2$O	0.898	-0.915	-0.885	1.000

Figure 3.17 shows the fit of the Texaco data. The temperature dependence of the data differs from the temperature dependence imposed by the heat of mixing data which caused a consistent overprediction of the Texaco data. Figure 3.18 shows the predicted fits of the remaining data sets. The Sandall data is predicted within 10% except for a few outliers and the Kennard data is fit within approximately 10%. The Dow data is underpredicted by as much as 20% at high mole fractions due to its inconsistency with the Texaco data . The freezing point data is fit well as shown in figure 3.19.
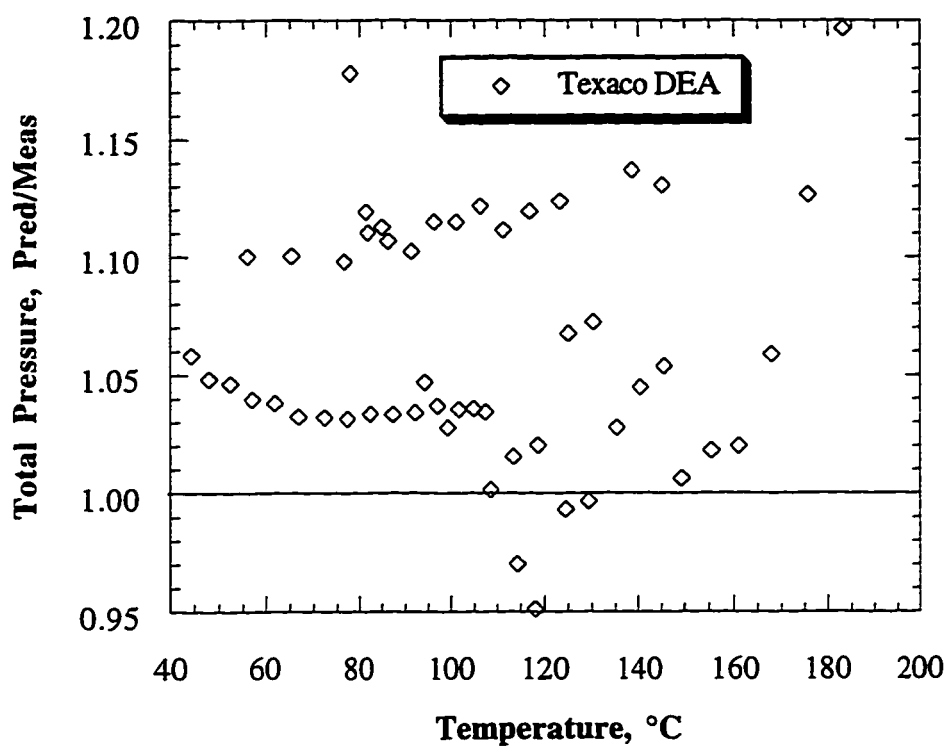
Figure 3.17. Ratio of predicted and measured total solution vapor pressure versus
temperature for the Texaco data from the regression of the NRTL
model for the DEA-H$_2$O system.
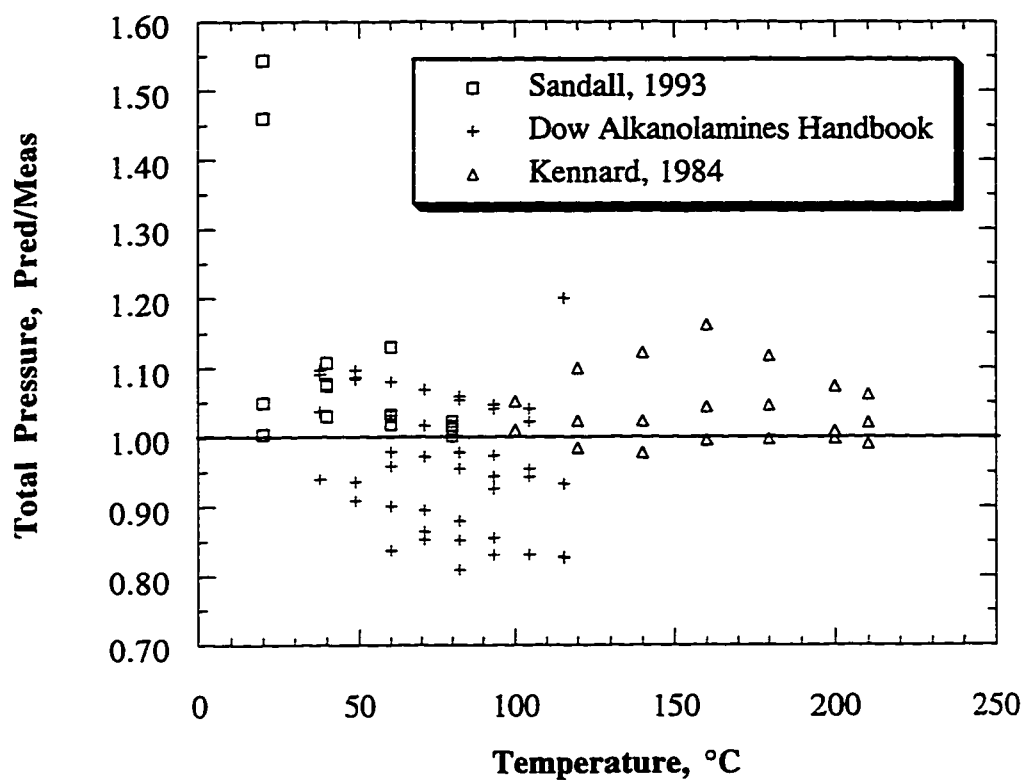
Figure 3.18. Ratio of predicted and measured solution total vapor pressure. These data sets were not included in the regression of the binary DEA-H$_2$O system, therefore this plot is a true prediction.

65
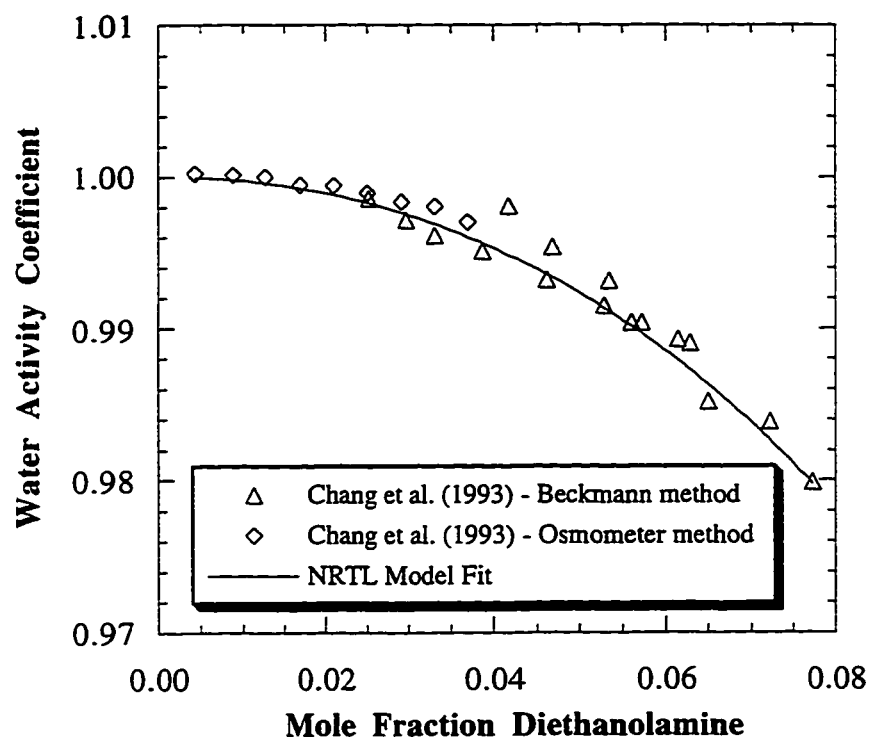
Figure 3.19. Experimental freezing point data for the DEA-H$_2$O system, given as water activity coefficient, is shown compared to its prediction from the NRTL regression.

Figures 3.20 and 3.21 illustrate the predictions of the model for the binary DEA-H$_2$O system at 40°C, 70°C and 120°C for activity coefficients and excess Gibbs energy, respectively. Figure 3.22 gives the activity coefficient of DEA by the asymmetric convention. Note the moderate temperature dependence of the activity coefficient at industrial compositions.
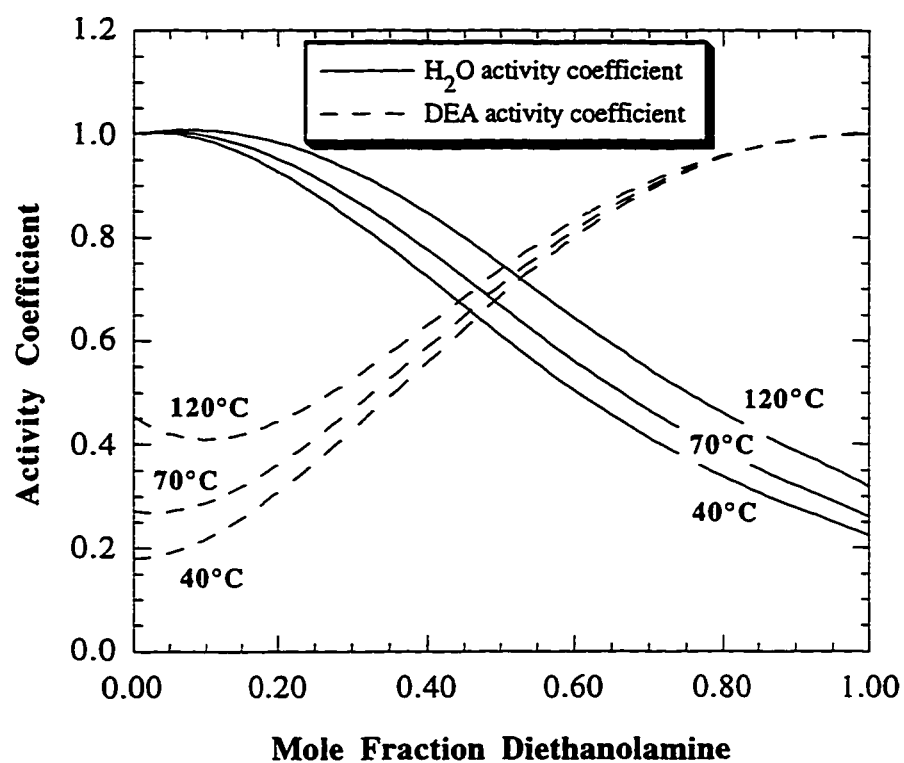
Figure 3.20. NRTL model predictions of water and diethanolamine activity coefficients at 40°C, 70°C and 120°C over the entire mole fraction range using the symmetric convention of activity coefficients.
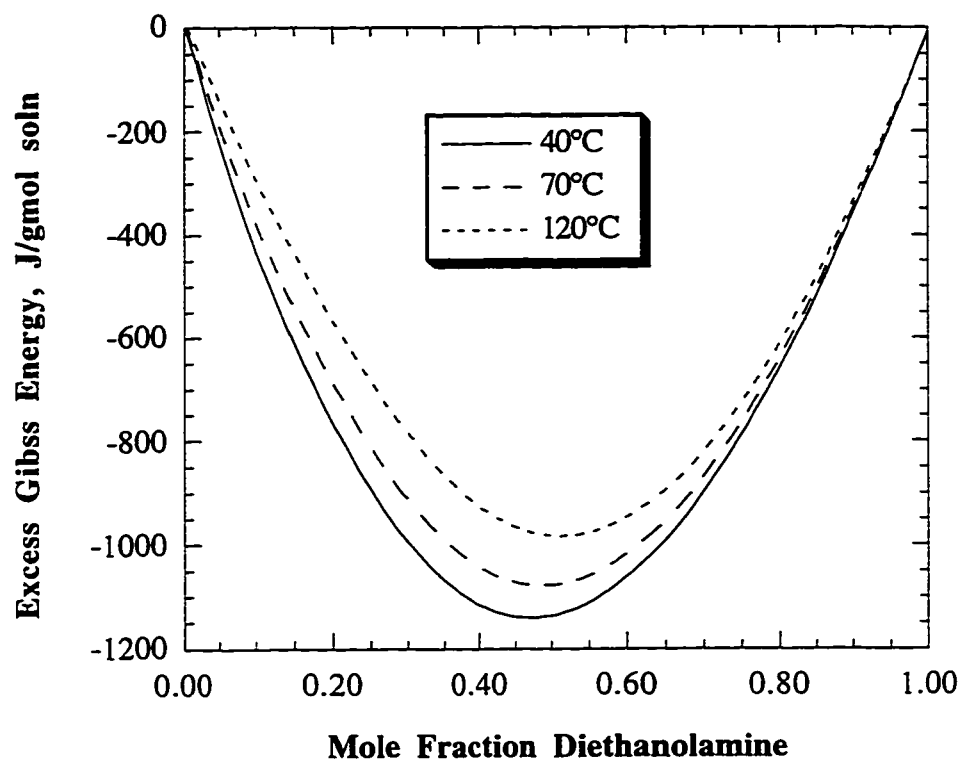
Figure 3.21. NRTL model predictions of excess Gibbs energy for DEA-H$_2$O mixtures at 40°C, 70°C and 120°C.
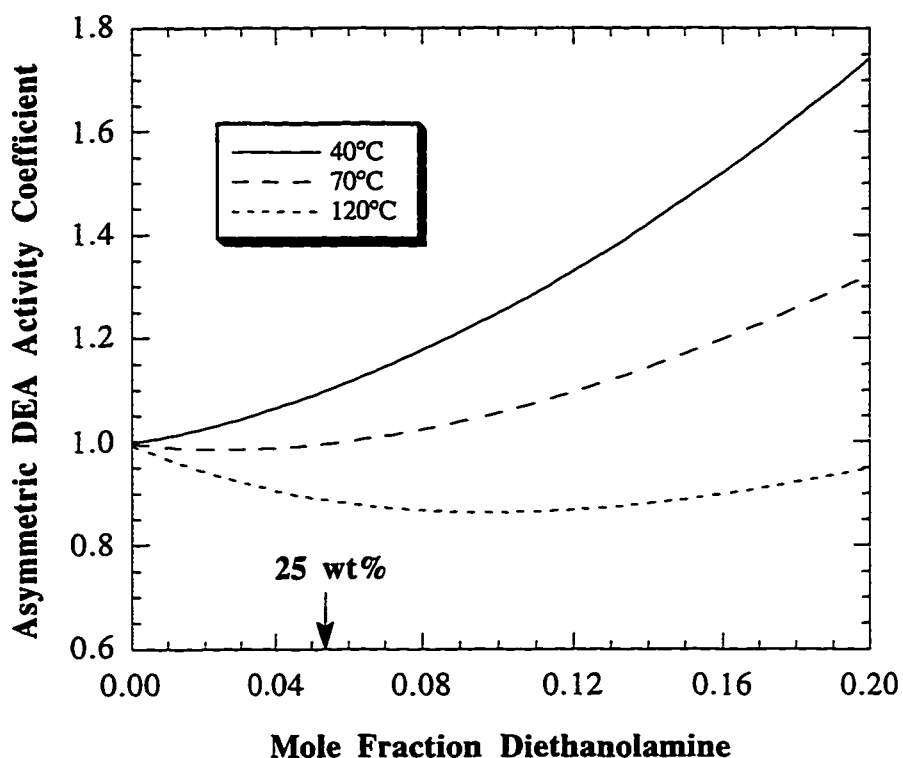
Figure 3.22. NRTL model predictions of DEA activity coefficient at 40°C, 70°C and 120°C by the asymmetric convention.

3.5.4 MDEA-DEA-H₂O

The Sandall (1993) data is the only set we have for total pressure of mixed amines. Figure 3.23 shows the prediction of this data using the previously found binary parameters from Table 3.8. and setting the MDEA-DEA parameters to zero. Notice that the 20°C and 40°C data are overpredicted just as occurred for the DEA-H$_2$O system. A regression of this data set using the MDEA-DEA parameters did not improve the predictions enough to warrant inclusion of these parameters to the model. This finding is reasonable since we did not expect any

significant interactions of MDEA with DEA. In general, with adequate binary amine-water parameters the behavior of amine1-amine2-water systems can be well predicted with the amine1-amine2 parameters set to zero.
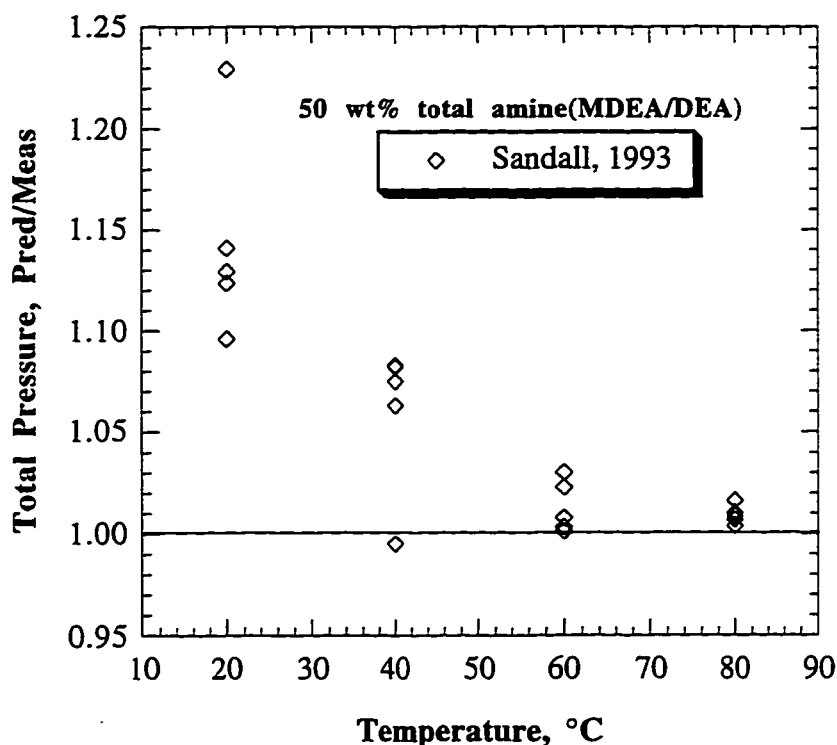
Figure 3.23. Predicted divided by measured solution total vapor pressure of 50 wt% total amine concentration in water with DEA/MDEA molar ratios of 1/20, 1/4, 1/2 and 2/3. This data was predicted from binary parameters with the MDEA-DEA parameters set to zero.

3.5.5 Infinitely Dilute Amine Activity Coefficient

Equilibrium constants are usually given in the literature with the convention that all activity coefficients go to one as the concentration goes to zero. To convert to the symmetric convention for activity coefficients, the

70

infinitely dilute amine activity coefficient is needed. Using the NRTL model parameters, we calculated the infinitely dilute amine activity coefficients and converted them into the common temperature dependent form used for equilibrium constants in Table 3.11.

Table 3.11. Equations for infinitely dilute amine activity coefficients

	A	B	C	D
MEA	147.7	-6295	-23.75	0.0255
DEA	58.45	-3505	-9.03	$9.37*10^{-3}$
MDEA	9.30	-2394	-0.50	$5.00*10^{-4}$

$$\ln \gamma^{\infty}_{amine} = A + B/T + C*\ln(T) + D*T$$

3.6 CONCLUSIONS

Accurate measurements for the heat of mixing of pure amines into 0.1N NaOH for MDEA, DEA and MEA have been made. The magnitude of the heat of mixing is significant for all three amines. The change in the heat of mixing with temperature is greatest for MDEA and MEA with the DEA heat of mixing changing only slightly from 25°C to 70°C. Therefore, temperature extrapolations of amine-water behavior without the use of heat of mixing data can lead to serious errors. Extrapolations beyond the range of the heat of mixing data will be most accurate for DEA due to its consistent temperature dependence and would be least accurate for MDEA, but the extrapolations are much better than if this data was not utilized at all.

The conclusion to be drawn on total pressure data is that there is not enough data available in the open literature. More data is needed for MDEA and DEA at all temperatures with an emphasis on high accuracy at high amine mole

fractions where modeling is the most sensitive. Some of the data regressed in this work was not intended to be used for amine-water modeling. The accuracy of the freezing point data and heat of mixing data is sufficient for amine water modeling, but it would be useful to have heat of mixing data at more temperatures.

An analysis has been made on the effect of different types of data on the ability of the Nonrandom Two-Liquid model to make accurate predictions. It has been shown that simply having total pressure data over the temperature range of interest will not produce the proper temperature dependence of the system over that same range. In addition, temperature extrapolation of a model based only upon total pressure data can lead to serious errors. Having accurate amine activity coefficients is important for the estimation of amine losses from absorber columns.

By using other types of data such as freezing point depression and heat of mixing data, excess Gibbs energy activity coefficient models that contain temperature dependence can be significantly improved. The fit of the data will be just as good, the model parameters will be known with more confidence, and the temperature dependence of the model will be improved.

Chapter 4: Simple Vapor-Liquid Equilibrium Model

Any equilibrium model for alkanolamine-acid gas systems will have to be based, at least in part, on vapor-liquid equilibria (VLE) data. Collection of accurate VLE data, especially at low loading, is not a trivial task. It requires vapor concentration measurements in the ppm range and liquid analyses of dissolved gases which can easily escape the system. Given the above, it is easy for two experimenters to reach different results. Literature data has been collected over various ranges of temperature, amine concentration and acid gas loading leaving no possibility for direct comparisons between data sources. In order to determine which data sets agree and which data sets or points are far from the norm, a simple model was constructed. This model allows a two-dimensional preview of the data sets with a minimal expenditure of computation time. Based on this work we were able to discard a few data sets that were far from the norm.

Although the model was created for comparing data sets, it is quite accurate and ideal for quick calculations. The model form is based on solution thermodynamic theory, but is a direct expression which does not require the solution of a set of equations. The model form can easily be entered into a handheld calculator or spreadsheet program. This model is useful for laboratory calculations, rough design calculations, and estimates of acid gas partial pressures in the field.

73

4.1 MODEL DEVELOPMENT

The reaction of acid gases with alkanolamines can frequently be approximated by a single equilibrium expression, equation 4.1 or 4.2.

$$AmineH^+ + HCO_3^- \Leftrightarrow Amine + CO_2 \text{ (aq)} + H_2O \tag{4.1}$$

$$AmineH^+ + HS^- \Leftrightarrow Amine + H_2S \text{ (aq)} \tag{4.2}$$
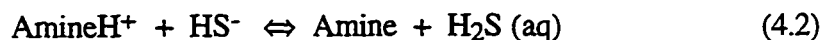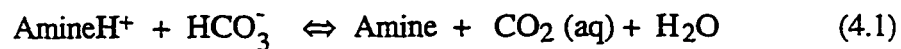
These two expressions neglect the presence of carbamate, carbonate $(CO_3^=)$, sulfide $(S^=)$, and hydroxide (OH^-) ions since their concentrations will be small. DEA is known to react directly with CO_2 to form carbamate species. Therefore, there are actually two important equilibria in the DEA-CO_2 system. To keep the model simple, the single equilibria in equation 4.1 is also assumed for the DEA-CO_2 system. The validity of this assumption is addressed later.

From equation 4.1, the equilibrium constant can be written as follows with concentrations in mole fractions. Activity coefficients are assumed equal to one and the water term is omitted since its concentration does not vary significantly over the range of practical conditions.

$$K'_{CO_2} = \frac{(CO_2 \text{ (aq)}) \, (Amine)}{(HCO_3^-) \, (AmineH^+)} \tag{4.3}$$

Rearranging, we obtain equation 4.4. Notice that the direction equations 4.1 and 4.2 are written makes K'_{gas} a desorption equilibrium constant.

$$(CO_2 \text{ (aq)}) = K'_{CO_2} \frac{(HCO_3^-) \, (AmineH^+)}{(Amine)} \tag{4.4}$$

The (Amine) and (AmineH$^+$) terms can be approximated on a basis of total loading, L_T, as follows.

$$(Amine) = (1-L_T) \, X^o_{amine} \qquad (4.5)$$

$$(AmineH^+) = (L_T) \, X^o_{amine} \qquad (4.6)$$

Where X^o_{amine} is the amine mole fraction concentration neglecting the presence of the acid gases. Equation 4.7 can be formed by combining 4.4, 4.5 and 4.6.

$$(CO_2 \, (aq)) = K'_{CO_2} \, (HCO_3^-) \, \frac{L_T}{(1-L_T)} \qquad (4.7)$$

Henry's Law can be expressed as:

$$(CO_2 \, (aq)) = \frac{P_{CO_2}}{H_{CO_2}} \qquad (4.8)$$

Substituting equation 4.8 into equation 4.7, we obtain equation 4.9.

$$P_{CO_2} = K'_{CO_2} \, H_{CO_2} \, (HCO_3^-) \, \frac{L_T}{(1-L_T)} \qquad (4.9)$$

We then combine K'_{CO_2} and H_{CO_2} into a single constant, K_{CO_2}. We assume that the bicarbonate mole fraction, (HCO_3^-), accounts for all forms of the absorbed CO_2 and replace its symbol with X_{CO_2} to get the simple model form given in equation 4.10.

$$P_{CO_2} = K_{CO_2} \, X_{CO_2} \, \frac{L_T}{(1-L_T)} \qquad (4.10)$$

The equilibrium constant, K_{CO_2}, in equation 4.10 is a function of temperature, acid gas loading and amine concentration as given below in equation 4.11.

$$\ln K_{CO_2} = A + \frac{B}{T} + C\, L_T\, X^o_{amine} + D\, (L_T\, X^o_{amine})^{0.5} \qquad (4.11)$$

Where:

P_{CO_2} = Acid gas partial pressure, kPa

X_{CO_2} = Acid gas liquid mole fraction = $\dfrac{CO_2}{Amine+H_2O+H_2S+CO_2}$

K_{CO_2} = Equilibrium constant for CO_2, kPa, defined above

L_T = Total Loading = $\dfrac{mole\ H_2S + mole\ CO_2}{mole\ Amine}$

T = Temperature, Kelvin

X^o_{amine} = gas free amine mole fraction = $\dfrac{Amine}{Amine + H_2O}$

Coefficients A and B in equation 4.11 represent the standard temperature dependence for reaction equilibrium constants. The total loading terms in equation 4.11 approximate an ionic strength dependence suggested by Astarita et al. (1983). The 1-L_T term serves to account for the reduced gas absorption capacity of the solution as the loading increases. This is the term where mixed acid gas systems are taken into account. For example, as H_2S loading increases, L_T increases which would in turn increase the CO_2 partial pressure. The mole fraction of the acid gas, X_{gas}, accounts for the specific acid gas loading and the amine concentration.

Derivation of the H_2S system is identical and H_2S predictions are made by replacing the CO_2 subscripts in equations 4.10 and 4.11 with H_2S subscripts. Table 4.1 gives the regressed parameters for CO_2 and H_2S to be used with equations 4.10 and 4.11.

Table 4.1. Regressed parameters for the acid gas equilibrium constants

	A	B	C	D
MDEA-H₂S	24.97 ± 0.64	-5554 ± 207	-16.8 ± 7.0	-1.8 ± 2.1
MDEA-CO₂	32.45 ± 0.43	-7440 ± 146	33 ± 5	-18.5 ± 1.6
DEA-H₂S	21.54 ± 0.92	-4452 ± 314	11.84 ± 11.2	-8.25 ± 3.6
DEA-CO₂	23.18 ± 0.7	-5267 ± 210	9.17 ± 11.6	-1.55 ± 3.95

$$*\mathrm{Ln}\ K_{gas} = A + B/T + C\ L_T\ X_{amine}^{\circ} + D\ (L_T\ X_{amine}^{\circ})^{0.5}$$

4.2 DATA REGRESSION METHOD

Experimental values of the equilibrium constants, K_{H_2S} and K_{CO_2}, were calculated for each experimental data point from equation 4.12.

$$\ln (K_{CO_2,exp.}) = \ln \left(\frac{P_{CO_2}exp.\ (1-L_T)}{X_{CO_2}\ L_T} \right) \qquad (4.12)$$

The natural logarithm of the equilibrium constant was then fit by linear regression using equation 4.11. By fitting the parameters to ln K_{CO_2}, rather than to P_{CO_2}, we avoid the problem of having high pressure data weighted more heavily than low pressure data. The four parameters for each acid gas were regressed separately using equilibrium data for the specific acid gas, including mixed acid gas data. The resulting parameters and 95% univariate confidence intervals for the regressions are given in Table 4.1. The parameters are more accurate than implied by the confidence intervals because of the correlation between them. The parameters have already been rounded off to an acceptable accuracy level and additional rounding will introduce error into the model predictions.

77

4.3 MDEA-H₂S

For the MDEA-H_2S regression no data points were omitted, but three known data sets were not included in the regression. The 191 data points that were regressed were fit with an average absolute percent error in H_2S partial pressure of 22%. Figure 4.1 compares the experimental to calculated H_2S partial pressure for the MDEA-H_2S system. Only Jou et al. (1993b) contains mixed acid gas data and it has the greatest scatter at higher loadings. Overall, the data is fit reasonably well and the model goes through the middle of the data.

The resulting simple equilibrium model is valid for MDEA concentration between 35 and 50 wt%, temperature from 25°C to 120°C and total acid gas loading between 0.003 and 0.8. The mathematical form of the model breaks down as total loading approaches one and should not be used with a total acid gas loading above 0.8.
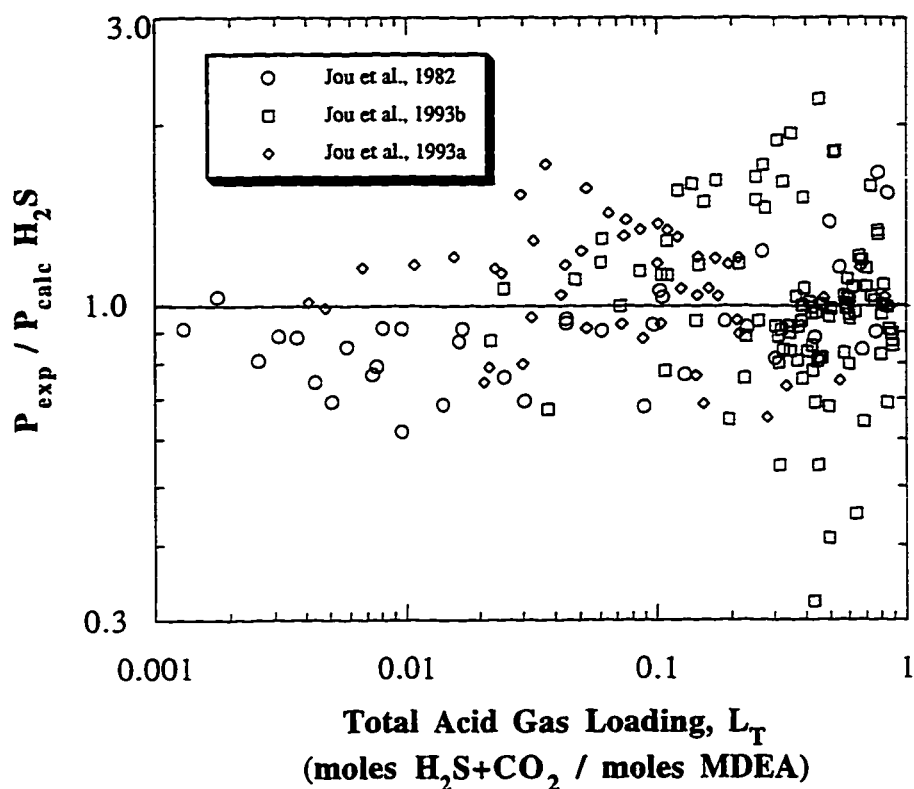
Figure 4.1. Comparative fit of experimental vapor-liquid equilibrium data to model calculated values for the MDEA-H_2S system. The data includes 25°C to 120°C, 35 wt% to 50 wt% MDEA, and 0.001 to 0.8 total acid gas loading.

Figure 4.2 compares H_2S partial pressure predictions of this model with Austgen et al. (1989). The two models generally agree down to a loading of 0.01. Agreement below this point is not expected since the model presented here was regressed on data above a loading of 0.003 and has no theoretical justification for its predictions below this point. Predictions of H_2S partial pressure by Austgen et al. (1989) below a loading of 0.01 are higher than predicted by this model.

79
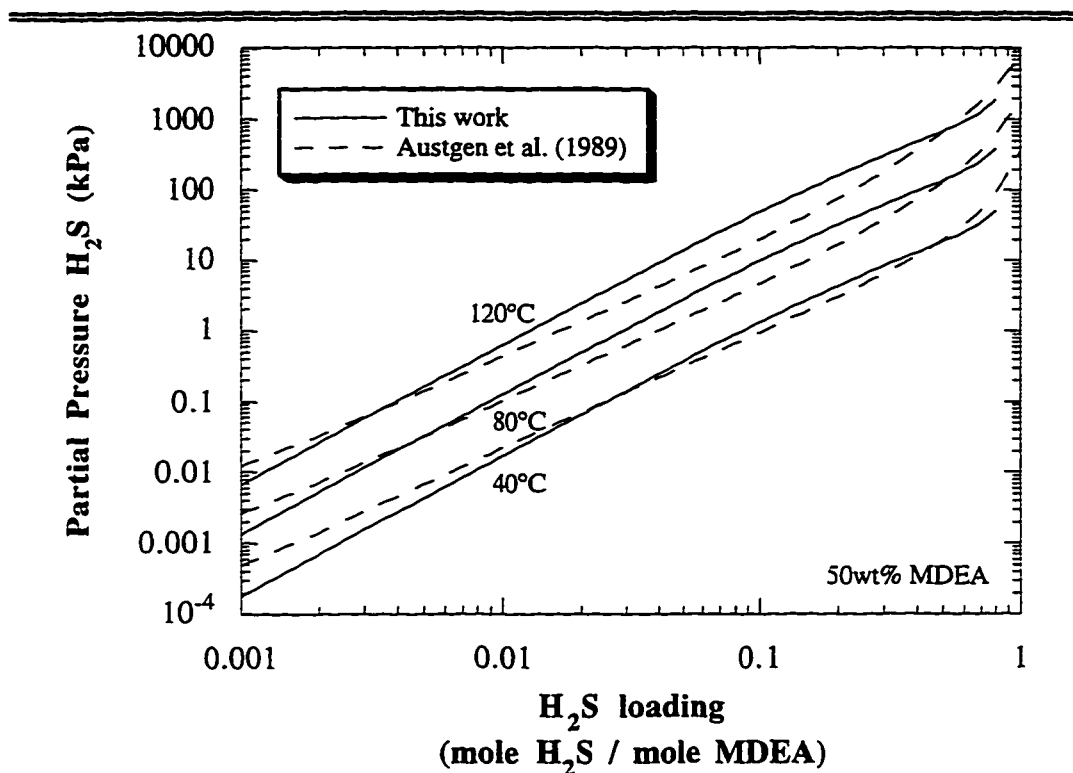
Figure 4.2. Comparison of model predicted H_2S partial pressures for 50 wt% MDEA solutions as a function of temperature and H_2S loading.

Figure 4.3 compares the model predictions to three unregressed data sets. The Li and Shen (1993) data was lower than the other data sets by as much as a factor of ten. Their data also had a significantly different loading trend and will not be included in the electrolyte-NRTL model. The Ho and Eguren (1988) data was fit satisfactorily and was included in the final electrolyte-NRTL regressions. The Huang and Ng (1995) data set was omitted from final regressions due to strong positive deviations from the norm at H_2S loadings less than 0.1.

The deviation of the Huang and Ng (1995) data at low loadings could be due to absorption of CO_2 from the atmosphere. To investigate, we used the

simple model to calculate the required CO_2 loading to make the Huang and Ng

(1995) data match model predictions. Figure 4.4 illustrates the modified Huang

data and the required CO_2 loadings for groups of data points. Huang and Ng

(1995) state that atmospheric CO_2 absorption from solution preparation is less

than 0.0002 moles CO_2/mole MDEA. Our experimental work confirms this

estimated value. So, if a CO_2 loading is the cause of the data discrepancy it

would have to be absorbed after solution preparation to obtain the loadings shown

in figure 4.4. Huang and Ng (1995) H_2S data above a loading of 0.1 were fit well

and did not require any adjustments.
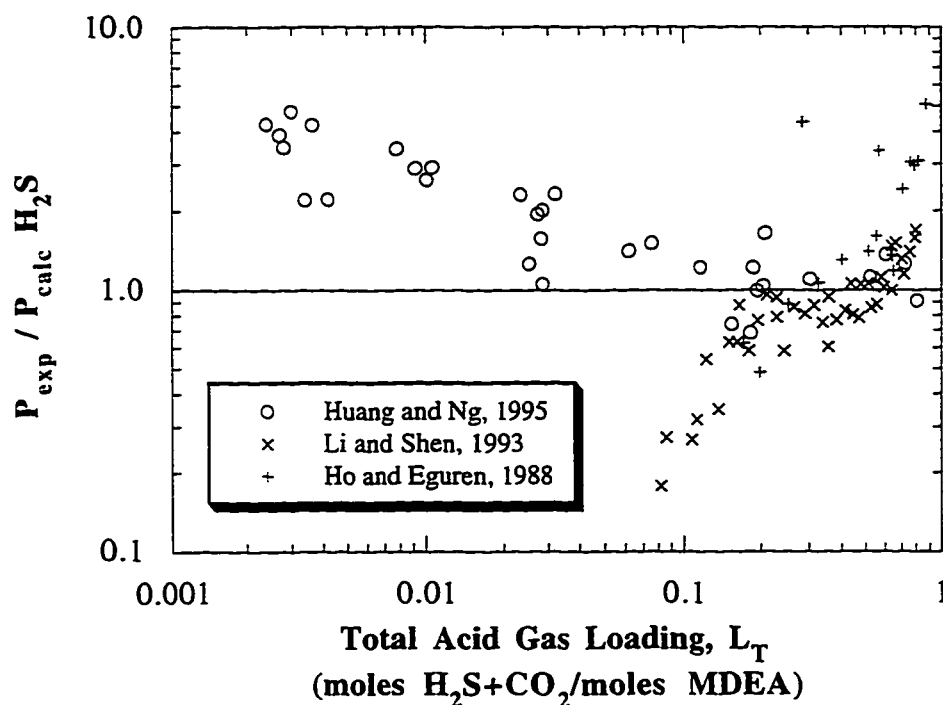
Figure 4.3. Unregressed data predictions for the MDEA-H_2S using the simple
semi-empirical model.
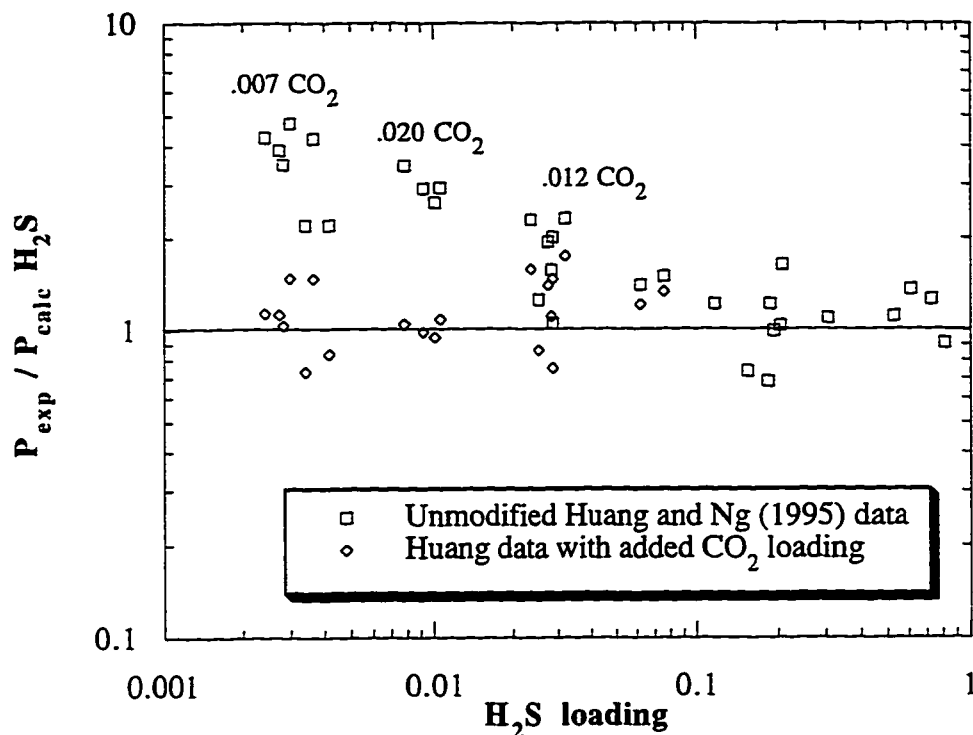
Figure 4.4 Comparison of experimental H_2S partial pressure data to the simple model predictions. The CO_2 loadings listed were applied to the groups of data below them resulting in the diamond symbols.

4.4 MDEA-CO2

The MDEA-CO_2 parameters were determined by regression of 212 data points. We excluded 23 outlying data points from the regression, approximately 10% of the total points, because the ratio of predicted and measured pressure was greater than 2.0 or less than 0.5. The average absolute percent error in CO_2 partial pressure was 20% for the MDEA-CO_2 model.

Figure 4.5 compares calculated and measured CO_2 partial pressure in the MDEA system. Only the data sets from Ho and Eguren (1988) and Jou et al.

(1993b) contain mixed gas equilibrium data. All of the data was fit within a factor of two over several orders of magnitude in loading and pressure.
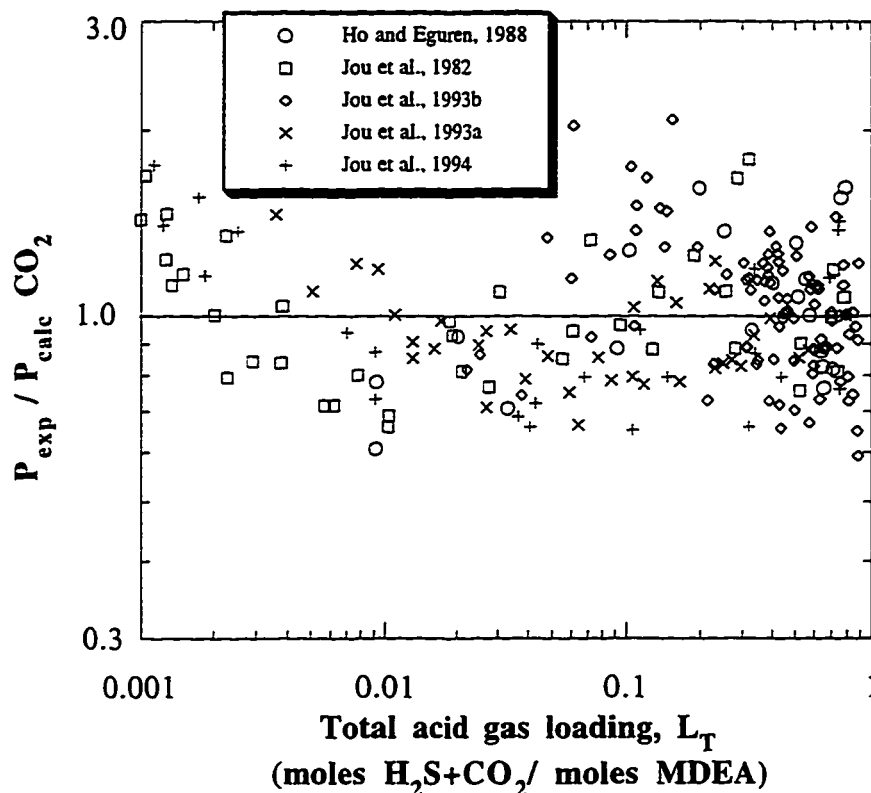
Figure 4.5. Comparative fit of experimental vapor-liquid equilibrium data to model calculated values for the $MDEA-CO_2$ system. The data includes 25°C to 120°C, 35 wt% to 50 wt% MDEA, and 0.001 to 0.8 total acid gas loading.

Figure 4.6 illustrates CO_2 partial pressure predictions by two models for a 50 wt% MDEA solution. The Austgen et al. (1989) model generally agrees with this work over the entire range of loadings and temperatures.
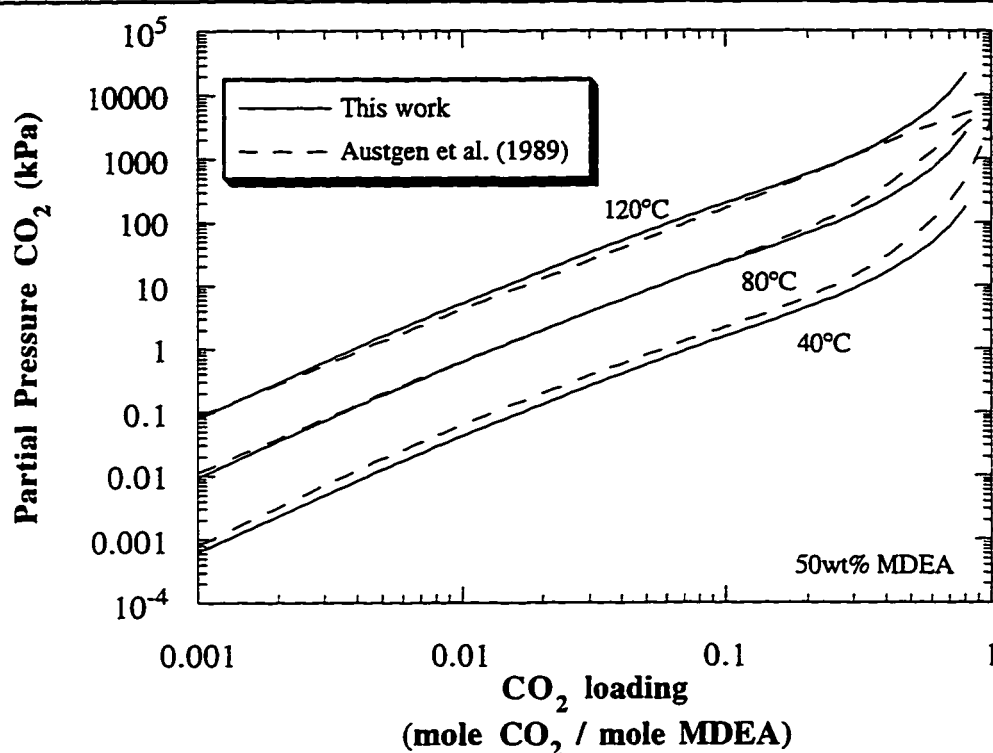
Figure 4.6. Comparison of model predicted CO_2 partial pressures for 50 wt% MDEA solutions as a function of temperature and CO_2 loading.

Figure 4.7 demonstrates the simple model predictions of unregressed data for the MDEA-CO_2 system. Data by Shen and Li (1992) is low by as much as two orders of magnitude and again has a different loading trend than the other data sets. Therefore, this data set will not be included in the final regressions of the electrolyte-NRTL model. The Huang and Ng (1995) and Austgen (1989) data compare well with the model predictions, although the model consistently underpredicts them. The data by Mshewa (1995) and Chakravarty (1992) are extracted from absorption experiments rather than from a VLE apparatus. Both of these data sets also fall consistently higher than the model predictions.
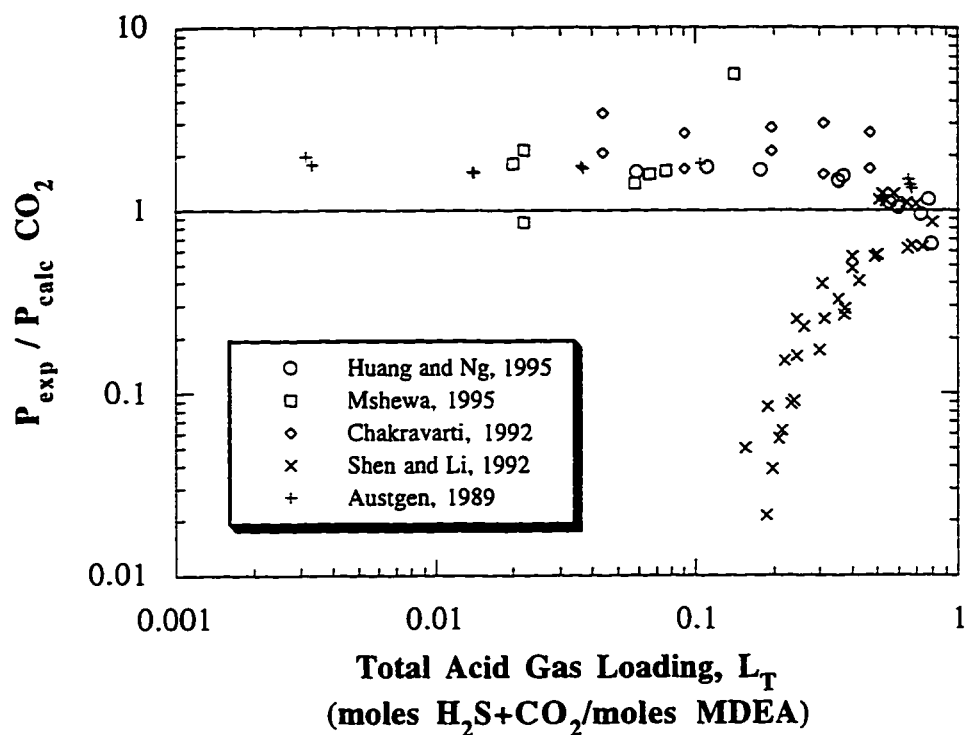
Figure 4.7. Unregressed data predictions for the MDEA-CO₂ system using the simple semi-empirical model.

4.5 DEA-H₂S

The regression of the DEA-H₂S model included 349 data points, 48 of which were mixed acid gas points from Lawson and Garst (1976). For this case, no data points were omitted. The average absolute percent error in H_2S partial pressure was 60%. This increase, as compared to MDEA-H₂S, is due to the wider range of amine concentrations and temperatures in the DEA-H₂S regression. DEA data ranged from 5 to 55 wt% DEA, 25°C to 150°C and an H_2S loading from 0.001 to 0.8.

Figure 4.8 compares calculated and measured H2S partial pressure. The model cuts through the middle of the scattered data and all of the data was fit within a factor of three. Lal et al. (1985) data fell consistently below the model predictions. The Huang and Ng (1995) data was again underpredicted at low H2S loadings similar to the MDEA system.
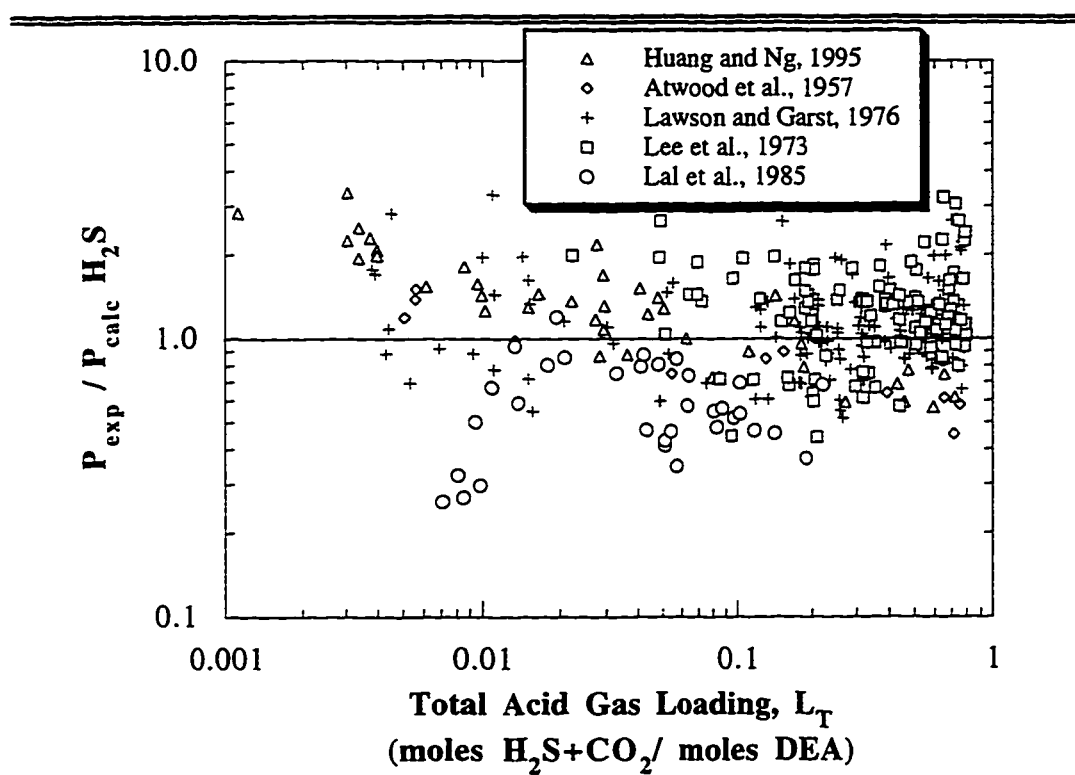
Figure 4.8. Comparative fit of experimental vapor-liquid equilibrium data to model calculated values for the DEA-H2S system. The data includes 25°C to 150°C, 5 wt% to 55 wt% DEA, and 0.001 to 0.8 total acid gas loading.

Figure 4.9 compares H2S partial pressure predictions by this work with predictions from Austgen et al. (1989). The models generally agree at 40°C and 80°C above a loading of 0.01. At 120°C, this model predicts consistently lower

86

pressures than Austgen over the entire loading range. Below 0.01, predictions by this model are lower than those by Austgen et al. (1989).
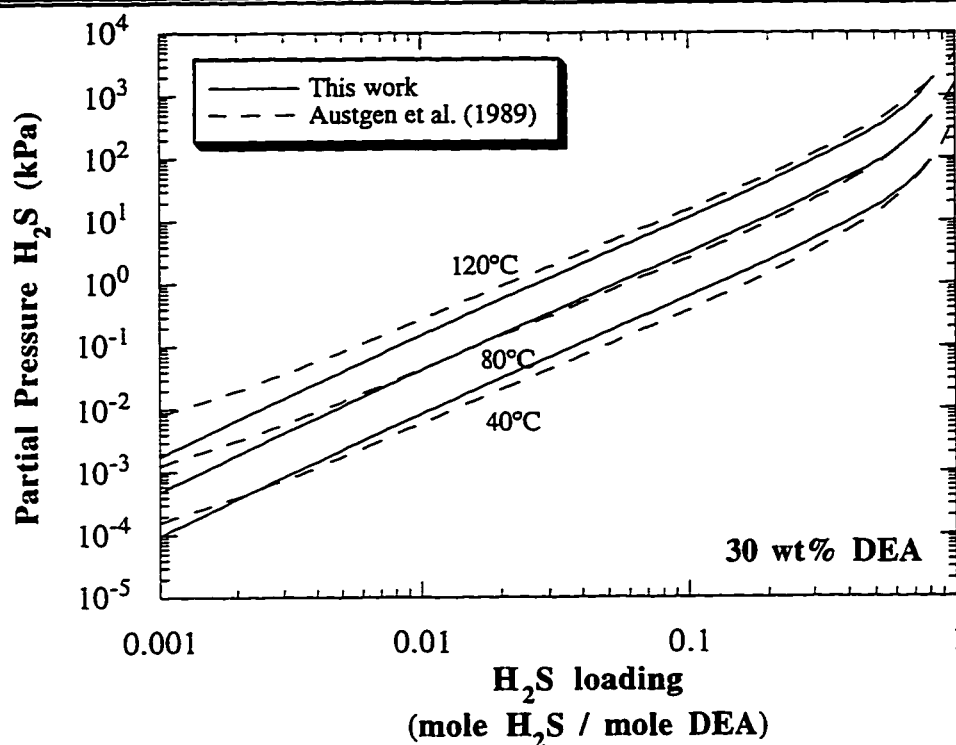
Figure 4.9. Comparison of model predicted H_2S partial pressures for 30 wt% DEA solutions as a function of temperature and H_2S loading.

4.6 DEA-CO$_2$

For the DEA-CO$_2$ system we allowed an even wider range of experimental conditions. The model was regressed for DEA concentrations between 2 and 55 wt%, temperatures from 0°C to 200°C, and acid gas loadings as high as 0.8. This data set consisted of 411 data points, some of which were mixed acid gas data. There were no data sets that were knowingly omitted from the regression, therefore no "unregressed" figures for the DEA systems are provided.

Figure 4.10 shows the fit of the DEA-CO_2 data. Recall that the model neglects the presence of $CO_3^=$ and $DEACOO^-$ and assumes a single equilibria. It is well known that in addition to the bicarbonate mechanism, DEA reacts directly with CO_2 to form a carbamate species. Thus, there are two reactions occurring between DEA and the CO_2 species. These violations of our basic assumptions, the wide range of experimental conditions, and the inherent scatter in the data explain the mediocre fit. However, most of the data is fit within a factor of 4 over many orders of magnitude in pressure.
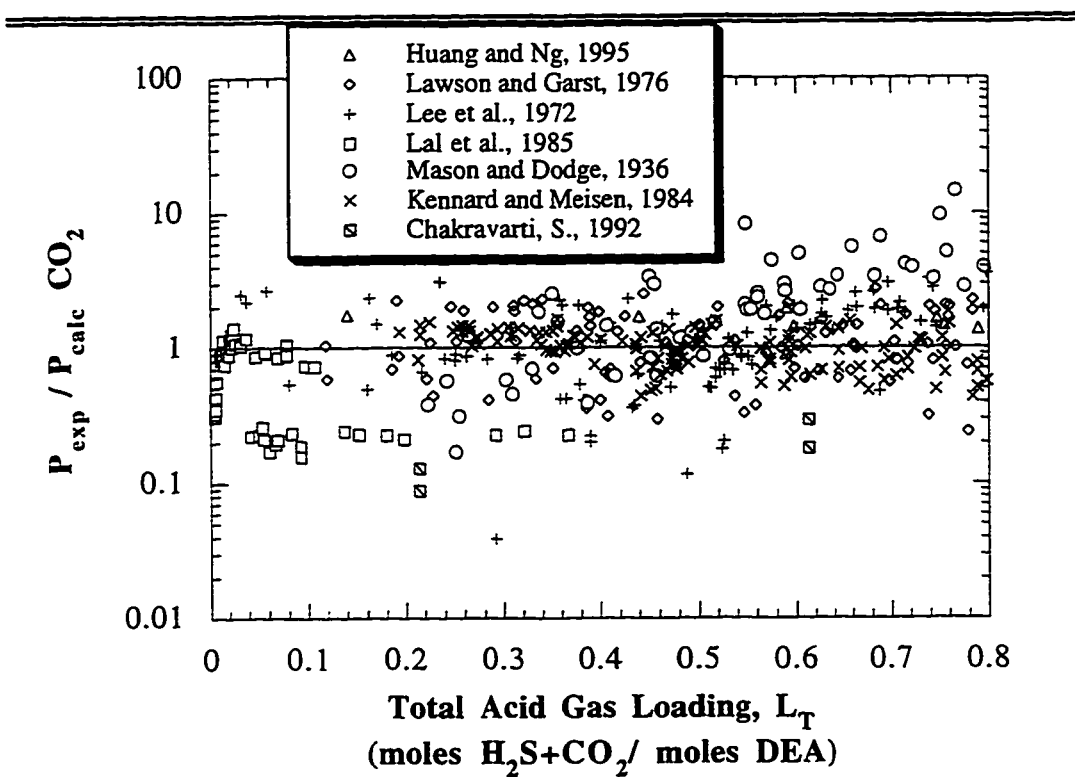
Figure 4.10. Experimental divided by calculated CO_2 partial pressure as a function of total acid gas loading. The data includes 0°C to 200°C, 2 wt% to 55 wt% DEA, and 0.0 to 0.8 total acid gas loading.

Figure 4.11 demonstrates the difference in VLE predictions between this simple model and Austgen et al. (1989). Austgen did not regress the Kennard and Meisen (1984) data which is at higher temperatures than the rest of the data sets. In hindsight, the two term temperature dependence of the simple model is too limiting to fit the very large temperature range from 0°C to 200°C. The two models compare well at 80°C, but the simple model greatly overpredicts at 40°C and underpredicts at 120°C. Regression of a more limited data set below 120°C, or adding another temperature parameter would improve the DEA-CO_2 predictions.
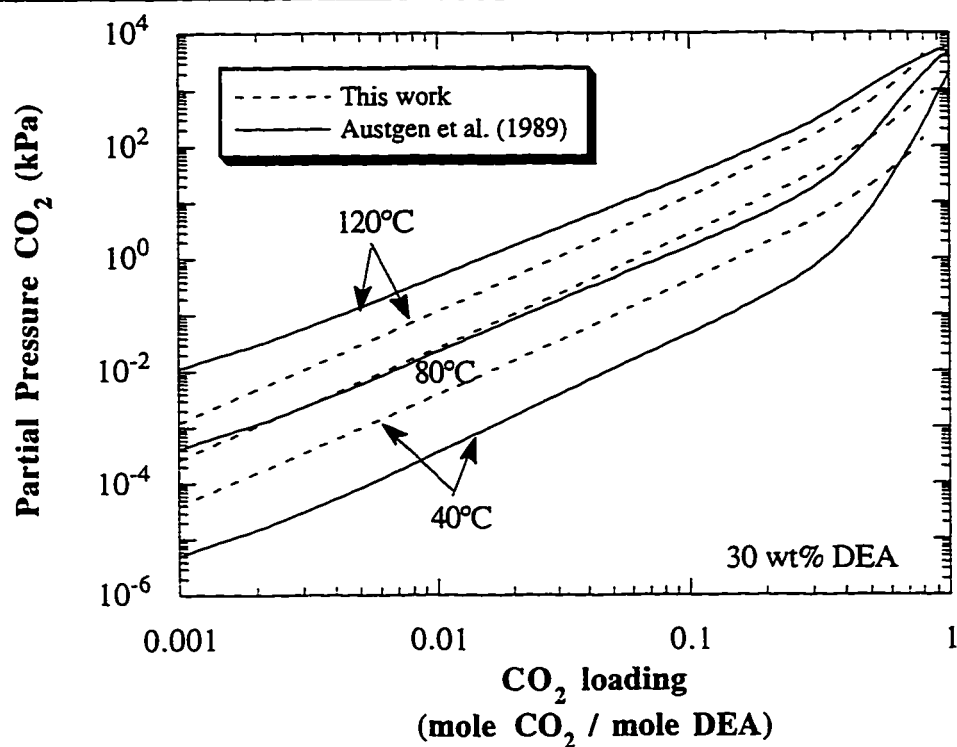
Figure 4.11. Comparison of model predicted CO_2 partial pressures for 30 wt% DEA solutions as a function of temperature and CO_2 loading.

89

4.7 HEAT OF ABSORPTION PREDICTIONS

An alternate method of verifying the model is to use it to calculate heat of absorption. The parameter "B" in equation 4.11 is directly related to the heat of absorption (ΔH_{abs}) of CO_2 and H_2S. From thermodynamics, Prausnitz et al. (1986), we obtain the relationship between the temperature dependence of the equilibrium constant and the heat of reaction given in equation 4.13.

$$\frac{d \ln K_{des}}{d \frac{1}{T}} = - \frac{\Delta H_{des}}{R} \qquad (4.13)$$

We can take the derivative of equation 4.11 and equating it to equation 4.13 we arrive at equation 4.14.

$$\Delta H_{des} = - BR \qquad (4.14)$$

In order to compare to literature values, we have written ΔH in terms of absorption.

$$\Delta H_{abs} = BR \qquad (4.15)$$

The calculated values of heat of absorption are given in Table 4.2 and correspond to the average experimental conditions of the data. The average MDEA-CO_2 data conditions are 38.4 wt% MDEA, 0.31 total acid gas loading and a temperature of 56.8°C. For MDEA-H_2S the averages are 38.8 wt% MDEA, 0.31 total acid gas loading and a temperature of 51.6°C. The average conditions for DEA-H_2S are 29.1 wt% DEA, 0.27 total acid gas loading and a temperature of 75.5°C. The average conditions for DEA-CO_2 are 26.5 wt% DEA, 0.43 total acid gas loading and a temperature of 94.4°C.

90

DEA heats of absorption are known to generally be higher than for MDEA. However, they are shown by our model to be lower than MDEA. This is due to averaging of the heat of absorption over a wide range of temperature and DEA concentration. Therefore, the numbers predicted by our model can only be compared to values obtained at the same average experimental conditions. Another reason for the low heat of absorption value calculated for DEA-CO_2 is the large temperature range and the model requirement that heat of absorption be constant.

Merkley et al. (1987) and Oscarson et al. (1989b, 1990, 1995) report experimentally measured heats of absorption. These references provide simple equations relating ΔH_{abs} to temperature and amine concentration which were used to calculate ΔH_{abs} at our average experimental data conditions. All of these references exhibited as much as ±10% scatter in their data. Jou et al. (1982, 1994) and Lee et al. (1973) predict ΔH_{abs} by modeling of experimental vapor-liquid equilibrium data. The predictions of Jou et al. (1982) and Lee et al. (1973) had to be interpolated to our average conditions. Table 4.2 shows that our predictions compare reasonably well with the experimental data and other model predictions considering the accuracy of the data and the error introduced in using average experimental conditions.

Table 4.2. Heat of Acid Gas Absorption

Author	Conditions	Heat of Absorption (kJ/gmol gas)			
		MDEA-CO_2	MDEA-H_2S	DEA-CO_2	DEA-H_2S
This model		-61.9	-46.2	-43.8	-37.0
Jou et al., 1982	~38wt%, L_T=0.3	-57.6	-40.7		
Jou et al., 1994	30wt%, L_T=0.3	-60			
Merkley et al., 1987	~38wt%, L_T=0.3	-53.4			
Oscarson et al. 1990	~38wt%, L_T=0.3		-36.5		
Oscarson et al. 1989b	~29wt%, 77°C				-43.6
Lee et al., 1973	~28wt%, L_T=0.27				-46
Oscarson et al. 1995	~26wt%,L_T=0.4,94°C			-77	

4.8 POSSIBLE MODEL IMPROVEMENTS

The temperature dependence of the model given in equation 4.11 is too simplistic, especially for DEA. A third temperature term of the form T or ln T would greatly improve regressions over wide temperature ranges. Equation 4.11 could become one of the following equations:

$$\ln K_{CO_2} = A + \frac{B}{T} + C T + D L_T X^o_{amine} + E (L_T X^o_{amine})^{0.5} \qquad (4.16)$$

$$\ln K_{CO_2} = A + \frac{B}{T} + C \ln T + D L_T X^o_{amine} + E (L_T X^o_{amine})^{0.5} \qquad (4.17)$$

This would allow a much better fit of the DEA data which covered a temperature range of 200°C. The model could also be modified in some way to be consistent with the DEA-CO_2 system. For DEA-CO_2, two moles of amine are reacted for every mole of CO_2 absorbed at loadings below 0.5. The current model assumes

one mole of amine reacts with one mole of acid gas. A final enhancement would be the ability to calculate partial pressures in mixed alkanolamine systems.

4.9 CONCLUSIONS

A simple model has been developed for predicting the solubility of hydrogen sulfide and carbon dioxide in aqueous alkanolamine solutions. The model uses four parameters for each acid gas that are regressed from experimental data. This model is valid over wide ranges of amine concentrations, temperatures, and acid gas loadings and can be used for mixed acid gas systems. All of the data regressed for the MDEA system, which includes mixed acid gas data, was predicted with an average absolute percent deviation (AAPD) of 20% for CO_2 and 22% for H_2S over seven orders of magnitude in pressure. The DEA model predicts the partial pressure data with an AAPD of 60% and 77% in H_2S and CO_2, respectively, also over seven orders of magnitude.

From theory, we have related model parameters to the heat of absorption of acid gases. The heat of absorption values calculated from the model are consistent with experimental data and predictions by other models. We have also shown that partial pressure predictions by this model agree with those of much more complicated models over many orders of magnitude in pressure.

Although originally created as a tool for comparing data sets, the model presented here is also useful for quick desktop calculations. It can be used for checking the consistency of experimental data and as a good initial guess for more complex equilibrium calculations. It represents an improvement over the Kent and Eisenberg (1976) model in that it does not require the solution of a set of

equations. Because of this simplicity, the current model can be easily implemented in a spreadsheet program or entered into a handheld calculator. The model structure is general and can be applied to other simple alkanolamine systems.

Chapter 5: Electrolyte Nonrandom Two-Liquid Model

In this chapter all of the details of the electrolyte-NRTL model are given. In that sense, this chapter serves to document the constants and equations used in this work. The first section discusses the basic properties of the amines, ions and water. Relationships that were used to calculate density, volume, heat capacity, dielectric constant, etc. are provided and discussed. Antoine equations have been previously discussed in section 3.4.1 of Chapter 3 and are not repeated here. In addition, improvements and detailed analyses on the equilibrium and Henry's constants are given. Plots comparing experimental data to model equations are given for Henry's constants and equilibrium constants.

Discussions then turn to the structure of the electrolyte-NRTL model itself. Each component of the model is discussed and additional equations and properties are introduced as they become needed. The Redlich-Kwong-Soave (Soave, 1972) model was used for vapor phase non-idealities. Details on its model form and necessary parameters are also given. The activity coefficient portion of the model contains three terms, a Debye-Hückel term, Born correction for mixed solvents and the local interactions term. Equations for each are given and details on parameters and their structure and determination are discussed. For details that might not be covered here, the reader is referred to the dissertation by Austgen (1989), the following papers: Chen et al. (1979, 1982), Chen and Evans (1986) and Mock et al. (1986) and the Aspen Plus™ User Guide for Release 9 (1994).

5.1 PHYSICAL PROPERTIES

5.1.1 Constant Properties

Before any calculations can be made the basic physical properties of the important chemical species must be known. Table 5.1 was taken from Austgen (1989) and represents the values of the basic properties that are used with Aspen Plus™. The sources that Austgen referenced are restated in this table. The critical constants are utilized in the vapor phase equation of state. Critical volumes are used to obtain the molar volume, or density, of the solution.

Table 5.1. Pure component properties for molecular species

Comp.	MW	T_c (°K)	P_c (kPa)	V_c (m³ kmol⁻¹)	Z_c	ω	Source
H_2S	34.08	373.2	8936.9	0.0986	0.284	0.100	a
CO_2	44.01	304.2	7376.5	0.0939	0.274	0.225	a
H_2O	18.02	647.3	22090.0	0.0568	0.233	0.344	b
DEA	105.14	715.0	3270.0	0.3490	0.192	1.046	b
MDEA	119.16	677.8	3876.1	0.3932	0.192	1.242	c

a - Reid et al., (1977); b - Daubert and Danner, DIPPR Data Tables (1985); c - Peng (1987)

5.1.2 Heat capacity

Although heat capacity does not directly effect calculations of VLE, we have taken the equation forms used in Aspen and recreated them here. Heat capacities are very important in simulation of full scale plants since they are needed to calculate solution temperatures and heat exchange. Since Aspen bases its calculations of liquid heat capacity on the ideal gas heat capacity and the heat of vaporization, accurate values of those variables are needed. Unfortunately, little data exist for the ideal gas heat capacity of the amines due to their low vapor pressures. Therefore, our calculations of heat capacity are slightly suspect.

Wendell Kensell (1996) of The M.W. Kellogg Company was gracious enough to compare our predictions to experimental data. Predictions from this work generally agreed with data from Dow Chemical, but were significantly lower than experimental data and curves from Union Carbide, Elf Atochem and Weiland (1996). For example, in lean 40 wt% MDEA solutions our values were 0.8 compared to 0.87 cal/g°C. The difference is larger at high loadings with this model predicting 0.67 compared to 0.79 and 0.83 cal/g°C. One explanation for the difference is that this work's predicted pure MDEA heat capacity is lower than that given by the above references. This discrepancy then propagates into prediction of heat capacity of 50 wt% MDEA aqueous solutions. The best solution to this discrepancy would be to regress experimental data to the Aspen equation forms, however that effort is not in the current scope.

Table 5.2 provides the coefficients for the ideal gas heat capacity polynomial to be used with equation 5.1. All of the values listed were taken from Austgen (1989).

$$C_p^{*\,ig} = A + B*T + C*T^2 + D*T^3 + E*T^4 + F*T^5 \qquad (5.1)$$

Table 5.2 Coefficients for temperature dependence of the ideal gas heat capacity polynomial model

Compound	A	B	C	D	E	F
MDEA	4.917E4	5.595E2	-3.134E-1	1.102E-4	0	0
MDEAH+	0.208E5	0	0	0	0	0
DEAH+	0.208E5	0	0	0	0	0
DEACOO-	0.208E5	0	0	0	0	0

Aspen data banks contain coefficients for the DIPPR ideal gas heat capacity equation. Most of the compounds will use the DIPPR equation form given as equation 5.2 below. The value for DEA was obtained from Austgen (1989).

$$C_p^{*\,ig} = A + B*\left(\frac{C/T}{\sinh(C/T)}\right)^2 + D*\left(\frac{E/T}{\cosh(E/T)}\right)^2 \tag{5.2}$$

Table 5.3 Coefficients for temperature dependence of the DIPPR ideal gas heat capacity model

Compound	A	B	C	D	E
DEA	6.89E4	4.568E5	1.85E2	8.092E-1	0

Of course there are many species that contribute to the overall solution heat capacity. Determination of the solution heat capacity is also derived from the excess heat capacity which is the derivative of the excess enthalpy.

5.1.3 Heat of Vaporization

Heat of vaporization for each chemical species is required in order to calculate liquid heat capacities using the ideal gas heat capacities. Aspen provides several model forms from which to choose. Austgen used both the Watson equation form, equation 5.3, and DIPPR equation form, equation 5.4. If parameters for both models are given for a compound, Aspen defaults to the Watson equation.

$$\Delta H_{vap,\,i}(T) = \Delta H_{vap,\,i}(T_1) * \left(\frac{1-T/T_{ci}}{1-T_1/T_{ci}}\right)^{ai+bi*(1-T/Tc)} \tag{5.3}$$

$$\Delta H_{vap,\,i} = A *(1-T_{ri})^{(B+C*T_{ri}+D*T_{ri}^2+E*T_{ri}^3)} \tag{5.4}$$

where $T_{ri} = T / T_{ci}$

Table 5.4 Watson heat of vaporization model coefficients

Component	$\Delta H_{vap} (T_1)$	T_1	a_i	b_i
MDEA	6.18132E7	293.15	0.38	0

Table 5.5 DIPPR heat of vaporization model coefficients

Component	A	B	C	D	E
DEA	1.034E8	3.33E-1	0	0	0

5.1.4 Dielectric constant

Dielectric constant is related to a compound's ability to stabilize ions. The higher the dielectric constant, the more likely it is that ions will form and remain as ionic species. Dielectric constant for pure fluids is a function of temperature only. Equations and the coefficients for this temperature dependence were taken from Austgen (1989). The coefficients for the dielectric constant of water were obtained from the Aspen data banks.

Table 5.6. Dielectric constants for DEA and MDEA as a function of temperature

DEA:	$D = 28.01 + 9277.0 \, [1/T - 1/273.15]$
MDEA:	$D = 24.76 + 8989.31 \, [1/T - 1/273.15]$

Since we have a mixed solvent, the mixed dielectric constant must be determined. Equation 5.5 below shows the concentration weighted calculation of dielectric constant in a mixed solvent. Although a reasonable effort has been made to obtain good values for the dielectric constant, sensitivity studies have shown that variations in D do not significantly affect partial pressure predictions.

$$D_m = \sum_i x_{m_i}^{sf} D_i \qquad (5.5)$$

where $x_{m_i}^{sf}$ is the solute free, solvent mass fraction

5.1.5 Density and molar volume

As stated in Chapter 2, densities of the solutions are often needed to convert between the concentration units. For some experimental work and calculations the density of a solution had to be determined. Most often, density was experimentally measured using an accurate 250 μL syringe and an analytical balance. However, relationships have been developed by other authors relating density as a function of temperature, amine concentration and acid gas loading. Licht and Weiland (1989) have regressed an empirical equation for solution density as a function of amine concentration, temperature and acid gas loading. Weiland et al. (1994) provided a relationship for the density of MDEA, MEA and DEA as a function of amine concentration and CO_2 loading at 25°C.

In general, Aspen Plus™ does not use density relationships directly. Instead, it calculates the molar volume and inverts the number when density is required. The molar volume is calculated by the Brevli and O'Connel (1975) model. It utilizes the critical properties of the solvent and the critical volume of the Henry's component. The molar volume of the supercritical components is also required to calculate the pressure correction to the Henry's constant.

5.2 HENRY'S CONSTANT

Henry's Law constants are an important part of any equilibrium model. Without accurate constants VLE can still be predicted, however there will be error

introduced into the activity coefficients and speciation of the model. Aspen uses a volume weighted mixing rule for calculating Henry's solubility in a mixed solvent. Equations 5.6 and 5.7 demonstrate how the volume weighting is applied. If a Henry's constant for one of the solvents is not given, then w_A is renormalized and H_i is recalculated. For our calculations, Henry's solubility of the acid gases in pure alkanolamines was not provided as this data does not exist. Therefore, the constants a, b, c and d in equation 5.9 are given for the Henry's components in water only.

$$\ln\left(H_i / \gamma_i^\infty\right) = \sum_A w_A * \ln\left(H_{iA} / \gamma_{iA}^\infty\right) \tag{5.6}$$

$$w_A = \frac{x_A (V_{cA})^{2/3}}{\sum_B x_B (V_{cB})^{2/3}} \tag{5.7}$$

$$H_{iA} = H_{iA}^* \exp\left(\frac{1}{RT} \int_{p_A^*}^{p} V_{iA}^\infty \, dp\right) \tag{5.8}$$

$$\ln H_{iA}^* = a_{iA} + b_{iA}/T + c_{iA} \ln T + d_{iA} T \tag{5.9}$$

with H_{iA}^* in (Pa / mole fraction) and T in Kelvin.

5.2.1 Henry's Constant Regression

We have compiled data on the Henry's Constant for CO_2 and H_2S. For all data sets and equations we have assumed the following definition for solubility, S. At low partial pressures, the fugacity equals the partial pressure and solubility, S, is identical to Henry's Constant, H. Fugacity corrections to the partial pressure are generally not needed as long as the pressure remains below approximately 20 atmospheres.

$$S_{gas} = P_{gas} / X_{gas} \qquad\qquad (5.12)$$

where P_{gas} is the acid gas partial pressure, Pascals

X_{gas} is the liquid phase molecular acid gas mole fraction.

Henry's Law constants are strong functions of temperature and weak functions of pressure. Pressure dependence of this constant is partially due to gas phase non-idealities, fugacity, and interaction effects in solution that are pressure dependent. We have assumed S as being independent of pressure as stated above. This assumption is valid for acid gas partial pressures below 20 atm.

Solubility data from five literature sources are shown in figure 5.1. The Lee and Mather (1977) tabular data were derived from total pressure of the system instead of H_2S partial pressure, so the Raoult's Law partial pressure of water was subtracted from all of the data. We have omitted Lee and Mather (1977) data above 20 atm to prevent non-ideal effects on Henry's Constant. The vertical scatter at each temperature in their data indicate that not all of the effects are removed at pressures below 20 atm.

Most of the data in figure 5.1 agree well at low temperatures. However, near 120°C the Lee and Mather (1977) data are higher than measured by Selleck et al. (1952) and Kozintseva (1965). The curve given in the dissertation by Austgen (1989) is compared to the curve proposed by Lee and Mather (1977). Both agree at temperatures below 100°C, but the Lee and Mather curve predicts a slightly higher H_2S Henry's constant from 100°C to 180°C. The Lee and Mather curve was used in this work and its coefficients are given in Table 5.7.

Table 5.7. Temperature dependent Henry's Law constants

Units of Pascal / mole fraction	A	B	C	D
H_2S	18.1937	-2808.5	2.5629	-0.01868
Data References: Selleck et al. (1952), Kozintseva (1965), Clarke and Glew (1971), Wright and Maass (1932), Lee and Mather (1977)				
CO_2	110.034525	-6789.04	-11.4519	-0.010454
Data References: Harned and Davis (1943), Versteeg and van Swaaij (1988), Ellis (1959), Stewart and Munjal (1970), Wiebe and Gaddy (1939)				
$\ln H = A + B/T + C*\ln T + D*T$				
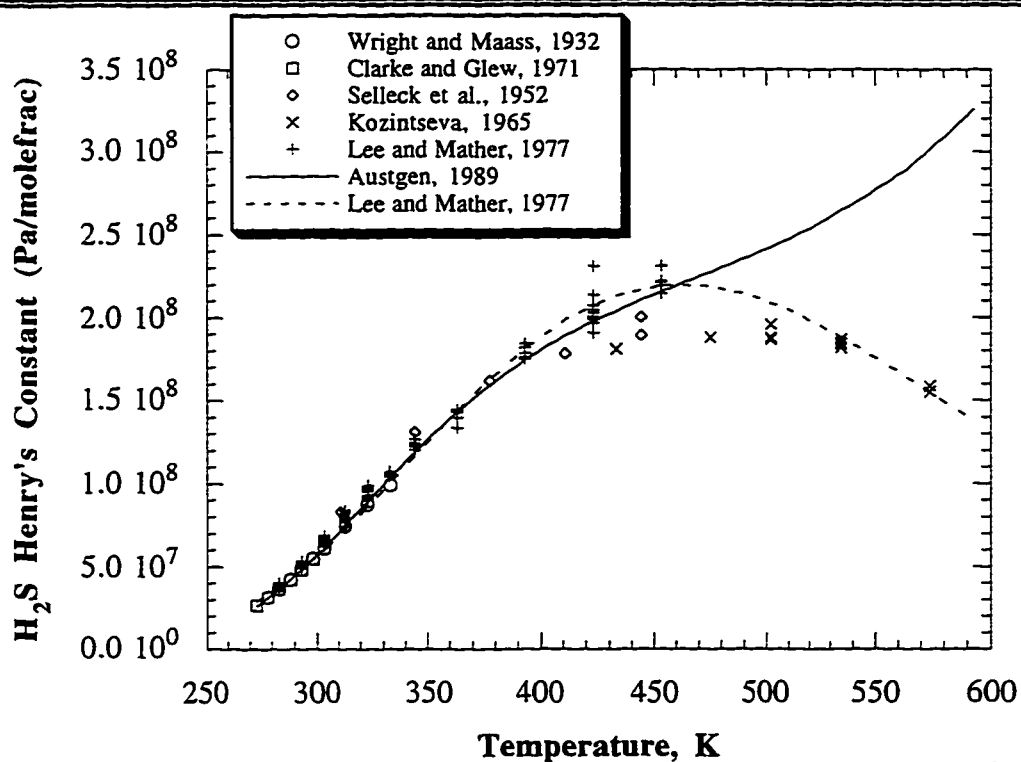
Figure 5.1 H_2S Henry's constant in water assuming ideal liquid and vapor phases.

For Henry's Law constants, more data existed for the CO_2 system compared to H_2S. The data presented for CO_2 in figure 5.2 was truncated to

partial pressures below 20 atm. Above this pressure, the gas solubility increased with pressure. Most of the Ellis (1959) CO_2 data are above this pressure limit. Note the disagreement between the Ellis (1959) data and the data by Wiebe and Gaddy (1939) and Zelvenskii (1937) at 120°C. The Ellis data is not included in the curve since it is probably non-ideal and many other data sets disagree with it. The curve by Edwards et al. (1978) fits all of the data except Ellis (1959) and has been used in this work. Its coefficients for the temperature dependence are given above in Table 5.7
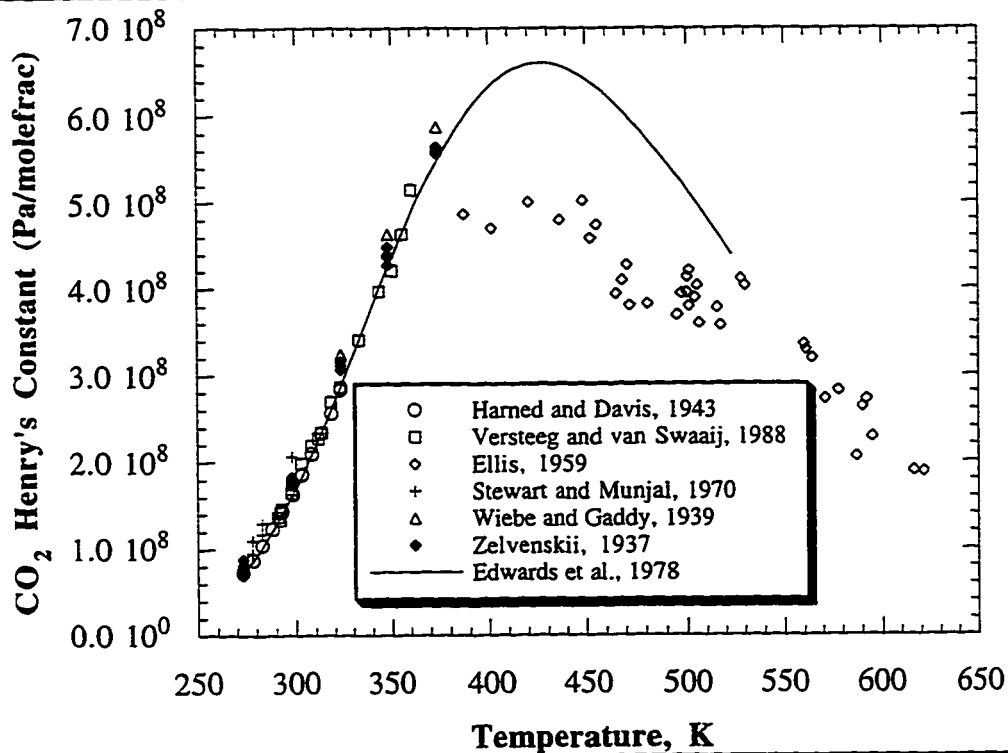
Figure 5.2 CO_2 Henry's constant assuming ideal gases, defined as CO_2 partial pressure in Pascals divided by molecular CO_2 concentration in mole fraction. Dissociation was assumed negligible.

5.2.2 Henry's Constant in Mixed Solvents

Since data for the solubility of CO_2 and H_2S in pure alkanolamines does not exist, the coefficients for this Henry's law have been assumed to be zero. Therefore, we have assumed that the Henry's constant in the mixed solvent is equivalent to its value in pure water. Physical solubility measurements in aqueous alkanolamine solutions are impossible due to immediate reaction of the molecular gas species. However, for CO_2 the solubility of non-reactive N_2O in alkanolamines can be measured. Then using the "N_2O analogy", which is based on the fact that CO_2 and N_2O have similar sizes and molecular weights, the physical solubility of CO_2 can be deduced. There is no analogous molecule to H_2S to allow a measurement of its physical solubility in alkanolamine solutions.

Figure 5.3 below shows CO_2 physical solubility as a function of MDEA concentration and temperature. The lines are calculated at an arbitrary low loading from the electrolyte-NRTL model parameters in this work. The weight percent lines cross near 40°C and follow the proper trend at higher temperatures. Solubilities as a function of amine concentration unexpectedly invert at temperatures below 40°C. In general, predicted CO_2 solubility matches the data within a factor of 1.5 and does not affect other species concentrations at low loadings. At acid gas loadings greater than 1.0, where concentrations of molecular acid gases are significant, calculated speciation and partial pressures will not be correct.

105
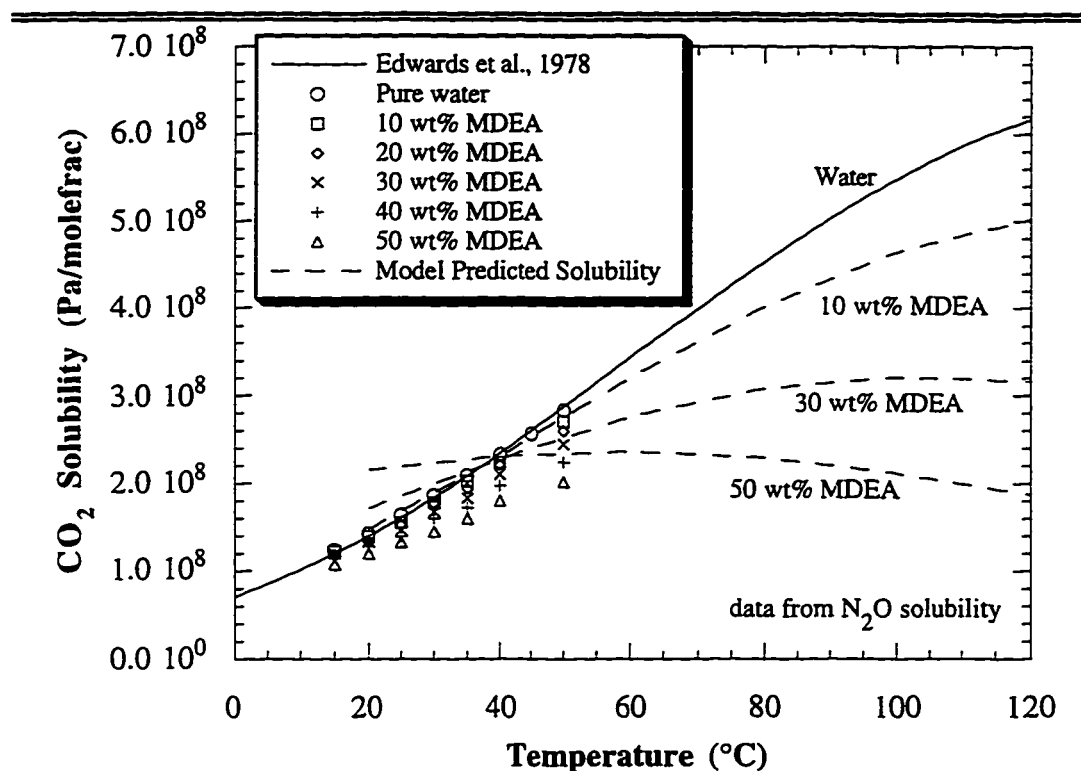
Figure 5.3 CO_2 physical solubility measured in water and predicted in MDEA-
H_2O solutions from experimental N_2O solubility data by Sandall
(1993) compared to model predictions.

5.3 EQUILIBRIUM CONSTANTS

For most constants we have tried to obtain all of the available data within

reason. We present all of the equilibrium constants on the molality basis with the

asymmetric activity coefficient convention for all species ($\gamma \to 1$ as $x \to 0$).

Conversion of these equilibrium constant equations to the mole fraction basis and

the symmetric activity coefficient convention for the amines may be necessary

depending on the VLE model structure.

Table 5.8. Temperature dependent equilibrium constants on molality basis.

Reaction	A	B	C	D
*$MDEAH^+ + H_2O \Leftrightarrow MDEA + H_3O^+$	-59.55	-1709	8.01	0.0
Data References: Schwabe et al. (1959), Oscarson et al. (1989), Kim et al. (1987)				
*$DEAH^+ + H_2O \Leftrightarrow DEA + H_3O^+$	-26.5	-4035	3.44	0.0
Data References: Bower et al. (1962), Oscarson et al. (1989)				
$CO_2 + 2 H_2O \Leftrightarrow HCO_3^- + H_3O^+$	235.482	-12092.1	-36.7816	0.0
Data References: Harned and Davis (1943), Ellis (1959), Read (1975), Ryzhenko (1963)				
$HCO_3^- + H_2O \Leftrightarrow CO_3^= + H_3O^+$	220.067	-12431.7	-35.4819	0.0
Data References: Harned and Scholes (1941), Cuta and Strafelda (1954), Ryzhenko (1963)				
$H_2S + H_2O \Leftrightarrow HS^- + H_3O^+$	218.599	-12995.4	-33.5471	0.0
Data References: Tsonopoulos et al. (1976), Ellis and Milestone (1967), Loy and Himmelblau (1961), Wright and Maass (1932)				
$2 H_2O \Leftrightarrow OH^- + H_3O^+$	140.932	-13445.9	-22.4773	0.0
Data References: Harned and Robinson (1940), Ackermann (1958), Noyes et al. (1907)				
$\ln K_m = A + B/T + C*\ln T + D*T$				
*Amine protonation reaction given on asymmetric activity coefficient convention. T in Kelvin.				

5.3.1 H₂O

The equilibrium constant for water is given in figure 5.4. The data agree very well in the low temperature ranges. Fisher and Barnes (1972) measured pK_w between 100 and 300°C, but their experimental data exhibited large deviations and are not included. Parameters in the Edwards et al. (1978) equation were based on a curve by Tsonopoulos et al. (1976) which in turn was based on data by Ackermann (1958), Harned and Robinson (1940) and Noyes et al. (1907) (not shown).
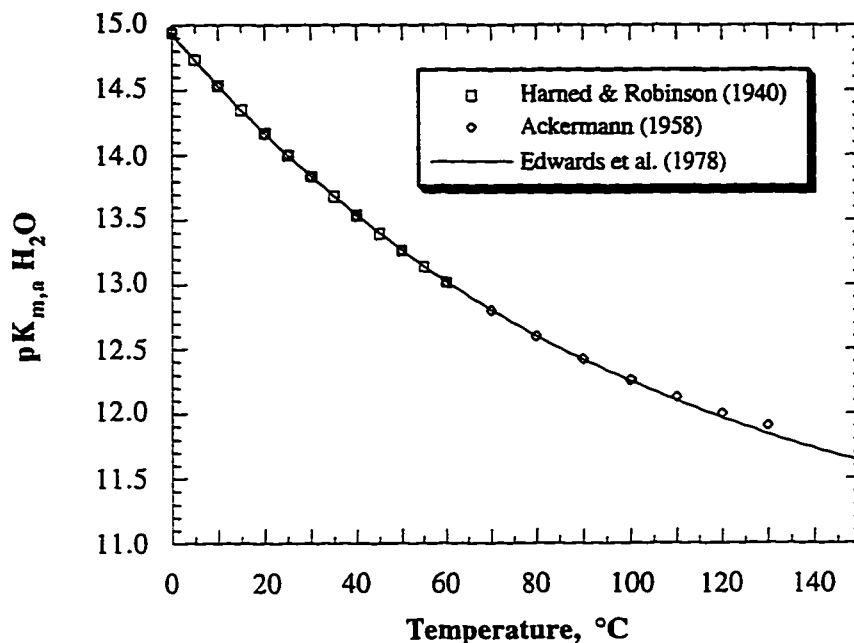
Figure 5.4 Ionization constant of water on the molality basis.

5.3.2 CO₂

Figure 5.5 plots four experimental data references for the first ionization

constant of CO_2, equation 2.31, versus the curves by Edwards et al. (1978),

Ryzhenko (1963). The Ellis (1959) data was at low, but not zero, ionic strength

and was averaged at each temperature. The curve by Edwards et al. (1978) was

based on the data of Harned and Davis (1943), Ellis (1959) and Ryzhenko (1963)

and is recommended for use. The parameters are given in Table 5.8. The

Ryzhenko curve is based on his own data and that of Harned and Davis (1943)

and is included for comparison since several literature sources utilize Ryzhenko's

equation. All three equations agree reasonably well with each other. Note that

the pK curve changes direction and therefore the ΔH_{rxn} changes sign at approximately 60°C.
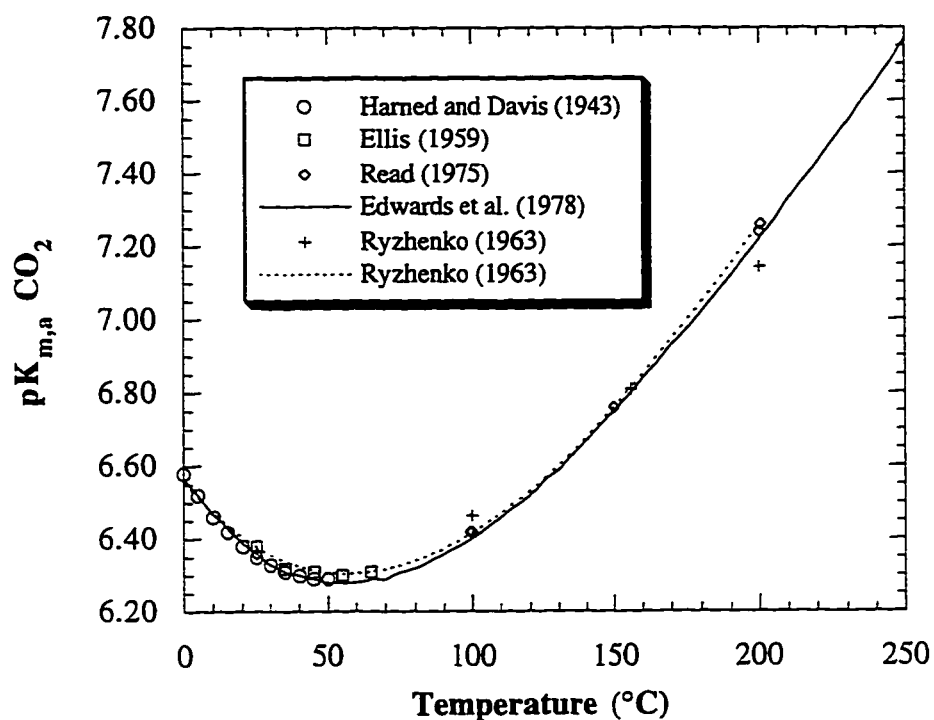
Figure 5.5 First ionization constant for CO_2 in water based on the molality scale compared to literature curve fits.

5.3.3 HCO_3^-

Figure 5.6 gives the second dissociation constant for CO_2 on the molality basis defined at zero ionic strength. Cuta and Strafelda (1954) data was not at zero ionic strength which explains its positive deviation from the curves. The curve by Edwards et al. (1978) fits well and is recommended for use up to 200°C.

The Ryzhenko curve is included for comparison and generally agrees with Edwards.
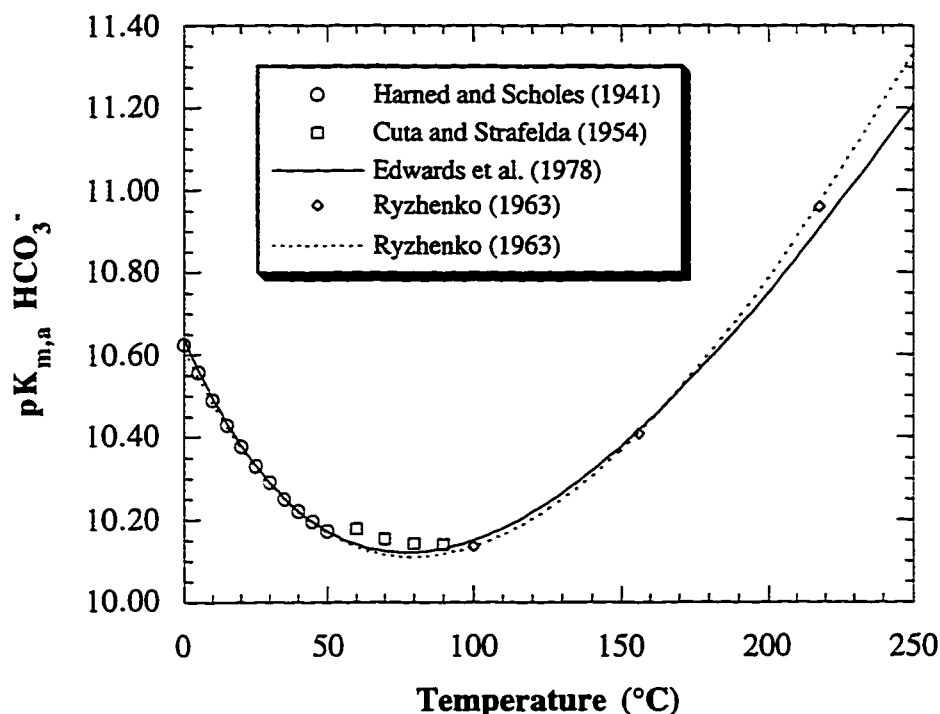
Figure 5.6 Second ionization constant for CO_2 in water based on the molality scale compared to literature curve fits. Cuta and Strafelda data was not at zero ionic strength.

5.3.4 H_2S

Figure 5.7 presents the first ionization constant for H_2S on the molality scale. All of the data follow the same temperature dependent trends with slight variations in the absolute magnitude of the pK. Tsonopoulos et al. (1976) provide an equation for the temperature dependence of the pK_a based on the data sets in figure 5.7, but they used base ten logs instead of natural logs. Edwards et al.

(1978) modified the Tsonopoulos parameters to the natural log form and the results are given in Table 5.8 and plotted in figure 5.7.
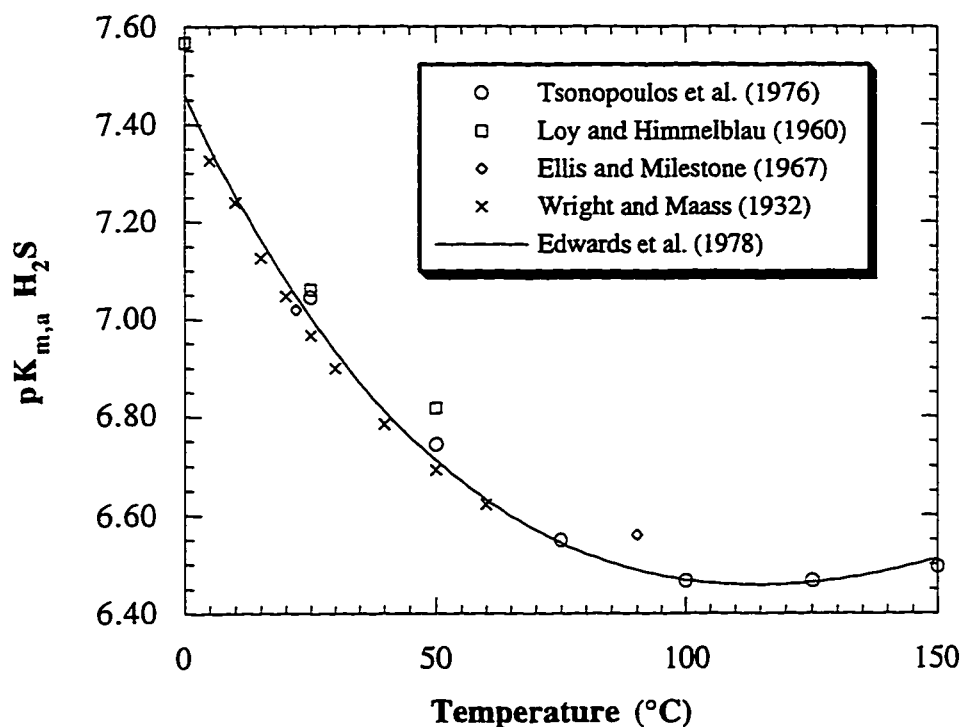
Figure 5.7 First ionization constant for H_2S in water based on the molality scale compared to literature curve fits.

5.3.5 HS⁻

Obtaining the second dissociation constant for H_2S is experimentally very difficult. To obtain measurable amounts of $S^=$ very concentrated solutions of NaOH, 15 N to 20 N, must be used. At these concentrations the solutions can no longer be considered aqueous making analysis more difficult. Oxygen contamination has also been said to cause low pK_a's due to formation of polysulfides and thiosulfates (Giggenbach, 1971 and Meyer et al., 1983).

Giggenbach gives a pK_a for HS^- as 17.2 at 14°C and 16.4 at 70°C. Meyer et al. (1983) give a value of pK_a for HS^- as 17 ± 1. At typical gas treating solution pH the concentration of $S^=$ is much lower than H^+ or OH^- and therefore negligible.

5.3.6 MDEA

For MDEA the most notable conclusion is that most literature sources use an MDEA deprotonation equilibrium constant (equation 2.35) based on only four data points between 25°C and 60°C, collected in 1959. This is shown as the dashed curve below in figure 5.8. We have found three other original references for this equilibrium constant. Fortunately, two of the three references confirm the values of Schwabe et al. (1959). The Oscarson et al. (1989) data extend the temperature range to cover stripper conditions. Littel et al. (1990) data was not included in the regressed curve and deviates consistently lower than the other data sets for no known reason.

Regression of only the Schwabe data results in a constant heat of reaction of 35.2 kJ/gmol. However, we know from Oscarson that the heat of reaction varies from 32 to 42 kJ/gmol between 25°C and 150°C, respectively. Using a constant heat of reaction for MDEA protonation results in a 50% difference in K for MDEA and a 10% low prediction in the heat of absorption at stripper conditions. The offset in the K could affect a rate-based model by significantly changing activity coefficients and solution speciation to fit the data.
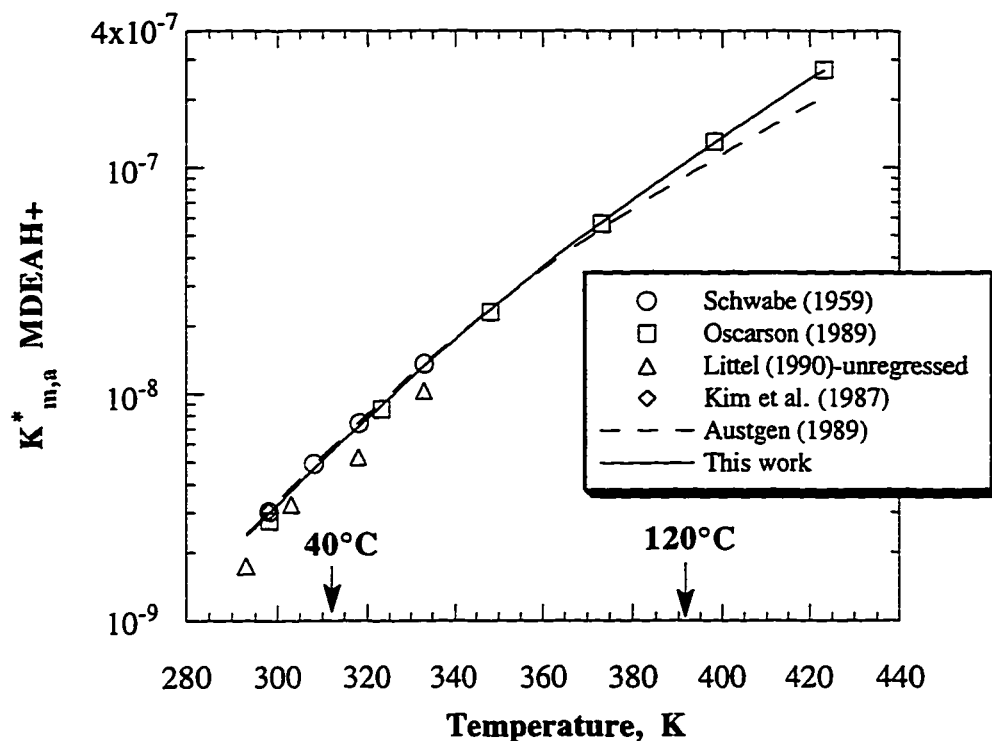
Figure 5.8 MDEA deprotonation reaction equilibrium constant at zero ionic strength based on molality scale and asymmetric activity coefficients. Dashed line was fit on Schwabe (1959) only. The solid line was fit on Schwabe, Oscarson and Kim data.

Differences in the heat of absorption will affect the calculated steam rate in the stripper. Figure 5.9 illustrates the difference in the heat of absorption predictions resulting from the different temperature dependencies. The equilibrium constant that should be used for reaction 2.35 is given in Table 5.8.
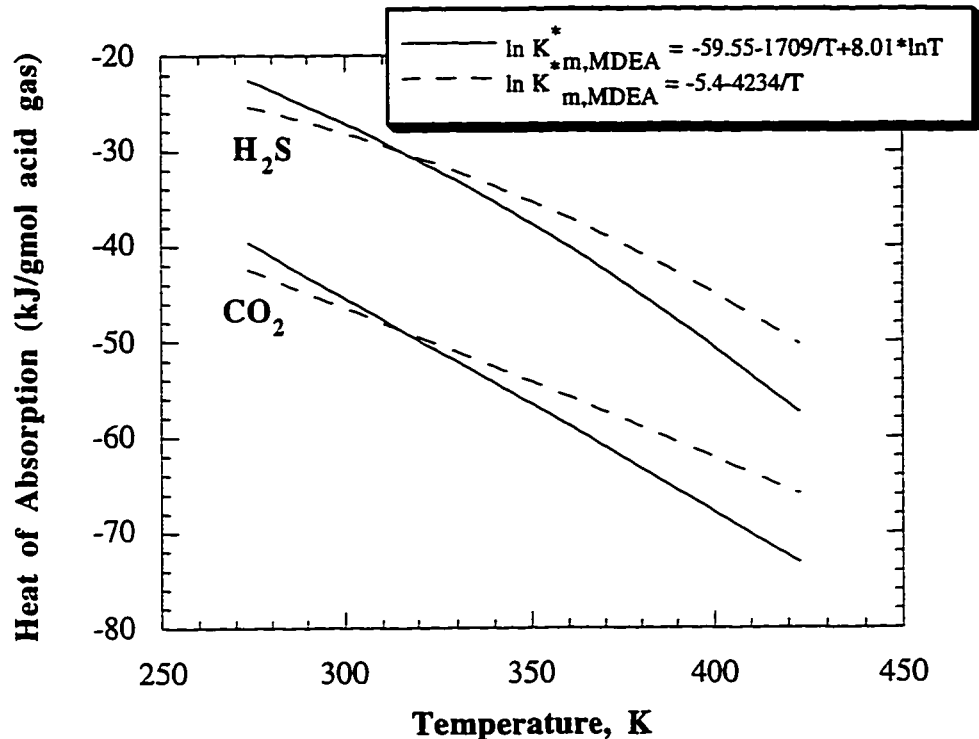
Figure 5.9 Ideal heat of absorption for MDEA-H$_2$S and MDEA-CO$_2$ calculated from the heats of solution and reaction at infinite dilution.

5.3.7 DEA

The pK$_a$ values for the DEA deprotonation reaction (equation 2.36) are given in figure 5.10. The curve, which was fit to the data sets in the figure, agrees well with what little experimental data was found. Please note that the equilibrium constant is based on the molality scale and asymmetric activity coefficient convention.

114
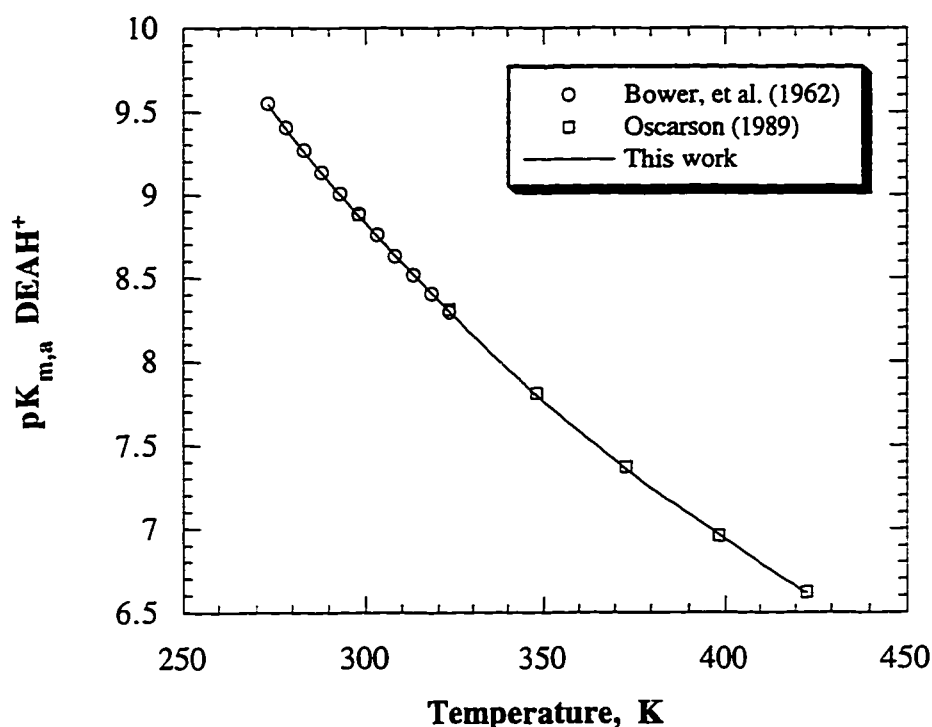
Figure 5.10 DEA deprotonation reaction equilibrium constant at zero ionic strength based on molality scale and asymmetric activity coefficients.

The above equilibrium constant plots for MDEA and DEA were obtained by assuming that all activity coefficients approach one as pure water is approached. However, this model assumes the amine activity coefficients approach one as pure amine is approached. Therefore, to utilize the equilibrium constants they have to be normalized by the infinitely dilute amine activity coefficient as described in Chapter 2. In addition, all of the above equilibrium constants are based on molality concentration units. This work uses the mole fraction concentration scale. Chapter 2 also describes the procedure to convert the

equilibrium constants to the mole fraction basis. Table 5.9 provides the equilibrium constants as used in Aspen Plus™ after the above conversions have been made.

Table 5.9. Temperature dependent equilibrium constants on mole fraction basis.

Reaction	A	B	C	D
*$MDEAH^+ + H_2O \Leftrightarrow MDEA + H_3O^+$	-56.2	-4044.8	7.848	0.0
Data References: Schwabe et al. (1959), Oscarson et al. (1989), Kim et al. (1987)				
*$DEAH^+ + H_2O \Leftrightarrow DEA + H_3O^+$	-9.4	-6457	0.81	0.0
Data References: Bower et al. (1962), Oscarson et al. (1989)				
$CO_2 + 2 H_2O \Leftrightarrow HCO_3^- + H_3O^+$	231.465	-12092.1	-36.7816	0.0
Data References: Harned and Davis (1943), Ellis (1959), Read (1975), Ryzhenko (1963)				
$HCO_3^- + H_2O \Leftrightarrow CO_3^= + H_3O^+$	216.049	-12431.7	-35.4819	0.0
Data References: Harned and Scholes (1941), Cuta and Strafelda (1954), Ryzhenko (1963)				
$H_2S + H_2O \Leftrightarrow HS^- + H_3O^+$	214.582	-12995.4	-33.5471	0.0
Data References: Tsonopoulos et al. (1976), Ellis and Milestone (1967), Loy and Himmelblau (1961), Wright and Maass (1932)				
$HS^- + H_2O \Leftrightarrow S^= + H_3O^+$	-32.0	-3338.0	0.0	0.0
Data References: Giggenbach (1971), Meyer et al. (1983)				
$2 H_2O \Leftrightarrow OH^- + H_3O^+$	132.899	-13445.9	-22.4773	0.0
Data References: Harned and Robinson (1940), Ackermann (1958), Noyes et al. (1907)				
$\ln K_x = A + B/T + C*\ln T + D*T$				
*Amine protonation reaction has been normalized by the infinitely dilute amine activity coefficient. T in Kelvin.				

116

5.4 VAPOR PHASE MODEL

Soave's (1972) modification of the Redlich-Kwong (Redlich and Kwong, 1949) equation of state (RKS) is used to represent the equilibrium behavior of the vapor phase. Soave (1972) replaced the temperature-dependent term $\frac{a}{T^{0.5}}$ by a function $a(T, \omega)$ involving temperature and the acentric factor. In pressure explicit form, the RKS equation of state is (Aspen Plus™, 1994):

$$P = \frac{RT}{V_m - b} - \frac{a}{V_m\,(V_m + b)} \tag{5.13}$$

where
$$a = \sum_i \sum_j x_i\, x_j\, (a_i\, a_j)^{0.5}\,(1 - k_{ij}) \tag{5.14}$$

$$b = \sum_i x_i\, b_i \tag{5.15}$$

$$k_{ij} = k_{ji} \tag{5.16}$$

$$b_i = 0.08664\, \frac{RT_{ci}}{p_{ci}} \tag{5.17}$$

$$a_i = \alpha_i\, 0.42747\, \frac{R^2 T_{ci}^2}{p_{ci}} \tag{5.18}$$

$$\alpha_i = [1 + m_i(1 - T_{ri}^{0.5})]^2 \tag{5.19}$$

$$m_i = 0.48 + 1.57\omega_i - 0.176\omega_i^2 \tag{5.20}$$

Equation 5.13 then is rearranged to solve the expression for the volume term. The integral from equation 2.12 can then be calculated to obtain vapor fugacities for use in VLE calculations.

5.5 ACTIVITY COEFFICIENT MODEL

Chen et al. (1982) suggested a model for electrolyte systems that accounts for long range ion-ion interactions and short range molecule-molecule and molecule-ion interactions. Two guiding assumptions of their model are that like-ion repulsions are large and that local electroneutrality is satisfied. Their initial model only covered the case of one solvent and one completely dissociated electrolyte. They state that the model is valid for concentrations ranging from a molecular mixture to dilute electrolytes to fused salts. They use Pitzer's (1980) formulation of the Debye-Hückel theory to account for the ion-ion long range interactions. For short range interactions Chen used the Nonrandom Two-Liquid (NRTL) model of Renon and Prausnitz (1968).

Chen and Evans (1986) extended their previous model to cover the case of a single solvent with multiple electrolytes. They show the model to work well for many different electrolyte systems. Here, vapor phase fugacity coefficients were calculated by the Redlich-Kwong-Soave equation of state.

Mock et al. (1986) extended the electrolyte-NRTL model to cover mixed solvent electrolyte systems. They used the same local and long range interactions as Chen and Evans (1986). However, they mention but do not account for the change that must be made in the reference state of ionic activity coefficients. They are defined to approach one at infinite dilution in water, but in actuality the ion approaches infinite dilution in a mixed solvent. Mock et al. mention the possible use of a term to account for the dielectric constant of the mixed solvent to adjust for the new ion reference state due to two solvents. Aspen Technology

118

(1988) added a Born correction (Robinson and Stokes, 1970) to the model to account for the change in reference state. The electrolyte-NRTL model is made up of three separate terms to arrive at a total excess Gibbs energy which is converted to activity coefficients using thermodynamic relationships.

$$\frac{g_{ex}^*}{RT} = \frac{g_{ex\ PDH}^*}{RT} + \frac{g_{ex\ Born}^*}{RT} + \frac{g_{ex\ NRTL}^*}{RT} \tag{5.21}$$

5.5.1 Long-Range Contribution

The first term in equation 5.21 accounts for the long range ion-ion interactions that occur at low ionic strengths.

$$\frac{g_{ex\ PDH}^*}{RT} = -\sum_k x_k \left(\frac{1000}{M_s}\right)^{0.5} \left(\frac{4A_\phi I_x}{\rho}\right) \ln\left(1+\rho\ I_x^{0.5}\right) \tag{5.22}$$

where

M_s Molecular weight of solvent

ρ "Closest approach" parameter

I_x Ionic strength on mole fraction scale

$$I_x = 0.5 \sum_i x_i\ z_i^2 \tag{5.23}$$

x_i = mole fraction of component i
z_i = charge of component i

A_ϕ Debye-Hückel parameter

$$A_\phi = \frac{1}{3}\left(\frac{2\pi N_o d}{1000}\right)^{0.5}\left(\frac{e^2}{D_w kT}\right)^{1.5} \tag{5.24}$$

N_o = Avogadro's number
d = Solvent density
e = electron charge
D_w = dielectric constant of water
T = temperature, K
k = Boltzmann constant

5.5.2 Born Correction

The Born correction term accounts for the change in reference state for ions from infinitely dilute in water to infinitely dilute in amine-water liquids.

119

This difference is mainly represented by a change in the dielectric constant of the solvent. When the radius of an ion is not provided or available in a databank, a value of 3×10^{-10} m is assumed.

$$\frac{g^*_{ex\ Born}}{RT} = \left(\frac{e^2}{2kT}\right)\left(\frac{1}{D_m} - \frac{1}{D_w}\right)\frac{\sum_i X_i\ z_i^2}{r_i}\ 10^{-2} \tag{5.25}$$

where
r_i = Born radius
D_m = Dielectric constant of mixed solvent

5.5.3 Local Contributions

The most important interactions in acid gas treating electrolyte solutions are the short range interactions. These are accounted for by the NRTL structure for multicomponent mixtures. The subscripts m, c and a represent molecules, cations, and anions, respectively.

$$\frac{g_{ex\ NRTL}}{RT} = \sum_m X_m \frac{\sum_j X_j\ G_{jm}\ \tau_{jm}}{\sum_k X_k\ G_{km}} + \sum_c X_c \sum_{a'} \left(\frac{X_{a'}}{\sum_{a''} X_{a''}}\right)\frac{\sum_j G_{jc.a'c}\ \tau_{jc.a'c}}{\sum_k X_k\ G_{kc.a'c}}$$

$$+ \sum_a X_a \sum_{c'} \left(\frac{X_{c'}}{\sum_{c''} X_{c''}}\right)\frac{\sum_j G_{ja.c'a}\ \tau_{ja.c'a}}{\sum_k X_k\ G_{ka.c'a}} \tag{5.26}$$

with

$$G_{cm} = \frac{\sum_a X_a\ G_{ca.m}}{\sum_{a'} X_{a'}} \qquad G_{am} = \frac{\sum_c X_c\ G_{ca.m}}{\sum_c X_{c'}}$$

$$\alpha_{cm} = \frac{\sum_a X_a\ \alpha_{ca.m}}{\sum_{a'} X_{a'}} \qquad \alpha_{am} = \frac{\sum_c X_c\ \alpha_{ca.m}}{\sum_c X_{c'}}$$

where $\quad X_j = x_j\ C_j$ ($C_j = Z_j$ for ions and C_j = unity for molecules)
α = nonrandomness parameter
τ = binary energy interaction parameter
and

120

$$G_{jc,a'c} = \exp(-\alpha_{jc,a'c}\, \tau_{jc,a'c}) \qquad G_{ja,c'a} = \exp(-\alpha_{ja,c'a}\, \tau_{ja,c'a})$$

$$G_{im} = \exp(-\alpha_{im}\, \tau_{im}) \qquad G_{ca,m} = \exp(-\alpha_{ca,m}\, \tau_{ca,m})$$

$$\tau_{ma,ca} = \tau_{am} - \tau_{ca,m} + \tau_{m,ca} \qquad \tau_{mc,ac} = \tau_{cm} - \tau_{ca,m} + \tau_{m,ca}$$

In this work the τ, "tau", parameters have the temperature dependence, $\tau = A + B/T$. The model structure actually allows two additional constants for τ to add more complexity to its temperature dependence. This work assumes default values of zero for all of the temperature dependent parameters. Default values of the A parameter in this work are the same as Austgen (1989) and are based on average τ values obtained in Chen and Evans (1986) and Mock et al. (1986) for numerous electrolyte systems.

These defaults are different than those listed in Chapter 3 of Physical Property Methods and Models (Aspen Plus™, 1994). Aspen's values listed on page 3-59 seem to be transposed and have been reported in table 5.10 below as they should have been. The default values in this work, which differ from Aspen's, are explicitly declared in the input files so that Aspen's default values will not be invoked.

121

Table 5.10 Default electrolyte-NRTL parameters specified in this work

Parameter	This work (Aspen 8.5 defaults)		Aspen version 9.2 defaults	
	$A_{1,2}$	$\alpha_{1,2}$	$A_{1,2}$	$\alpha_{1,2}$
(ca) H_2O	-4	0.2	-4	0.2
H_2O (ca)	8		8	
(ca) Amine	-8	0.1	-2	0.2
Amine (ca)	15		10	
(ca) Solute	-8	0.1	-2	0.2
Solute (ca)	15		10	
(c'a') (c"a")	0	0.1	0	0.2
(c"a") (c'a')	0		0	
m_1 m_2	0	0.2	0	0.3
m_2 m_1	0		0	

Solute = CO_2 or H_2S, (ca) = cation, anion pair, ml = solvent or solute.

From thermodynamic relationships (Prausnitz et al., 1986) we can get activity coefficients from Gibbs excess energy.

$$\ln \gamma_i = \left(\frac{\delta(n_t\, g^*_{ex}/RT)}{\delta n_i} \right)_{T,P,n_{j\neq i}} \tag{5.27}$$

By substituting equations 5.22, 5.25 and 5.26 into equation 5.27, equations for the contributions to the activity coefficient are obtained. The explicit activity coefficient equations are given in Appendix C. The activity coefficients are then applied to equation 2.17 along with mole fractions and Antoine equations to predict the acid gas equilibrium vapor pressure.

5.6 VAPOR-LIQUID EQUILIBRIA CALCULATIONS

Once all of the above variables are calculated, equilibrium between the vapor and liquid can be determined. From Chapter 2 we know that the liquid fugacity must equal the vapor fugacity. Equation 2.17 is the resulting working relationship for calculation of VLE for amine and water species. Equation 2.19 shows the relationship used for supercritical components such as CO_2 and H_2S. The main difference between these two equations is the use of Henry's constant instead of pure component vapor pressure as the liquid fugacity reference state. Recall that the Poynting correction factor has already been included in the solubility parameter, H_i^o, in equation 2.19.

$$\varphi_i \, y_i \, P = \gamma_i \, x_i \, P_i^o \, \exp\left(\frac{\upsilon_i \, (P\text{-}Pi^o)}{RT}\right) \tag{2.17}$$

$$\varphi_i \, y_i \, P = \gamma_i^* \, x_i \, H_i^o \tag{2.19}$$

An inconsistency in Aspen Plus™ has been found in the normalization of solute, H_2S or CO_2, activity coefficients. Solute activity coefficients are defined to approach one as their concentrations approach zero. However, since the electrolyte-NRTL model treats molecules as being symmetrically normalized the solute activity coefficient at infinite dilution, γ_i^∞, is not zero when solute-solvent parameters are non-zero. To account for this, Aspen defines the asymmetric acid gas activity coefficient as:

$$\gamma_i^* = \frac{\gamma_i}{\gamma_i^\infty} \tag{5.28}$$

The definition in equation 5.28 is correct, however the error is in the calculation of γ_i^∞. It should be the acid gas activity coefficient at infinite dilution in the

amine-water solution and should only be a function of amine concentration and temperature. However, it is seen to also be a function of acid gas loading. It is believed that Aspen calculates γ_i^∞ at any acid gas loading by simply setting the molecular acid gas concentration to zero while allowing all of the other ionic species to remain at their loaded solution values. However, in a truly infinitely dilute solution all ionic concentrations except those associated with the basicity of the amine should be zero. The end result is that γ_i^∞ varies with acid gas loading due to the varying ionic concentrations which affect the activity coefficient calculations.

Figure 5.11 below quantitatively illustrates the effect of this incorrect normalization. Calculations were made by keeping the infinitely dilute activity coefficient constant at the true infinite dilution value and comparing to Aspen calculated values. The greatest differences occur at high loadings where molecular acid gas species play a more important role in VLE calculations and where ionic concentrations are large enough to greatly affect activity coefficients.
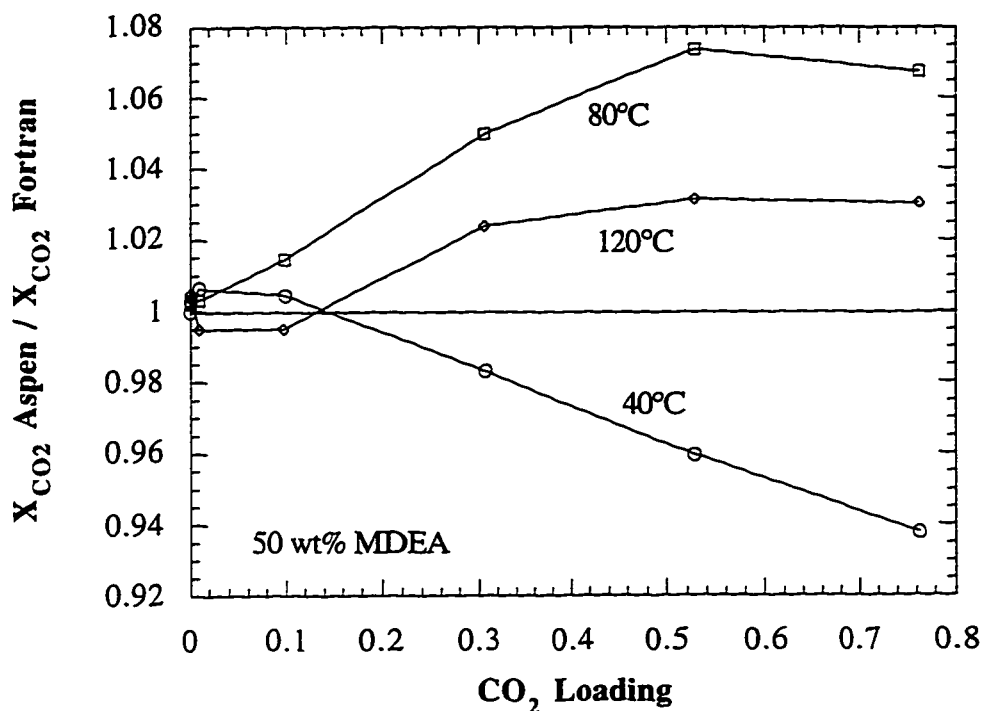
Figure 5.11 Effect of the different normalization of molecular acid gas infinitely dilute activity coefficient.

5.7 DATA REGRESSION SYSTEM

The above sections describe the model used in this work and how thermodynamic data is calculated. The thermodynamic structure must now be applied to the fitting of experimental data. Some of this effort for the binary amine-water thermodynamic system has already been discussed in Chapter 3. This section will describe in slightly more detail the method of data regression. Aspen Plus™ has built-in algorithms for the fitting of data called the Data Regression System™ (DRS). Having these algorithms already coded into Aspen

allowed this work to focus on the thermodynamic behavior of the system rather than on convergence criteria, step sizes, etc.

Aspen performs a non-linear optimization by varying the parameters to minimize Q in the following objective function.

$$Q = \sum_k \left(\sum_j \left(\sum_i \left(\frac{Z_{exp} - Z_{pred}}{\sigma_Z} \right)^2_i \right)_j \right)_k \qquad (5.29)$$

The objective function is summed over all i variables (Z) for each j data point and all k data sets. The standard deviations, σ_Z, serve to equally weigh the variables so, for example, pressure in Pascals is not more important than composition in mole fractions. Estimates of the standard deviations are entered for every variable in every data set. In general, the standard deviations were set to 0.2 for temperature and 10% and 5% for total pressure and liquid mole fraction concentrations, respectively. Deming's method (1943) was used to determine step sizes and to converge upon the solution.

Since error is assumed to exist in all of the variables, a classic treatment of error in the dependent variable is not possible. Values of the independent variables are normally assumed to be correct with error existing only in the dependent variables. However, the Aspen DRS assumes error in all of the variables and moves the data to match model predictions. One benefit of this method is that it is more realistic for acid gas VLE data. Both acid gas loading and acid gas partial pressures contain error, with loading being the larger error in some cases. One drawback is that logical standard deviations must be chosen for the variables. If pressure is given too high of a standard deviation in relation to

126

the mole fractions, then only the pressure data will be fit and vice versa. In addition, if very large standard deviations are given, then the data will move to fit the model predictions rather than the model adjusting its parameters to fit the data.

To add further flexibility, Aspen also allows weighting factors upon the data sets and parameter values. The values of the "A" parameters are on the order of one and the "B" parameters are on the order of 1000. Therefore, the A parameters were given a weight of 1.0 and the B parameters a weight of 0.01. In this way, the B parameters were not given greater consideration during regressions due to their larger values. Data sets included in the regressions were all given an equal weighting of 1.0.

Chapter 6: Methyldiethanolamine Systems

Methyldiethanolamine (MDEA) is one of the favored alkanolamines in acid gas treating. It is receiving increased use due to its lower heat of reaction and lower corrosivity compared to the other amines. In light of its increasing industrial importance, it was determined that this work would emphasize modeling MDEA and its mixtures with diethanolamine (DEA). This chapter describes the data regression and model predictions for the $MDEA-H_2S-CO_2$ system. Discussions of the DEA model and the complete mixture, MDEA-DEA-H_2S-CO_2, are given in Chapter 7. Also discussed in this chapter are model driven experiments that have been performed. These data serve to fill the voids where VLE data does not exist and provide additional information on solution thermodynamics that cannot be obtained accurately from VLE data.

The regression of VLE data in the individual gas systems, $MDEA-CO_2$ and $MDEA-H_2S$, are discussed first. Parameters obtained and model predictions are compared to Austgen et al. (1991). This work has utilized a unique set of parameters from the electrolyte-NRTL model and differences from Austgen are discussed. Parameters used here stem from experience with the model, sensitivity studies of Chang (1992), and from necessity to properly fit the experimental data.

VLE data was regressed to determine parameters for the high loading regions. Then predictions at low acid gas loadings were improved by manipulating the hydroxide parameters to match results from conductivity experiments. The model has also been confirmed to be correct in the low loading

128

region by comparison to pH data. Comparing model predictions to the experimental data also allows comparison between the data sets. Outlying data sets and discrepancies between data sets are discussed.

Model driven experiments are then discussed and details are given for the experimental procedures, results and how they relate to the electrolyte-NRTL model predictions. Conductivity measurements are shown to be an ideal method of obtaining speciation in unloaded solutions. pH data has been measured and is compared to model predictions. The last section describes predictions for the mixed gas MDEA-H_2S-CO_2 system. It is shown that mixed gas calculations can be made from single gas systems without the need for additional parameters. A good fit of the mixed acid gas data also confirms that the MDEA-CO_2 and MDEA-H_2S systems are correct.

6.1 MDEA-CO_2

The creation of the MDEA-CO_2 model begins with the VLE data. Six data sets from the literature have been regressed with the electrolyte-NRTL model. The resulting parameters are given in Table 6.1. Recall that the model has a temperature dependence in the taus of A + B/T. Therefore, the A's and B's listed in Table 6.1 are the temperature dependent terms of the parameters. The B parameter values and standard deviations have been given in Table 6.1 after being divided by 313K. This allows comparison of the various values on the same basis and shows that standard deviations on the temperature parameters are on the same order of magnitude as the A parameters. Most of the parameters are well predicted as indicated by the low standard deviations. The parameter for ($C5^+$

$CO_3^=$) MDEA was not well predicted and is quite different from the default value of -8 used by Austgen et al. (1991). Carbonate species concentration in this work was much lower than Austgen's as a result. Note that "C5$^+$" is shorthand notation for the protonated MDEA ions, MDEAH$^+$.

Austgen et al. (1991) only regressed the first four parameters in Table 6.1. The remaining parameter values listed are the default values used in their work. Note also that Austgen et al. (1991) set their MDEA-H$_2$O binary parameters equal to zero. This results in an ideal solution which has been shown in chapter 3 to not be the case. Binary MDEA-H$_2$O parameters for this work are given in Table 3.8. Austgen et al. (1991) did have non-zero binary parameters, but could not achieve a good regression utilizing them. This is not because their binary parameters were bad, but is a direct result of only utilizing the water parameters at the top of Table 6.1. It has been determined that MDEA parameters are required when amine-water systems are not ideal. A difference in amine-water parameters propagates into the electrolyte parameters making direct comparisons of the parameters more difficult between this work and Austgen et al. (1991).

The true effect of the amines on solution behavior can only be modeled by utilizing parameters with the amine. Although the water interaction parameters contain protonated amine species, this is not sufficient to determine amine interactions. It is not the absolute amine interactions that are important, but the differences in salt interactions between amine and water. Since the amine is further than water from its defined reference state on a concentration basis, it has the most freedom of movement and therefore can have a greater effect on model

130

predictions. When Austgen et al. (1991) set the MDEA-H_2O system to be ideal, the amine parameters were not required because there was no longer a significant difference in sensitivity between the water and amine parameters.

Notice that the parameter for ($C5^+$ OH^-) H_2O has no standard deviation listed. That is because this parameter was not regressed with the Data Regression System™ in Aspen Plus™. Instead, it was varied manually to match the hydroxide concentration obtained from conductivity data. Conductivity experiments are discussed in detail later in this chapter.

Table 6.1 Electrolyte-NRTL parameters for MDEA-CO_2-7.13

parameter	A or B	value	std dev	α	Tau at 40°C	Austgen Model
H_2O ($C5^+$ HCO_3^-)	A	7.503	0.33	0.2	7.5	9.5
H_2O ($C5^+$ HCO_3^-)	B / 313K	0	N/A			
($C5^+$ HCO_3^-) H_2O	A	-5.837	0.20	0.2	-3.6	-4.5
($C5^+$ HCO_3^-) H_2O	B / 313K	2.22	0.30			
($C5^+$ HCO_3^-) MDEA	A	0.839	0.49	0.1	-5.8	-8
($C5^+$ HCO_3^-) MDEA	B / 313K	-6.604	0.56			
($C5^+$ $CO_3^=$) MDEA	A	-8	N/A	0.1	-2.0	-8
($C5^+$ $CO_3^=$) MDEA	B / 313K	5.98	3.83			
($C5^+$ OH^-) H_2O	A	-5.6	N/A	0.2	-5.6	-4
($C5^+$ OH^-) H_2O	B / 313K	0	N/A			

Table 6.2 provides the parameter correlation matrix for the MDEA-CO_2 system. This table was obtained from the original regression in which the hydroxide parameter was fit in Aspen. The hydroxide parameter was then moved manually as discussed above. Table 6.2 shows that the hydroxide parameter is not

131

sensitive to the VLE data. This justifies our method of using conductivity data and also indicates that the hydroxide parameter can be moved without significantly affecting the acid gas VLE predictions. High correlations are usually seen and expected for the A with the B term of the same parameter. This is seen for parameter 2 with 3 and 4 with 5. Note that the carbonate parameter 6 is not correlated strongly with any of the other parameters. This is a secondary indicator that this parameter is difficult to obtain accurately.

Table 6.2 Parameter correlation matrix for MDEA-CO_2-7.13.

	1	2	3	4	5	6	7
1	1.00						
2	0.28	1.00					
3	-0.71	-0.88	1.00				
4	0.01	0.54	-0.40	1.00			
5	-0.35	-0.60	0.61	-0.94	1.00		
6	0.17	0.27	-0.30	-0.12	0.06	1.00	
7	0.04	0.11	-0.10	0.29	-0.28	0.23	1.00

Parameter Legend

1	H_2O ($C5^+$ HCO_3^-)	A
2	($C5^+$ HCO_3^-) H_2O	A
3	($C5^+$ HCO_3^-) H_2O	B
4	($C5^+$ HCO_3^-) MDEA	A
5	($C5^+$ HCO_3^-) MDEA	B
6	($C5^+$ $CO_3^=$) MDEA	B
7	($C5^+$ OH^-) H_2O	A

VLE data regression

Most of the data was fit within ±30% and the model goes through the center of the data scatter as illustrated in figure 6.1. Note that at loadings less than 0.01 there seems to be an upward trend in that data. The hydroxide parameter allowed better fitting of the high amine concentration data, seen as the

132

circular symbols, below a loading of 0.01. However, lower amine concentration data was unmoved by this hydroxide parameter. The parameter loses its sensitivity at MDEA concentrations below 25 wt%. It is unclear if this effect is a true solution behavior which would signify a deficiency in the parameter set used. Austgen (1989) also shows this trend in his dissertation figure 6.27.
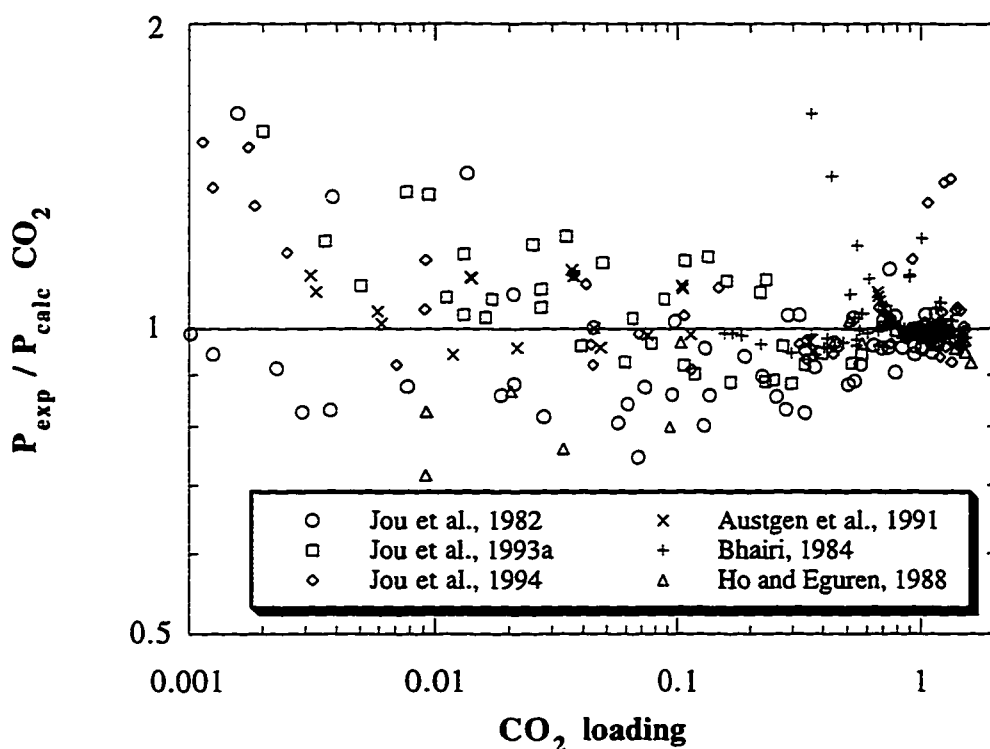
Figure 6.1 Ratio of experimental to model calculated CO_2 partial pressures as a function of CO_2 loading for the MDEA-CO_2-7.13 parameter set. Mole fractions were simultaneously fit.

During regressions of experimental data it is also assumed that there is error in the concentrations reported. In fact, very often the majority of the experimental error in a data point resides in the determination of the solution

loading. Based on this knowledge, the concentrations are also manipulated during regression of the model. Figure 6.2 shows how well the CO_2 mole fraction was predicted by the electrolyte-NRTL model. Most of the data were fit within 20%. Notice the inverse nature of figure 6.1 with figure 6.2. Where pressure is being over predicted, the regression reduces the mole fractions to help fit the partial pressures.
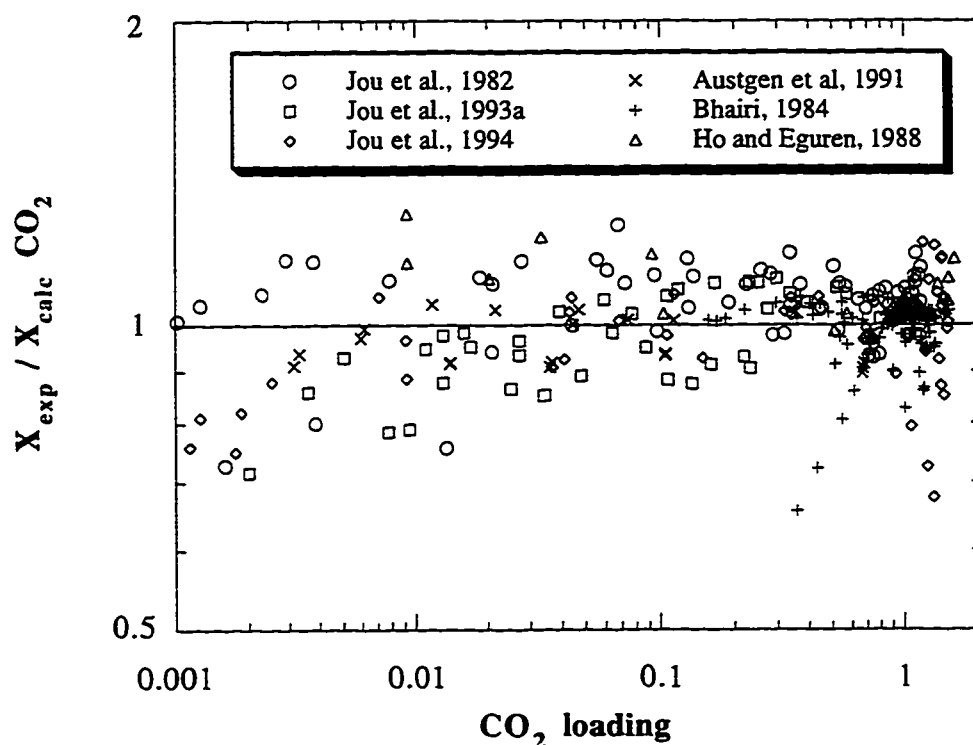
Figure 6.2 Ratio of experimental to model predicted CO_2 mole fractions as a function of CO_2 loading for the MDEA-CO_2-7.13 parameter set. Partial pressures were simultaneously fit.

Table 6.1 gives the resulting parameter set from the regression of the six data sets given in figures 6.1 and 6.2. These parameters must be used with our

previously reported MDEA-H$_2$O binary system parameters, equilibrium constants and Henry's law equations. CO$_2$-H$_2$O and H$_2$S-H$_2$O binary NRTL parameters used in this work were taken from Austgen (1989). Parameters not listed here were set to the default values suggested by Austgen et al. (1991) and are given in Table 5.10 and Appendix D.

6.1.1 Model predictions

Partial Pressure

Figure 6.3 below compares partial pressure predictions of the current model to our simple model from Chapter 4 and to Austgen et al. (1991). Notice that all three models roughly agree at 40°C where data is abundant. This work, however, does predict a lower partial pressure at 40°C at loadings above 0.3. The difference is partly due to the different data sets that were included in our regression that Austgen et al. (1991) did not use. The data of Ho and Eguren (1988) and Jou et al. (1994) was not available at the time they developed their model. The simple model, which agrees with this work, also regressed the data of Ho and Eguren (1988) and Jou et al. (1994). Note that our "Jou et al. 1993a" reference has the same data listed in Austgen et al. (1991) as "Jou et al. (1986)". The difference at 120°C over the lower loading ranges is due to the different value for the MDEA protonation reaction at temperatures greater than 100°C. Predictions for 25 wt% MDEA are nearly identical between this work and Austgen et al. (1991), except for CO$_2$ loadings below 0.001 at 40°C.

135
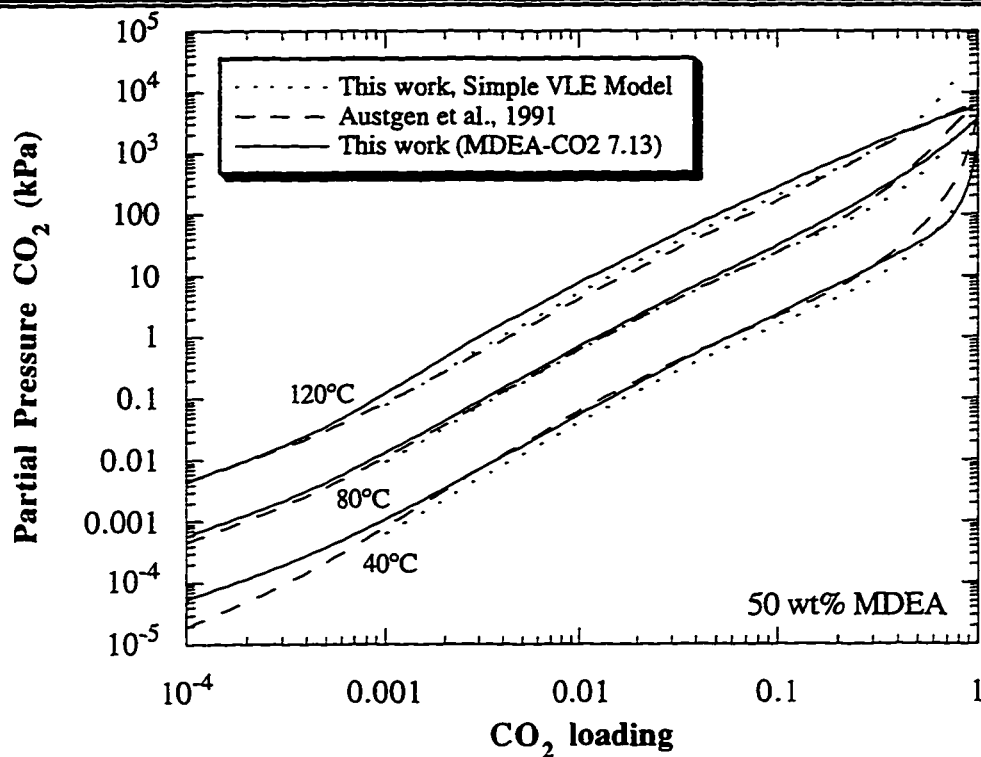
Figure 6.3 Calculated CO_2 partial pressures in kPa at 40, 80 and 120°C by three different models in 50 wt% MDEA.

The many orders of magnitude in pressure make comparisons in figure 6.3 difficult. Therefore, partial pressure in kPa was divided by the CO_2 loading squared. This normalization procedure reduces the number decades in the y-axis and makes differences in the models easier to see in figure 6.4.
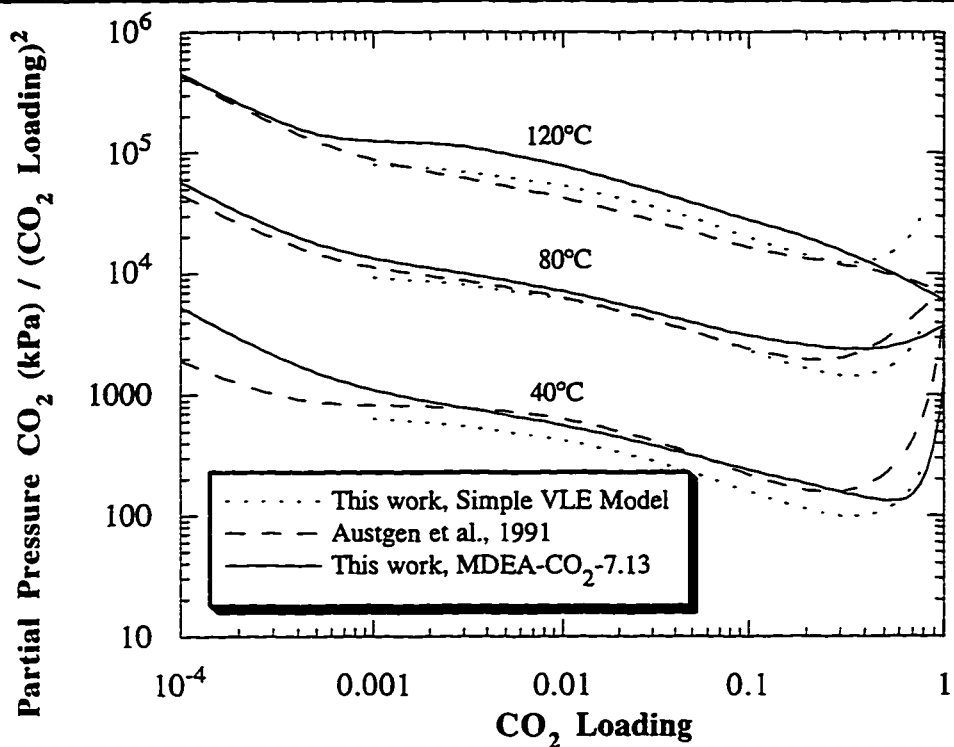
Figure 6.4 Calculated CO_2 partial pressure divided by CO_2 loading squared for three models in 50 wt% MDEA.

Commercial absorbers can run at a variety of amine concentrations. Therefore, figure 6.5 is given which nearly collapses the different weight percent curves by dividing CO_2 partial pressure by the MDEA mole fraction which is assumed to be acid gas free and the CO_2 loading squared. While this requires more effort to obtain partial pressures from the plot, it reduces the y-axis to only two decades greatly improving readability of the curves.
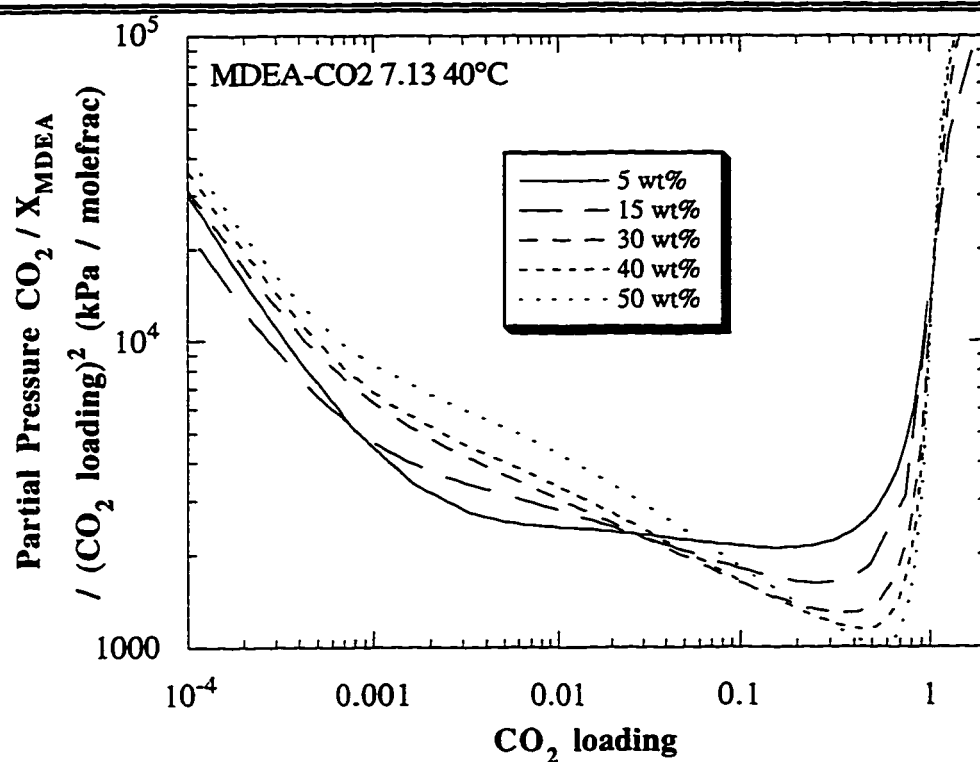
Figure 6.5 CO_2 partial pressure normalized by the gas free MDEA concentration and the loading squared as a function of MDEA weight percent in aqueous solutions at 40°C.

Speciation

Even when partial pressure plots appear similar, model behavior can be quite different. This is due to different parameters which result in unique activity coefficient behavior. Changes in model predictions are accomplished by manipulating mole fractions and activity coefficients, while activities can remain essentially the same. Figure 6.6 below shows the predicted mole fractions from this work at 40°C for 50 wt% MDEA. The carbonate concentration shown is too low based on experience with the DEA models.

138
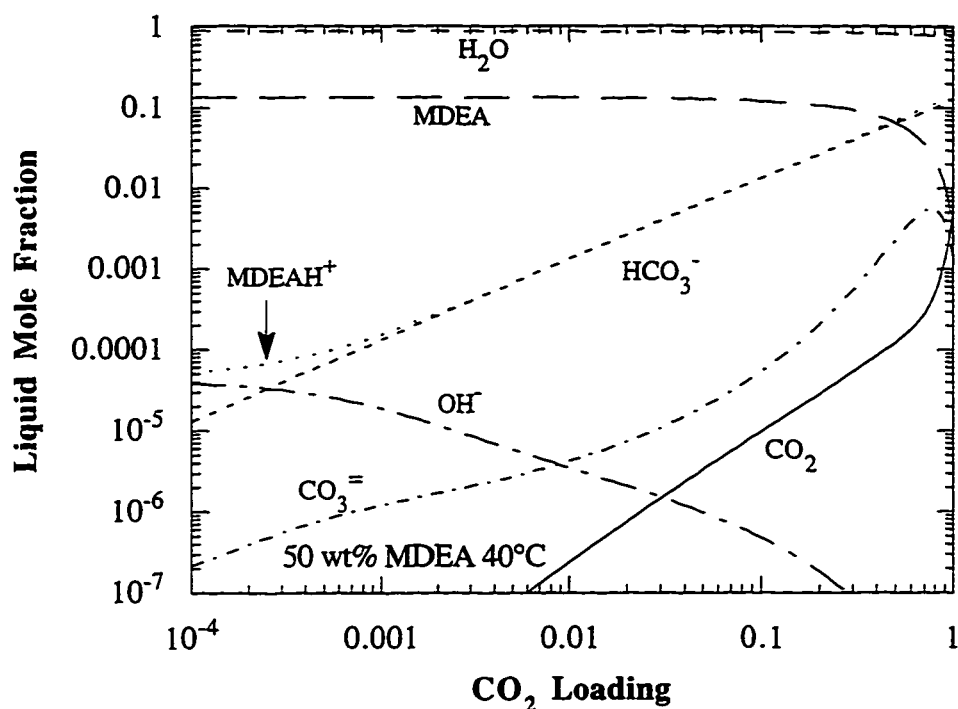
Figure 6.6 Liquid species mole fractions predicted by the current CO_2-7.13
electrolyte-NRTL model parameter set for a 50 wt% MDEA solution
at 40°C.

The Henry's constant for CO_2 is the only regressed parameter for CO_2 solubility. No parameters accounting for solubility changes with amine concentration or ionic strength were regressed. Therefore, the absolute value of the molecular concentration of CO_2 could be wrong by a factor of two or more. Unfortunately, little data exists for the concentration of molecular CO_2 in acid gas treating solutions to improve these predictions. Note that the lack of knowledge of molecular CO_2 concentration does not significantly affect VLE predictions at loadings less than 1.0.

Figure 6.7 compares calculated hydroxide and carbonate mole fractions for a 50 wt% MDEA solution at 40°C from this work with Austgen et al. (1991). Recall that Austgen et al. (1991) have used default values for the $CO_3^=$ parameters of -8.0 compared to a regressed value of -2.0 at 40°C in this work.
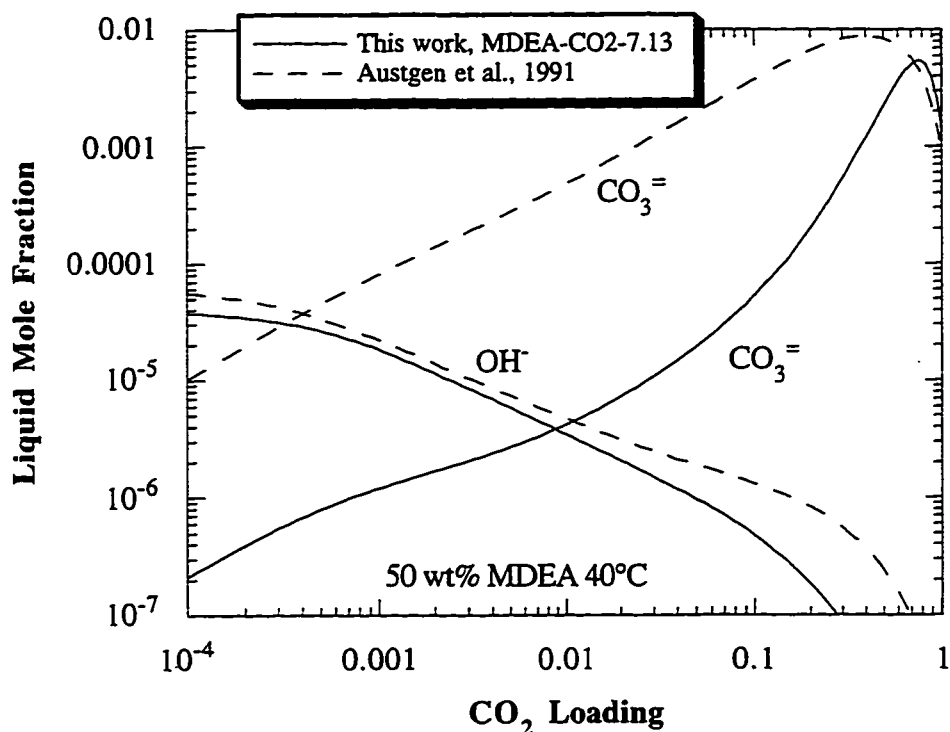
Figure 6.7 Liquid species mole fractions calculated from this work compared to those calculated by the Austgen et al. (1991) electrolyte-NRTL model parameter set for a 50 wt% MDEA solution at 40°C.

From DEA-CO_2 work discussed in chapter 7, it is believed the correct value for this parameter lies between these two values at approximately -5.6. This parameter value would result in more carbonate than reported in this work, but less than reported in Austgen et al. (1991).

Another difference illustrated in figure 6.7 is the mole fraction of MDEAH$^+$ and OH$^-$ at very low loadings. Since VLE data did not exist below a CO_2 loading of 0.001, other data was needed to determine where the model should predict. Therefore, a few conductivity measurements have been undertaken to determine the true ionic concentrations at low loading. These experiments are discussed in detail in section 6.3. The OH$^-$ parameter listed in Table 6.1 has been adjusted to match our hydroxide mole fraction calculated from conductivity measurements in Table 6.6. Figure 6.8 gives the speciation in 50 wt% MDEA solutions at 120°C calculated from this work. It also shows a carbonate concentration which is unreasonably low.
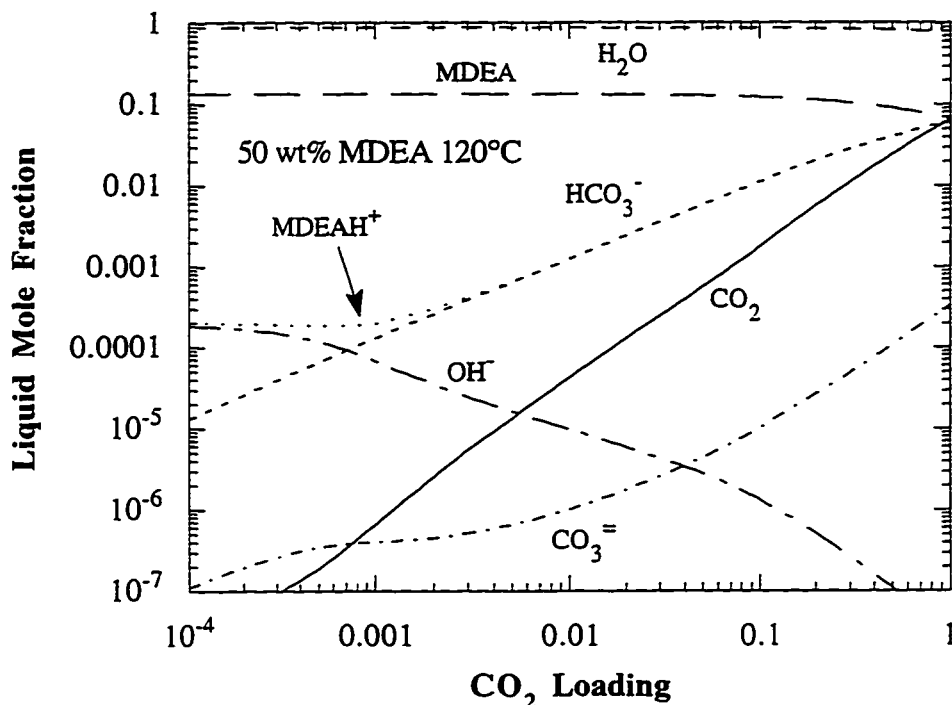
Figure 6.8 Liquid species mole fractions predicted by the CO_2-7.13 electrolyte-NRTL model parameter set for a 50 wt% MDEA solution at 120°C.

Activity Coefficients

Figure 6.9 illustrates the activity coefficient predictions for this work in 50 wt% MDEA at 40°C. Note that the activity coefficients of MDEAH$^+$ and HCO$_3^-$ are not independent above a loading of 0.003. The CO$_3^=$ activity coefficient approaches an unreasonable high value of near 1000 at zero loading. This corresponds to the low concentrations of this ion and is another factor suggesting our carbonate speciation is not correct. Note that the CO$_2$ activity coefficient shown here is symmetrically normalized and not the asymmetrically normalized value used for VLE calculations.
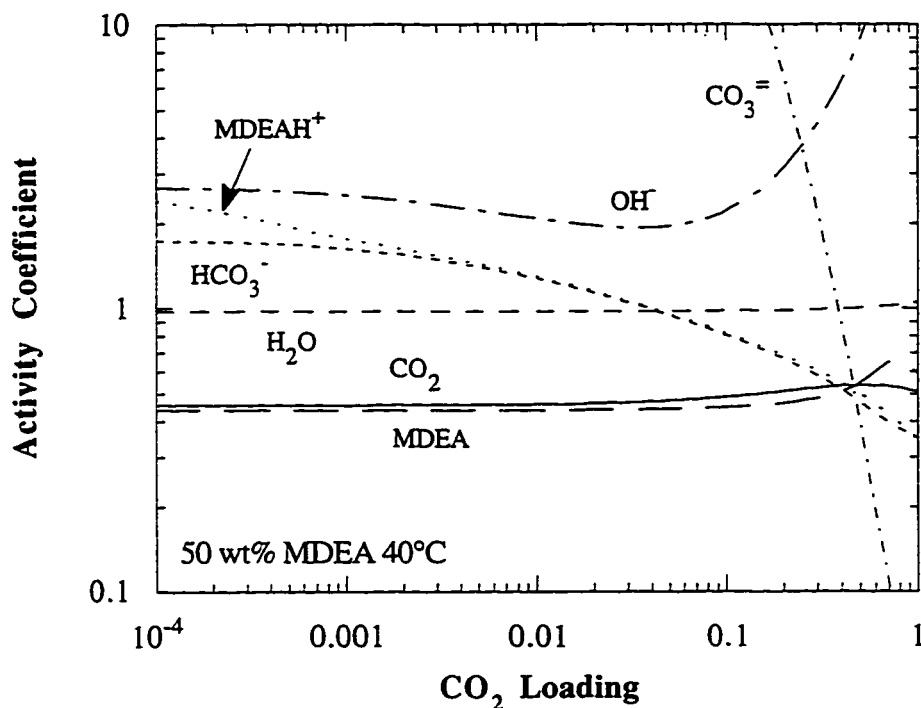
Figure 6.9 Liquid phase activity coefficients for 50 wt% MDEA at 40°C
calculated from the electrolyte-NRTL "MDEA-CO$_2$-7.13" model.

142

Heat of Absorption

One important variable in acid gas treating thermodynamics is the acid gas heat of absorption. In the absorber the temperature rise of the solution resulting from the acid-base reactions and the slight increase in partial pressure that results from this temperature rise must be determined. The negative of these numbers, the heat of desorption, is required to calculate the steam requirement for the stripper. In that respect, a smaller magnitude of the heat of absorption results in less reboiler steam use and a more economical process if all other factors are constant.

Heat of absorption can be calculated in two ways. First, it can be calculated rigorously by determining the enthalpy of the solution before and after the acid gas is absorbed. A second method is to apply the derivative of pressure at constant acid gas loading shown in equation 6.1 below.

$$\left(\frac{d \ln P}{d\ 1/T}\right)_x = -\frac{\Delta H_{abs}}{R} \qquad (6.1)$$

The heat of absorption presented here is calculated by equation 6.1 from acid gas partial pressures as a function of loading and temperature. Figure 6.10 shows the calculated heat of absorption for CO_2 into 50 wt% MDEA solutions.

The solid line in figure 6.10 is calculated from averaging values from the 25, 40, 80 and 120°C curves. It demonstrates the behavior that we would expect for heat of absorption as a function of loading. Heat of absorption has contributions for all of the reactions and the physical heat of absorption for gas molecules dissolving into the solution. Of course as the solution becomes

143

saturated at high loadings, only physical absorption is occurring and the heat of absorption should approach the physical heat of absorption.
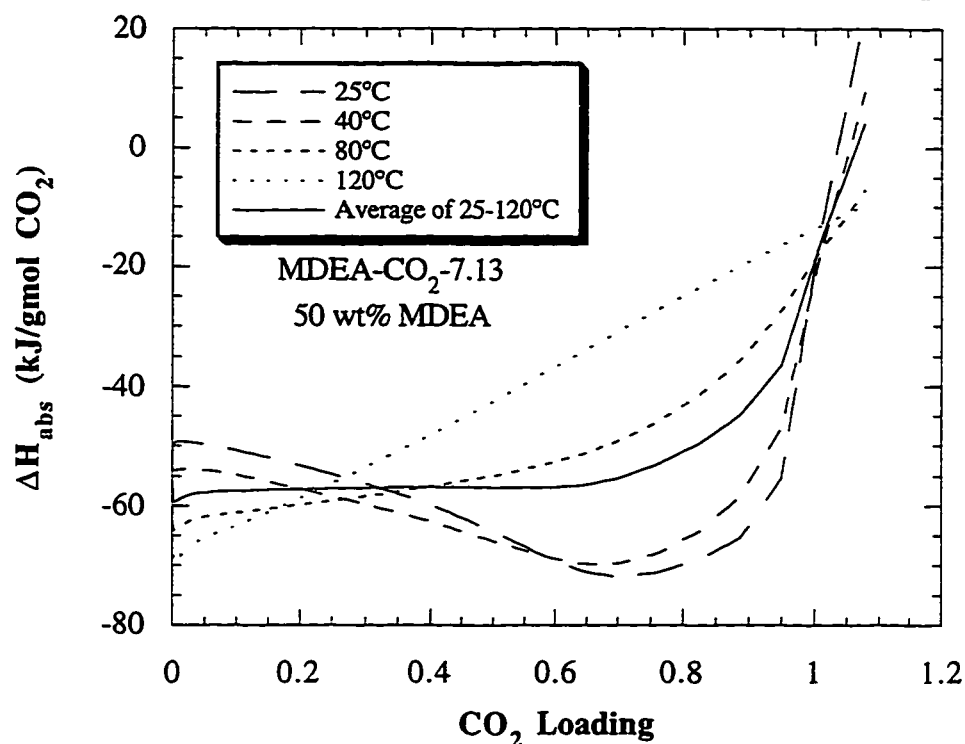
Figure 6.10 Calculated heat of absorption for CO_2 into 50 wt% MDEA solutions as a function of temperature and CO_2 loading.

Heat of absorption calculated as a function of temperature is a less accurately determined quantity. First of all, it requires a second derivative of all of the equilibrium constants. In most cases, the values we have for the second order temperature dependence of the equilibrium constants are not well determined. This uncertainty propagates into uncertainty in the temperature dependence of the heat of absorption. Secondly, the temperature derivative of the heat of absorption is the heat capacity of absorption.

144

$$\left(\frac{d\,\Delta H_{abs}}{d\,T}\right)_{x} = C_{p,\,abs} \qquad (6.2)$$

To determine $C_{p,\,abs}$ one must know the differences in the heat capacities of all of the ions and molecules. Values supplied to the model for heat capacities of the ions are uncertain at best. Therefore, temperature dependence of the heat of absorption at loadings away from zero will not be determined with accuracy or certainty. In support of this conclusion, Jou et al. (1982) state in their paper that heat of absorption is independent of temperature within the accuracy of their data.
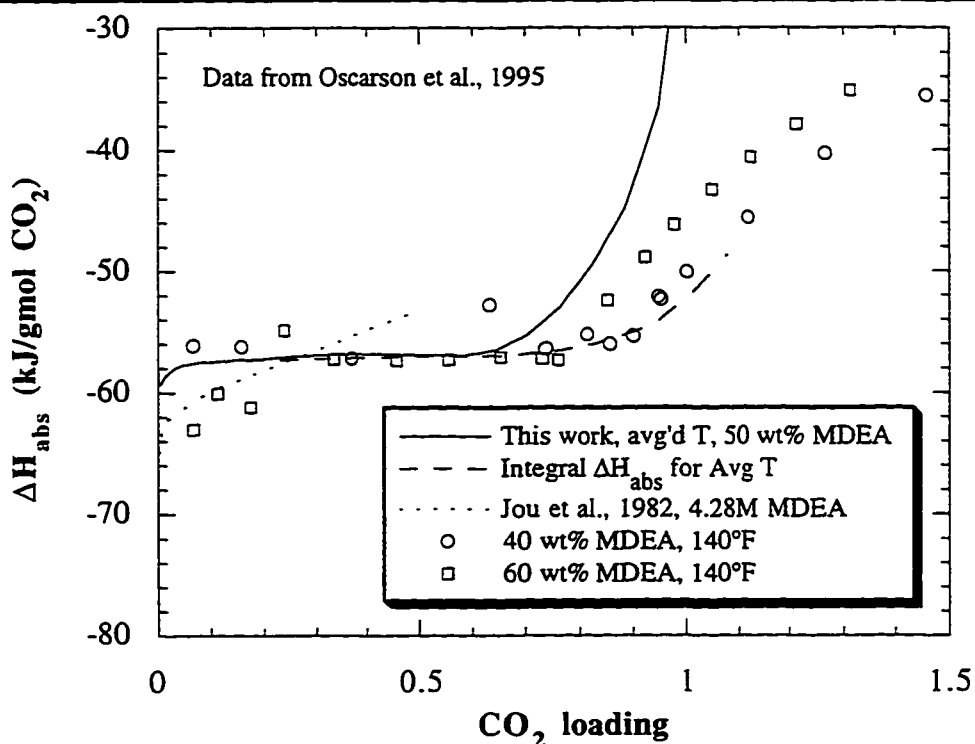
Figure 6.11 Heat of absorption of CO_2 into aqueous MDEA solutions calculated from partial pressures compared to experimental calorimetric data denoted by squares and diamonds.

Figure 6.11 compares heat of absorption calculated from partial pressures in this work and Jou et al. (1982) with experimental data by Oscarson et al. (1995). This work does not exhibit a loading dependence of the heat of absorption until a loading of 0.7 is approached and is consistent with the data by Oscarson. Jou et al. (1982) show a slight loading dependence, but generally agree with this work and Oscarson's data.

Note that the Oscarson et al. (1995) data is an integral heat of absorption. They measure the total heat in bringing an amine solution from zero loading to the desired loading and then divide by the total moles of acid gas added. Calculations from the models are the heat of absorption at a given loading. To properly compare with the Oscarson data the model curve has been numerically integrated. At a given loading, every heat of absorption below that loading is included in the numerical integration. This has no effect on calculations below a loading of 0.6 since the curve is constant. However, comparisons to the Oscarson data have greatly improved at high loadings as seen by the dashed line in figure 6.11.

6.1.2 Unregressed Data

There exists vapor-liquid equilibrium (VLE) data that was not regressed to form the CO_2-7.13 parameter set. This data is compared to predictions by the model and most of the data are fit well as shown in figure 6.12. The equilibrium data by Chakravarty (1992) and Mshewa (1995) were obtained from rate measurements of absorption and desorption in MDEA solutions. Shen and Li (1992) data have a significantly different trend than the other data at a loading range where experimental measurements should be relatively easy. Therefore,

146

careful consideration should be given before utilizing their data. The data by Bullin et al. (1996) generally agrees with our model, except for two points at very low CO_2 loading. Data by Huang and Ng (1995) agree well for this MDEA-CO_2 system, but show a slight upward trend at low loading. Bullin et al. (1996) show a slight downward trend at low loading.
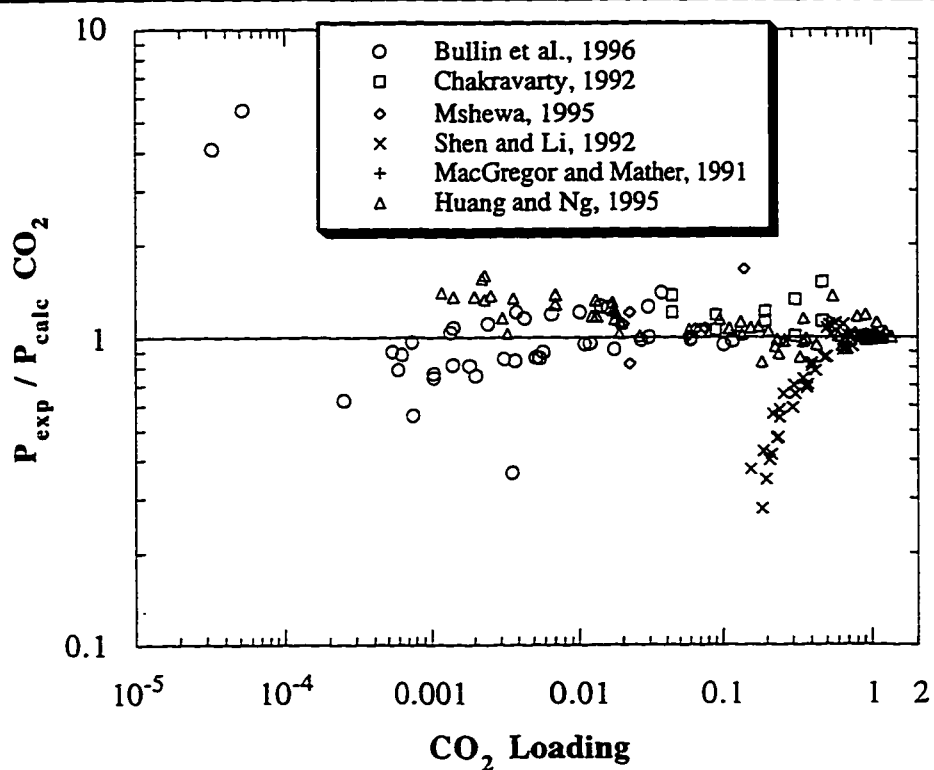
Figure 6.12 Model prediction comparison of CO_2 partial pressures for data sets that were not included in the regression of the parameters.

Due to the method of this calculation in Aspen, mole fractions were also assumed to contain error and were predicted simultaneously. Notice in figure 6.13 that the mole fraction curve is the inverse of the partial pressure plot. By manipulating the mole fractions in the opposite direction, the pressure data

147

appears to fit slightly better than it would if no movement of mole fractions were allowed.
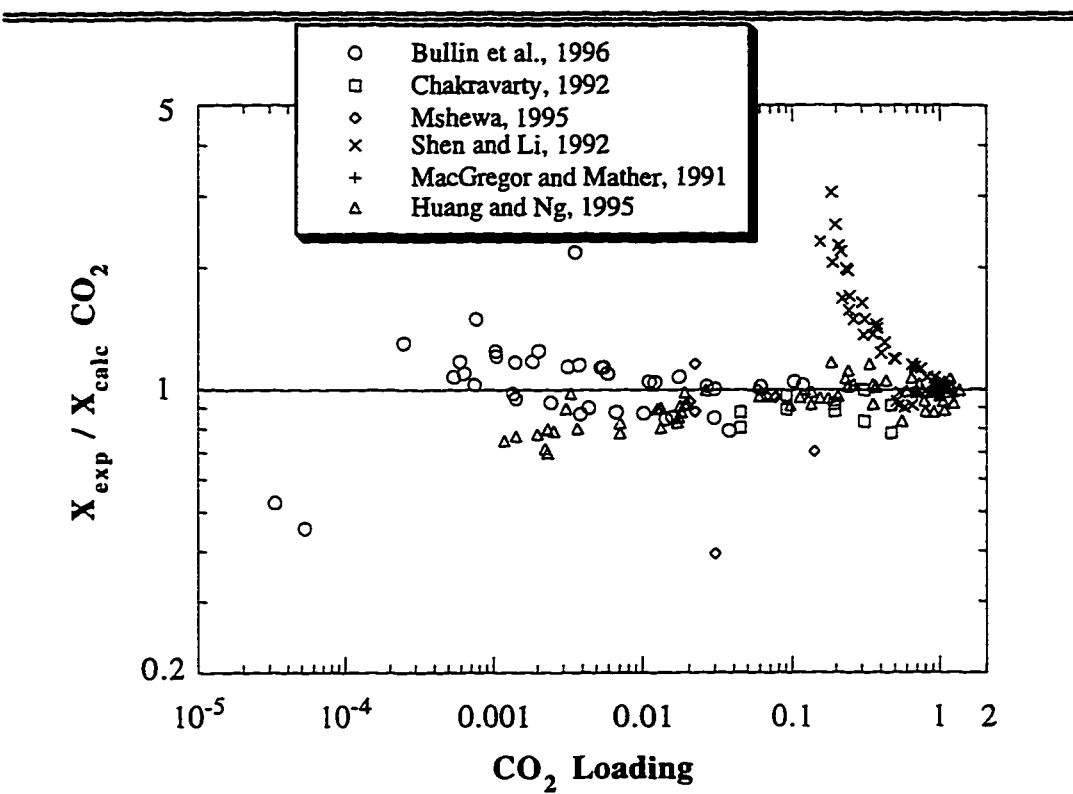
Figure 6.13 Model prediction comparison of CO_2 mole fractions for data sets that were not included in the regression of the parameters.

6.2 MDEA-H₂S

Much less data exists for the MDEA-H₂S system compared to the MDEA-CO_2 system. We have regressed three data sets to obtain the electrolyte-NRTL parameter set called "MDEA-H₂S-6.5" in this work. Figure 6.14 shows how well the three data sets were fit by the model. Jou et al. (1982) mention errors in their data at very low and very high loadings. Therefore, this data set has been cut to

H2S loadings above 0.01 and below 1.2. The data sets are fit well with an average error of approximately 20% in H2S partial pressure. The two Jou data sets seem to be following a slightly lower trend than the model at loadings below 0.01.
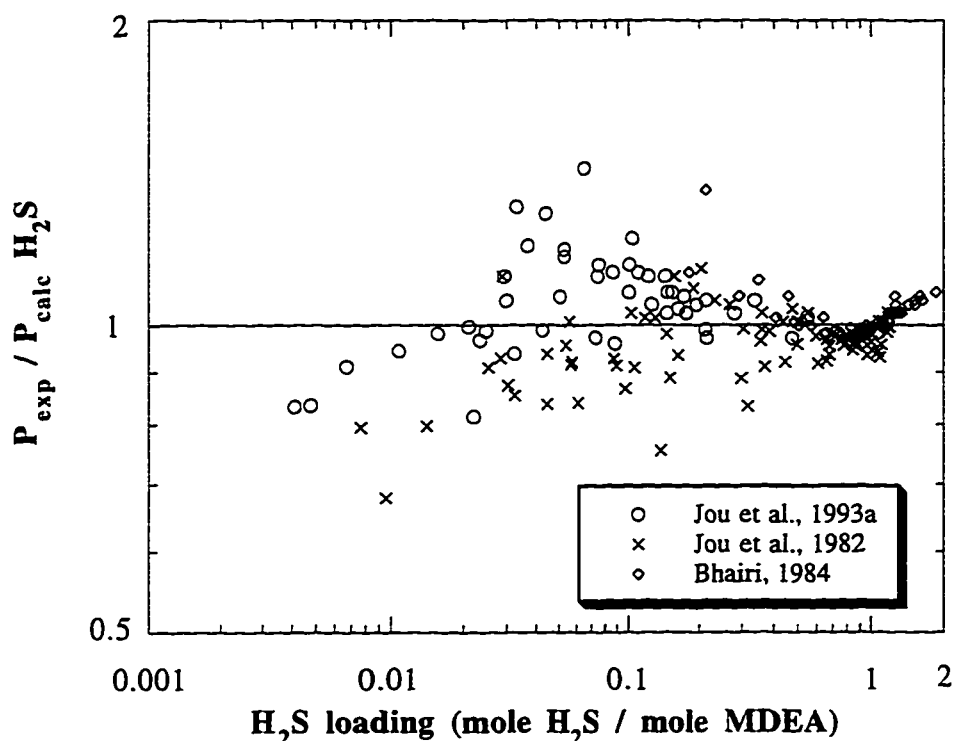
Figure 6.14 Ratio of experimental to model predicted H2S partial pressures as a function of H2S loading for the MDEA-H2S-6.5 parameter set. Mole fractions were simultaneously fit.

As with CO_2, mole fractions were simultaneously regressed and model predictions are given in figure 6.15. Table 6.3 provides the parameters which are to be used with the previously reported MDEA-H2O parameters and other constants.
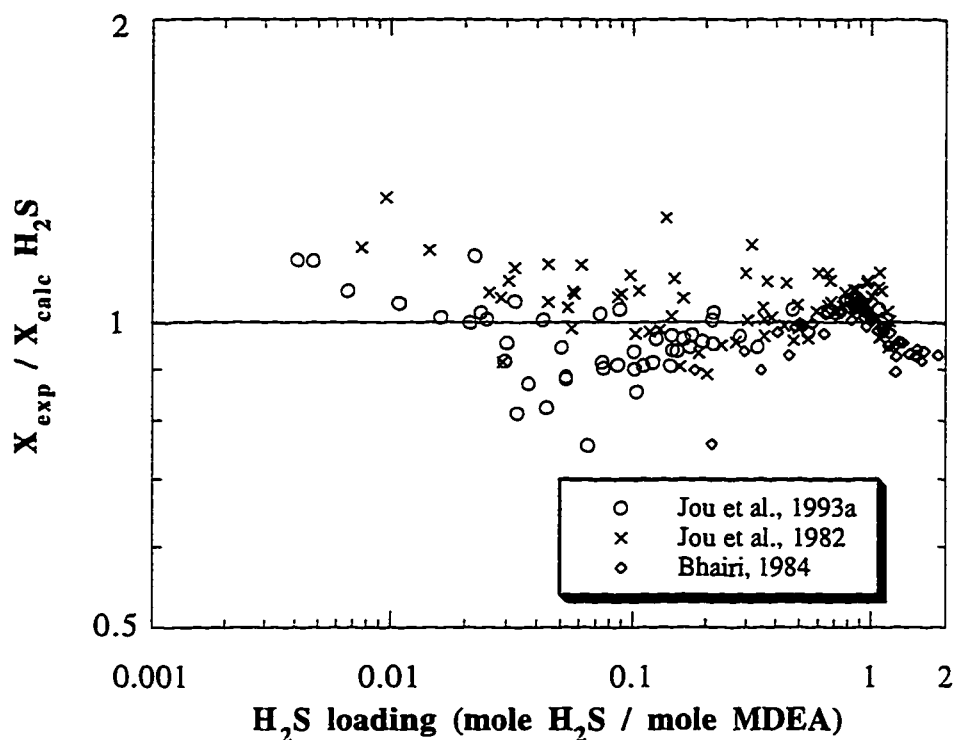
Figure 6.15 Ratio of experimental to model predicted H_2S mole fractions as a function of H_2S loading for the MDEA-H_2S-6.5 parameter set. Partial pressures were simultaneously fit.

Table 6.3 provides the resulting parameters from the above regression. Standard deviations listed as "N/A" indicate a parameter that was not regressed. They are included in the table so that the values for the A and B temperature dependent parameters are clear. The ($C5^+$ OH^-) H_2O parameter is identical to that listed in Table 6.1 to maintain consistency for the MDEA-H_2S-CO_2 system.

150

Table 6.3 Electrolyte-NRTL parameters for MDEA-H$_2$S system, "H$_2$S-6.5"

Regressed parameters	A or B	value	standard deviation	α	Tau at 40°C	Austgen Model
H$_2$O (C5$^+$ HS$^-$)	A	5.00	0.71	0.2	5.0	7.0
H$_2$O (C5$^+$ HS$^-$)	B / 313K	0	N/A			
(C5$^+$ HS$^-$) H$_2$O	A	-2.625	0.45	0.2	-2.4	-3.2
(C5$^+$ HS$^-$) H$_2$O	B / 313K	0.207	0.42			
(C5$^+$ HS$^-$) MDEA	A	0.0416	0.66	0.1	-4.5	-8
(C5$^+$ HS$^-$) MDEA	B / 313K	-4.588	0.78			
(C5$^+$ OH$^-$) H$_2$O	A	-5.6	N/A	0.2	-5.6	-4
(C5$^+$ OH$^-$) H$_2$O	B / 313K	0	N/A			

Austgen et al. (1991) only regressed the first four parameters listed in Table 6.3. They set the other parameters to defaults of -8 and -4 as shown. Recall also that they set the MDEA-H$_2$O parameters to zero. The electrolyte parameters are correlated to the binary parameters making comparisons between this work and Austgen et al. (1991) less straight forward. It was found that to regress the data satisfactorily when MDEA is not assumed to be ideal, the (C5$^+$ HS$^+$) MDEA parameter must be used. MDEA-H$_2$O systems are known to be highly non-ideal and to have a strong temperature dependence as demonstrated by the high heats of mixing. Therefore, the Austgen parameter set compensated for this error at 40°C where most of the data was, but was unable to also predict correctly at 120°C where data is sparse. Figure 6.16 illustrates that the greatest difference between this model and Austgen et al. (1991) is at 120°C.

Parameter correlation between the electrolyte parameters helps identify relationships between the different species. Table 6.4 shows the correlation matrix for the MDEA-H$_2$S-6.5 parameter set given in Table 6.3. All of the parameters are moderately correlated which indicates that they all have some

effect on model predictions. A correlation of one would indicate that a parameter has been duplicated and can be removed. As occurred for the CO_2 system, the parameters with the highest correlation are the A and B for the same parameter, 2 with 3 and 4 with 5. Moderate correlations also exist between the other important parameters.

Table 6.4 Parameter Correlation matrix for MDEA-H_2S-6.5

	1	2	3	4	5
1	1.00				
2	-0.54	1.00			
3	-0.25	-0.68	1.00		
4	-0.15	0.67	-0.65	1.00	
5	-0.42	-0.32	0.75	-0.83	1.00

Parameter Legend
1 H_2O (C5$^+$ HS$^-$)   A
2 (C5$^+$ HS$^-$) H_2O A
3 (C5$^+$ HS$^-$) H_2O B
4 (C5$^+$ HS$^-$) MDEA   A
5 (C5$^+$ HS$^-$) MDEA   B

6.2.1 Model Predictions

Partial Pressure

Our model generally agrees with Austgen at 40°C and 80°C, but predicts differently at 120°C for 50 wt% MDEA in figure 6.16. This difference comes from a combination of factors such as different amine-water behavior, different pKa of MDEA at T>100°C, different electrolyte-NRTL parameters used in the regression, and a lack of VLE data to determine proper behavior.

152
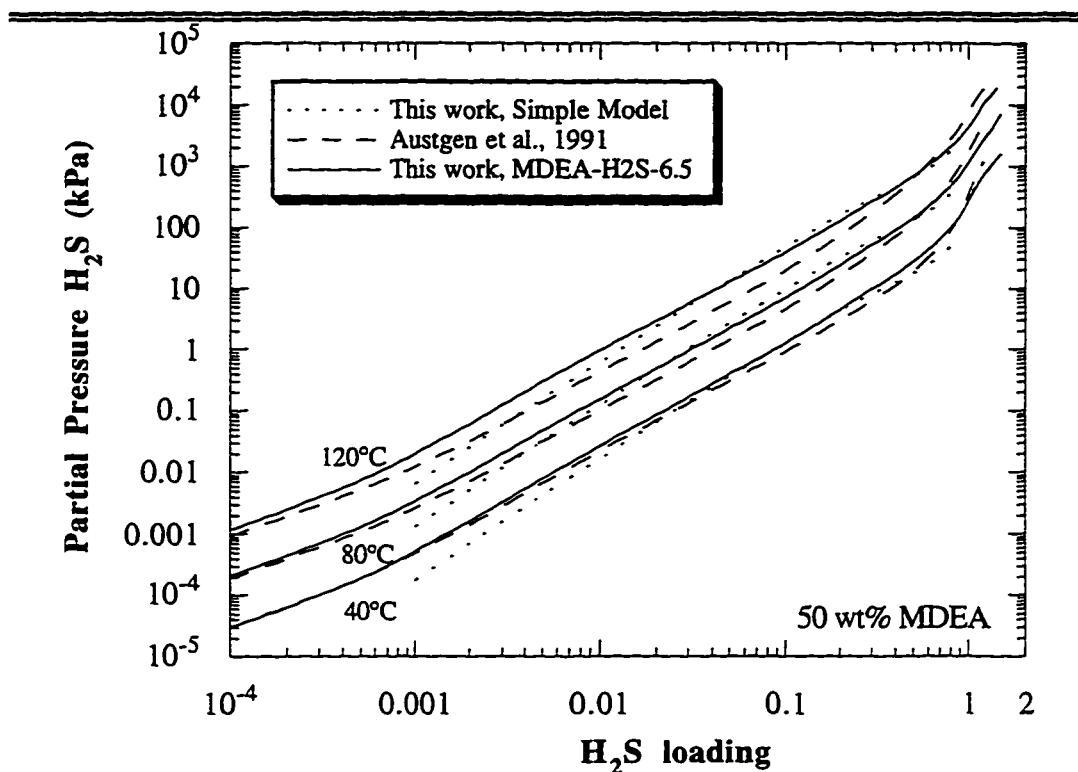
Figure 6.16 Electrolyte-NRTL model predicted H2S partial pressure in kPa by three different parameter sets for a 50 wt% MDEA solution at 40, 80 and 120°C.

From our work with the simple model we have shown that partial pressure in MDEA systems is directly proportional to MDEA concentration. Therefore, we have divided partial pressure by the acid gas free MDEA mole fraction and H2S loading squared and plotted it versus H2S loading. The result is figure 6.17 which can be used to calculate partial pressures in kPa at 40°C for any MDEA concentration.
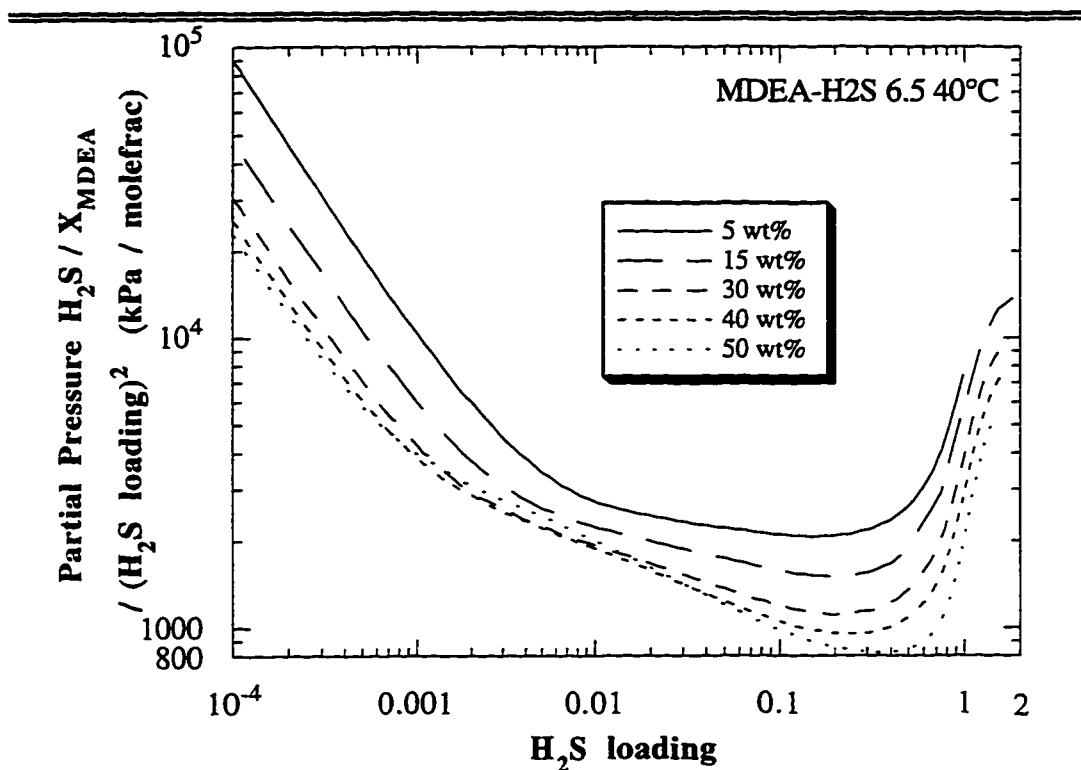
Figure 6.17 Model calculated H_2S partial pressure divided by gas free MDEA mole fraction and the loading squared, as a function of MDEA weight percent in aqueous solutions at 40°C.

Speciation

Solution speciation in H_2S systems is more straight forward than for CO_2 systems. $S^=$ ions are never found in any significant concentrations and do not contribute to the overall H_2S balance. Therefore, speciation as a function of H_2S loading is a straight line with one mole of $MDEAH^+$ and one mole of HS^- being formed for every mole of H_2S added as seen in figure 6.18. The hydroxide parameter that was used for MDEA systems is not acid gas dependent. Therefore, predictions of hydroxide concentration are identical at very low loadings in CO_2

154

and H_2S systems. Properly predicting molecular H_2S concentration has the same difficulties as given for CO_2. No data exists for H_2S that could be regressed to improve predictions beyond the simple Henry's Law solubility for molecular H_2S in acid gas treating solutions.
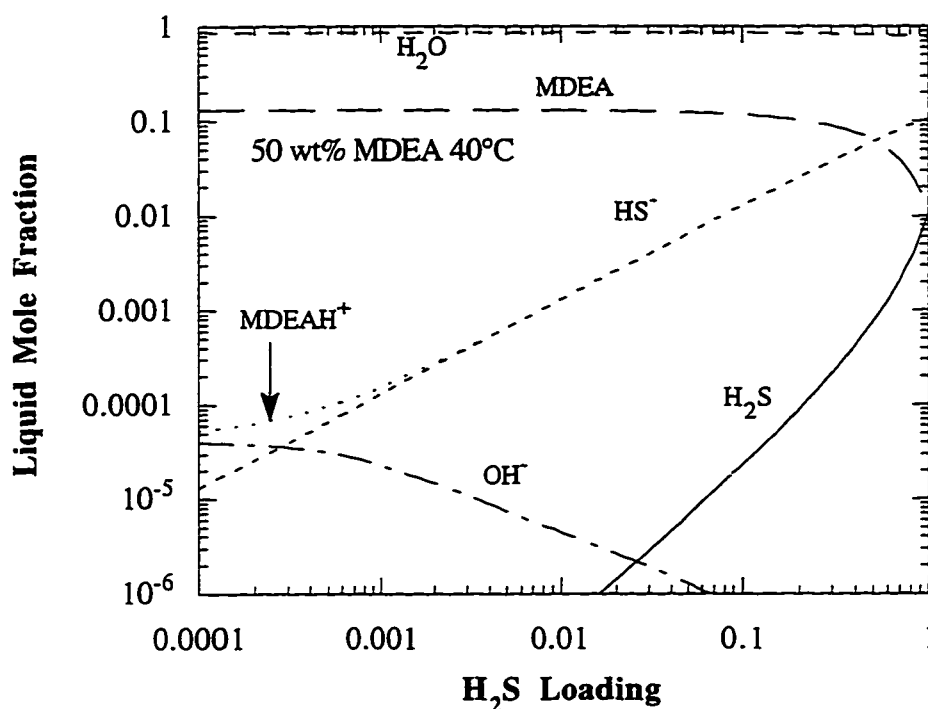
Figure 6.18 Calculated liquid mole fraction concentrations in 50 wt% MDEA at 40°C for the MDEA-H_2S-6.5 electrolyte-NRTL model.

Activity Coefficients

Figure 6.19 below shows the activity coefficient predictions for this work in 50 wt% MDEA at 40°C. Note that the activity coefficients of MDEAH$^+$ and HS$^-$ again are not independent above a loading of 0.001. Note that the H_2S

155

activity coefficient shown here is symmetrically normalized and not the asymmetrically normalized value used for VLE calculations.
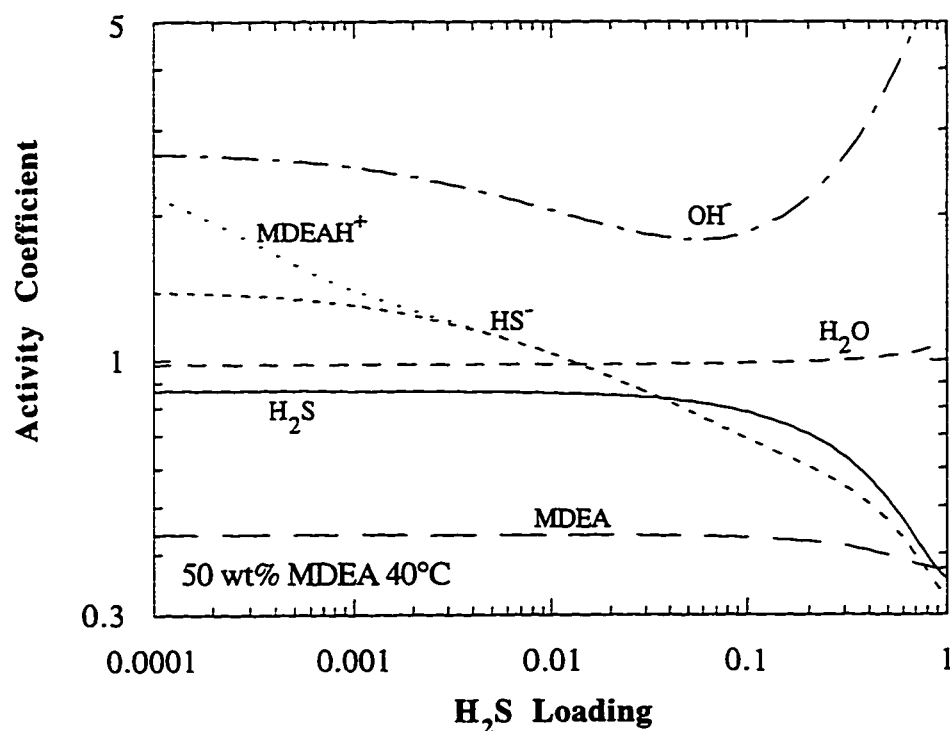
Figure 6.19   Calculated liquid activity coefficients in 50 wt% MDEA at 40°C for the MDEA-H_2S-6.5 electrolyte-NRTL model.

Heat of Absorption

Heat of absorption for the MDEA-H_2S system is somewhat more smooth than the CO_2 system. Calculations from the model were performed based on partial pressure derivatives as given in equation 6.1. Values at high loadings in figure 6.20 do not approach zero as in the CO_2 system. It also appears that the curves do not approach the physical heat of absorption for H_2S of approximately -20 kJ/gmol H_2S. It is believed that model predictions above a loading of 1.0 are

not good and result in the unsmooth behavior. Also unlike the CO_2 system, the curves show a slight H_2S loading dependence in the heat of absorption. The solid line is a simple average of the four temperature curves.
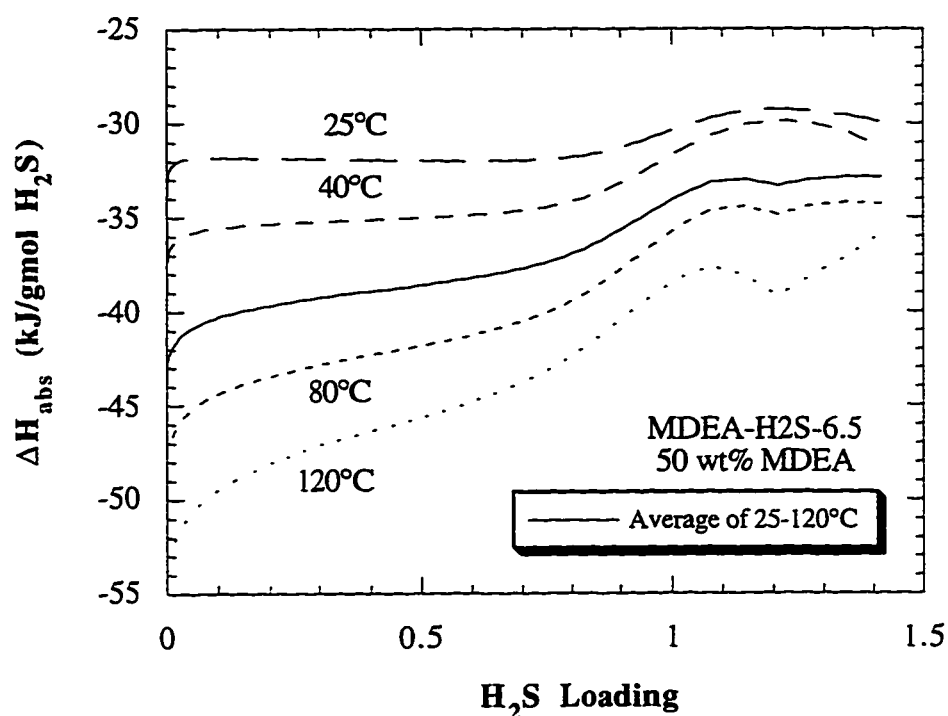
Figure 6.20 Calculated heat of absorption of H_2S into 50 wt% MDEA solutions as a function of temperature and H_2S loading.

The average heat of absorption from figure 6.20 has been compared to values by Jou et al. (1982) calculated from their VLE data and experimental data by Oscarson et al. (1995) in figure 6.21. Note that the Oscarson data does not show trends in amine concentration or temperature within the accuracy of the data. After integration of the heat of absorption curve from this work, agreement is good with the Oscarson data up to a loading of 1.0. If the Jou et al. (1982) were

also integrated, it would very closely match the Oscarson data. However, again note that this work does not approach the physical heat of absorption demonstrated in the Oscarson data. The Jou curve does approaches a more reasonable physical absorption limit than the solid line representing this work.
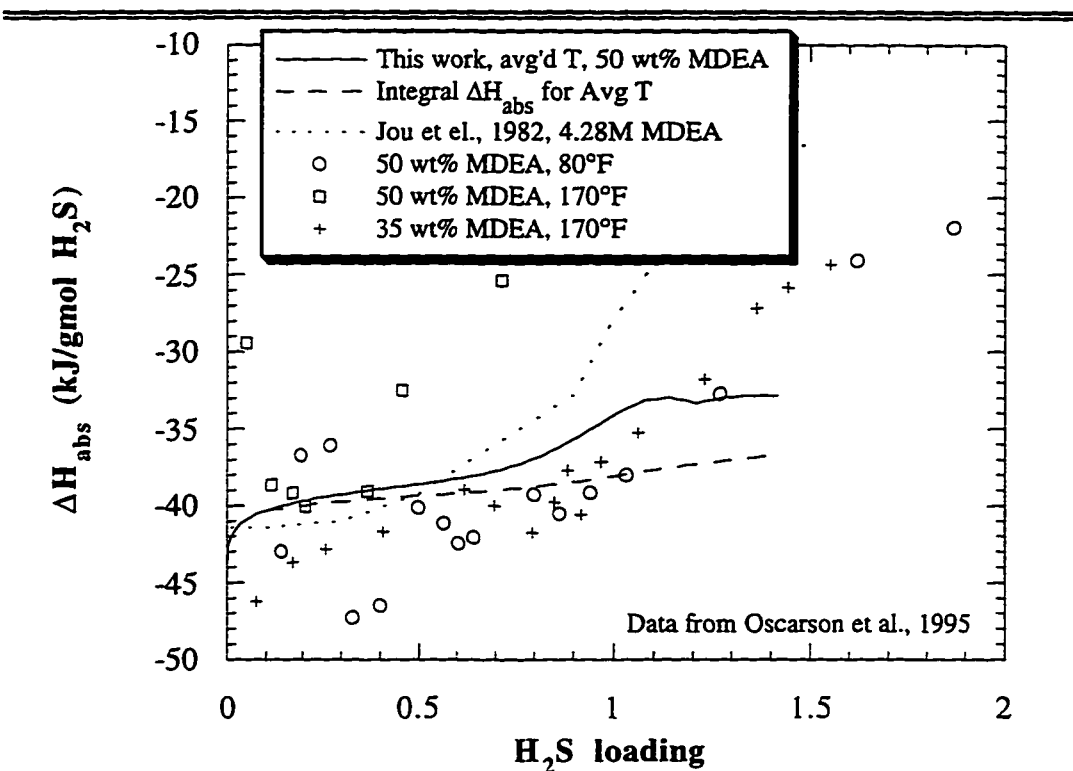
Figure 6.21 Heat of absorption of H_2S into aqueous MDEA solutions calculated from partial pressures compared to experimental calorimetric data.

6.2.2 Unregressed Data

There are three data sets for the MDEA-H_2S system that were not included in the regression and they are compared to the model below in figure 6.22. The Huang and Ng (1995) data was not included because it was known from our simple model work that it would not agree with the data of Jou et al. (1982,

158

1993a). Rather than have the model split the difference between the two data sets, we decided to use only the Jou data, which is available in the open literature and then explore the differences between the data sets.
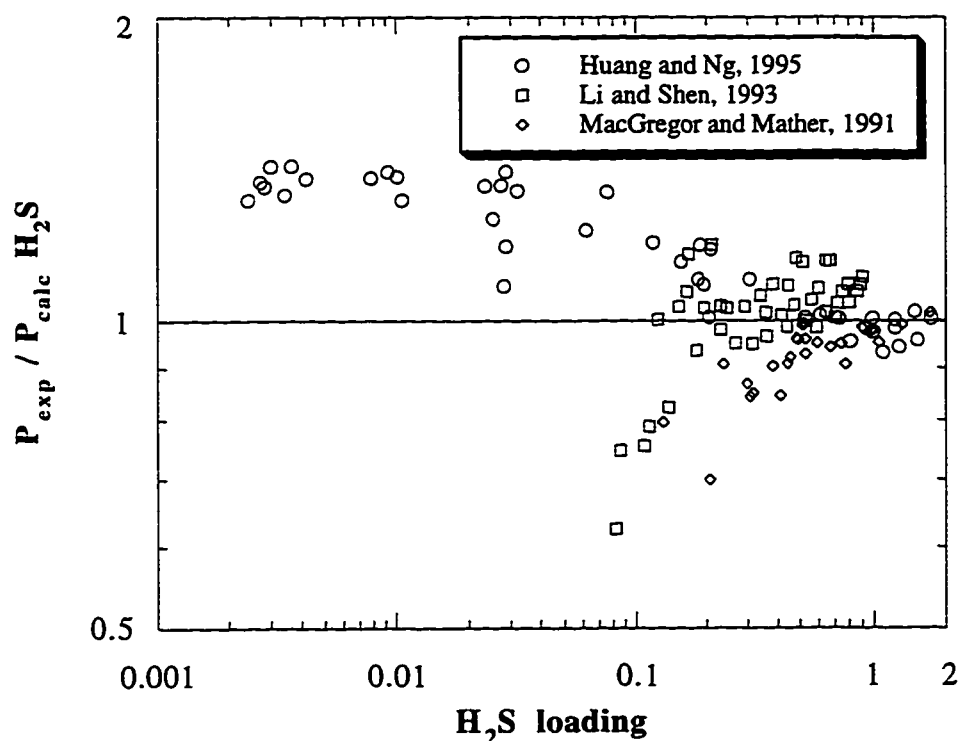
Figure 6.22 Model prediction comparison of H_2S partial pressures for data sets that were not included in the regression of the MDEA-H_2S-6.5 parameters.

A separate regression of the electrolyte parameters was performed on only the Huang and Ng (1995) data. A good fit was obtained by regressing the hydroxide parameter listed in Table 6.1. This set of parameters will be referred to as the Huang model. The main difference is the (C5$^+$ OH$^+$) H_2O parameter which is -4.6 for the Huang and Ng (1995) data compared to -5.6 in this work. Since

there is no way of determining which set of pressure data is correct, we have compared predictions of pH and hydroxide concentration. The Huang model predicts consistently lower pH compared to this work and Austgen et al. (1991) from an H_2S loading of 0.001 to 0.3. These curves are compared against experimental data in figures 6.24 and 6.25. pH predictions are different, unfortunately the curves are close enough that the pH data in this work is not accurate enough to draw a strong conclusion. However, we also compare the hydroxide concentrations in Table 6.6 and the Huang model predicts too little hydroxide consistent with their lower pH. Therefore, it is concluded that the slightly higher partial pressures of the Huang and Ng (1995) data are not correct.

The data of Li and Shen (1993) is shown to deviate significantly from the other data sets and should be scrutinized carefully before use. Data by MacGregor and Mather (1991) seems to follow the same trend as Li and Shen away from the norm of the data. It is unclear why these two data sets exhibit this downward trend in a region where experimental measurements should not be very difficult. It is possible that H_2S was adsorbing onto the walls of their equilibrium cells or analytical devices. This error would be more pronounced in the low pressure, low loading region which is the trend noted in figure 6.22.

Due to the method of this calculation in Aspen Plus™, mole fractions were also assumed to contain error and they were predicted simultaneously. Notice in figure 6.23 that the mole fraction curve is the inverse of the partial pressure plot. By manipulating the mole fractions in the opposite direction, the pressure data appears to fit slightly better than it would if no movement of mole fractions were allowed.
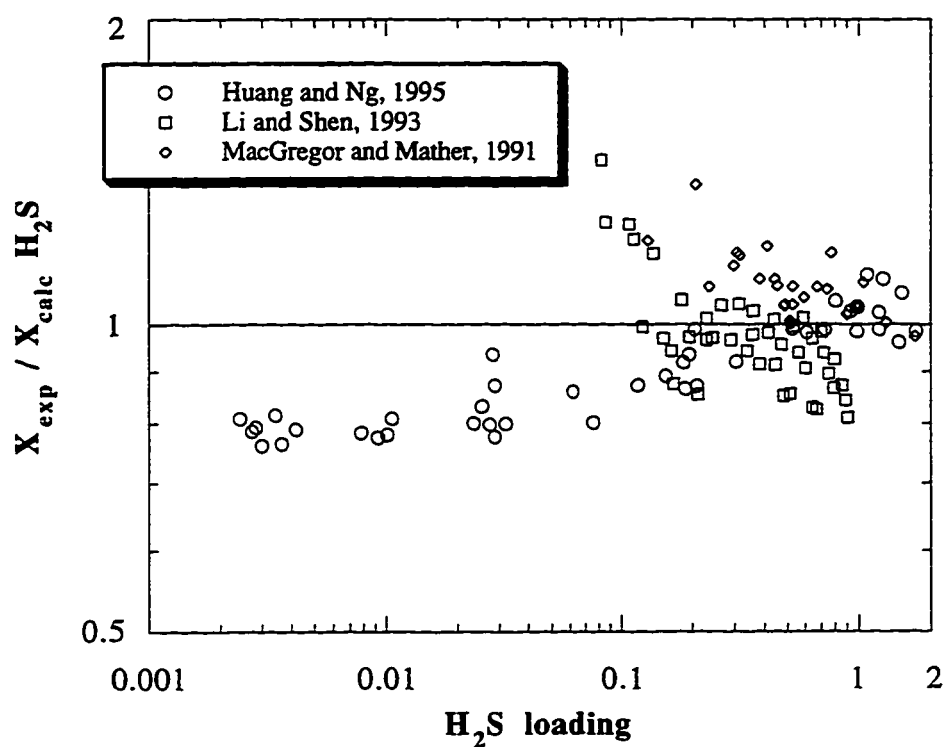
Figure 6.23 Model prediction comparison of H_2S mole fractions for data sets that were not included in the regression of the MDEA-H_2S-6.5 parameters.

6.3 Model Driven Experiments

From work with the simple VLE model described in Chapter 4, it was determined that existing experimental VLE data was not always consistent and did not cover the loading ranges desired for acid gas modeling. VLE data below a loading of 0.01 moles acid gas per mole of amine is sparse and even then exhibits significant variations between experimenters. Therefore, to model the acid gas treating system well at low loading data other than VLE has to be utilized. This approach was demonstrated in Chapter 3 for the binary amine-water systems. Total pressure data was shown to be insufficient for accurate modeling and heat of mixing and freezing point depression data was utilized to improve the overall model.

Unfortunately, the majority of the experimental data collected have been of the pressure-concentration type. Oscarson et al. (1995) measured heat of absorption data for several acid gas systems at a variety of temperatures and amine concentrations. However, the experimental method and data are not of sufficient quality to improve upon the current VLE data set. Therefore, different thermodynamic data was sought that could be accurately measured where VLE data is lacking.

6.3.1 Conductivity

As a method of obtaining more information about low loading conditions, conductivity measurements have been made. Since the conductivity of a solution is directly related to the ionic strength, concentrations of the ionic species can be

inferred. Specifically, the concentration of hydroxide and protonated amine ions were desired.

6.3.1.1 Conductivity Theory

Conductance of a solution holds much more information than simply how much charge can be carried by the solution. Conductance in a solution is created by the movement of ionic species in that solution when placed under a driving force. In the case of conductance measurements, the conductivity probe has small parallel plates across which a high frequency AC voltage is applied. The charge difference between the plates causes the ions to move towards the opposite charged plate. This movement of ions is measured as the electrical resistance of the solution, the inverse of which is conductance. Therefore, ionic species concentrations can be obtained directly from calibrated conductance measurements.

At infinitely dilute concentrations of ions in water the specific ionic conductivities can be assumed to be independent of the presence of the other ions. This is known as the law of independent migration of ions (Atkins, 1986). Equation 6.1 demonstrates the relationship and allows the calculation of any electrolyte conductivity given its constituent ionic molar conductivities at infinite dilution.

$$\Lambda_m^o = v_+ \lambda_+ + v_- \lambda_-$$ (6.3)

Where Λ_m^o is the molar conductivity of the dissociated electrolyte, $S \ cm^2/mol$

S is conductance, siemens ($1 \ S = 1$ mho)

$v_{+ \ or \ -}$ is the stoichiometry of the ion in the molecule, unitless

$\lambda_{+ \ or \ -}$ is the molar conductivity of the ion, $S \ cm^2/mol$

Infinite dilution conductivities in water for the common ions are available in the literature at 25°C (Atkins, 1986; CRC, 1988). Conductivity of an ion is also a function of the ionic concentration. Kohlrausch's Law relates the conductivity to the square root of the concentration as given in equation 6.4. This relationship is only valid for concentrations below an ionic strength of 0.1.

$$\Lambda_m = \Lambda_m^o + K\, C^{0.5} \tag{6.4}$$

where K is a coefficient determined from experimental data

C is the concentration in mol/cm^3

We can also make use of the relationship between conductivity and ionic mobility. The Nernst-Einstein relation describes the correlation between ionic conductivity and diffusion coefficients for the ions. This very powerful equation allows direct calculation of diffusivity from conductivity data.

$$\Lambda_{m\,i}^o = \frac{z^2 F^2 D_i}{RT} \tag{6.5}$$

where $\Lambda_{m\,i}^o$ is molar conductivity of species i, S cm^2/mol

z is the charge number of the ion, unitless

F is Faraday's constant, 9.64846×10^4 C/mol

D is diffusion coefficient, cm^2/sec

R is gas law constant, 8.314 J/gmol-K

T is temperature in Kelvin

It would appear that the units do not cancel. However, they will cancel without the need for additional constant factors once the definitions of coulombs,

C=A sec, and Siemens, $S=A^2$ sec / J, are utilized. Equation 6.5 is used to calculate diffusivities to confirm our experimental conductivity results.

Stokes-Einstein theory (Atkins, 1986) is also very useful in extracting information from conductivity measurements. It states that the ratio of

164

diffusivities between two solutions is inversely proportional to the viscosity ratio to the power of one if hydrodynamic radius and temperature are kept constant.

$$\frac{D_{i\,1}}{D_{i\,2}} = \left(\frac{\mu_2}{\mu_1}\right)^{1.0} = \frac{\Lambda^o_{i\,1}}{\Lambda^o_{i\,2}} \qquad (6.6)$$

This relationship is logical as the diffusivity is expected to decrease in a more viscous solution. Since conductivity is directly proportional to diffusivity, equation 6.6 also shows that conductivity is inversely proportional to viscosity. Many authors have regressed upon experimental diffusivity data a coefficient for the viscosity ratio that ranges from 0.6 to 1.0. Ratios lower than one are due to ionic association and hydrogen bonding effects in amine-water mixed solvents that do not occur in pure water.

6.3.1.2 Probe Calibration

A Yellow Springs Instrument Co. (YSI) Model 32 Conductance Meter was utilized for these measurements. The conductivity cell was a YSI 3417 with a cell constant of 1.0/cm. The meter outputs the conductance of the solution in millimhos or micromhos. In official SI units, mhos are known as siemens, S. This value is then multiplied by the cell constant in 1/cm to derive the conductivity in mho/cm. Temperatures were obtained using a controlled water bath and solution temperatures were measured directly using a thermistor probe which was accurate to 0.01°C.

The conductivity probe and readout were calibrated using 0.1M KCl and 0.1 M NaCl solutions. KCl and NaCl were gravimetrically added into 50 mL volumetric flasks on a scale accurate to 0.0001g. The flasks were then filled to

the appropriate fill line with deionized (DI) water. The solution conductances were measured from 24°C to 40°C as given below in Table 6.5. Literature values for KCl and NaCl were obtained from the YSI (1989) manual, which were acquired from International Critical Tables Vol. 6 (1930) and CRC Handbook 42nd ed. (1961) respectively. The DI water was confirmed not to significantly contribute to the conductivity of the solutions due to its very low ionic strength. The resulting cell constant for the probe is 1.088 ± 0.01 1/cm. Note also that conductivity is affected by fluid dynamics. Therefore, the probe was calibrated in the same physical position and the same beaker in which the experiments were performed.

Table 6.5 Conductivity probe calibration measurements

System	Temp., °C	Conductance, millimhos or millisiemens	Literature Conductivity, mmho/cm or mS/cm	Conductivity Probe constant, 1/cm
DI water	22.62	0.0020		
DI water	39.92	0.0041		
0.1M KCl in DI water	24.24	11.68	12.67	1.08476
0.1M KCl in DI water	40.00	15.35	16.70	1.08795
0.1M NaCl in DI water	24.40	9.62	10.53	1.0946
0.1M NaCl in DI water	39.94	12.89	13.98	1.08456
Average				**1.088 ± 0.01**

6.3.1.3 Analysis Procedure

The conductance is read directly from the meter and conductivity is then obtained by multiplying conductance by the cell constant, 1.088. Tables A.1 to A.7 contain the series of experiments designed to obtain the molar conductivity of $MDEAH^+$, $DEAH^+$, and OH^- ions in typical amine solutions.

First, one can assume that the molar conductivity ratio of K^+ and Cl^- is roughly constant in all solutions because these simple ions do not exhibit

166

significant interactions. From the literature (Atkins, 1986) we have the molar conductivity at infinite dilution of K^+ and Cl^- in water. These and values for other ions are given in Table A.6. Keep in mind that the following calculations have to all be made at the same temperature. The example below was calculated at 25°C.

$$\lambda\,_{K^+}^{H_2O}(\infty) = 73.5\,\frac{mho\text{-}cm^3}{cm\text{-}mol} \quad \lambda\,_{Cl^-}^{H_2O}(\infty) = 76.4\,\frac{mho\text{-}cm^3}{cm\text{-}mol} \tag{6.7}$$

$$R = \left(\lambda\,_{K^+} / \lambda\,_{Cl^-}\right) = 0.962 \tag{6.8}$$

Conductivity of 0.1M KCl is then measured in water. This demonstrates the magnitude of the concentration effect on the conductivity in equation 6.4.

$$\lambda\,_{K^+Cl^-}^{H_2O}(0.1M) = 128.6\,\frac{mho\text{-}cm^3}{cm\text{-}mol} = \lambda\,_{K^+}^{H_2O}(0.1M) + \lambda\,_{Cl^-}^{H_2O}(0.1M) \tag{6.9}$$

Using the ratio, R, from equation 6.8 we can solve for both conductivities in the right side of equation 6.9.

$$\lambda\,_{K^+}^{H_2O}(0.1M) = 63.0\,\frac{mho\text{-}cm^3}{cm\text{-}mol} \quad \lambda\,_{Cl^-}^{H_2O}(0.1M) = 65.5\,\frac{mho\text{-}cm^3}{cm\text{-}mol} \tag{6.10}$$

Conductivity of 0.1M KCl in the amine solution, 49wt% MDEA for this case, is then measured. See Tables A.1 to A.7 for detailed reporting on the measured conductivities. Following the same procedures from equations 6.8 to 6.10, we obtain equation 6.11. This measurement confirms the validity of equation 6.6 relating conductivity ratios to viscosity ratios. Viscosity of 49wt% MDEA is approximately 6.3 times higher than water at 25°C.

$$\lambda\,_{K^+}^{MDEA}(0.1M) = 10.0\,\frac{mho\text{-}cm^3}{cm\text{-}mol} \quad \lambda\,_{Cl^-}^{MDEA}(0.1M) = 10.4\,\frac{mho\text{-}cm^3}{cm\text{-}mol} \tag{6.11}$$

Now that conductivity of K^+ in the amine is known, 0.1M KOH in the amine is measured. Using the K^+ value from 6.11, the hydroxide conductivity is determined.

$$\lambda\,_{K^+OH^-}^{MDEA}(0.1M) = 24.3 = \lambda\,_{K^+}^{MDEA}(0.1M) + \lambda\,_{OH^-}^{MDEA}(0.1M) \tag{6.12}$$

$$\lambda \, ^{MDEA}_{OH^-} (0.1M) = 14.3 \, \frac{mho\text{-}cm^3}{cm\text{-}mol} \tag{6.13}$$

Note that equation 6.6 holds for K^+ and Cl^-, but it does not hold for associating ions such as OH^- and $amineH^+$ especially at concentrations above infinite dilution. An amine solution is then completely neutralized with HCl and diluted with water to a concentration of approximately 0.0005M. The conductivity of this solution is then measured and assumed to contain only $MDEAH^+$ and Cl^- ions. Knowing the Cl^- conductivity in water, the $amineH^+$ value in water is obtained.

$$\lambda \, ^{H_2O}_{MDEAH^+Cl^-} (\infty) = 127.3 = \lambda \, ^{H_2O}_{MDEAH^+} (\infty) + \lambda \, ^{H_2O}_{Cl^-} (\infty) \tag{6.14}$$

$$\lambda \, ^{H_2O}_{MDEAH^+} (\infty) = 50.9 \, \frac{mho\text{-}cm^3}{cm\text{-}mol} \tag{6.15}$$

Since no significant interactions occur at infinite dilution, the viscosity ratio from equation 6.6 is applied to obtain the protonated amine conductivity in the amine solution.

$$\lambda \, ^{MDEA}_{MDEAH^+} (\infty) = \frac{50.9}{6.3} = 8.08 \, \frac{mho\text{-}cm^3}{cm\text{-}mol} \tag{6.16}$$

Most conductivities were to decrease by a factor of two from 0.1M to infinite dilution in 49 wt% MDEA. This factor is applied to the value in equation 6.13 and on combining with equation 6.16 the conductivity of the pair is obtained.

$$\lambda \, ^{MDEA}_{MDEAH^+OH^-} (\infty) = 8 + 28 = 36 \, \frac{mho\text{-}cm^3}{cm\text{-}mol} \tag{6.17}$$

Finally, conductance of an amine-water solution at the desired amine concentration is measured and divided by the molar conductivity to obtain the ionic concentrations after some conversions. Contributions to the conductivity from impurities and the water itself must be subtracted from the solution conductivity at this point.

168

$$C = \frac{K_{MDEAH^+OH^-}}{\lambda_{MDEAH^+OH^-}^{MDEA}} = \frac{0.0515 \text{ E-3 mho/cm}}{36 \frac{\text{mho-cm}^3}{\text{cm-mol}}} = 1.43 \text{ E-6 mol/cm}^3 \qquad (6.18)$$

$$X_{OH^-} = \frac{1.43 \text{ E-6 mol/cm3} * 1000 \text{ cm3/L} * 0.1313}{4.38 \text{ M MDEA}} = 4.2 \text{ E-5} \qquad (6.19)$$

It is important to note that absorbed CO_2 can greatly affect accuracy of the results. Therefore, care must be taken to exclude CO_2 or to accurately quantify its presence and subtract its contribution to conductivity. CO_2 loadings above 0.0001 begin to mask conductivity contributions from the basicity of the amine.

Another measurement which serves as a comparison to other amines is the conductivity of the amine infinitely dilute in water. The various amines can then be compared and the validity of equation 6.6 for protonated amines can be verified. Conductivity from lowest to highest is DEA < MEA < MDEA. Atkins (1986) stated that movement of an ion is related to its hydrodynamic radius. It is postulated that the methyl group on MDEA prevents hydration by water and therefore results in a lower effective radius for MDEA than the other two amines. DEA would be expected to be less mobile than MEA due to its larger size and molecular weight.

Another difficulty in analyzing conductivity measurements at high concentrations is ionic association. Cations and anions can pair up by association and not contribute to conductivity. This results in molar conductivities being overpredicted and is one of the major sources of experimental uncertainty. The difficulty lies in the fact that the degree of association is an unknown function of ionic strength.

169

6.3.1.4 Results and Discussion

Following the analysis procedure above, we arrive at a molar conductivity for ($MDEAH^+OH^-$) of 36 ± 5 mho-cm^3/cm-mol at 25°C and 65 ± 5 at 40°C, infinitely dilute in 49 wt% MDEA solutions. Using the values of the molar conductivity for $MDEAH^+$ and OH^- the mole fractions of these ions in a 49 wt% MDEA solution can be estimated.

The CO_2 loading of the first 49 wt% MDEA run was measured at 0.00018. A correction has been applied to this data set to account for the additional conductivity. Given all of the assumptions above, the hydroxide mole fraction has been calculated to be approximately (4.2 ± 2.0) E-5 at both 40°C and 25°C. This small difference is due to the fact that the measured conductivity increased by a factor of two while the molar conductivity of $MDEAH^+OH^-$ also increased by a factor of two.

Table 6.6 compares the calculated hydroxide mole fraction in 50 wt% MDEA solutions from the conductivity experiments compared to three sets of electrolyte-NRTL parameters. Our current CO_2-7.13 model is an improvement over the other models because its hydroxide parameter has been moved to fit the hydroxide mole fraction at 40°C in a 50 wt% MDEA solution. More conductivity data would be required to improve the predicted temperature dependence of the hydroxide concentration in Table 6.6. Parameters by Austgen et al. (1991) predicted the values calculated from the conductivity experiments fairly well without adjustments. The predictions of hydroxide mole fraction from the Huang

model described above are consistently lower than the other models and the experimental data.

Table 6.6 Calculated hydroxide mole fraction concentration in 50 wt% MDEA solutions

Conditions	Conductivity	Austgen	CO2-7.13	Huang
50 wt% 25°C	(4.2±2.0)E-5	5.0E-5	2.6E-5	1.4E-5
50 wt% 40°C	(4.2±2.0)E-5	6.0E-5	4.1E-5	1.9E-5
50 wt% 120°C	N/A	9.0E-5	2.0E-4	4.1E-5

Equation 6.5 illustrated how conductivity is related to diffusivities. We have taken the infinitely dilute conductivities of $MDEAH^+$ and $DEAH^+$ in 49 wt% MDEA and 29 wt% DEA, respectively, from Table A.7 and calculated their diffusivities. These values for the protonated amines are compared to literature data for the molecular amines in the same solutions at the same temperatures. There could be a difference in the diffusivity of the amine versus its protonated counterpart, however they are usually assumed to be equal. Diffusivities in MDEA agree very well with data by Snijder et al. (1993) at 25°C and 40°C. Values presented for Snijder were obtained from his equations describing diffusivity as a function of temperature and amine concentration. Calculations for DEA agree very well with Thomas and Furzer (1962) at 25°C, but are approximately 40% lower than values by Snijder et al. (1993). Therefore, the conductivities in the concentrated amines are confirmed to be roughly accurate and equation 6.5 is shown to be appropriate.

Table 6.7 Calculated diffusion coefficients from the Nernst-Einstein relation
compared to experimental data

	Diffusion Coefficient, cm^2/sec		
Conditions	This work	Snijder et al. (1993)	Thomas and Furzer (1962)
49 wt% MDEA, 25°C	2.14 E-6	2.3 E-6	
49 wt% MDEA, 40°C	4.03 E-6	3.8 E-6	
29 wt% DEA, 25°C	3.27 E-6	4.52 E-6	3.4 E-6
29 wt% DEA, 40°C	4.64 E-6	6.56 E-6	

6.3.2 pH

pH by definition is directly related to the activity of hydronium ions and indirectly related to all of the other species activities. pH data supplements VLE data as another source of thermodynamic information to be used in modeling. Unfortunately, very little pH data exists for acid gas loaded solutions. This data is somewhat difficult to collect due to the loss of the absorbed gases. Collecting this data can also be dangerous in the case of H_2S systems. However, an alternative method to using dangerous H_2S is to use an analogous acid such as hydrochloric acid (HCl). For the Amine-H_2S systems, we can assume that its pH behavior is similar to the Amine-HCl system at equal acid loadings. Since none of the species are volatile, this experiment can be easily completed by standard wet chemistry techniques. By this analogy we can perform the much easier pH titrations of amine solutions and infer the thermodynamics in the Amine-H_2S system. This analogy will not work for CO_2 systems at low loadings due to the second dissociation of H_2CO_3. Therefore, a few measurements have been made using CO_2 as the acid titrant.

6.3.2.1 pH Theory

The pH measurement system was originally defined for use in aqueous systems using molality concentrations. pH_m is defined as the negative base ten logarithm of hydronium ion activity where concentrations are in molality.

$$pH_m = -\log[a_{H_3O^+}] \qquad (6.20)$$

However, this work utilizes the mole fraction scale and the following conversion can be applied to convert between molality and mole fraction based pH values.

$$pH_m = pH_x - 1.7447 \qquad (6.21)$$

Calculations of pH_x in this work were made by calculating the pOH_x, then applying the relationship in equation 6.22 for the equilibrium constant of water.

$$pH_x = pK_w - pOH_x \qquad (6.22)$$

Our model, however, includes the activity of water in the equilibrium constant given in equation 2.38 below.

$$K_{mw} = \frac{a_{OH^-} \, a_{H_3O^+}}{a_{H_2O} \, a_{H_2O}} \qquad (2.38)$$

Therefore, in 50 wt% MDEA solutions at high loading, calculated pH_m can be as much as 0.2 pH units higher than experimental pH_m data. This difference between the two methods approaches zero as the acid gas loading and amine concentration approach zero. In general, the difference in not including the activity of water was less than the experimental uncertainty in the data.

6.3.2.2 Experimental Procedures

Titrate Solution Preparation

Approximately 100g of a 50 wt% MDEA solution was prepared gravimetrically with vacuum distilled, deionized water on a scale accurate to

±0.0001 g. The MDEA, CAS No. 105-59-9, was from Huntsman Chemical and was called "JeffTreat® M" lot #305224A. The stock MDEA concentration was found to be 98.0 ± 0.5 wt% MDEA by titration with standard 1M HCl and the remaining 2% was assumed to be water. The stock amine purity was determined after the following experiments were performed and the actual amine concentration was propagated throughout our calculations. This explains why the experiments are carried out at 49 wt% instead of the intended 50 wt% MDEA.

The prepared 49 wt% MDEA solution was placed in an Erlenmeyer flask and subjected to a light vacuum for several minutes to remove any dissolved gases. In general, bubbles were seen leaving the solution and the vacuum was removed when the evolution stopped.

HCl Titrant Preparation- 2/12 & 2/16 experiments

The following procedure applies to acid titrant preparation for the experiments listed in Table B.1 and B.2 only. The acid titrant concentration was chosen such that the desired loading range would be covered while using a maximum of 5 mL of acid. This minimizes the change in amine concentration resulting from the water added with the acid. Even with this procedure, the acid-free amine concentration changed from 49 wt% to approximately 46 wt% at the end of the titration for the 2/12 and 2/16 experiments. The dilute HCl titrant was prepared volumetrically using a 36.5 wt% stock hydrochloric acid and vacuum distilled DI water. The concentration of the stock acid was determined to be 11.658 N by titration with a standard NaOH solution from Fisher. The density of the concentrated acid was measured to be 1.1644 ± 0.0009 g/mL.

174

Titrant Solution Preparation-remaining experiments

The maximum desired acid loading was determined first. Then, a titrant solution was made that contains approximately 2 times the desired final solution acid loading. For example, if a final acid loading (mol acid/mol amine) of 0.1 in a 50 wt% MDEA (acid-free basis) solution is desired, a clean 50 wt% MDEA solution would be titrated with a 0.2 loaded 50 wt% solution. Therefore, the acid free MDEA concentration remained constant at 50 wt% and pH measurements were made as the acid loading is increased. A vacuum was pulled on these titrant solutions before the experiment since they have the capacity to absorb CO_2.

6.3.2.3 pH Calibration and Measurement

A new Fisher "AccupHast" pH electrode was used for the experiments listed in Tables B.1 through B.7. The data in Table B.8 was measured using a new Corning pH probe, cat. no. 476531, which was similar to the previously used probe. The readout was a Corning model 130 with slope, intercept and temperature calibration knobs. The probe was calibrated in standard pH 7 and pH 10 buffer solutions at room temperature or 40°C depending on the experimental temperature. The temperature compensation was set to the experimental temperature before the calibrations at that temperature were performed.

The amine solution was continuously stirred and the pH probe remained submerged in the solution throughout the experiments. Attempts were made to limit the atmospheric exposure of the solutions, but the experiment was by no means air tight. The titrant was added incrementally by volume using a 25mL burette with 0.1mL graduations. The experiment was carried out in a temperature

175

controlled water bath and the actual solution temperature was monitored. Table 6.4 archives the MDEA experimental conditions. An equivalent table is given in Chapter 7 for the DEA experiments. Some of the solutions were analyzed for CO_2 content before and/or after the experiment. Procedures for liquid CO_2 analysis can be found in the dissertation by Mshewa (1995).

Table 6.8 MDEA titration experimental conditions neutralized with HCl or CO_2

date	solution temperature	acid free amine wt%	CO_2 ldg before exp.	CO_2 ldg after exp.	acid ldg range
HCl					
2/12/96	22 to 28°C	48.8 - 46.4	N/A	0.00011	0.001 - 0.1
2/16/96	~22°C	48.8 - 45.7	N/A	N/A	0.0001 - 0.01
2/21/96	~22°C	48.97 ±0.03	N/A	N/A	0.01 - 1
3/25/96	25.53 - 25.70	48.89±0.05	N/A	0.00018	0.0001 - 0.01
3/27/96	39.48 - 40.65	48.95	N/A	0.00021	0.0001 - 0.01
4/5/96	39.97 - 41.15	48.96	0.00011	0.00020	0.001 - 0.1
CO_2					
8/19/96	~22	49	0.0001	0.279	0 - 0.28

6.3.2.4 Results and Conclusions

Recall from Chapter 4, figure 4.3, that two distinctly different data sets exist at low loading for the MDEA-H_2S system. In an attempt to reconcile the differences between the Jou et al. (1982, 1993a, 1994) and Huang and Ng (1995) data sets, an electrolyte-NRTL parameter set was regressed upon the Huang data only. Plots of calculated partial pressure match the upward trends seen in figure 4.3. pH was then calculated for this "Huang only" parameter set and compared with the current model, Austgen et al. (1989) and the experimental data.

Figure 6.24 illustrates that we cannot conclude which data set is correct based on the current pH data. The Huang curve does not include any correction for a CO_2 loading of 0.0002 and therefore would predict a slightly lower pH at

lower loadings. A CO_2 loading of 0.0002 was typical of the CO_2 absorption during the experiment and therefore is assumed applicable to those experiments where CO_2 content was not quantified. After a CO_2 correction is applied to the Huang model, the present model would best agree with the data at loadings between 0.0001 and 0.001. No strong conclusions can be made on the overall validity of the Huang data from figure 6.24. Note that the Austgen curve has "over-corrected" for the CO_2 loading and it is believed that his model predicts the presence of too much $CO_3^=$.
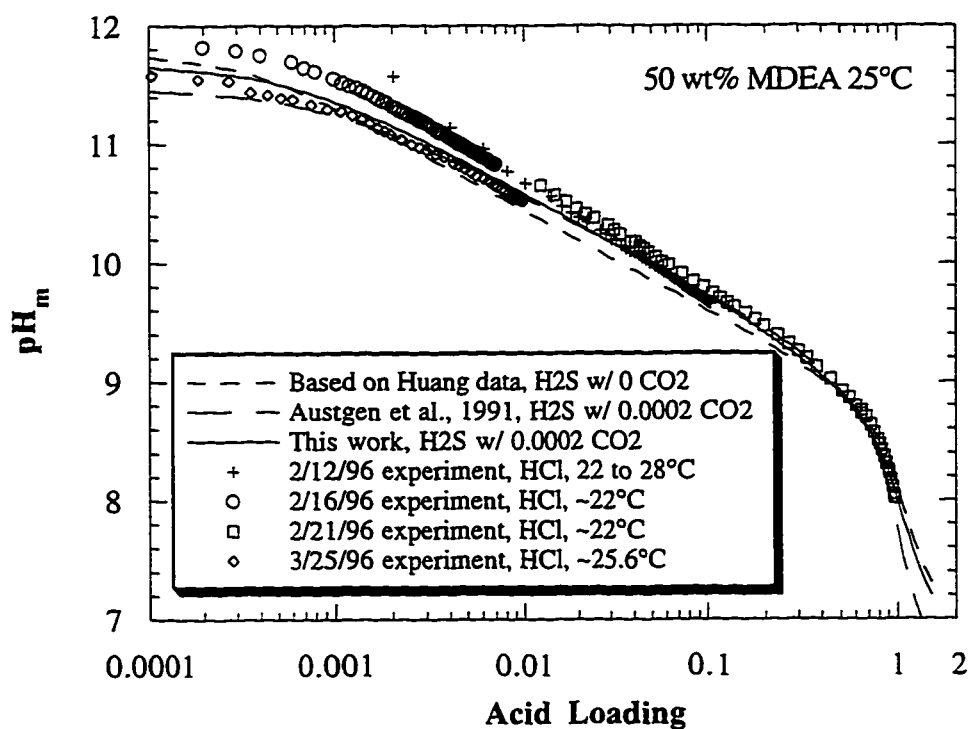
Figure 6.24 pH predicted by the electrolyte-NRTL model for three different
MDEA parameter sets for a 50 wt% MDEA solution at 25°C
compared to four experimental data sets.

177

Figure 6.25 for 40°C shows even smaller differences between the models and the data. This leads to several conclusions for the MDEA-H_2S system. One being that models with different pressure predictions can predict the same pH behavior. This is due to the correlation between mole fractions and activity coefficients in the hydronium activity. This can limit the ability to use pH data as a tool for comparing VLE data sets.
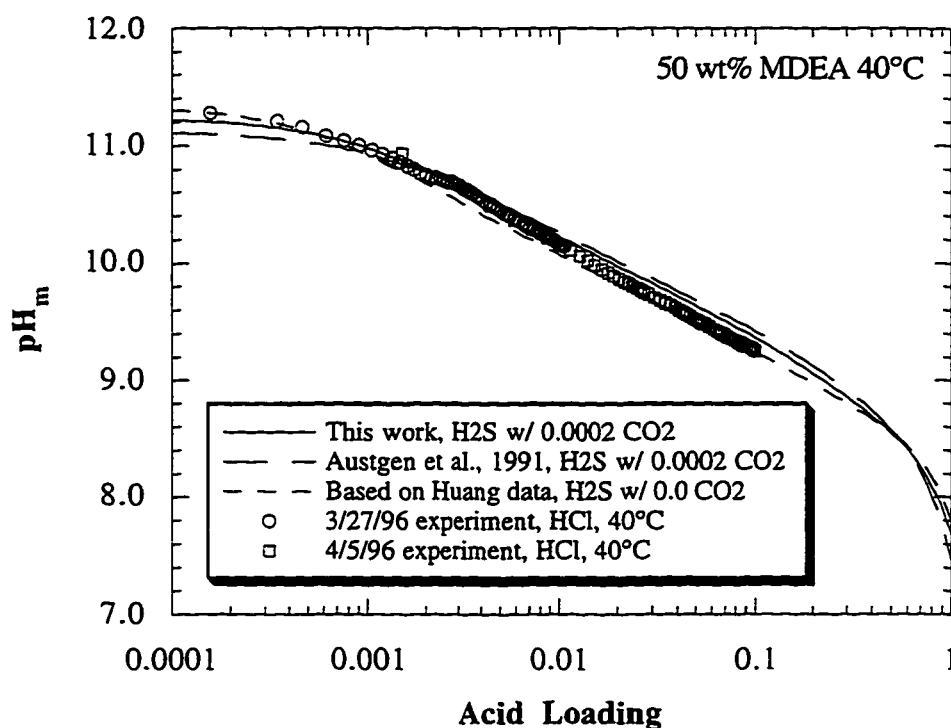
Figure 6.25 pH predicted by the electrolyte-NRTL model for three different MDEA-H_2S parameter sets for a 50 wt% MDEA solution at 40°C compared to two experimental data sets.

Another conclusion is that this model is properly predicting pH data. Therefore, with this model pH data can be used as a simple measurement

technique in the field for determining acid gas loading. A final conclusion is that our HCl-H$_2$S analogy is correct with respect to pH measurements.
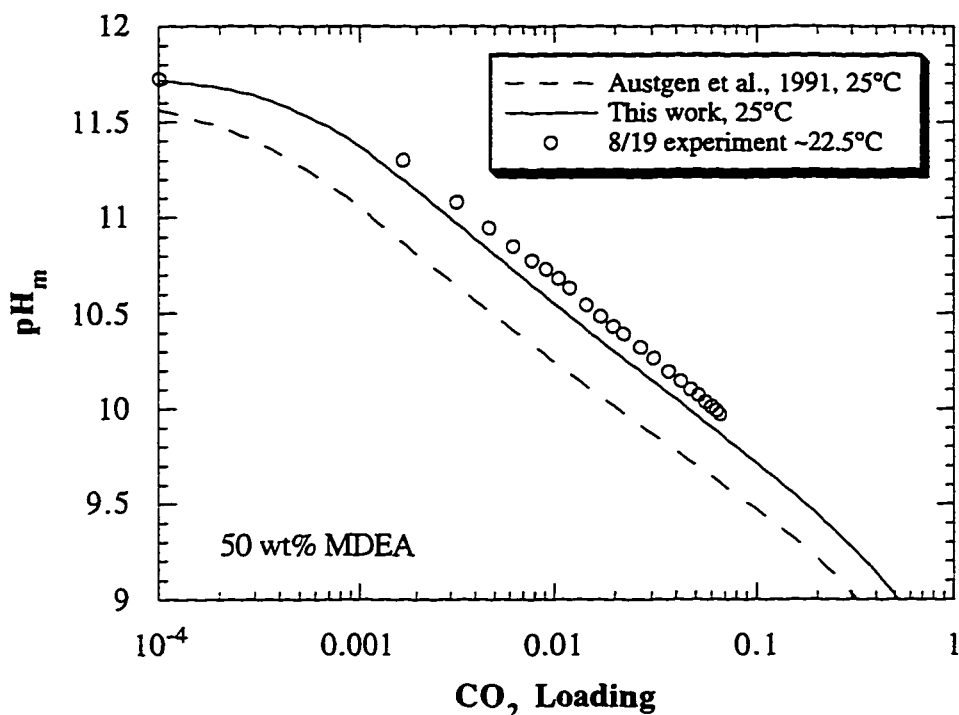
Figure 6.26 pH predicted by the electrolyte-NRTL for MDEA-CO$_2$ for a 50 wt% MDEA solution at 25°C compared to experimental data that varied from 22.3 to 23.3°C.

A different situation exists for the MDEA-CO$_2$ system. Speciation for CO$_2$ systems is more complex than H$_2$S systems since the second dissociation of CO$_2$ to CO$_3^=$ is significant at low loadings. Even though the equilibrium constants are known, due to the activity coefficients CO$_3^=$ concentration can vary widely.

Figure 6.26 compares electrolyte-NRTL model predictions at 25°C of this work and Austgen et al. (1991) against experimental data. The Austgen model predicts

179

much lower pH which corresponds to its higher $CO_3^=$ compared to this work.

Note also that Austgen et al. (1991) did not regress any parameters specific to $CO_3^=$ while the present work has. Both models have the proper slope, but this work fits the data with much more accuracy. If predictions were made at 22°C instead of 25°C, this work would coincide with the data and Austgen would still be significantly different.

6.4 MDEA-CO$_2$-H$_2$S

6.4.1 Data Comparisons

Many authors have stated that mixed gas equilibria can be predicted from the component single acid gas models. This work also concludes that mixed acid gas data can be reasonably predicted from accurate single acid gas parameter sets. Parameters from the "MDEA-CO$_2$-7.13" and "MDEA-H$_2$S-6.5" systems have been combined into a single Aspen input file so that calculations can be made for the MDEA-CO$_2$-H$_2$S system. It is imperative that all of the parameters, including the default values, be specified exactly as listed in this work since the default parameters have changed in version 9.0 of Aspen Plus™. When making calculations for this MDEA mixed gas system, the combined parameter set is referred to as "7.13/6.5" or variations upon these two numbers.

Predictions of unregressed data for the mixed acid gas system are performed exactly as they were for the single acid gas systems, with one exception. Since there are now two components contributing to acid gas partial pressure, the pressure ratio in figure 6.27 is the total acid gas partial pressure ratio. Also similar to the single acid gas calculations, error is assumed in both partial

pressure and acid gas mole fractions. Predicted acid gas mole fractions are given in figure 6.28 and 6.29 as a function of the total acid gas loading.
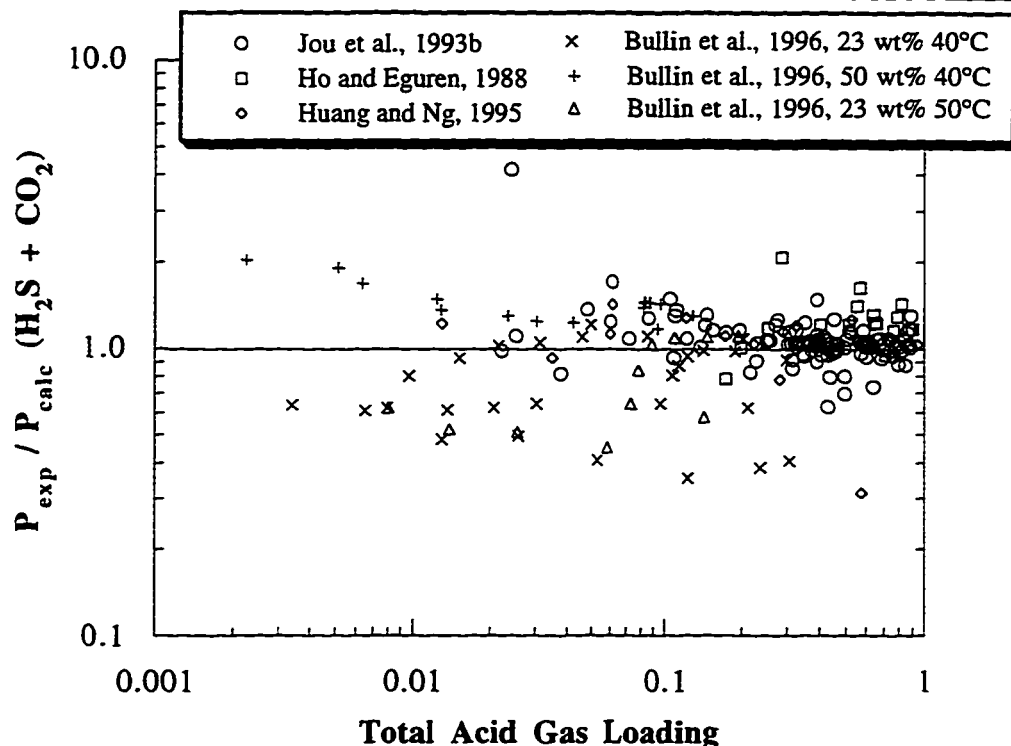
Figure 6.27 Ratio of experimental to model predicted total acid gas partial pressures as a function of total acid gas loading for the combined MDEA-CO_2-7.13-H_2S-6.5 parameter set. Mole fractions were simultaneously predicted.

Most of the data is fit well and is centered around 1.0. The Bullin et al. (1996) data which exists at the lowest loadings also exhibits the greatest scatter of the data sets. Actual scatter of the Bullin data is reduced by fitting of the CO_2 mole fractions. Figure 6.28 shows that some the Bullin data has significant errors in the predicted CO_2 mole fractions. The three Bullin data "sets" contain within each of them several distinct data series. This explains why some of the 23 wt%

181

40°C and 23 wt% 50°C data is fit very well and disagrees by a factor of two or three. It is believed that CO_2 was not at equilibrium in these discrepant data series. The Jou et al. (1993b), Ho and Eguren (1988) and Huang and Ng (1995) data sets were all predicted very well by the model considering no new parameters were utilized for the mixed acid gas predictions. The upward trend of the Huang data seen in the MDEA-H_2S system is not evident here.
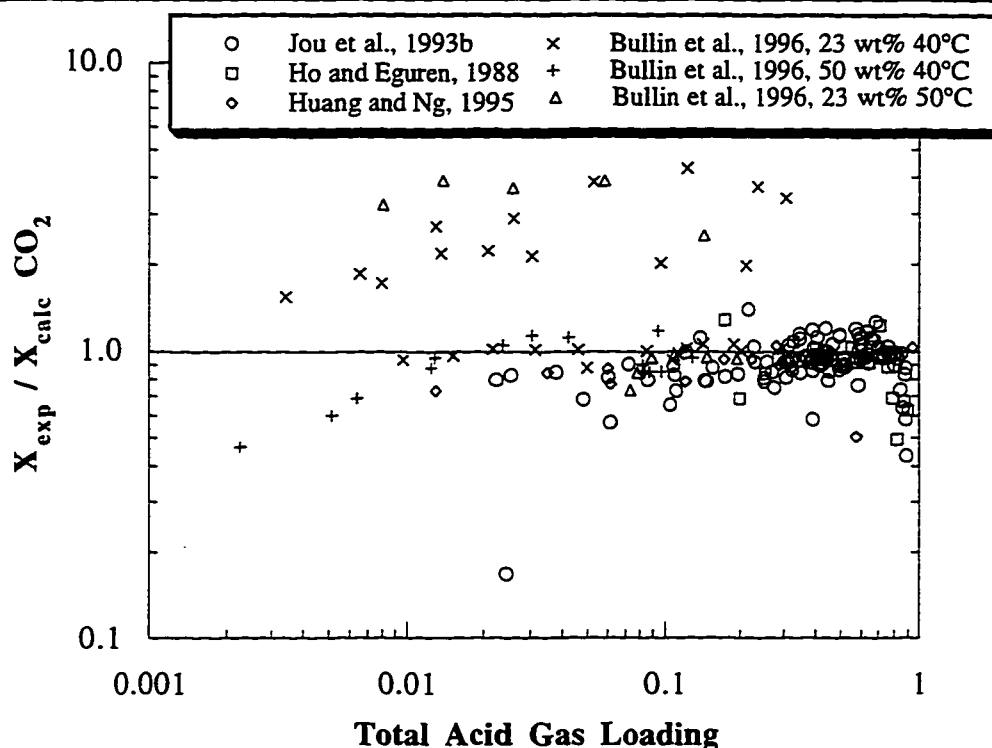
Figure 6.28 Ratio of experimental to model predicted CO_2 mole fractions as a function of total acid gas loading for the combined MDEA-CO_2-7.13-H_2S-6.5 parameter set. Acid gas partial pressures were simultaneously predicted.

Figure 6.29 shows that, in general, H_2S mole fractions were fit more closely than were CO_2. Again, some of the Bullin data series are fit well while

others deviate significantly from a perfect fit of 1.0. All of the data sets are predicted within a factor of two in H_2S mole fraction.
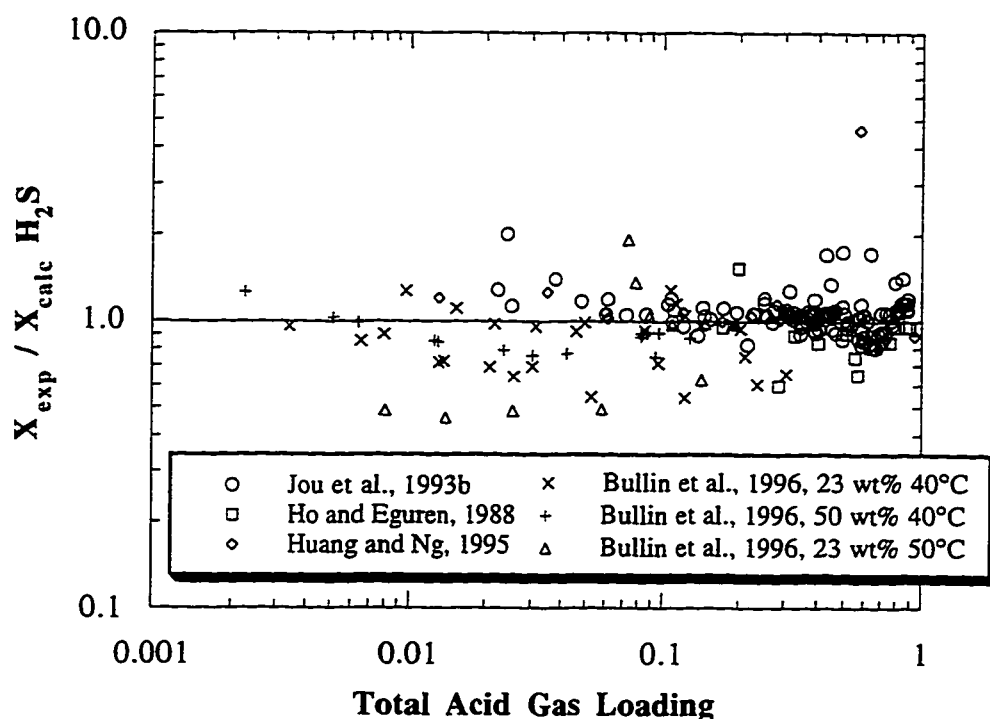
Figure 6.29 Ratio of experimental to model predicted H_2S mole fractions as a function of total acid gas loading for the combined MDEA-CO_2-7.13-H_2S-6.5 parameter set. Acid gas partial pressures were simultaneously predicted.

6.4.2 Model Predictions

The following four figures are given as useful tools for determining approximate acid gas partial pressures in the mixed acid gas MDEA system. Calculations were made using the Aspen input file given in Appendix D. In a mixed acid gas system the partial pressures are a function of both acid gas loadings. However, the curves can be collapsed by normalizing the acid gas

183

value is then plotted versus total loading and figure 6.30 shows the results for 50

wt% MDEA at 40°C. By normalizing we can now read H_2S partial pressure

versus many different CO_2 loadings on a single plot. In addition, the number of

decades in pressure on the y-axis have been reduced improving readability of the

plot.
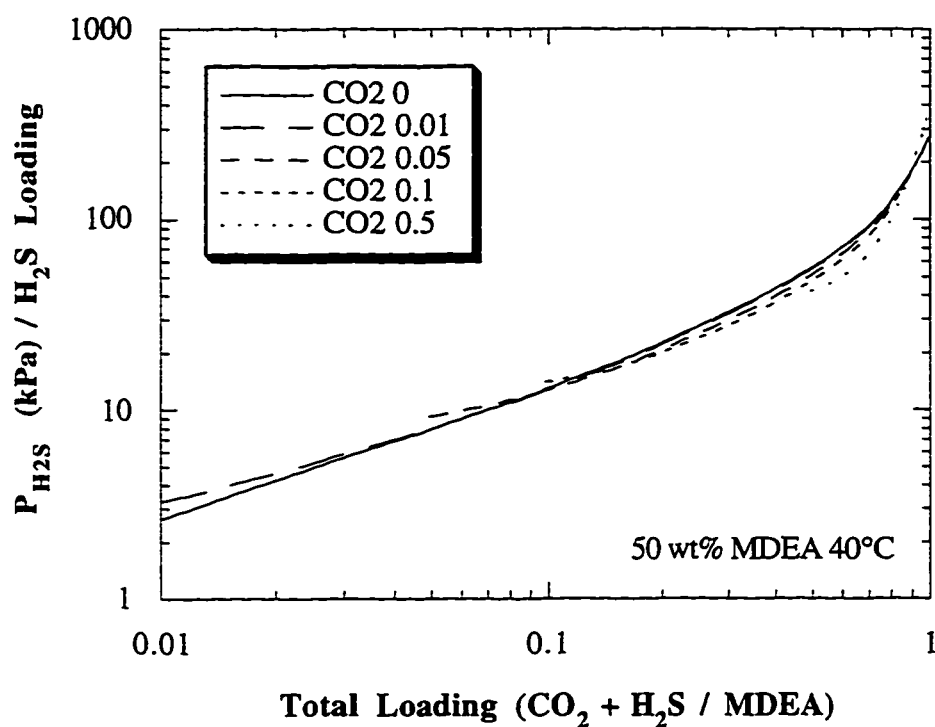
Figure 6.30 H_2S partial pressure in kPa divided by the H_2S loading, calculated
from the combined MDEA-6.5-7.13 model parameters. CO_2
loadings remained constant for each curve in 50 wt% MDEA
solutions at 40°C.

Normalization of the 50 wt% MDEA plot at 120°C did not produce as consolidated of a single line as with the 40°C plot. It does, however, still collapse a good region of the plot and reduce the decades on the y-axis. Some of the reason for the failure of the normalization at 120°C is that it does not account for the appreciable concentrations of molecular acid gases at the higher loadings. It might also be a result of the carbonate/bicarbonate buffer occurring at low loadings.
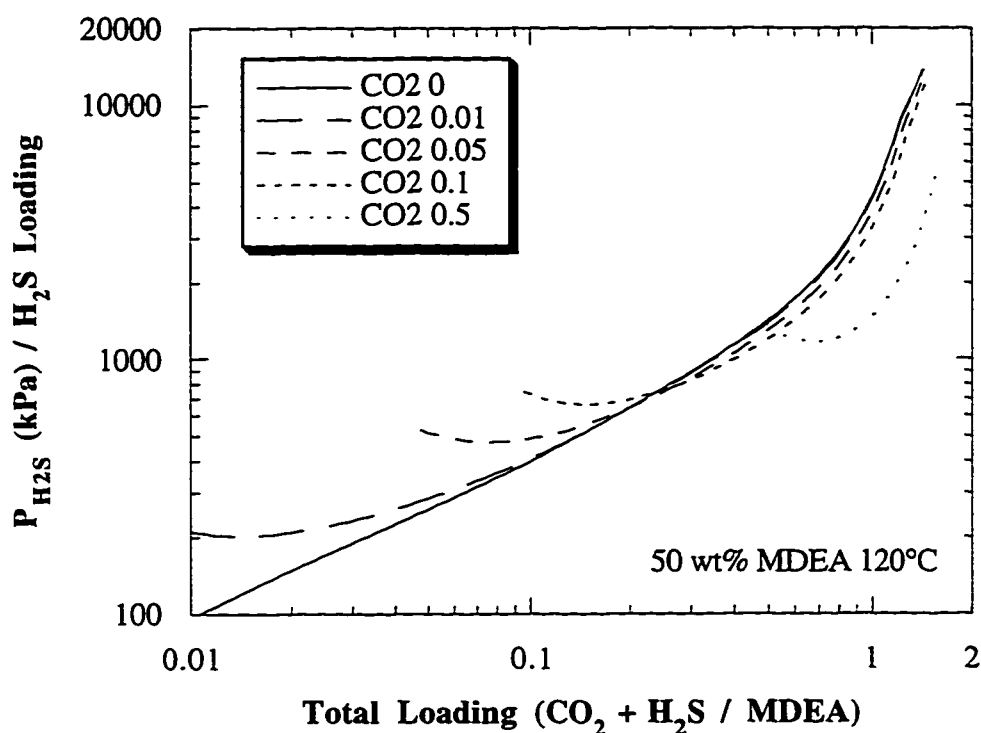
Figure 6.31 H_2S partial pressure in kPa divided by the H_2S loading, calculated from the combined MDEA-6.5-7.13 model. CO_2 loadings remained constant for each curve in 50 wt% MDEA solutions at 120°C.

185

CO_2 partial pressures also collapsed nicely onto a single line when pressure in kPa was divided by the CO_2 loading at 40°C. Comparing figure 6.32 to 6.30 demonstrates why MDEA is used for selective removal of H_2S. In addition to having a slower rate of reaction with CO_2 compared to other amines, MDEA is more thermodynamically favorable for H_2S than CO_2. Values for normalized H_2S pressure vary from 3 to 200 while CO_2 pressures vary from 5 to 1000 over the same loading range.
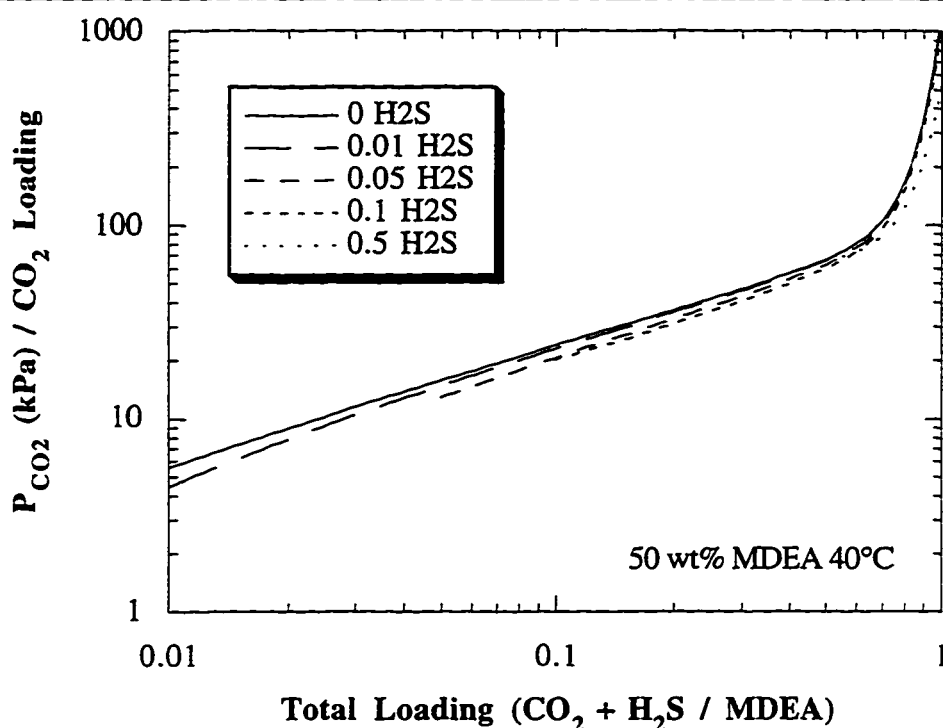
Figure 6.32 CO_2 partial pressure in kPa divided by the CO_2 loading, calculated from the combined MDEA-6.5-7.13 model. H_2S loadings remained constant for each curve in 50 wt% MDEA solutions at 40°C.

186

Partial pressure of CO_2 at 120°C in 50 wt% MDEA collapsed the least of the four presented curves. It does, however, still reduce the orders of magnitude in the y-axis to improve readability.
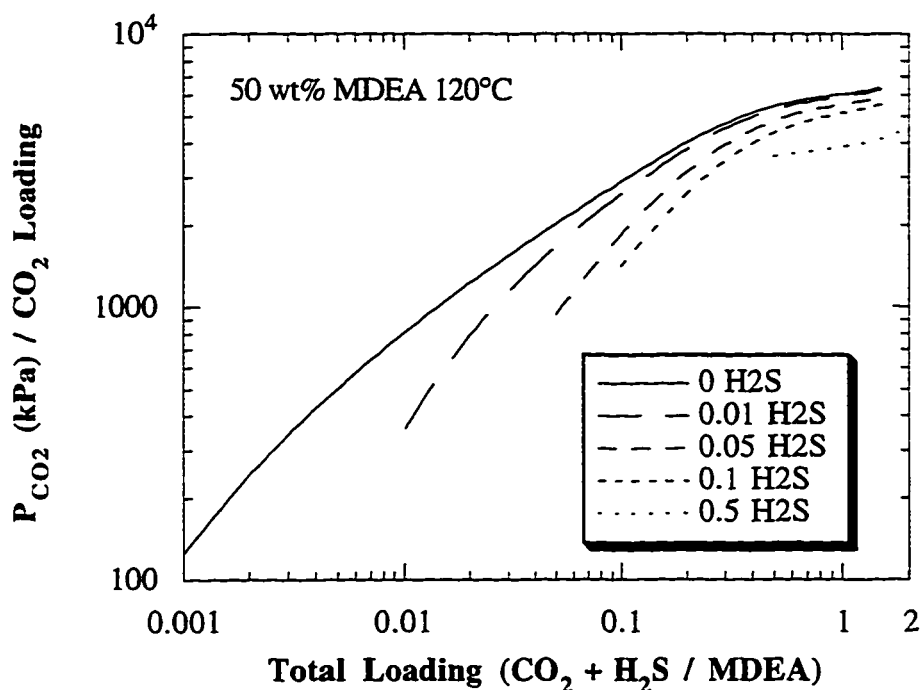
Figure 6.33 CO_2 partial pressure in kPa divided by the CO_2 loading, calculated from the combined MDEA-6.5-7.13 model. H_2S loadings remained constant for each curve in 50 wt% MDEA solutions at 120°C.

6.5 CONCLUSIONS

The model for the $MDEA-H_2S-CO_2$ system begins with a strong underlying amine-water model. Rather than assuming the $MDEA-H_2O$ system to be ideal, we have utilized freezing point and heat of mixing data to improve our predictions of MDEA activity coefficient in aqueous MDEA solutions. MDEA activity coefficients are important not only in the acid gas VLE calculations, but also are required to calculate the amount of amine in the vapor phase. Amine losses from the top of the absorber are an important operational consideration and only with good values of the MDEA activity coefficients can they be accurately quantified.

After improving the amine-water model, the equilibrium constant for the reaction of MDEA with H_2O was improved. Heat of reaction data has been used to improve the temperature extrapolation of the equilibrium constant past the previous upper limit of 60°C. Values for the pKa of this reaction are different from previously reported values at temperatures greater than 100°C.

This work has also utilized a unique set of parameters from the electrolyte-NRTL model. The choice of parameters stems from experience with the model, sensitivity studies of Chang (1992), and from necessity to properly fit the experimental data. First, VLE data was regressed to determine parameters for the high loading regions. Predictions at acid gas loadings lower than where VLE data exists were improved by manipulating the hydroxide parameters to match results from conductivity experiments. The models were also confirmed to be correct in the low loading region by comparison to pH data.

188

Partial pressure predictions of this model generally agree with Austgen et al. (1991) at 40°C and 80°C, except for the CO_2 system below a loading of 0.001. The discrepancy is due to a much lower carbonate concentration being predicted in this work compared to Austgen. The actual carbonate concentration is most likely slightly less than predicted by Austgen and on the order of 10^{-6} at low loading in 50 wt% MDEA at 40°C. Independent measurements of the bicarbonate to carbonate ratio in aqueous amines would help clear up the discrepancy. However, calculations of pH in this work much more closely match experimental pH data for the MDEA-CO_2 than does Austgen et al. (1991). Pressure predictions in this work at 120°C are higher than predicted by Austgen due to our different MDEA activity coefficients and lower pKa at temperatures greater than 100°C.

A discrepancy exists for the MDEA-H_2S system at low loading. Data from Huang and Ng (1995) predicted higher partial pressures than data by Jou et al. (1982 & 1993a). The Huang data was analyzed using the electrolyte-NRTL model. Predictions of pH and hydroxide concentration appear to be slightly low, leading us to conclude that the partial pressure data of Huang and Ng (1995) is slightly too high.

Speciation predictions for the model seem to be reasonable for moderate and low loadings. However, the inconsistent reference state for acid gas molecules leaves some concern at high loadings. The model will still predict pressures properly, but the incorrect reference state will affect the calculated acid gas molecular concentrations. The reader is cautioned in using speciation predictions from this model, especially for the acid gases, at high loadings and amine concentrations.

Partial pressure predictions for the MDEA-H_2S-CO_2 system agree well with unregressed mixed acid gas data. It is concluded that good predictions can be made by combining the single acid gas parameters into a single model. Most of the data by Ho and Eguren (1988), Jou et al. (1993b) and Huang and Ng (1995) was fit very well by the model. Some of the data by Bullin et al. (1996) was fit very well and some not very well. For some of the data sets it appeared that CO_2 equilibrium had not been reached.

Overall, a model has been developed for the MDEA-H_2S-CO_2 system which is improved over previously existing models. Predictions for the MDEA-H_2O system are the most accurate to date due to the use of thermodynamic data in addition to total pressure data. The model fits all of the vapor-liquid equilibria data very well. In addition, we have improved model predictions and our understanding of low loading behavior by using conductivity data. Finally, the model is shown to predict partial pressures for the mixed acid gas system very well without the need for additional parameters.

Chapter 7: Diethanolamine and MDEA-DEA Systems

Diethanolamine (DEA) has long been used in acid gas treating systems. It originally served as a replacement to monoethanolamine (MEA) due to its lower corrosivity and vapor pressure. Like MEA, DEA reacts directly with CO_2 to form a carbamate species. The ability to quickly react with CO_2 has led DEA into a supporting role of "fine tuning" absorption of CO_2 in MDEA systems. By varying the ratio of DEA to MDEA a solution can be customized to the desired CO_2 removal given a specific acid gas feed stream. While meeting the CO_2 outlet specifications is important, excessive removal of CO_2 is costly and can hinder H_2S absorption.

Given the continued importance of DEA in acid gas treating, this chapter first covers equilibrium in the DEA-H_2S and DEA-CO_2 systems. Figures and discussions show that we have obtained a good model. Our DEA-H_2S model is similar to that of Austgen et al. (1989). The predictions for the DEA-CO_2 system also agree with Austgen et al. (1989) at 40°C, but differences between the two increase with temperature at low loading. Reasons for the differences and our predictions are further discussed.

Our resulting parameter sets are then combined with the MDEA parameter sets from Chapter 6 to form a complete MDEA-DEA-H_2S-CO_2 model. No additional parameters are regressed and predictions using the combined parameter set are compared to literature VLE data. Figures are then given allowing the reader to predict acid gas VLE in the mixed amine, mixed acid gas systems.

191

7.1 DEA-H₂S

Much more data exists for the DEA-H_2S system as compared to the MDEA-H_2S system. We have fit VLE data from five sources to the electrolyte-NRTL model. Table 7.1 lists our resulting parameters and some unregressed parameters are also listed for clarity. Parameters with "N/A" for the standard deviations were not regressed with the Aspen DRS. Tau values have been calculated at 40°C for this work and for that of Austgen et al. (1989) and are compared in the last two columns of Table 7.1. The last two parameters were set to default values of -8 in the parameter sets by Austgen. The values for those parameters in this work are less negative than the defaults. Due to the negative correlation between parameter 1 and 4, (DEAH⁺ HS⁻) DEA increases while H_2O (DEAH⁺ HS⁻) decreases. Therefore, these two seemingly different parameter sets can predict the same due to parameter correlation.

Standard deviations for the parameters must be viewed on a relative and not absolute basis. Therefore, the B parameters and their standard deviations given in Table 7.1 have been divided by 313K so that all parameters can be compared on the same order of magnitude. Standard deviations can also be compared between parameters to determine which are the most sensitive to the data regressed. A small standard deviation indicates that the parameter was very important in obtaining a good fit of the data.

192

Table 7.1 Electrolyte-NRTL parameters for DEA-H₂S system, "DEA-H₂S-6.3"

Regressed parameters	A or B	value	standard deviation	α	This work 40°C	Austgen 40°C
H_2O (DEAH⁺ HS⁻)	A	7.766	0.292	0.2	7.8	10.1
H_2O (DEAH⁺ HS⁻)	B / 313K	0	N/A			
(DEAH⁺ HS⁻) H_2O	A	-3.328	0.183	0.2	-3.9	-4.9
(DEAH⁺ HS⁻) H_2O	B / 313K	-0.591	0.111			
(DEAH⁺ HS⁻) DEA	A	-4.132	0.356	0.1	-5.4	-8
(DEAH⁺ HS⁻) DEA	B / 313K	-1.275	0.35			
(DEAH⁺ OH⁻) H_2O	A	-5.75	N/A	0.2	-5.8	-8
(DEAH⁺ OH⁻) H_2O	B / 313K	0	N/A			

Table 7.2 Parameter correlation matrix for the DEA-H₂S-6.3 parameter set

	1	2	3	4	5	6
1	1.00					
2	-0.85	1.00				
3	0.32	-0.77	1.00			
4	-0.43	0.56	-0.48	1.00		
5	0.00	-0.21	0.38	-0.90	1.00	
6	0.13	-0.11	0.04	0.09	-0.12	1.00

Parameter Legend

1 = H_2O (DEAH⁺ HS⁻)   A
2 = (DEAH⁺ HS⁻) H_2O A
3 = DEAH⁺ HS⁻) H_2O B
4 = (DEAH⁺ HS⁻) DEA   A
5 = (DEAH⁺ HS⁻) DEA   B
6 = (DEAH⁺ OH⁻) H_2O A

Table 7.2 is the resulting parameter correlation matrix which provides insight into the relationships and dependencies between the parameters. The (DEAH⁺ OH⁻) H_2O parameter was originally regressed, which is why it is included in Table 7.2 as the sixth parameter. However, the parameter value has been fit outside of the Aspen DRS to our measurements of hydroxide concentration and therefore a standard deviation is not provided for it in Table

193

7.1. Conductivity experiments to obtain the hydroxide concentration are discussed in section 7.3. The very low correlation of the hydroxide parameter to the others justifies the assumption that a complete refit of the data with the new hydroxide parameter is not necessary. It also illustrates that the hydroxide parameter is not sensitive to VLE data and therefore cannot be determined from it.

High correlations are noted and expected between the two components of each tau parameter, 2 with 3 and 4 with 5. There also tends to be significant correlation between parameters that are the reverse of one another. Parameters 1 and 2 have a correlation coefficient of 0.85 in Table 7.2.

7.1.1 Data Regression

Data used to regress parameters for the DEA-H_2S system is much more scattered than the MDEA data. Lal et al. (1985) state that errors in their data become large at low loadings and our preliminary analysis of their complete data set confirmed this. Therefore, the Lal et al. data set was reduced such that only data above an H_2S loading of 0.021 were used. H_2S partial pressure was predicted within ±30% as shown in figure 7.1 and none of the data sets were seen to deviate consistently from the norm. Mole fraction of H_2S was fit at the same time and comparisons to model predictions are given in figure 7.2. Mole fractions are predicted well with an error of ±20%. Resulting parameters are given in Table 7.1 and are analogous to the MDEA-H_2S system.

194
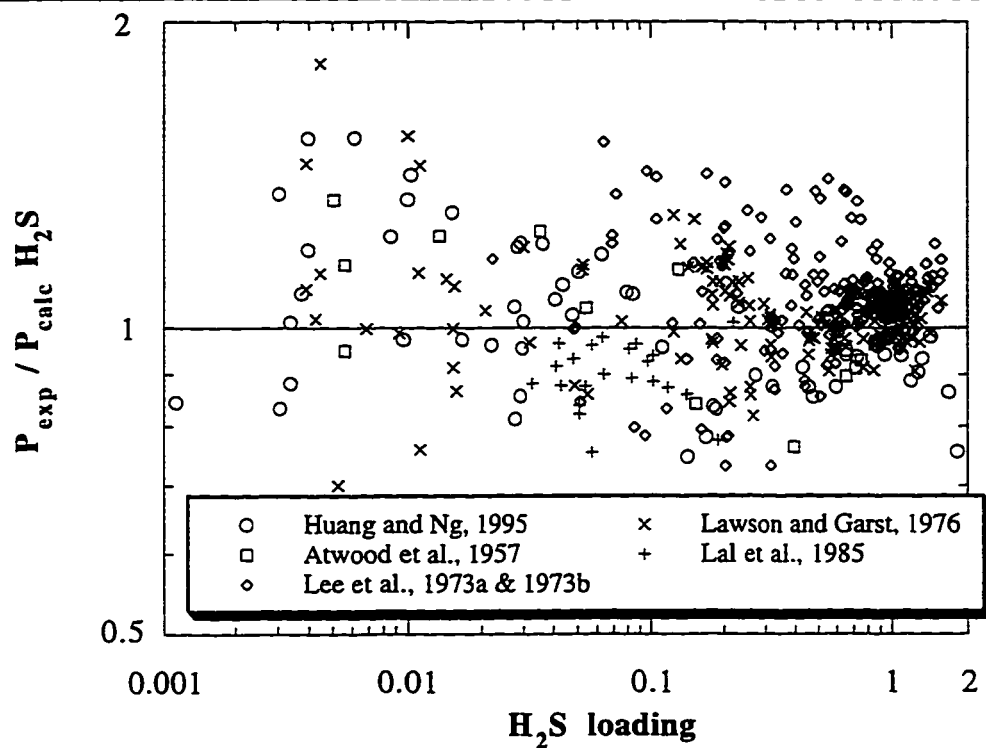
Figure 7.1 Ratio of experimental to model predicted H_2S partial pressures as a function of H_2S loading for the DEA-H_2S-6.3 parameter set. Mole fractions were simultaneously fit.

195
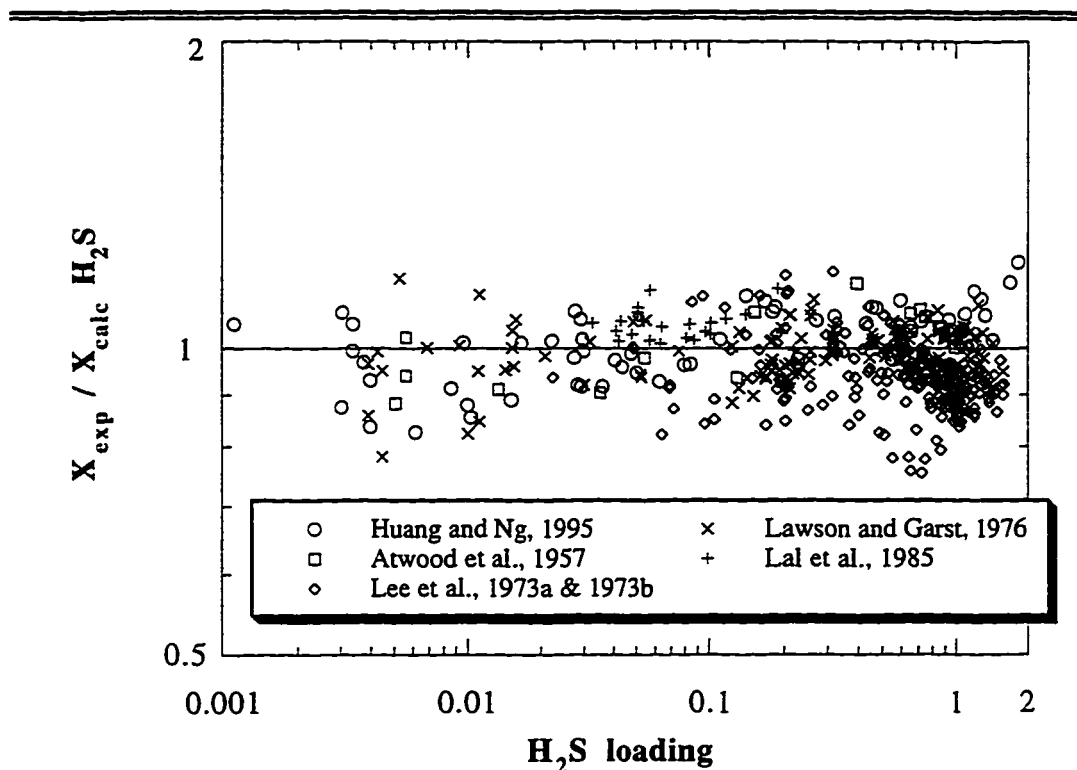
Figure 7.2 Ratio of experimental to model predicted H2S mole fractions as a
function of H2S loading for the DEA-H2S-6.3 parameter set. Partial
pressures were simultaneously fit.

7.1.2 Model Predictions

Partial Pressures

Model parameters from Table 7.1 have been utilized to make calculations
with the electrolyte-NRTL model. Parameters from Table 7.1 must be used with
our previously reported DEA-H2O parameters, Henry's law equations and
equilibrium constants. This work, Austgen et al. (1989) and the simple model
from this work agree very well at loadings above 0.01 (figure 7.3).

196
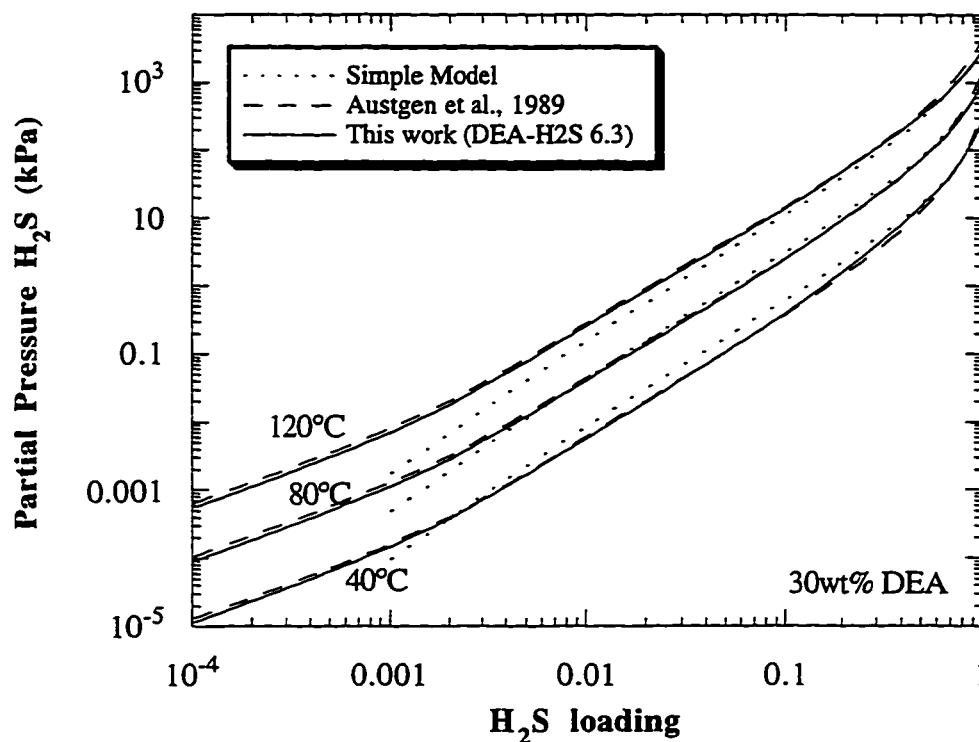
Figure 7.3 H$_2$S partial pressure predicted by the electrolyte-NRTL model with two different parameter sets for a 30 wt% DEA solution at 40, 80 and 120°C.

The electrolyte models continue to agree to lower loadings where the simple model does not account for hydroxide reactions. This work therefore corroborates the Austgen DEA-H$_2$S model. It also shows that different parameter sets can predict the same partial pressure behavior. Austgen et al. (1989) accounted for non-idealities in DEA-H$_2$O which is one reason the DEA-H$_2$S models predict much closer than the MDEA-H$_2$S models do as shown in figure 6.3.

Equilibrium analysis concludes that, to a first approximation, H_2S partial pressure is directly proportional to the amine concentration (Austgen, 1989). Therefore, if the partial pressure is normalized by the acid gas free amine concentration, then calculated pressures at different amine concentrations will collapse onto a single line. Figure 7.4 demonstrates these assumptions hold and allow the reader to calculate H_2S partial pressure at 40°C at any amine concentration and H_2S loading.
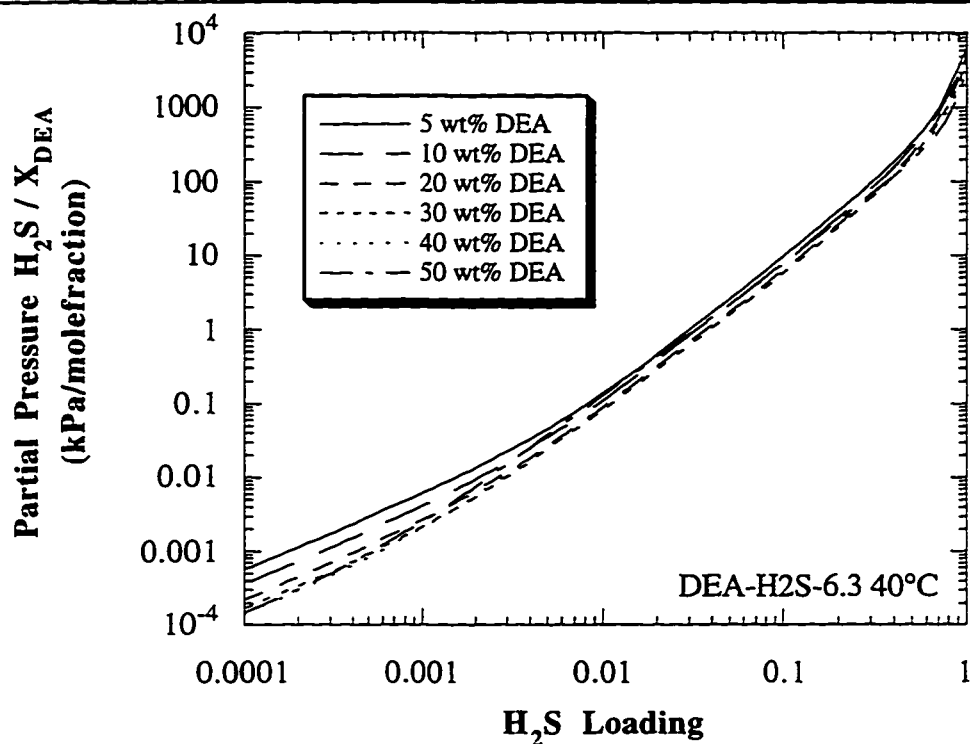
Figure 7.4 H_2S partial pressure in kPa divided by the acid gas free DEA mole fraction at 40°C for the DEA-H_2S-6.3 model.

Speciation

An important result from rigorous equilibrium modeling is the ability to predict liquid species concentrations. Figure 7.5 plots the liquid phase mole fractions of the important species in a 30 wt% DEA solution at 40°C. The interesting areas of the graph are where the hydroxide ion and bisulfide ion change roles as the dominant anion. This corresponds with the change in slope of the partial pressure plots at an H_2S loading of approximately 0.003.
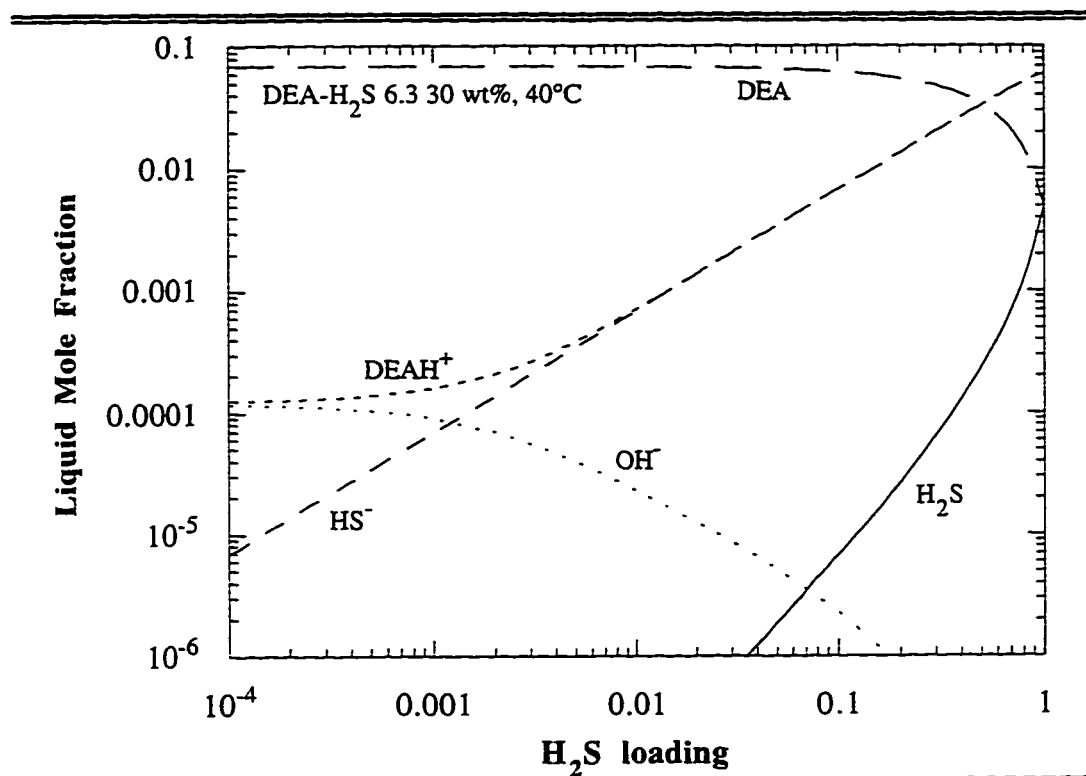
Figure 7.5 Liquid phase mole fractions for a 30 wt% DEA solution at 40°C from the DEA-H_2S-6.3 electrolyte-NRTL model.

199

It also illustrates why simple models that do not account for hydroxide ions fail in low loading predictions. Sulfide ion concentrations are on the order of 10^{-10} and were deleted from figure 7.5 to improve readability.

Activity Coefficients

Activity coefficients shed some light on the interactions occurring in the solution. They also are necessary for calculation of vapor-liquid equilibrium. One should be careful not to put too much emphasis on a single activity coefficient value. Activity coefficients can vary with the data regressed, the model structure, the parameters used and the equilibrium constants. They also are highly correlated with each other and should be viewed only in the context of a complete model. Completely different model structures, with different parameters, can have different activity coefficients and still predict partial pressure and VLE data exactly the same. Figure 7.6 gives our calculated activity coefficients at 40°C for a 30 wt% DEA solution. Curves for HS^- and $DEAH^+$ exactly coincide above an H_2S loading of 0.01 and split towards values of 1.03 and 0.93, respectively, at very low loadings.
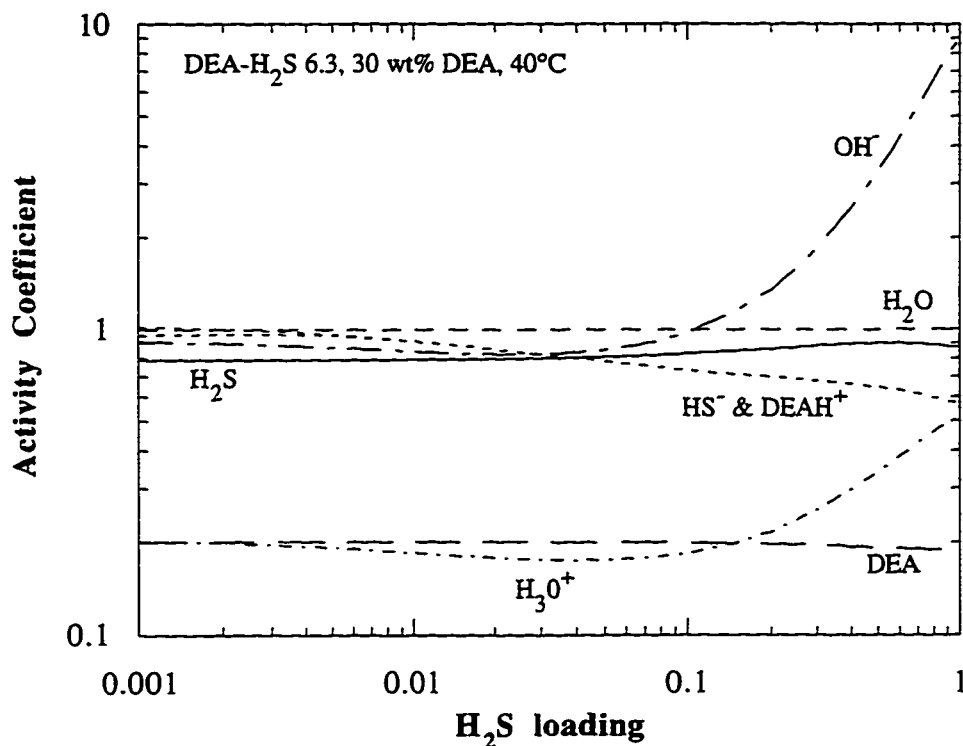
Figure 7.6 Activity coefficients for a 30 wt% DEA solution at 40°C from the DEA-H$_2$S-6.3 electrolyte-NRTL model.

Heat of absorption

An important variable in acid gas treating is the heat of absorption. It governs the heat rise in the absorber and determines the steam required in the stripper. In addition, good values of the heat of absorption are an ideal way to thermodynamically verify a model regressed upon VLE data. Figure 7.7 plots our calculated heat of H$_2$S absorption in a 30 wt% DEA solution as a function of temperature. These values were calculated by taking the derivative (equation 6.1) of our partial pressure predictions as was done for MDEA. The solid line is an average heat of absorption from the other four lines. The DEA-H$_2$S model seems

to be better behaved than in the MDEA systems. The various temperatures are nicely spaced and all of them approach the physical heat of absorption for H_2S at a loading of one.
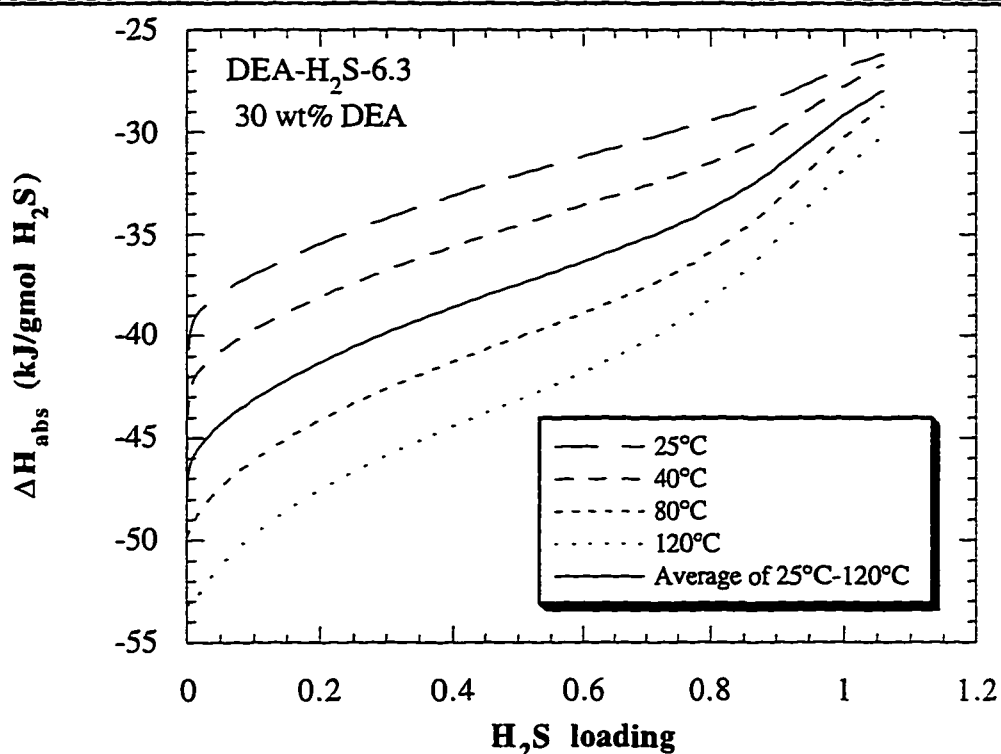
Figure 7.7 Heat of H_2S absorption into 30 wt% DEA calculated from pressure predictions of the DEA-H_2S-6.3 electrolyte-NRTL model.

To confirm our calculations, the average heat of absorption from figure 7.7 has been compared to literature values in figure 7.8. This work tends to be slightly higher than the data of Lee et al. (1973a) and Oscarson et al (1995). The Lee data assumes that heat of absorption is not a function of temperature. As a result, the values reported in this work might not be at the same average temperature as Lee et al. (1973a).

202

Note that the data by Oscarson et al. (1995) is a cumulative heat of absorption. Their experiments involved absorbing acid gases into clean amine solutions at various ratios to obtain various final H_2S loadings. Therefore, their heat of absorption at, for example, an H_2S loading of 0.6 is an integrated value of all of the heats of absorption from zero to 0.6. So, to compare to the differential heat of absorption of this work and that of Lee et al. (1973a), the heats of absorption at each loading must be averaged with all of the preceding heat of absorption values. This has been done numerically for our average heat of absorption and is indicated in figure 7.8 by the dashed line.
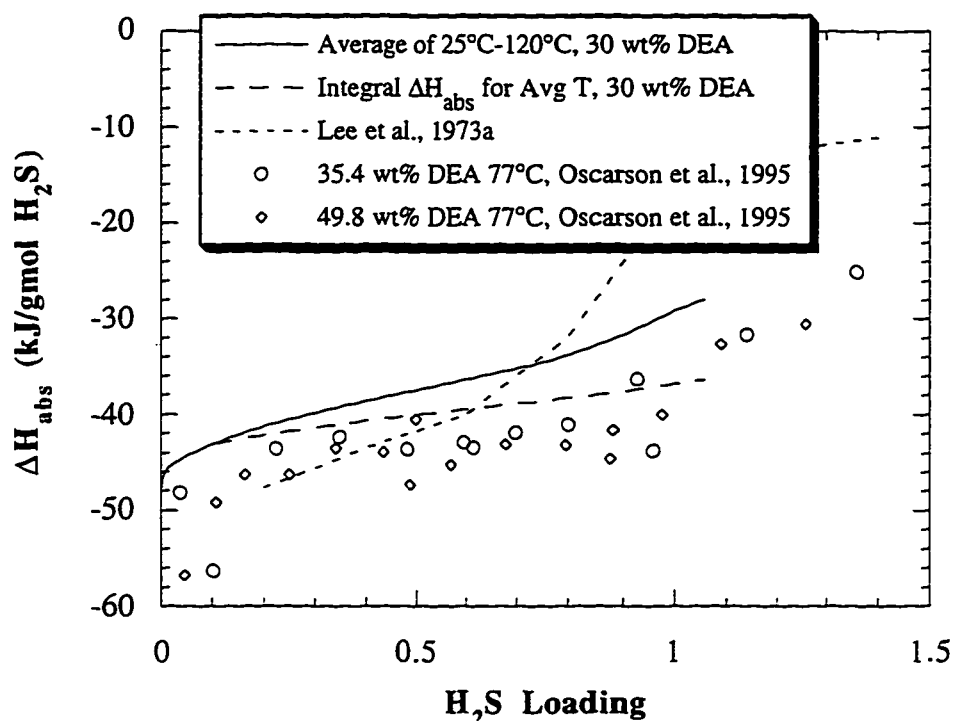
Figure 7.8 Heat of absorption of H_2S into DEA solutions calculated by this work and Lee et al. (1973a) from partial pressures compared to integral heat of absorption calorimetric data.

Note that the Oscarson et al. (1995) data is more closely represented by the integral heat of absorption curve. The Oscarson data do not show an amine dependence within the accuracy of their data. Experimental data is presented for 77°C, however their data also do not show temperature dependence with the scatter of the data.

7.2 DEA-CO$_2$

The DEA-CO$_2$ system is the most complex of the binary systems studied here. It has all of the reactions of the MDEA-CO$_2$ system with the addition of the carbamate reaction. The carbamate reaction adds complexity because it is not independently known with accuracy from the literature. Since the carbamate reaction only occurs in the presence of DEA and all the other CO$_2$ reactions, its equilibrium constant is difficult to isolate. Any attempts to measure the constant at high amine concentrations fail because of the fast reversion of carbamate to bicarbonate. This makes precipitation experiments impossible. Therefore, the equilibrium constant for the carbamate reaction must be regressed.

We have regressed electrolyte-NRTL parameters and the carbamate equilibrium constant to four VLE data sets and pH data from this work. A preliminary parameter set did not agree with our pH data. Therefore, the pH and VLE data have been simultaneously regressed and the resulting parameter set is presented in Table 7.3. Calculated values of the tau parameter at 40°C are also compared to the parameters of Austgen et al. (1989). Again the temperature parameters have been divided by 313K for easier comparison in Table 7.3. The

natural log of the carbamate equilibrium constant at 40°C is -8.0 in this work compared to -6.4 for Austgen et al. (1989).

Table 7.3 Electrolyte-NRTL parameters for DEA-CO_2 system, "DEA-CO_2-10.4"

Regressed parameters	a or b	value	standard deviation	α	This work 40°C	Austgen 40°C
H_2O (DEAH$^+$ HCO_3^-)	A	2.460	0.85	0.2	2.5	9.3
H_2O (DEAH$^+$ HCO_3^-)	B / 313K	0	N/A			
(DEAH$^+$ HCO_3^-) H_2O	A	-5.408	0.56	0.2	-1.6	-4.4
(DEAH$^+$ HCO_3^-) H_2O	B / 313K	3.776	0.75			
(DEAH$^+$ HCO_3^-) DEA	A	4.865	0.93	0.1	-6.1	-8
(DEAH$^+$ HCO_3^-) DEA	B / 313K	-10.965	0.90			
(DEAH$^+$ $CO_3^=$) DEA	A	-8	N/A	0.1	-5.6	-8
(DEAH$^+$ $CO_3^=$) DEA	B / 313K	2.387	2.355			
H_2O (DEAH$^+$ DEACOO$^-$)	A	11.799	0.29	0.2	11.8	11.9
(DEAH$^+$ DEACOO$^-$) H_2O	A	-6.898	0.14	0.2	-6.9	-5.6
(DEAH$^+$ OH$^-$) H_2O	A	-5.75	N/A	0.2	-5.8	-4
(DEAH$^+$ OH$^-$) H_2O	B / 313K	0	N/A			
ln K_x carbamate	A*	0.2616	0.81		-8.0	-6.4
ln K_x carbamate	B*	-2585	242			

* Temperature dependent form for equilibrium constants as given in Table 5.9

Most of the parameters are fit well with low standard deviations. However, the carbonate parameter again has a high standard deviation, 2 on a tau basis, as occurred for the MDEA-CO_2 system. A conclusion might be to omit this carbonate parameter. However, its standard deviation is only twice that of the other B parameters and Table 7.4 illustrates that the carbonate parameter is correlated with the other parameters. This indicates that the model is sensitive to it. In addition, all regression cases that were attempted without this parameter failed to provide a reasonable representation of the data.

The (DEAH$^+$ OH$^+$) H_2O parameter was set to the same value as used for the DEA-H_2S system to maintain consistency for the zero loading case. The

temperature dependent parameters of the carbamate equilibrium constant were also regressed and predicted well with low standard deviations. Comparisons of the equilibrium constant value are given later.

Tau values for the water-carbamate electrolyte parameters are surprisingly similar between this work and Austgen, especially considering the different carbamate equilibrium constants. This work has utilized different parameters for the regressions than did Austgen. All values listed as "-8 or -4" for Austgen were set to defaults in his work and not regressed. The other electrolyte parameters differ significantly from the values obtained by Austgen. However, parameter correlation allows seemingly different sets of parameter values to predict the same pressure behavior. Some species concentrations and activity coefficients will be different, but until independent determinations can be made for these quantities there is no way to determine which predictions are correct. This further emphasizes the need for more thermodynamically related data, such as speciation and pH, to determine model behavior where VLE data is lacking.

Correlation of the parameters for the DEA-CO_2 system is given in Table 7.4. The electrolyte model calculates VLE and performs regressions using the tau values. Therefore, the A and B temperature terms of a parameter are always highly correlated. This can be seen in the 2/3, 4/5, and 9/10 correlation pairs. Also note that the carbonate parameter 6 is highly correlated with the second carbamate parameter. This could be a second reason that the carbonate parameter has such a high standard deviation. Parameters are also usually correlated highly with the reversed parameter. Parameter pairs 1/2 and 7/8 show this behavior.

Table 7.4 Parameter correlation matrix for the DEA-CO_2-10.4 parameter set

	1	2	3	4	5	6	7	8	9	10
1	1.00									
2	0.66	1.00								
3	-0.80	-0.98	1.00							
4	-0.13	0.24	-0.13	1.00						
5	-0.08	-0.37	0.29	-0.98	1.00					
6	0.27	0.49	-0.47	0.51	-0.54	1.00				
7	0.58	0.37	-0.49	-0.39	0.24	-0.34	1.00			
8	-0.05	0.04	0.00	0.56	-0.52	0.74	-0.72	1.00		
9	-0.20	-0.38	0.36	0.26	-0.21	0.36	-0.45	0.60	1.00	
10	0.25	0.44	-0.42	-0.23	0.17	-0.29	0.39	-0.47	-0.98	1.00

Parameter Legend

1 = H_2O ($C4^+$ HCO_3^-)   A   6 = (C_4^+ $CO_3^=$) DEA   B

2 = (C_4^+ HCO_3^-) H_2O A   7 = H_2O (C_4^+ $DEACOO^-$)   A

3 = (C_4^+ HCO_3^-) H_2O B   8 = (C_4^+ $DEACOO^-$) H_2O A

4 = (C_4^+ HCO_3^-) DEA   A   9 = ln $K_{carbamate}$ A

5 = (C_4^+ HCO_3^-) DEA   B   10 = ln $K_{carbamate}$ B

Data Fitting

Figure 7.9 compares CO_2 partial pressures from experiments to predictions by the electrolyte-NRTL model. Note that the majority of the data is at loading above 0.1. Very little data exists below 0.01. This lack of data at low loading is due to difficulty in measuring low CO_2 partial pressure and the fact that industrial absorbers rarely achieve loading below 0.01. The data by Lal et al. (1995) and Ho and Eguren (1988) seem to be following a trend lower than the model at low loading. Overall, the VLE data is fit well with an error in partial pressure predictions of roughly ±20%.
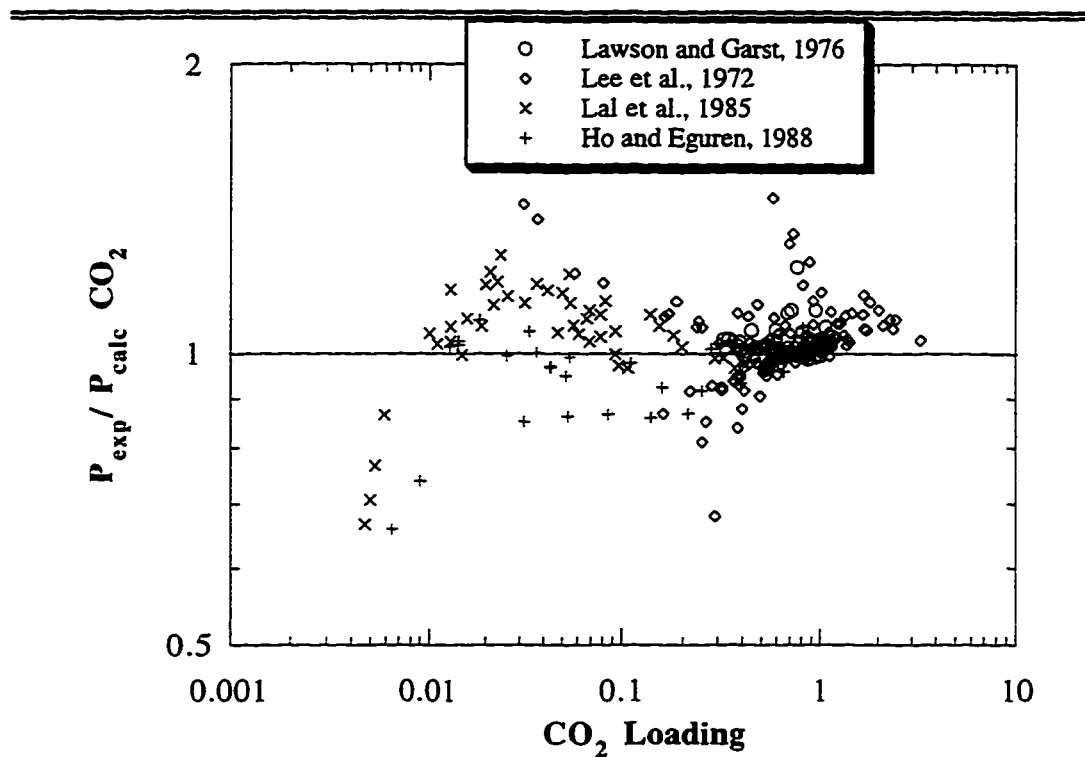
Figure 7.9 Ratio of CO_2 partial pressures from experiments to model predictions as a function of CO_2 loading for the DEA-CO_2-10.4 parameter set. Other data was simultaneously fit.

As in the other regressions, mole fractions are simultaneously fit. Figure 7.10 gives the model comparison to CO_2 mole fraction. This plot shows an inverse relationship to figure 7.9 and most of the mole fractions were fit within ±20%.
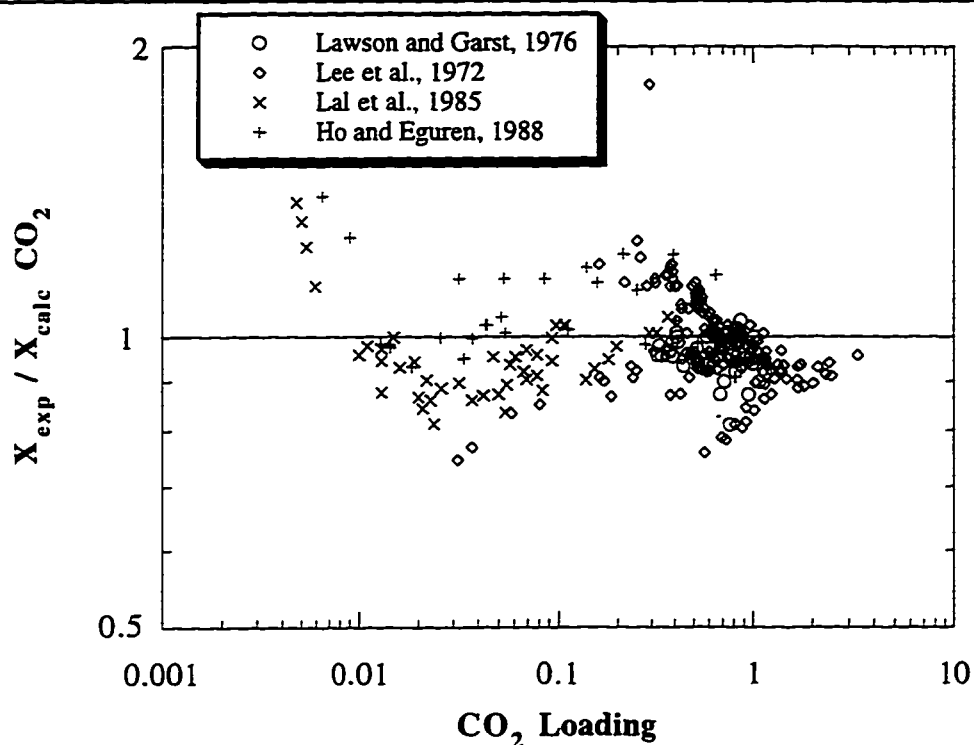
Figure 7.10 Ratio of experimental to model predicted CO_2 mole fractions as a function of CO_2 loading for the DEA-CO_2-10.4 parameter set. Other data was simultaneously fit.

Unlike all of the other binary systems, rather than just comparing model predictions to pH data, we have regressed pH data for the DEA-CO_2 system. The pH data was given the same regression weighting as the VLE data and standard deviations were set to 0.1 for temperature, 0 for liquid concentrations and 0.5% for pH. The data was collected in this work and is given in Table B.8. Figure 7.11 demonstrates that the model has done an excellent job of fitting the experimental DEA-CO_2 pH data.

209
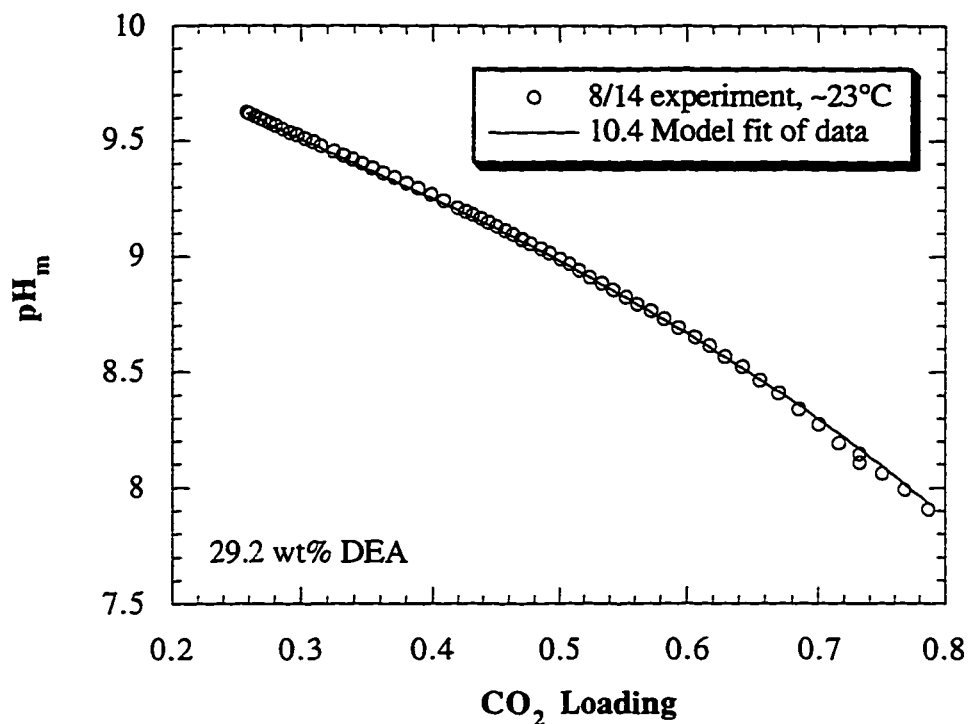
Figure 7.11 Experimental pH data compared to regressed predictions from the DEA-CO$_2$-10.4 model as a function of CO$_2$ loading.

7.2.1 Unregressed Data

Several VLE data sets for the DEA-CO$_2$ system exist that were not included in our regression. Data sets by Huang and Ng (1995) and Bullin et al. (1996) were not included mainly because they became available too late in the time frame of the current work. Another reason for their omission is that these data sets are not publicly available and would make recreating this work difficult. Data by Kennard and Meisen (1984) were not included since its temperatures reached as high as 200°C. Temperatures this high require questionably large

210

extrapolations of most of the fundamental equations such as Henry's and equilibrium constants.
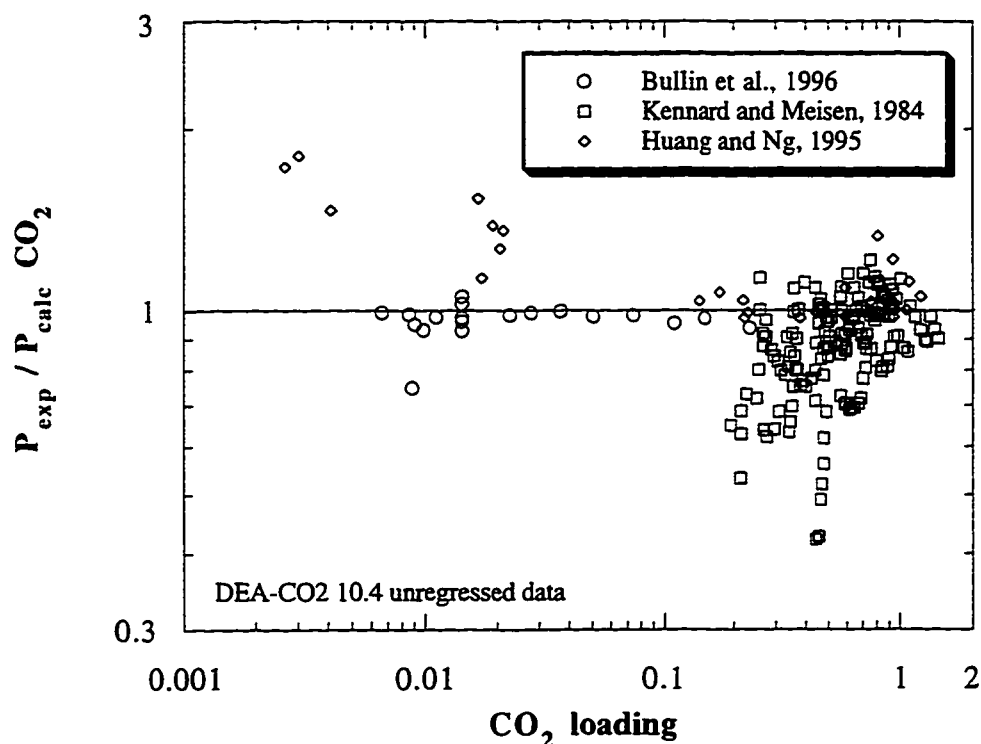
Figure 7.12 CO_2 partial pressure model fit of DEA-CO_2 data that was not included in the regression of the "DEA-CO_2-10.4" parameter set.

Data from Bullin et al. (1996) agree quite well with predictions of this work in figure 7.12. Huang and Ng (1995) data again show good fit at high loading, but an upward trend at low loading. Kennard and Meisen data is not fit well, shows large scatter, and is mostly overpredicted by this model.

Mole fractions were simultaneously fit and the Huang and Ng (1995) data show as much as a 40% error in figure 7.13. This means that if mole fractions

were assumed to be error free, partial pressures would be predicted with much less accuracy in figure 7.12.
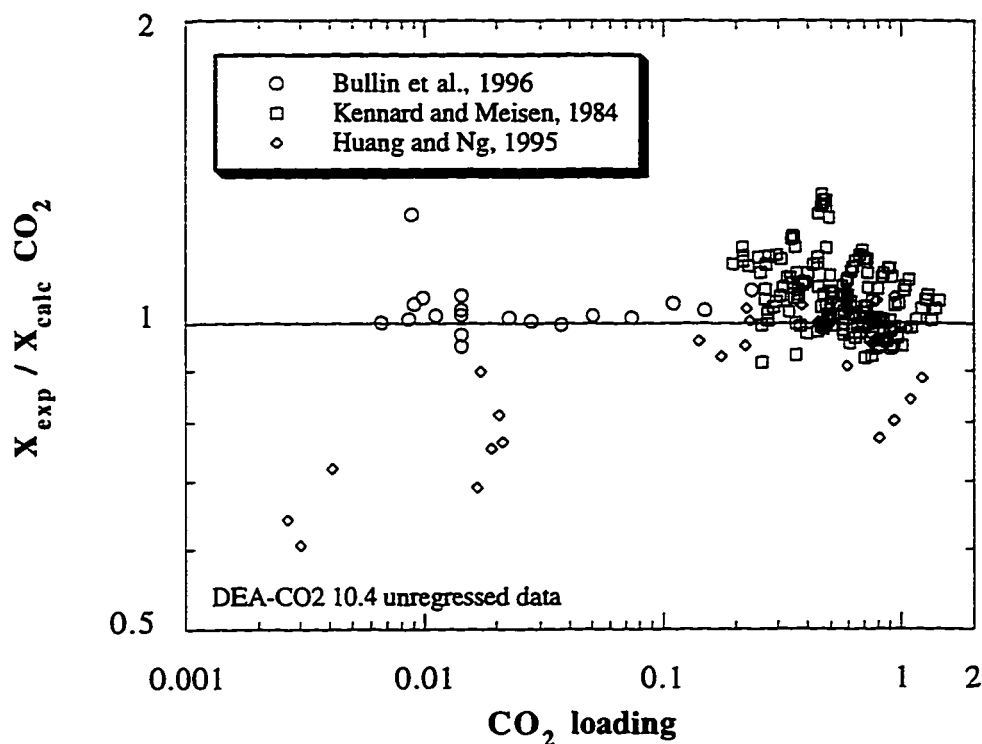
Figure 7.13 Experimental to calculated CO_2 mole fraction ratio of DEA-CO_2 data that was not included in the regression of the "DEA-CO_2-10.4" parameter set.

7.2.2 Model Predictions

Partial Pressure

CO_2 partial pressures predicted in this work are compared to the model of Austgen et al. (1989) below in figure 7.14. The models match well at all temperatures above a CO_2 loading of 0.1. Below a loading of 0.1, Austgen predicts higher than this work, with the greatest difference being at high

temperature and low loading. This is directly related to the lack of VLE data in that region. Remember that experimental data does not exist much below a CO_2 loading of 0.01. Therefore, both curves are model extrapolations at loadings below 0.01. The difference between the curves results from different temperature dependencies of the carbamate equilibrium constant and electrolyte parameters.
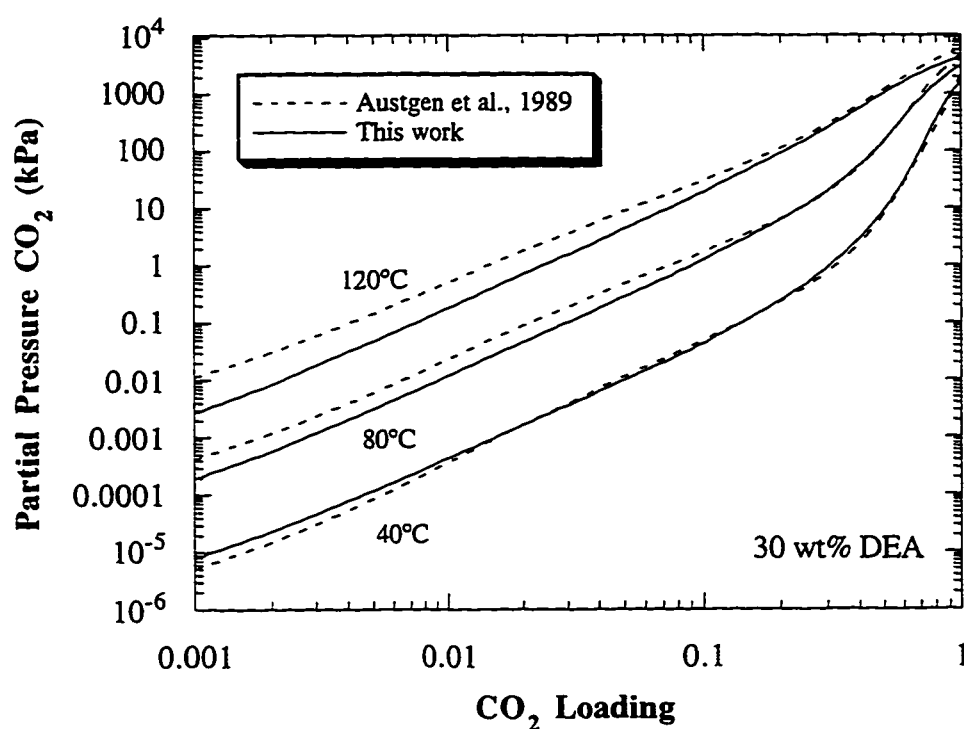
Figure 7.14 Calculated CO_2 partial pressure for two electrolyte-NRTL model parameter sets for 30 wt% DEA solutions.

The DEA-CO_2 system is different from the other binary systems in that CO_2 partial pressure at low loading is not a function of DEA concentration (Austgen, 1989). Figure 7.15 shows that below a loading of 0.1, CO_2 partial pressure at 5 to 50 wt% DEA is essentially the same. Above a loading of 0.1, the

reactions occurring for CO_2 absorption shift more towards bicarbonate and partial

pressure becomes a function of DEA concentration. Figure 7.16 plots the partial

pressure in kPa normalized by the DEA acid gas free mole fraction. The curves

have slightly collapsed, but have a larger spread than the other binary systems.
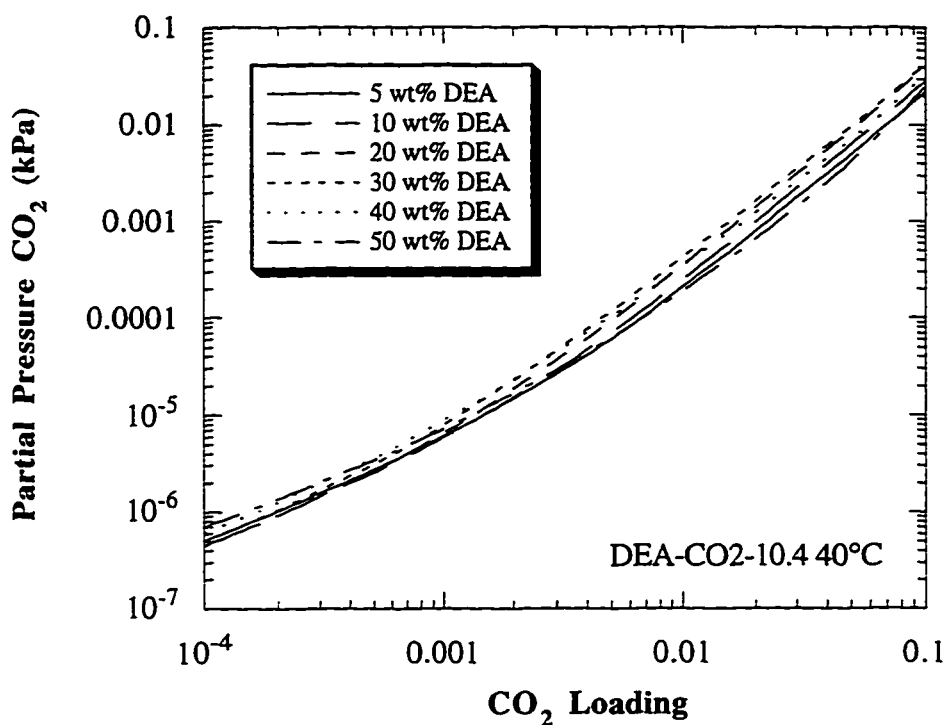
Figure 7.15 Calculated CO_2 partial pressure for the DEA-CO_2-10.4 electrolyte-NRTL model at 40°C.
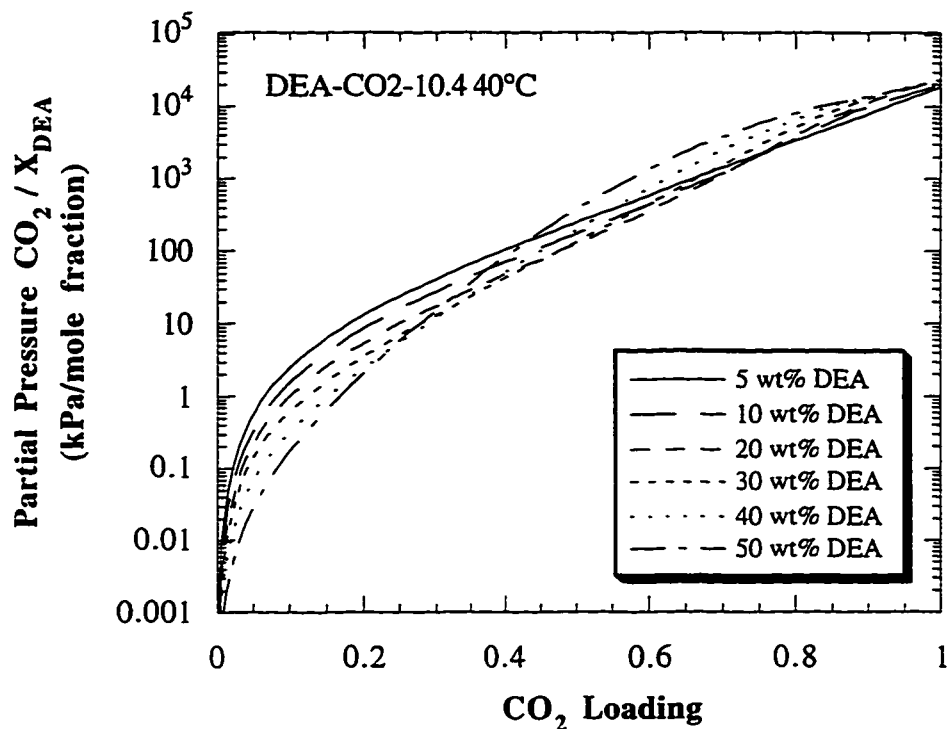
Figure 7.16 Calculated CO_2 partial pressure in kPa divided by the acid gas free DEA mole fraction for the DEA-CO_2-10.4 electrolyte-NRTL model at 40°C.

Speciation

As stated for the DEA-H_2S system, solution speciation is an important result of equilibrium modeling. Rate based mass transfer models require species concentration to calculate rates of diffusion and therefore the rate of absorption for acid gases. This is especially important for CO_2 absorption where reactions cannot be considered instantaneous.

In figure 7.17 carbamate equilibrium constant equations of this work (DEA-CO_2-10.4), Austgen et al. (1989), Kent and Eisenberg (1976) and

215

Chakravarty (1985) are compared with two experimentally obtained values. The comparison in figure 7.17 however, is not thermodynamically consistent. Kent and Eisenberg (1976) did not have activity coefficients in their model, therefore their equilibrium constant is a concentration based equilibrium constant. The two experimental references are extrapolated to zero ionic strength where they assume activity coefficients are all one. This work, Austgen, and Chakravarty represent the true equilibrium constant at infinite dilution in water.
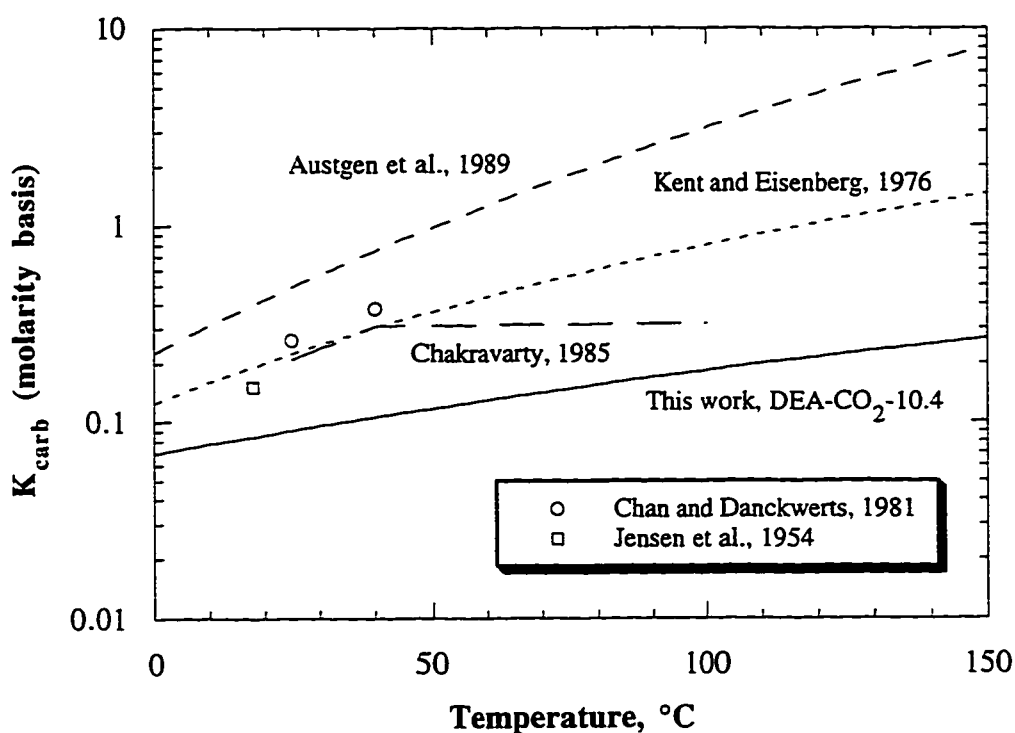
Figure 7.17 Carbamate equilibrium constant on the molarity concentration basis as a function of temperature.

Predictions of mole fraction concentrations for the Austgen model and this work have been compared to "experimental" data of Haji-Sulaiman et al. (1996).

216

Austgen and this work predict very similarly and both match the experimental data well as seen in figure 7.18. This work and Austgen et al. (1989) predict slightly less carbamate ions than indicated by the data. However, figure 7.17 shows significantly different carbamate equilibrium constants. This discrepancy is possible because the activity coefficients in each model compensate for the different equilibrium constants. The conclusion that is drawn is that when comparing between models for the DEA-CO_2 system, predicted concentrations should be compared and not the carbamate equilibrium constant.
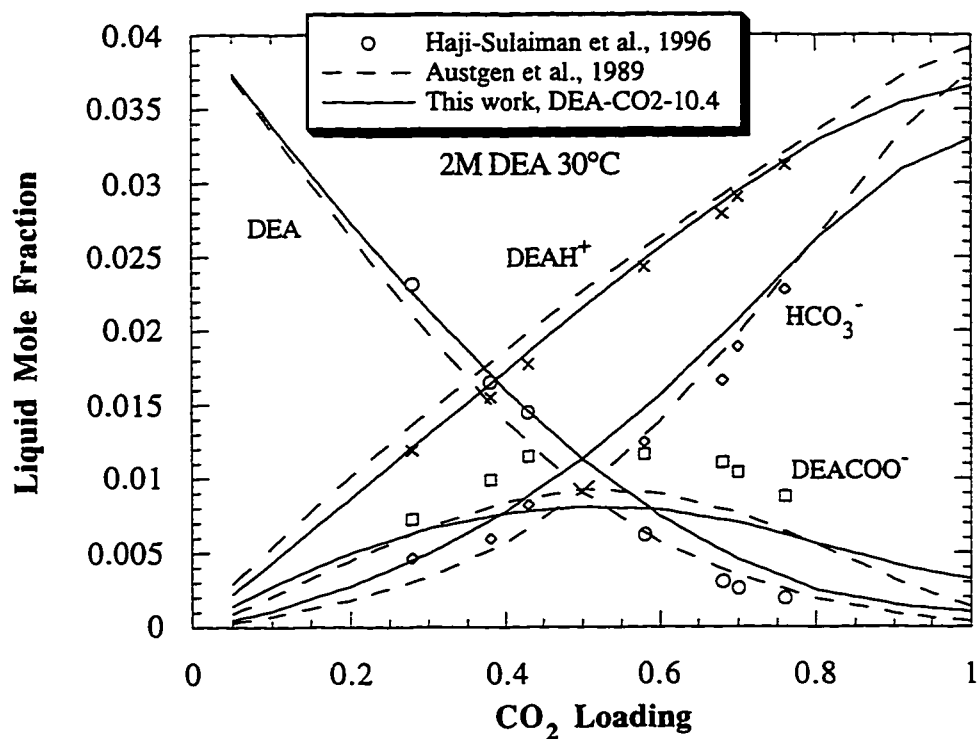
Figure 7.18 Comparison of concentration predictions from two parameter sets for the electrolyte-NRTL model to experimental data for 2M DEA at 30°C.

Liquid phase mole fractions are calculated in a 30 wt% DEA solution at 40°C in figure 7.19. The important feature is that bicarbonate exceeds carbamate concentration above a loading of 0.25. Other models (Austgen et al. 1989; Desmukh and Mather, 1981) have predicted that carbamate concentration equals bicarbonate concentration at a loading of approximately 0.6.
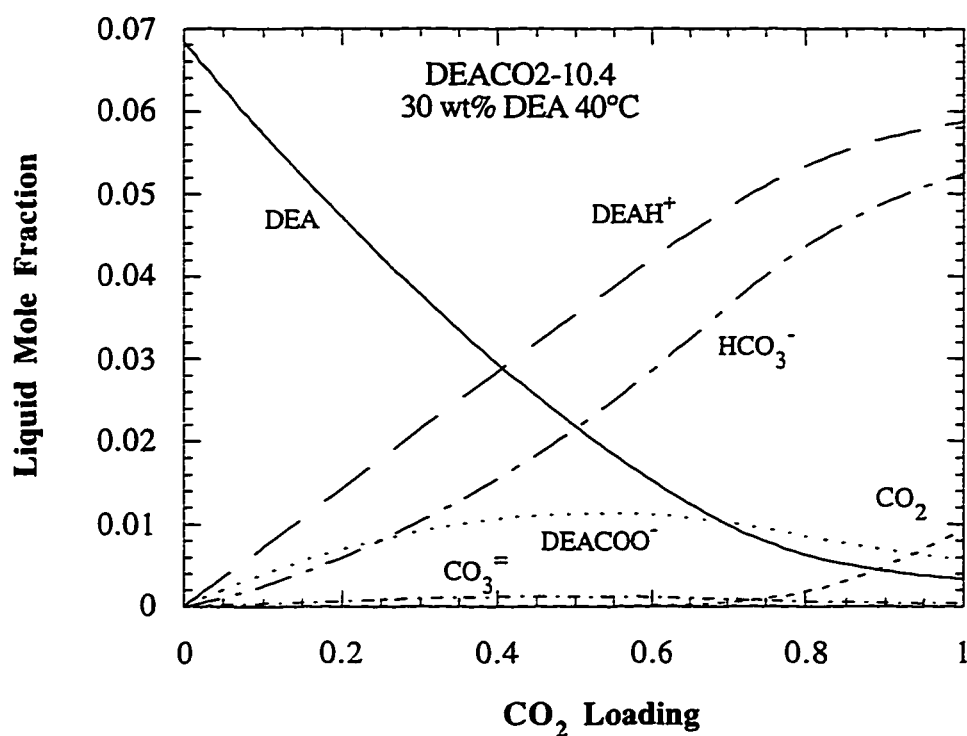
Figure 7.19 Liquid species concentrations predicted by the DEA-CO$_2$-10.4 electrolyte-NRTL for 30 wt% DEA at 40°C.

Interesting low loading details are lost when DEA-CO$_2$ speciation is plotted linearly versus loading. Figure 7.20 is identical to figure 7.19 with CO$_2$ loading on a log scale. First note that the carbamate and bicarbonate increase together as a function of loading until approximately 0.1. It is also evident that

carbonate ions become an important part of the CO_2 balance below a loading of

0.01. Also below a loading of 0.001, hydroxide becomes the dominant anion in

30 wt% DEA solutions at 40°C.
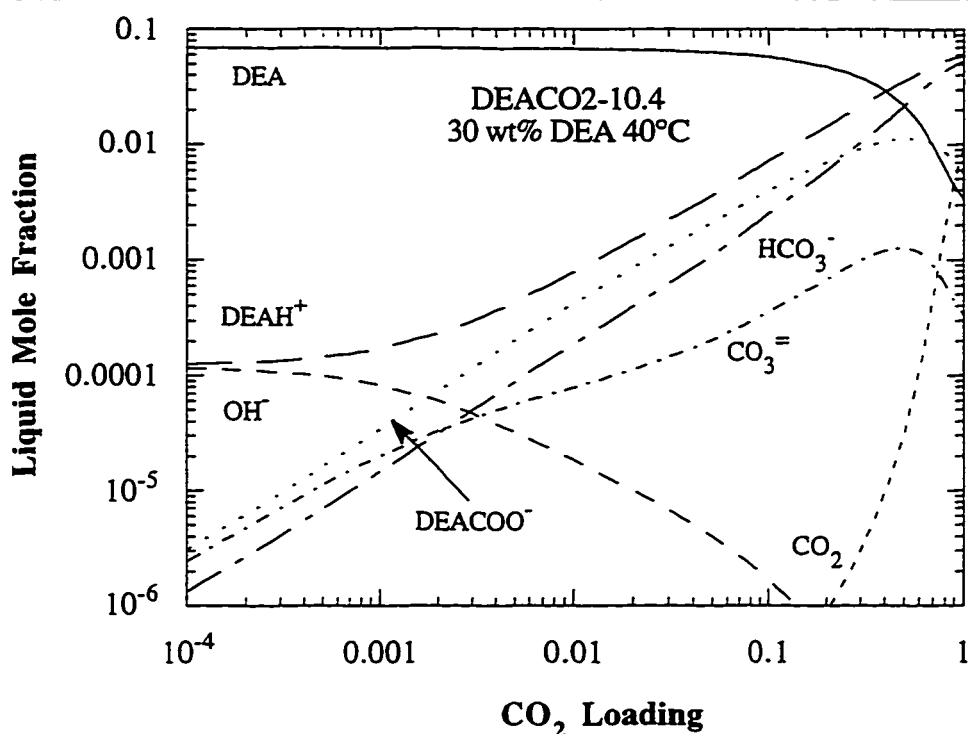
Figure 7.20 Liquid species concentrations predicted by the DEA-CO_2-10.4
electrolyte-NRTL for 30 wt% DEA at 40°C plotted on log scale to
show low loading behavior.

Figures 7.19 and 7.21 should be compared to examine the effects of

temperature on speciation. In 30 wt% solutions at 120°C, the molecular CO_2

concentration becomes important at loading as low as 0.5. The higher molecular

CO_2 results in lower ionic strength and bicarbonate concentration. It also

increases the CO_2 partial pressure which helps to remove CO_2 in the stripper.

219

Austgen (1989) showed that his model predicted the peak carbamate concentration to decrease approximately 50% from 40°C to 120°C. This work predicts that the carbamate speciation is relatively unchanged between 40°C and 120°C. This is possible even with the changing equilibrium constant due to the temperature dependence of the activity coefficients.
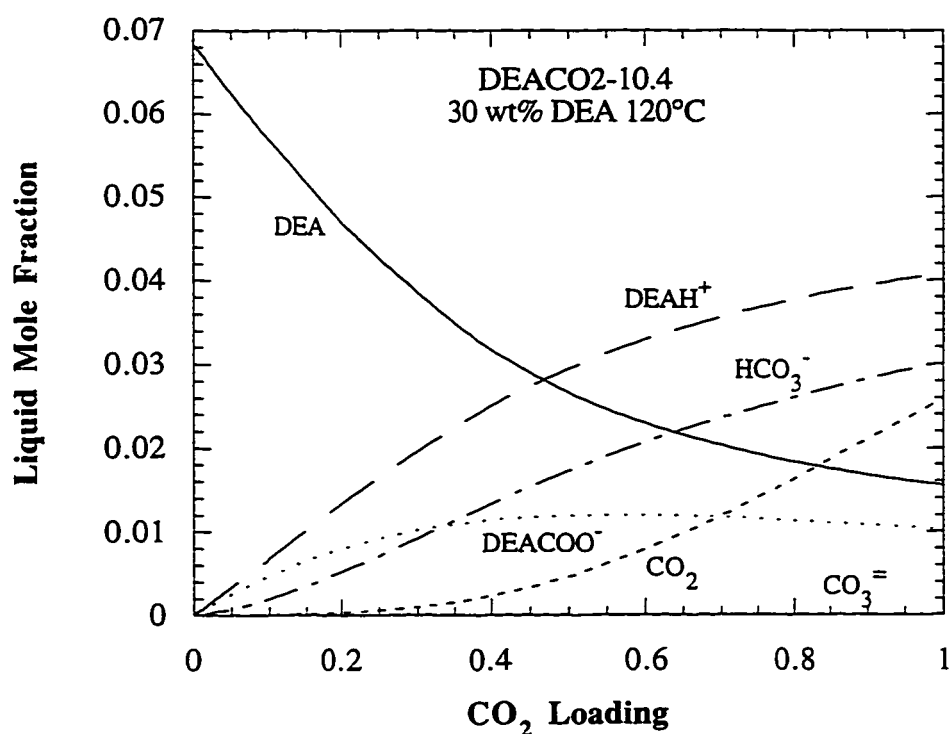
Figure 7.21 Liquid species concentrations predicted by the DEA-CO_2-10.4 electrolyte-NRTL for 30 wt% DEA at 120°C

Activity Coefficients

Activity coefficient behavior can sometimes help to decipher dependencies and trends in the model. First notice in figure 7.22 the carbonate activity coefficient is much more reasonable than for the MDEA-CO_2 system.

The (MDEAH$^+$ CO$_3$=) MDEA tau value was -2 at 40°C while (DEAH$^+$ CO$_3$=) DEA was -6. A difference of four in the tau value is significant and results in the high carbonate activity coefficients in MDEA. Since carbonate ions will always constitute a minor portion of the CO$_2$ balance, accurate determination of its concentration or activity coefficient will be difficult.
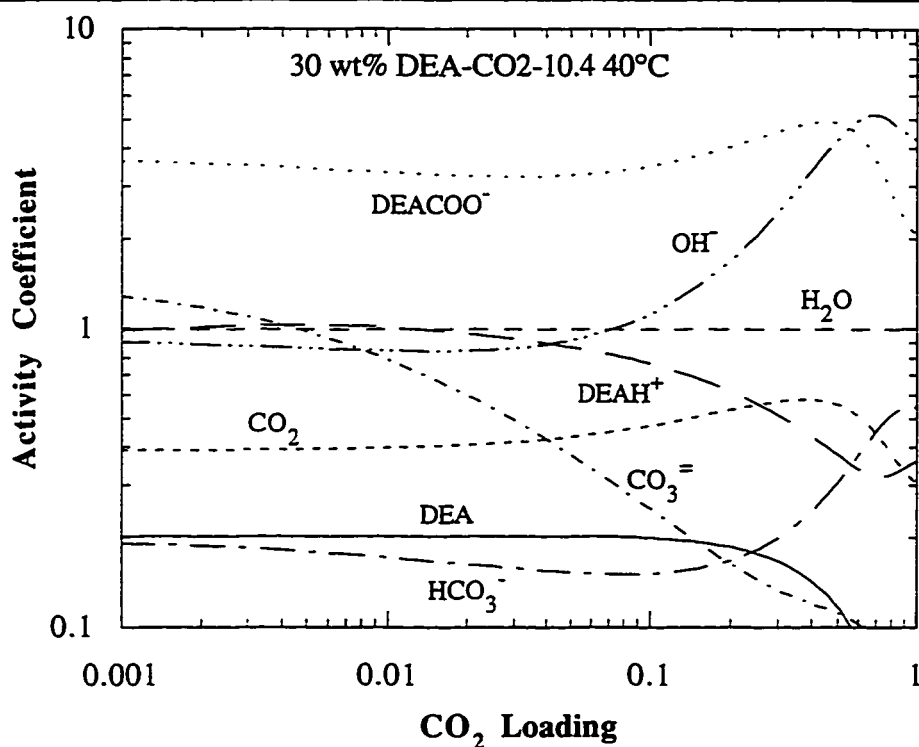
Figure 7.22 Predicted activity coefficients for 30 wt% DEA 40°C by the DEA-CO$_2$-10.4 electrolyte-NRTL model.

Heat of Absorption

Heat of absorption predictions are another thermodynamic check upon our model. As for the other systems, it was calculated from the temperature derivative of ln (pressure) as a function of loading and temperature. The

predictions at 25, 40, 80, and 120°C were averaged to obtain the solid line in figure 7.23. The DEA-CO_2 system shows a very strong loading dependence which results from the transition from the carbamate to bicarbonate absorption mechanism. The curves approach the heat of absorption corresponding to physical absorption of the acid gas.
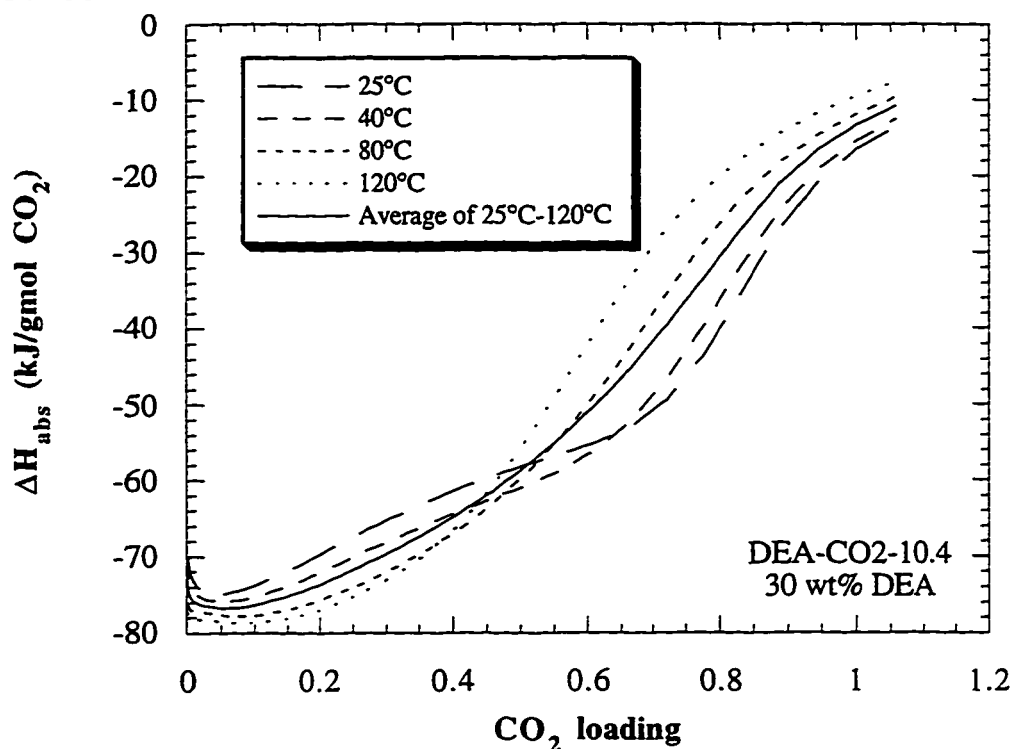
Figure 7.23 Heat of CO_2 absorption into 30 wt% DEA calculated from pressure predictions of the DEA-CO_2-10.4 electrolyte-NRTL model.

Figure 7.24 compares our average prediction to literature data. Note that data by Oscarson et al. (1995) is an integral rather than differential heat of absorption. To properly compare, we have taken discrete heats of absorption from

0.1 to 1.0 loading and numerically integrated the curve. The resulting dashed line

matches the Oscarson data well.
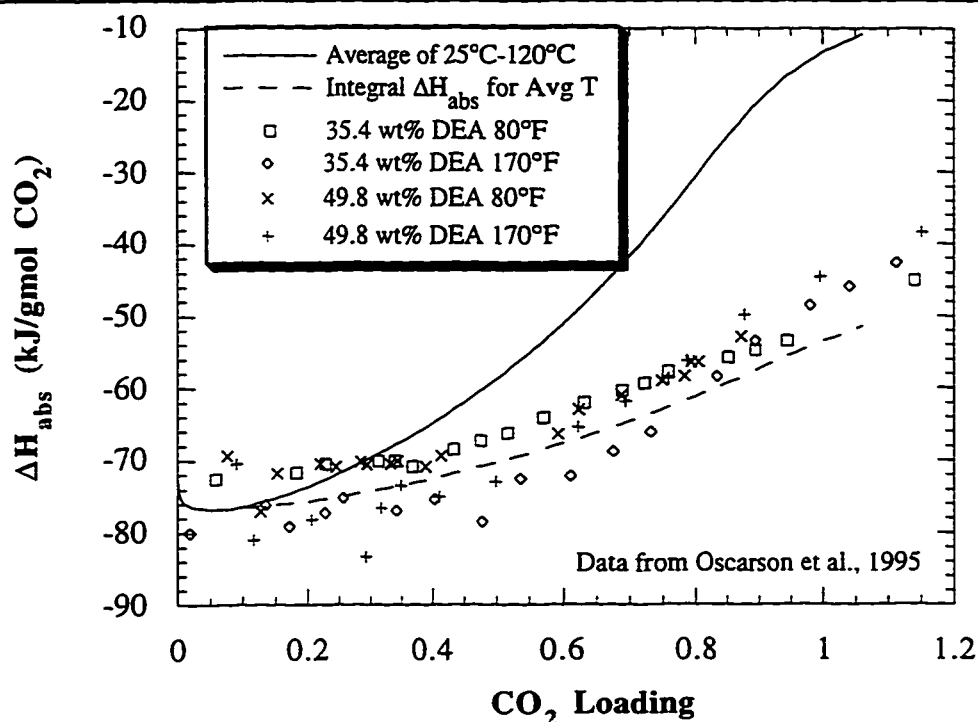
Figure 7.24   Heat of absorption of CO_2 into DEA solutions calculated by this work from partial pressures compared to integral heat of absorption calorimetric data.

7.3 MODEL DRIVEN EXPERIMENTS

7.3.1 pH

A few pH experiments have also been performed for the DEA system. Procedures for preparing the titrant and titrate solutions are the same as listed in Chapter 6 for MDEA. The first experiment listed in Table 7.5 is a titration of 29 wt% DEA with a 29 wt% DEA solution that was partially neutralized with

HCl. Hydrochloric acid is assumed to be analogous to H_2S for the purposes of pH measurements. Temperature was controlled at 40°C using a water bath.

Table 7.5 Experimental conditions for DEA pH titrations

Date	Solution Temp. °C	Acid free amine wt%	CO_2 ldg before exp.	CO_2 ldg after exp.	Acid ldg range
DEA					
4/24/96	39.71 - 40.26	29.7 - 29.9	0.00012	0.00019	0 - 0.013
8/14/96	23	29.2	N/A	N/A	0.2 - 0.8

Figure 7.25 below compares this experimental data to calculations from our current DEA-H_2S model. This data set is tabulated in Appendix B.7. The two curves do not include any CO_2 loading. If a CO_2 loading of 0.0002 were added, then the 40°C model would match the data even closer at acid loading less than 0.01.
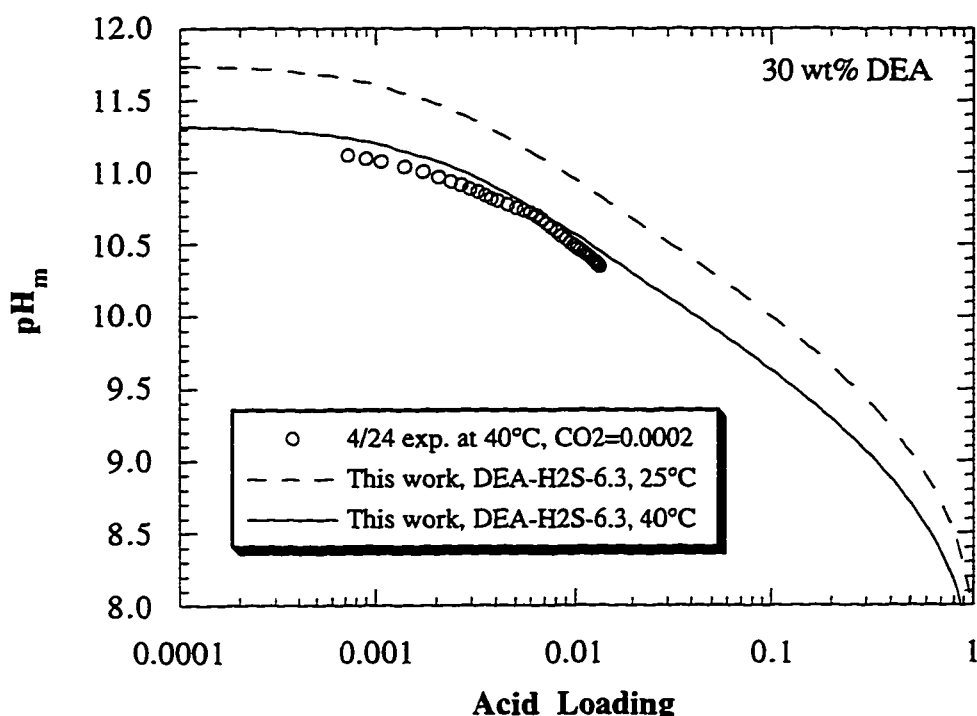
Figure 7.25 HCl titration results at 40°C in 30 wt% DEA compared to predictions at 25°C and 40°C from the DEA-H2S-6.3 model.

For the DEA-CO_2 system there were originally significant differences in the partial pressure predictions between this work and Austgen et al. (1989) at 40°C. Therefore, a titration of a 29 wt% DEA solution was carried out in a 29 wt% DEA solution with a 0.79 CO_2 loading. The result shown in figure 7.26 is a pH curve for 29 wt% DEA as a function of CO_2 loading. It demonstrates that our best parameter set at that time "DEA-CO_2-10.2" did not agree with pH predictions while Austgen et al. (1989) did. Therefore, we have regressed this pH data along with the VLE data to form an improved DEA-CO_2 parameter set as described above.
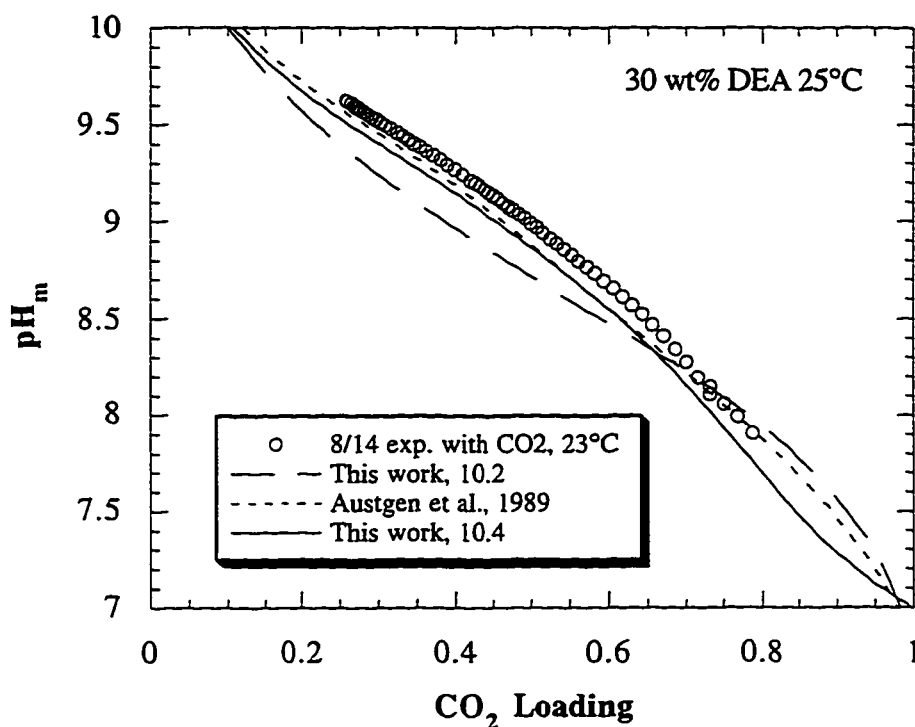
Figure 7.26 CO2 titration results at ambient (~23°C) temperature in 30 wt% DEA compared to predictions at 25°C from the electrolyte-NRTL model.

7.3.2 Conductivity

Conductivity measurements analogous to the MDEA system have been performed for DEA. The data and resulting ionic conductivities are reported in Tables A.1 through A.7. The (DEAH$^+$ OH$^-$) H$_2$O parameter reported above was varied to fit the calculated hydroxide mole fractions from Table 7.6. Only a small correction was necessary from the previous parameter value and the partial pressure predictions did not change. Of course, predictions of the hydroxide mole fraction by this model more closely match the conductivity data than does the model of Austgen et al. (1989) as shown in Table 7.6.

DEAH$^+$ diffusivity presented in Table 6.3, which was calculated from the conductivity data, compares well with literature diffusivity data. The confirmation of the conductivity data by diffusion coefficient data adds more certainty to the speciation and predictions at low loadings. It is interesting to note that DEA has a lower conductivity than MDEA even though its molecular weight is lower. This is the result of a smaller hydrodynamic radius for MDEA allowing it to move more freely through aqueous solutions.

Table 7.6 Hydroxide mole fraction in 30 wt% DEA determined from conductivity experiments compared to model predictions

Conditions	Conductivity	Austgen model	This model
30 wt% 25°C	(1.20±0.2)E-4	2.22 E-4	1.05 E-4
30 wt% 40°C	(1.14±0.2)E-4	2.23 E-4	1.20 E-4
30 wt% 120°C	N/A	1.60 E-4	1.44 E-4

7.4 DEA-H$_2$S-CO$_2$ SYSTEM

7.4.1 Data Comparisons

A few data sets have been found for the DEA-H$_2$S-CO$_2$ system. Parameters and constants from the DEA-H$_2$S and DEA-CO$_2$ systems have been combined to form a model for the DEA mixed gas system. Again, it is assumed that mixed gas predictions can be made without additional regressed parameters. Figure 7.27 illustrates the fit of total acid gas partial pressure by dividing experimental values by calculated values.
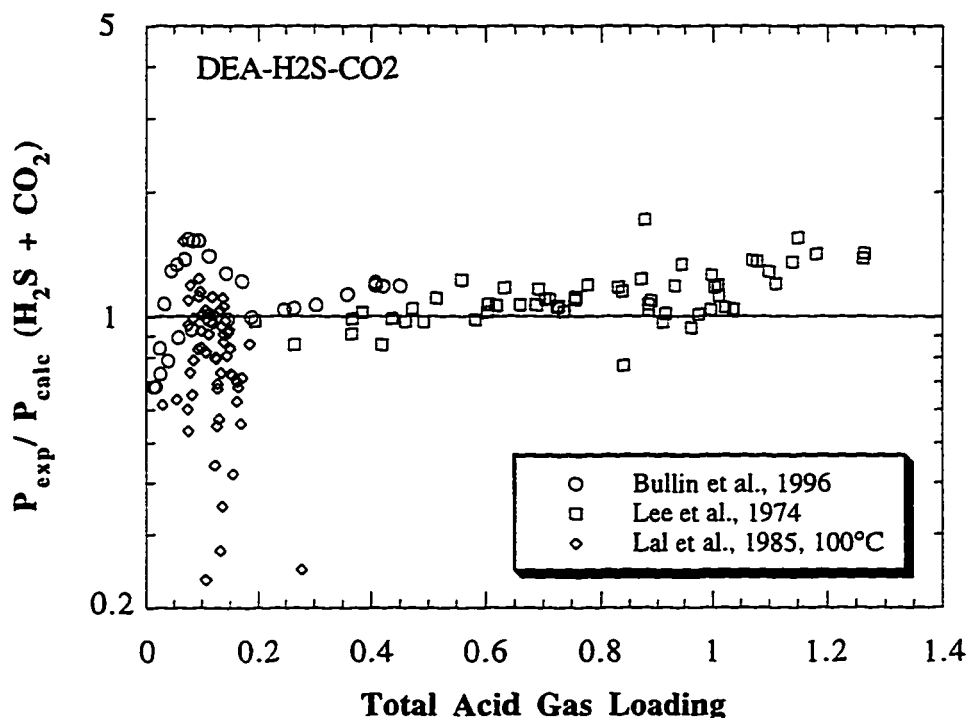
Figure 7.27 Total acid gas partial pressure ratio versus total loading calculated
from the electrolyte-NRTL model.

Since these data contain both H_2S and CO_2, the total acid gas partial

pressure is compared. Data from Bullin et al. (1996) and Lee et al. (1974) are

predicted well as shown in figure 7.27. The Lal et al. (1985) data is mainly at

lower loadings and shows a large scatter at low loading. This is generally

overpredicted by the model. Mole fractions are simultaneously compared to the

model and figure 7.28 shows the typical inverse relationship to figure 7.27. If

mole fractions were not allowed to move, then the error in the pressure data of

figure 7.27 would be even larger.

228
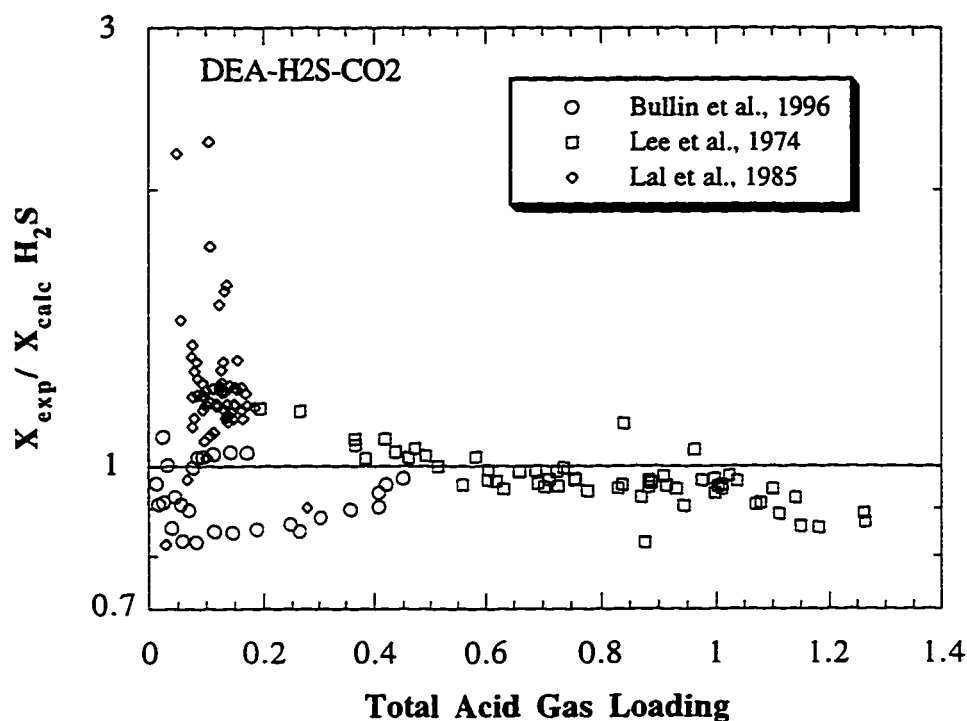
Figure 7.28 Calculated/experimental H₂S mole fraction versus total loading calculated from electrolyte-NRTL model.

It is interesting to note that the error in the CO_2 mole fraction in figure 7.28 follows the opposite trend from the H_2S mole fraction. This is required because if both CO_2 and H_2S mole fraction were increased, then the total pressure would increase thereby worsening the fit. In general, CO_2 mole fraction in figure 7.29 is predicted within 30%.
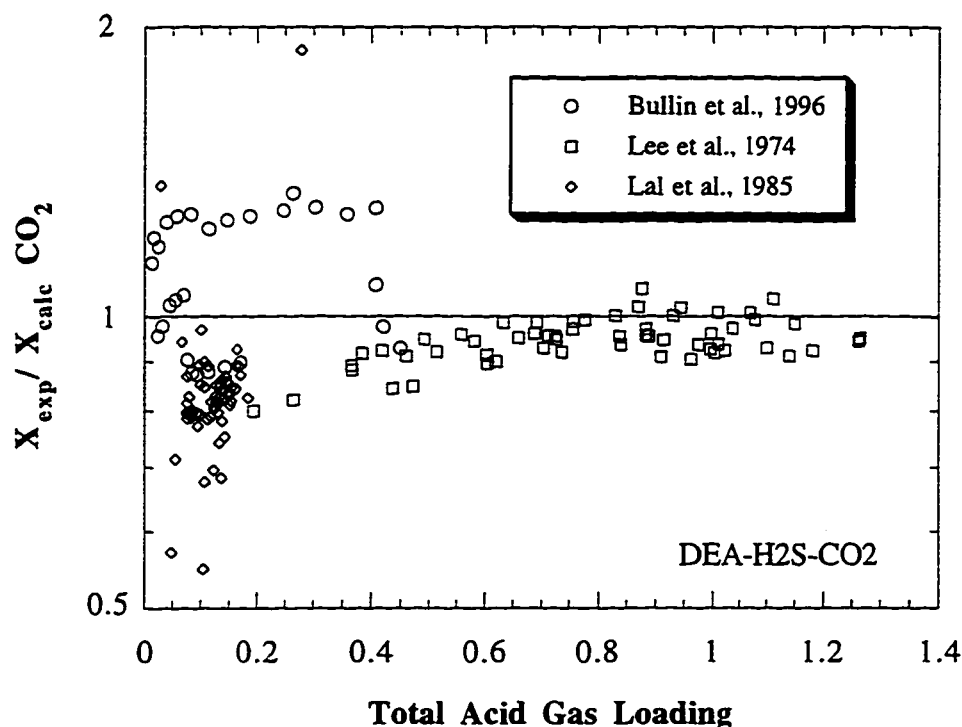
Figure 7.29 Calculated/experimental CO_2 mole fraction versus total loading calculated from electrolyte-NRTL model.

7.4.2 Pressure Predictions

The following graphs were calculated from the parameters for the DEA-H_2S-CO_2 system. They are provided to the reader as a way to extract predictions from our model without actually having to make calculations using the electrolyte-NRTL model. Figure 7.30 plots the H_2S partial pressure in kPa divided by the H_2S loading. By normalizing partial pressure by the loading, any mixture of CO_2 and H_2S loading are roughly combined onto a single line. The normalization works well at 40°C, but the curves exhibit deviations at 120°C when one acid gas loading is very small as compared to the other. The

normalization procedure also fails at acid gas loading of 0.5 and higher due to the presence of dissolved molecular acid gases.
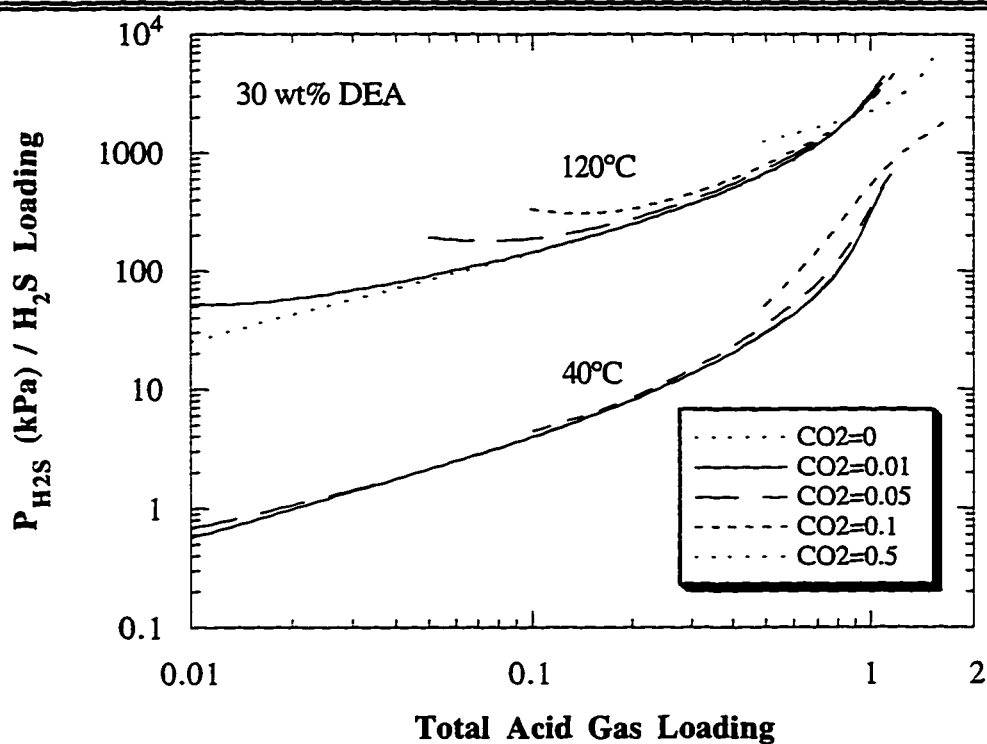
Figure 7.30 H_2S partial pressure in kPa normalized by the H_2S loading calculated from the electrolyte-NRTL model for 30 wt% DEA at 40°C and 120°C.

CO$_2$ partial pressures also fall onto one line when divided by the CO$_2$ loading at 40°C. Results at a loading of 0.5 and above did not match the other curves in figure 7.31. Curves for the mixed gases at 120°C also did not quite collapse when H$_2$S loading greatly exceeded CO$_2$ loading.
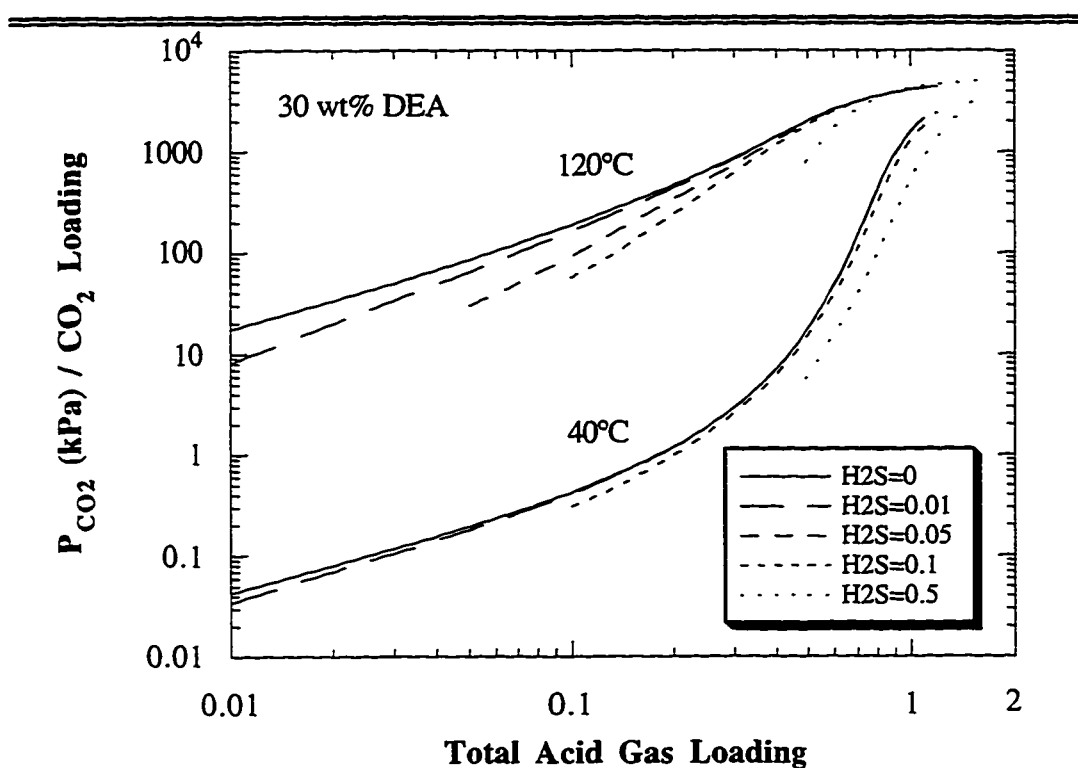
Figure 7.31 CO$_2$ partial pressure in kPa normalized by the CO$_2$ loading calculated from the electrolyte-NRTL model for 30 wt% DEA at 40°C and 120°C.

7.5 MDEA-DEA Mixed Amine System

Some very enlightening analogies can be made between the MDEA and DEA systems. Table 7.7 breaks down the important interaction parameters into sections so that they can be more clearly compared. The first similarity noticed is the hydroxide parameters. Recall that the (AmineH$^+$ OH$^-$) H$_2$O parameter was fit to hydroxide concentrations obtained from conductivity experiments in this work. The independently determined tau values for MDEA and DEA are amazingly similar at -5.6 and -5.75, respectively. The similarity leads to the possibility that this parameter is general for the alkanolamines and could be applied in monoethanolamine or diglycolamine systems.

Similarities are also seen in the H$_2$S systems. The (AmineH$^+$ HS$^-$) Amine parameter is also essentially the same for MDEA and DEA. This fact can be utilized when combining the parameter sets for mixed amine predictions. H$_2$O (AmineH$^+$ HS$^-$) parameters which are unique for each alkanolamine also had unique tau values.

CO$_2$ systems are more complex, however similarities were also seen in the amine parameters. Tau values for (AmineH$^+$ HCO$_3^-$) Amine parameter were almost identical between the MDEA and DEA versions of the parameter. Note however, that on the surface, the A and B constituents of the tau would appear very different. A conclusion drawn from this is that to compare electrolyte-NRTL parameter sets, the taus and not just the A and B parameters must be examined.

233

Table 7.7 Comparison of MDEA and DEA electrolyte parameters

Parameter	MDEA			DEA		
	A	B	Tau at 40°C	A	B	Tau at 40°C
Hydroxide						
H_2O (AmineH$^+$ OH$^-$)	8	0	8	8	0	8
(AmineH$^+$ OH$^-$) H_2O	-5.6	0	-5.6	-5.75	0	-5.8
Amine (AmineH$^+$ OH$^-$)	15	0	15	15	0	15
(AmineH$^+$ OH$^-$) Amine	-8	0	-8	-8	0	-8
H_2S						
H_2O (AmineH$^+$ HS$^-$)	5.00	0	5.0	7.766	0	7.8
(AmineH$^+$ HS$^-$) H_2O	-2.625	64.87	-2.4	-3.328	-185	-3.9
Amine (AmineH$^+$ HS$^-$)	15	0	15	15	0	15
(AmineH$^+$ HS$^-$) Amine	0.0416	-1436	-4.5	-4.132	-399	-5.4
CO_2						
H_2O (AmineH$^+$ HCO$_3^-$)	7.503	0	7.5	2.46	0	2.5
(AmineH$^+$ HCO$_3^-$) H_2O	-5.837	695	-3.6	-5.408	1182	-1.6
Amine (AmineH$^+$ HCO$_3^-$)	15	0	15	15	0	15
(AmineH$^+$ HCO$_3^-$) Amine	0.839	-2067	-5.8	4.865	-3432	-6.1
Amine (AmineH$^+$ CO$_3^=$)	15	0	15	15	0	15
(AmineH$^+$ CO$_3^=$) Amine	-8	1873	-2.0	-8	747	-5.6
H_2O (DEAH$^+$ DEACOO$^-$)	—	—	—	11.799	0	11.8
(DEAH$^+$ DEACOO$^-$) H_2O	—	—	—	-6.898	0	-6.9

Values for the (AmineH$^+$ CO$_3^=$) Amine parameter are quite different between MDEA and DEA. Recall in Chapter 6 that the carbonate concentrations and activity coefficients in MDEA were not credible. Standard deviations on the MDEA version of this parameter were 1200 compared to 700 for DEA. Carbonate concentrations also appeared more reasonable with what would be expected in DEA. Therefore, we have ignored the MDEA value for this parameter and assumed the DEA value to be adequate. Parameters for the water interactions are again unique to each alkanolamine. One extra parameter exists in the DEA-CO_2 system because MDEA cannot form the carbamate species.

Now that the similarities between the MDEA and DEA systems are clearly seen, that information can be used to improve parameter value selection in the mixed amine MDEA-DEA systems. Table 7.8 lists the parameter values that have been selected to represent interactions in the MDEA-DEA systems.

Since the Amine/Hydroxide parameters in the single amine systems were set to 15 and -8, they have also been set to 15 and -8 for the mixed amine hydroxide interactions. There might be interactions between the amines at low loading where hydroxide is present. To quantify this effect, conductivity experiments should be performed for the mixed amine system to determine if the hydroxide concentration is being properly predicted.

Only four parameters that might be significant arise in the mixed amine system. The other parameters which are not listed in Table 7.8 are with sulfide ions which have negligible concentrations. Therefore, those parameters remained at default values of 15 and -8 and do not affect model predictions. From the analogies in Table 7.7 we can set the $(AmineH^+ \ HS^-)$ Amine parameters to the average of MDEA and DEA values. MDEA and DEA taus were plotted as a function of temperature and the average curve between them, tau $= -1.73 -1026/T$, is given below in Table 7.8. Therefore, the two resulting tau parameters are all that are needed for predictions in the MDEA-DEA-H_2S system.

Table 7.8 MDEA-DEA mixed amine parameters

Parameter	A	B	Tau at 40°C
Hydroxide			
MDEA (DEAH+ OH-)	15	0	15
(DEAH+ OH-) MDEA	-8	0	-8
DEA (MDEAH+ OH-)	15	0	15
(MDEAH+ OH-) DEA	-8	0	-8
H₂S			
MDEA (DEAH+ HS-)	15	0	15
(DEAH+ HS-) MDEA	-1.73	-1026.7	-5.0
DEA (MDEAH+ HS-)	15	0	15
(MDEAH+ HS-) DEA	-1.73	-1026.7	-5.0
CO₂			
MDEA (DEAH+ HCO3-)	15	0	15
(DEAH+ HCO3-) MDEA	2.8	-2727	-5.9
DEA (MDEAH+ HCO3-)	15	0	15
(MDEAH+ HCO3-) DEA	2.8	-2727	-5.9
MDEA (DEAH+ CO3=)	15	0	.15
(DEAH+ CO3=) MDEA	-8	747	-5.6
DEA (MDEAH+ CO3=)	15	0	15
(MDEAH+ CO3=) DEA	-8	747	-5.6
MDEA (MDEAH+ DEACOO-)	15	0	15
(MDEAH+ DEACOO-) MDEA	2.8	-2727	-5.9
MDEA (DEAH+ DEACOO-)	15	0	15
(DEAH+ DEACOO-) MDEA	2.8	-2727	-5.9
DEA (MDEAH+ DEACOO-)	15	0	15
(MDEAH+ DEACOO-) DEA	2.8	-2727	-5.9
H₂O (MDEAH+ DEACOO-)	11.8	0	11.8
(MDEAH+ DEACOO-) H₂O	-6.9	0	-6.9

Again the CO_2 system is seen to be much more complex. As stated before, errors were noted in the MDEA carbonate predictions. Therefore, mixed amine carbonate parameters have been set to the values for DEA-CO_2 of 15 and

(-8 +747 / T). Amine-bicarbonate parameters have been set to the average tau parameters as a function of temperature from MDEA and DEA. The procedure is the same as used for the bisulfide parameters. Resulting tau parameters of 15 and (2.8 -2727 / T) are given above in Table 7.8.

It has been assumed that $MDEAH^+$ ions behave similarly to $DEAH^+$ ions. Therefore, the H_2O ($MDEAH^+$ $DEACOO^-$) parameter and its inverse have been set to the same values obtained for the H_2O ($DEAH^+$ $DEACOO^-$) parameters in Table 7.7. A less direct comparison can be made for the mixed amine-carbamate parameters. In the $DEA-CO_2$ system, the DEA ($DEAH^+$ $DEACOO^-$) parameter and its inverse were set to 15 and -8, respectively. To maintain consistency with the $DEA-CO_2$ system, this parameter was left at these defaults. However, it was believed that the other amine permutations of this carbamate parameter were important. Lacking a non-default analogous parameter, it has been assumed that the ($AmineH^+$ $DEACOO^-$) ion pair behaves similarly to the ($AmineH^+$ HCO_3^-) ion pair. Therefore, the other three Amine1 (Amine2H^+ $DEACOO^-$) parameters have been set to the same taus as given for the bicarbonate-amine interactions.

7.5.1 Data fitting

Now that a parameter set has been compiled for the MDEA-DEA systems, its predictions are compared to experimental VLE data. No other kind of data such as pH or heat of absorption were found for the mixed amine systems. Analysis begins with the MDEA-DEA-H_2S system. Only the data of Huang and Ng (1995) exist for this system. Figure 7.32 illustrates that the model has done an excellent job fitting the data considering no parameters were regressed upon this

237

data. Calculated values are slightly higher than the experimental values at low loading. However, predictions of this data set were low by a factor of ten when using the 15 and -8 default values for the bisulfide parameters. Therefore, this model represents a vast improvement over the Austgen et al. (1991) model, which used the incorrect default values for the mixed amine H_2S systems. If desired, the bisulfide tau values could be regressed to provide an even better fit of the Huang and Ng (1995) data.
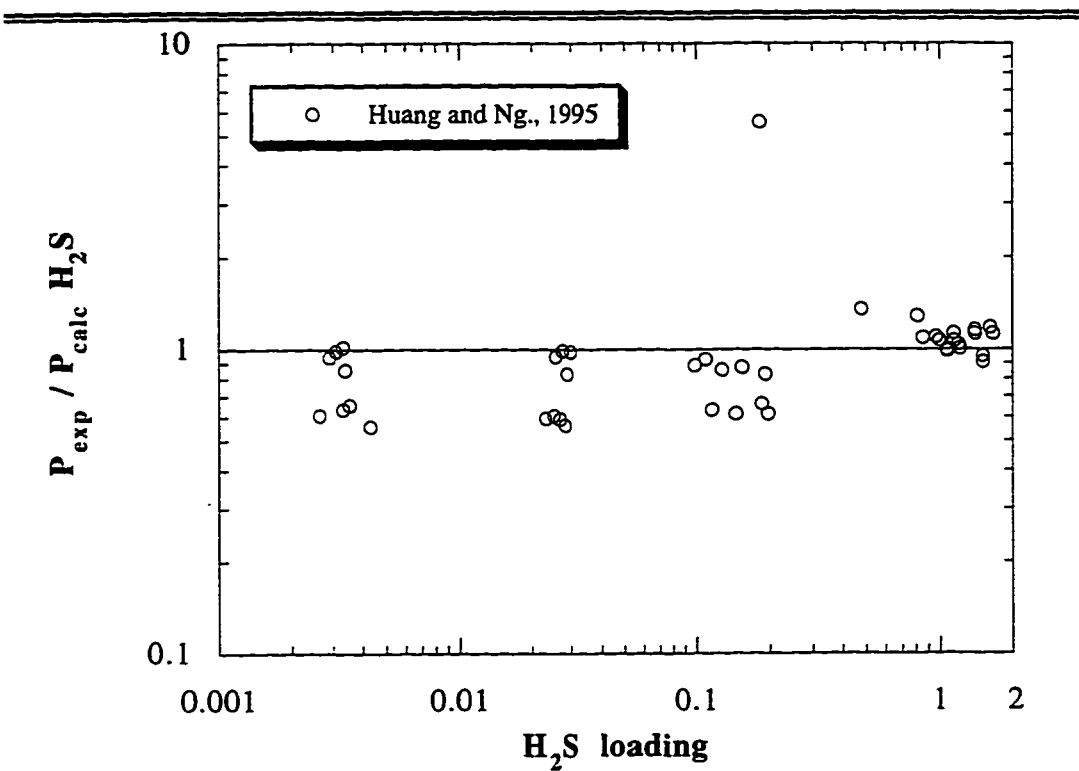
Figure 7.32 Ratio of experimental to model predicted H_2S partial pressures from the mixed amine parameter set. Mole fractions were simultaneously predicted.

Mole fractions are simultaneously predicted in this analysis method and the deviation is shown in figure 7.33. Mole fractions were predicted well with less than 15% error versus the experimental values.
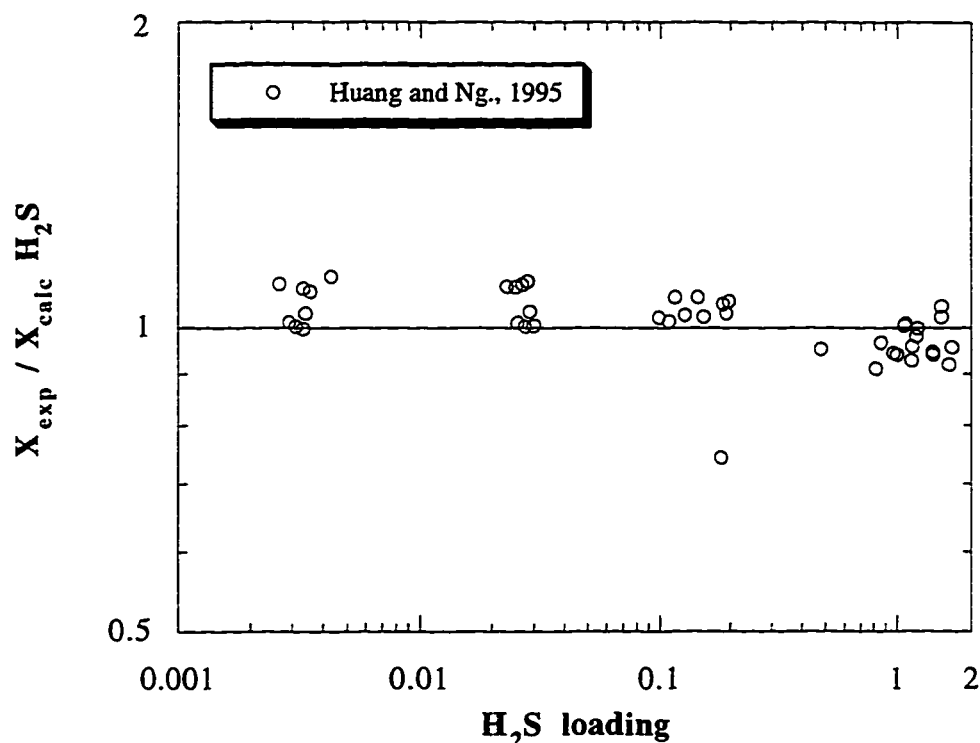
Figure 7.33 Ratio of experimental to model predicted H_2S mole fraction from the mixed amine parameter set. Partial pressures were simultaneously predicted.

As mentioned above, using ambiguous default values for the important amine mixture parameters can drastically affect model performance. Figure 7.34 compares predictions of the mixed model to MDEA-DEA-CO_2 data when parameters from Table 7.8 are set to the 15 and -8 defaults. Predictions above a loading of 0.1 match the experimental data very well. However, the model

239

underpredicts the data by two orders of magnitude at lower loadings. Mole fraction predictions, which are not shown here, were also wrong by as much as a factor of 10 at low loading. If mole fractions were assumed to have no error, then the pressures in figure 7.34 would be low by a factor of 1000 instead 100.
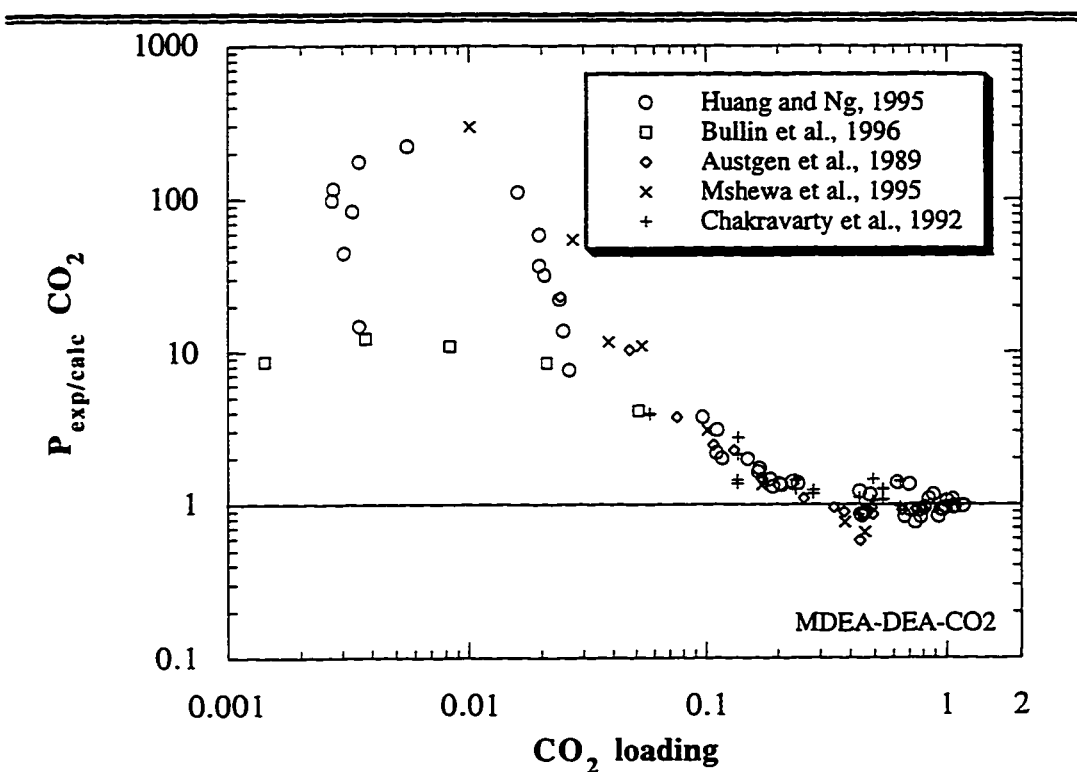
Figure 7.34 Ratio of experimental to model predicted CO_2 partial pressures from the electrolyte-NRTL model with default values of 15 and -8 for mixed amine parameters. Mole fractions were simultaneously predicted.

Proper mixed amine parameters from Table 7.8 were then used to compare to the MDEA-DEA-CO_2 data. Figure 7.35 illustrates the vast improvement in prediction of this data. All of the partial pressure data is now fit within a factor of three with most of the data being fit within 50%. The experimental data consists

of DEA/MDEA ratios ranging from 1/20 to 1/1. CO_2 partial pressure is still consistently underpredicted by the model with the better mixed amine parameter set. Therefore, some of the mixed amine parameters could be regressed to better fit this data. It was not performed in this work in order to properly quantify the method of parameter selection demonstrated in this work. This technique for mixed amine parameter selection will likely be applied to systems where no mixed amine data exist.
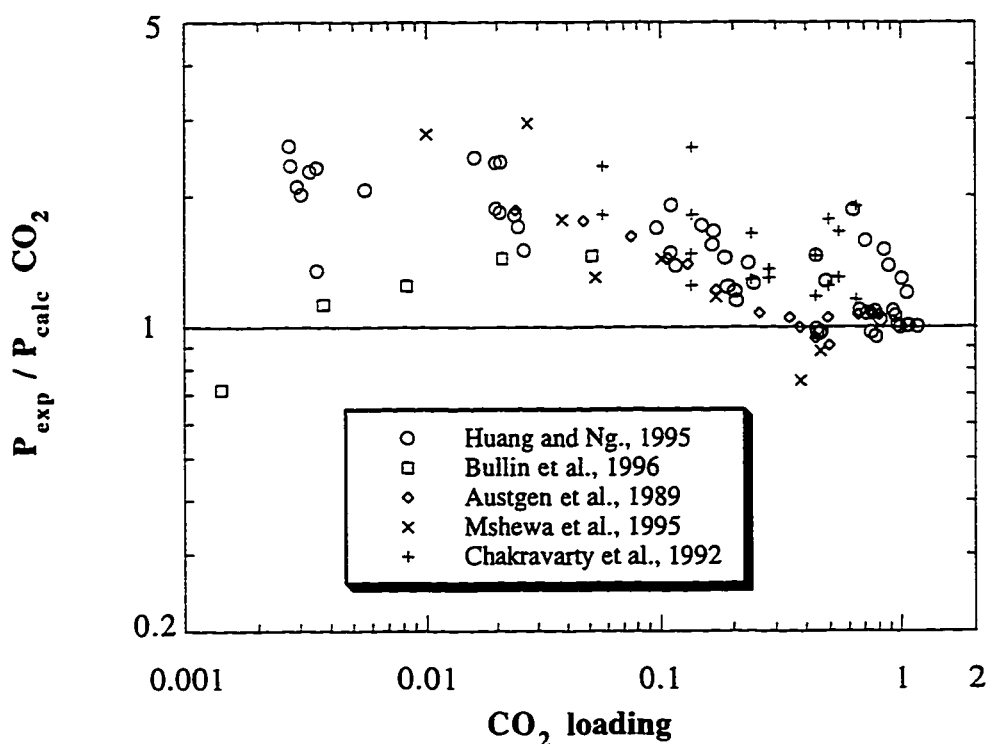
Figure 7.35 Ratio of experimental to model predicted CO_2 partial pressures as a function of H_2S loading for the correct parameter set in Table 7.8. Mole fractions were simultaneously predicted.

Mole fraction of the CO_2 is simultaneously predicted and shown in figure

7.36. Mole fractions are shown to be predicted within 20%, where errors as much

as 100% were seen when using incorrect default parameters.
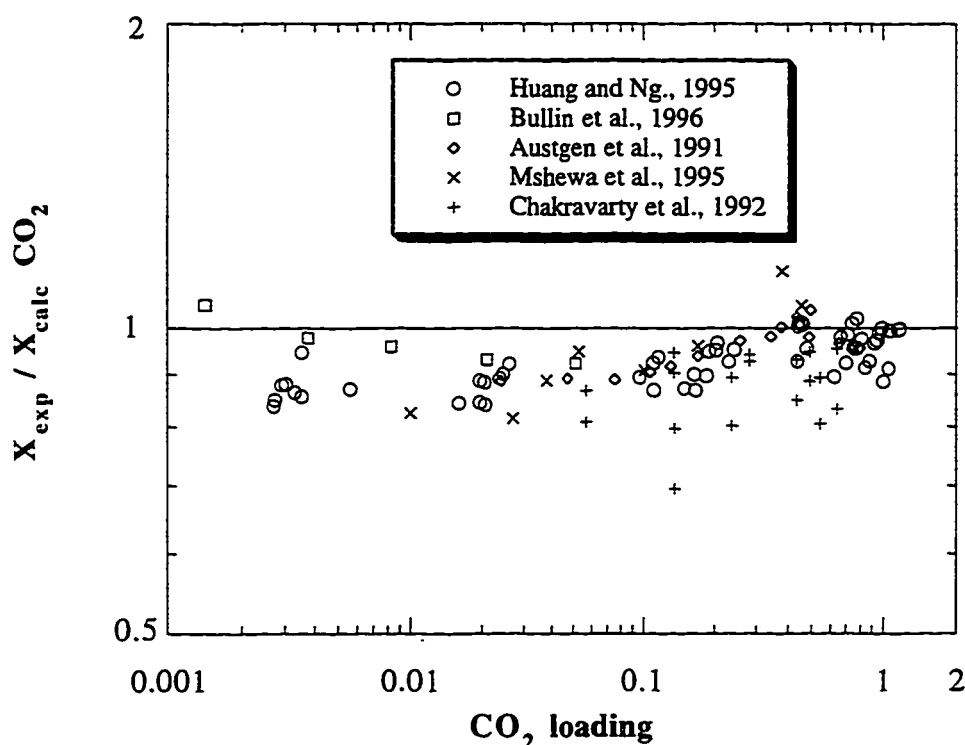
Figure 7.36 Calculated/experimental CO_2 mole fraction versus total loading calculated from electrolyte-NRTL model to unregressed data.

Only one data source was found that contained all four species of the

MDEA-DEA-CO_2-H_2S system. Data by Bullin et al. (1996) is compared in

figure 7.37 to model predictions. There were two series of data with H_2S loading

being approximately constant at the values indicated in the figure. Note that H_2S

constitutes the majority of the acid gas in the two series of data. Therefore,

predictions should be similar to the Huang and Ng (1995) data for

MDEA-DEA-H2S. Both data sets are overpredicted slightly at low loading by the model.
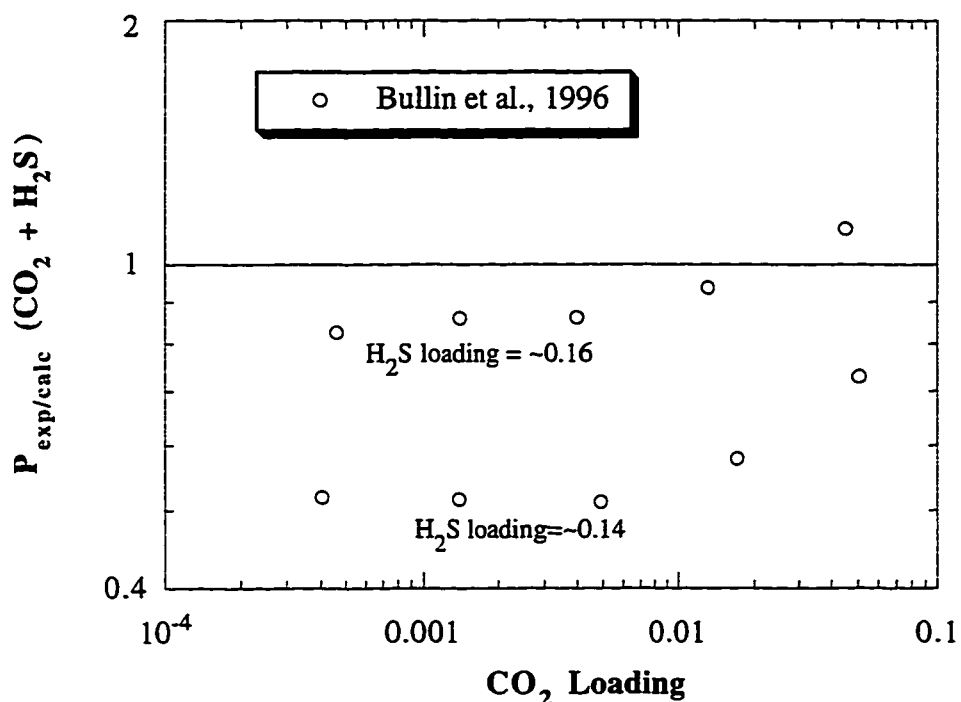
Figure 7.37 Ratio of experimental to model predicted total acid gas partial pressure as a function of CO_2 loading for the combined parameter set. Mole fractions were simultaneously predicted.

7.5.2 Pressure Predictions

Figures 7.38 through 7.41 present the predictions for the MDEA-DEA-H_2S-CO_2 model created in this work. The reported weight percent of the amines are based on the total grams of amine and water, neglecting acid gas concentrations. For example, in 100g of a 40 wt% MDEA/10 wt% DEA solution, there would be 40g of MDEA, 10g of DEA and 50g of water. Two MDEA/DEA

mixtures at 40 wt%/10 wt% and 25 wt%/25 wt% have been chosen due to their industrial significance and the likelihood that their predictions would be sufficiently different from pure MDEA or DEA to be interesting.

Acid gas partial pressures in kPa are divided by their loading to remove the first order effect of CO_2 loading on the H_2S partial pressure. This normalization also reduces the decades shown in the y-axis. This condensation of the partial pressures allows the effect of several different variables to be illustrated on a single plot. In a sense, dividing by the loading is also a modeling assumption on the direct relationship of partial pressure to loading. This assumption breaks down where CO_2 loading exceeds H_2S loading and at high loadings where significant concentrations of molecular gases exist. This explains why the curves are not combined where CO_2 exceeds H_2S and at 0.5 loading where significant amounts of acid gases already exist.
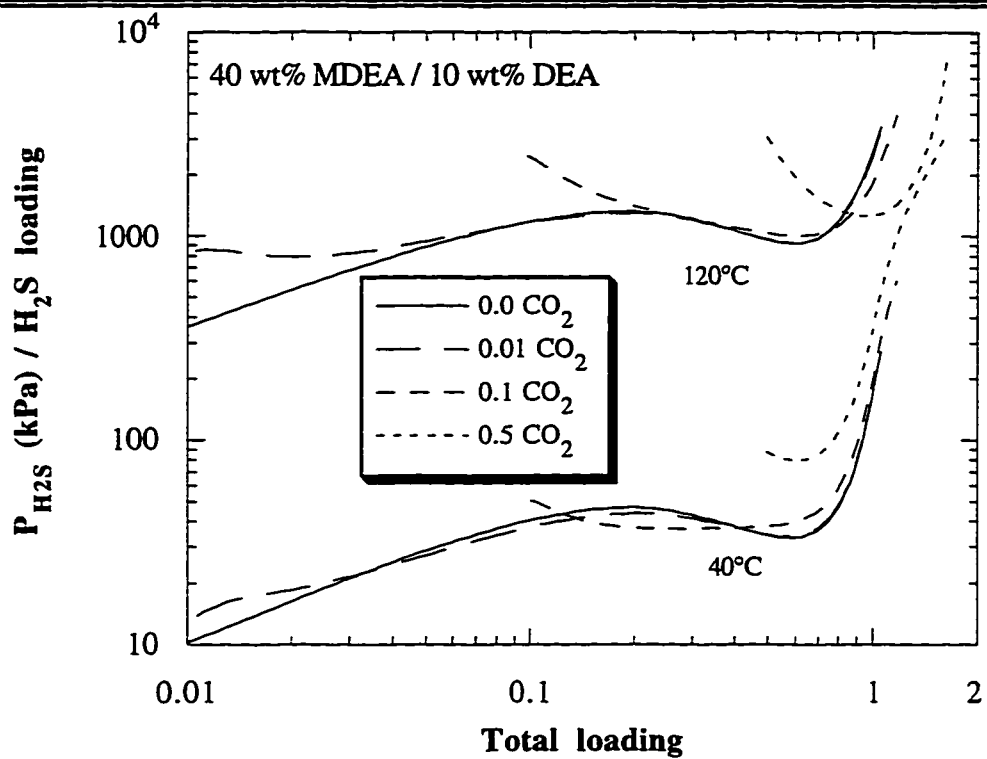
Figure 7.38 H_2S partial pressure in kPa divided by the H_2S loading at various constant CO_2 loadings at 40°C and 120°C in 40 wt% MDEA / 10 wt% DEA.
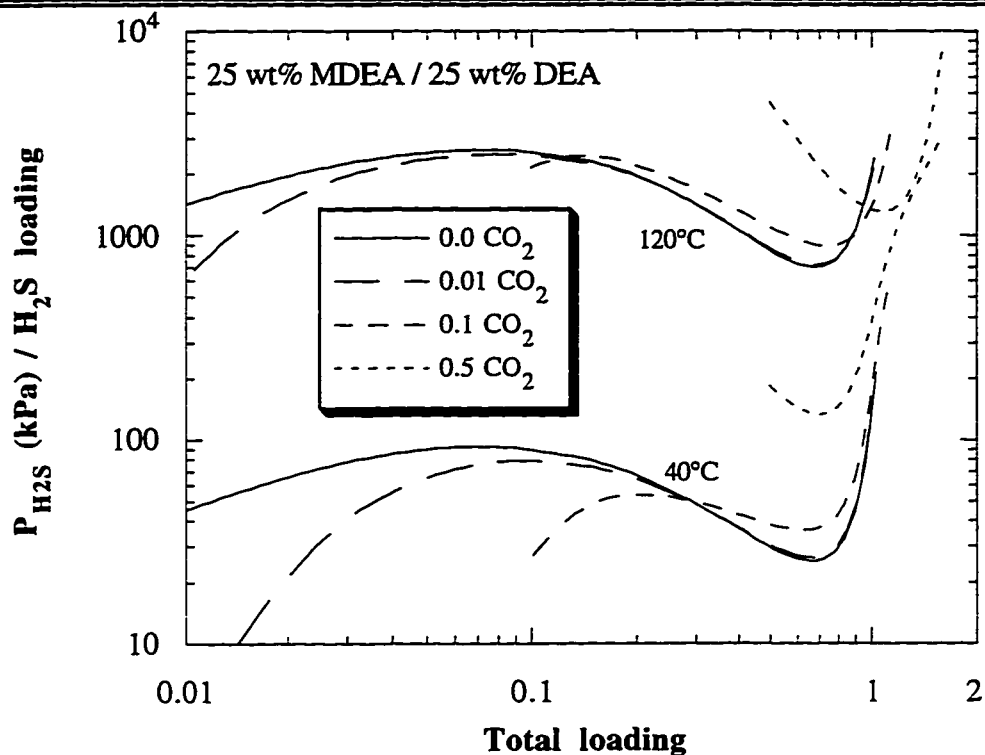
Figure 7.39 H₂S partial pressure in kPa divided by the H₂S loading at various constant CO_2 loadings at 40°C and 120°C in 25 wt% MDEA / 25 wt% DEA.

CO_2 predictions for the mixed amine systems are very similar to the single amine, mixed gas predictions. Note the reverse nature of the CO_2 curves to the H_2S curves in the above figures. While CO_2 forced the H_2S pressure curve downward in figures 7.38 and 7.39, H_2S increases the pressure curves in figures 7.40 and 7.41. The curves collapse reasonably well except for CO_2 loadings of 0.5 and above. These curves would not be expected to normalize well due to the presence of molecular CO_2.
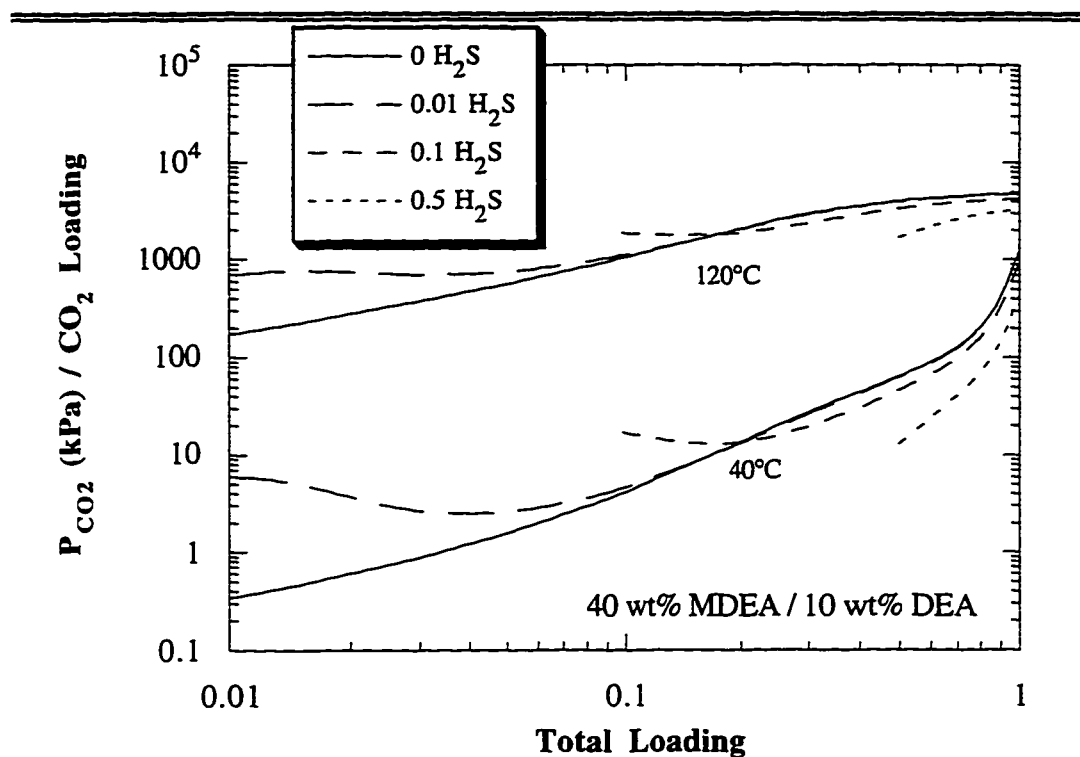
Figure 7.40 CO_2 partial pressure in kPa divided by the CO_2 loading at various constant H_2S loadings at 40°C and 120°C in 40 wt% MDEA / 10 wt% DEA.
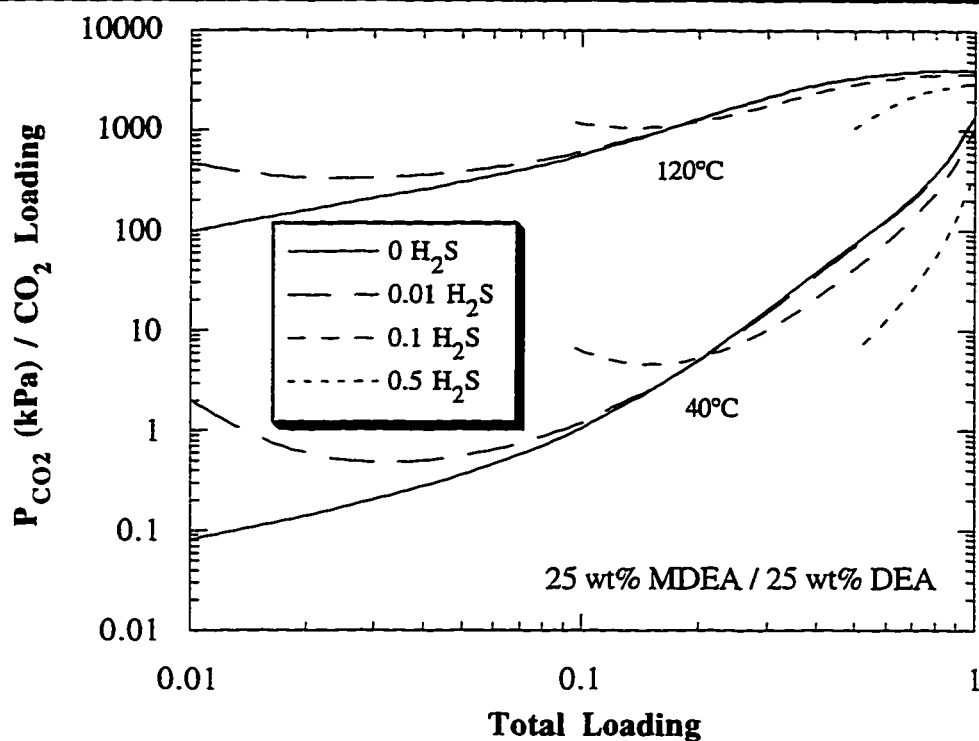
Figure 7.41 CO$_2$ partial pressure in kPa divided by the CO$_2$ loading at various constant H$_2$S loadings at 40°C and 120°C in 25 wt% MDEA / 25 wt% DEA.

One of the main reasons for using an amine mixture is to improve equilibrium towards CO$_2$. Figure 7.42 demonstrates the strong CO$_2$ absorption ability that DEA adds to an MDEA solution. By adding as little as 10 wt% DEA into a 50 wt% total amine solution, CO$_2$ partial pressure is reduced by a factor of ten.
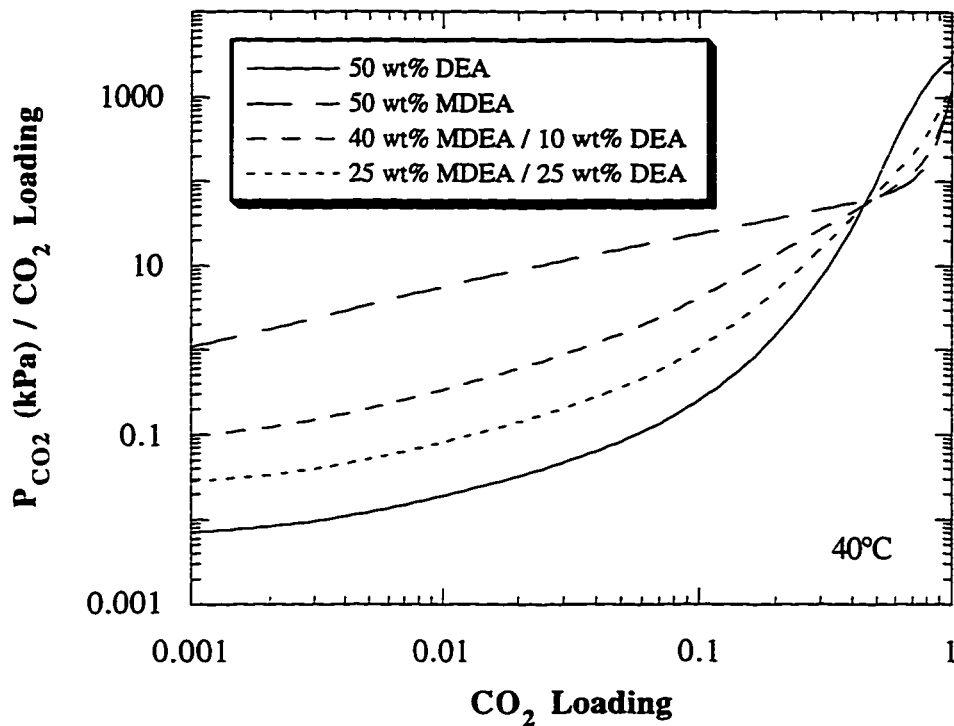
Figure 7.42 CO_2 partial pressure normalized by CO_2 loading for several 50 wt% amine mixtures at 40°C.

Stripper condition CO_2 partial pressures are predicted in figure 7.43 below. This curve demonstrates one reason why adding too much DEA to an MDEA solution should be avoided. Even at 120°C, the CO_2 partial pressure remains very low for the DEA/MDEA mixtures and will require more stages and reboiler steam to regenerate the solvent. Given the above conclusions, care must be taken in considering all of the factors involved in adding DEA to an existing MDEA-only gas treating design.
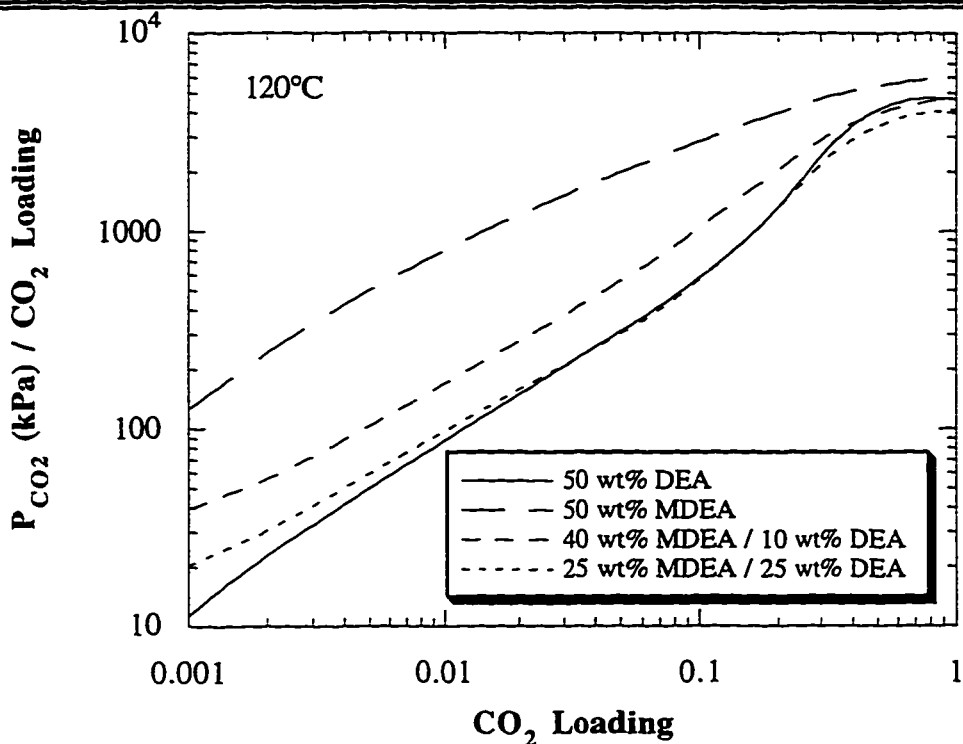
Figure 7.43 CO_2 partial pressure normalized by CO_2 loading for several 50 wt% amine mixtures at 120°C.

One other concern with DEA mixtures is that DEA has a higher heat of absorption with CO_2 than does MDEA. Our model confirms this trend and curves for heat of absorption in 50 wt% amine solutions and their mixtures are given in figure 7.44. At acid gas loadings below 0.4, which is where commercial absorbers operate, DEA significantly increases the heat of absorption with respect to CO_2. As little as 10% DEA increases the heat of absorption from -60 to -80 kJ/gmol CO_2 at low loading. The DEA heat of absorption curves decrease quickly above a loading of 0.4 due to the saturation of the carbamate mechanism.
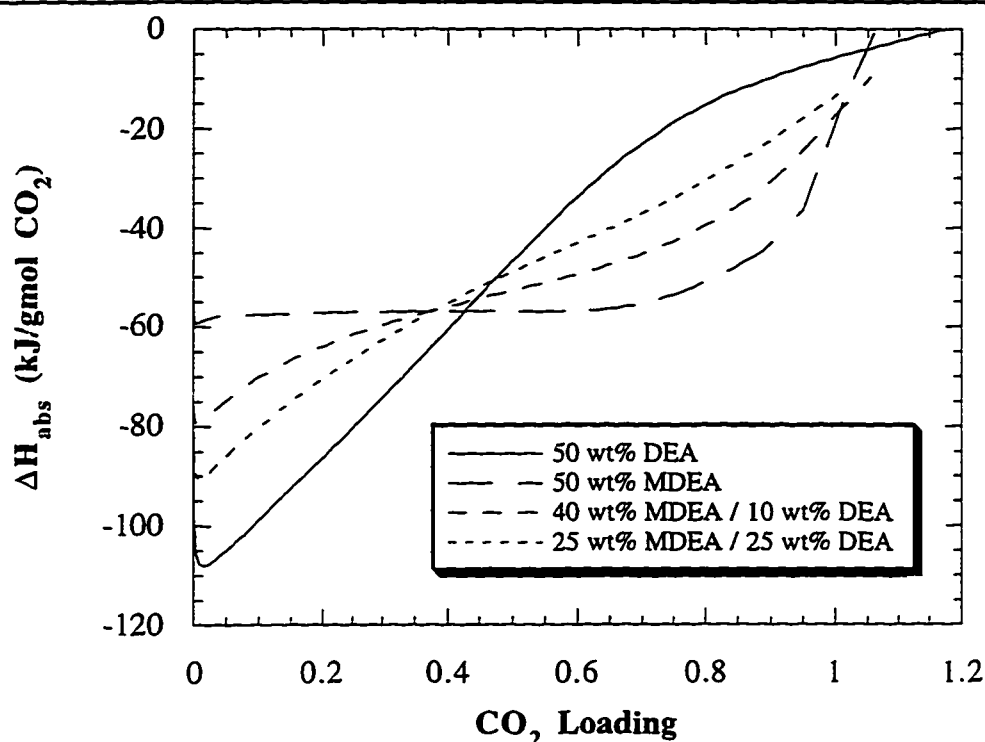
Figure 7.44 CO_2 heat of absorption in MDEA, DEA and their mixtures as a function of CO_2 loading and assumed independent of temperature.

Heat of absorption for H_2S in mixed amines is more constant, however. This is because absorption occurs under the same mechanism and all of the same reactions are involved. MDEA and DEA heats of absorption are not the same due to a small difference in the heats of reaction of the amines with water. There is little difference in the heat of absorption for a 40 wt%/10 wt% mixture compared to a 25 wt%/25 wt% mixture of MDEA and DEA.

251
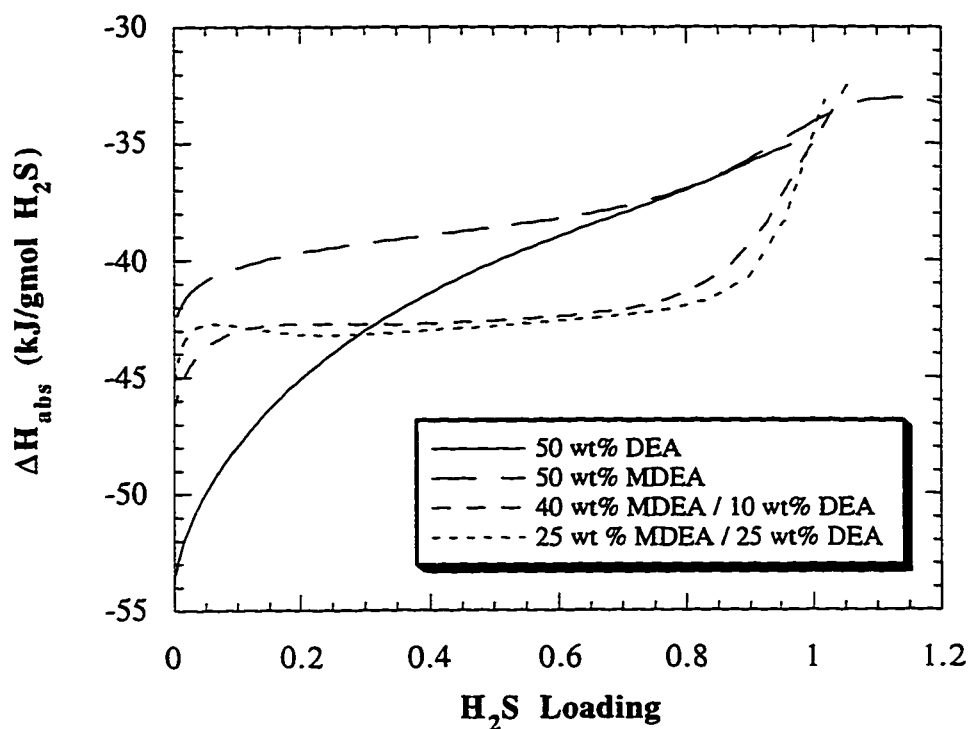
Figure 7.45 H₂S heat of absorption in MDEA, DEA and their mixtures as a function of H₂S loading and assumed independent of temperature.

7.6 CONCLUSIONS

DEA-H₂S

Modeling for the DEA-H₂S system was relatively trouble free. Using experience from regressing the MDEA-H₂S system, analogous parameters were regressed for DEA. Tau values at 40°C for the analogous parameters are similar between DEA and MDEA in this work. The hydroxide parameters are almost identical at -5.75 and -5.6 for DEA and MDEA, respectively. The similarity suggests that the hydroxide parameter used in this work might be general and the

value could be used for other amine systems. Predictions of partial pressure are approximately the same as predicted by Austgen et al. (1989), with our model being adjusted to properly predict hydroxide speciation at low loading. Predictions of heat of absorption and pH by the DEA-H_2S model match experimental data very well. VLE data was fit well and the standard deviations on the parameters were low, which leads to high confidence in this parameter set for the DEA-H_2S system.

DEA-CO₂

DEA-CO_2 is the most complex binary system to model. It has all of the analogous reactions and ionic species of the other binary systems, but in addition has an unknown carbamate equilibrium constant. Since this equilibrium constant must be regressed, the resulting values are correlated to the electrolyte parameters and can only be viewed in light of the total model. It is better to compare predictions of partial pressure and speciation rather than model parameters when comparing different DEA-CO_2 models.

The carbonate parameter is also not well determined as occurred for the MDEA-CO_2 system. Carbonate parameters are correlated with the carbamate parameters resulting in higher standard deviations. Carbonate concentration is also uncertain due to its insignificance in the overall CO_2 balance at the loading range where VLE data exists. However, unlike the MDEA system, carbonate activity coefficient predicted by the model is reasonable.

Partial pressures are fit well by this model and agree with Austgen at CO_2 loadings above 0.1. This work predicts lower partial pressures than Austgen at

loadings below 0.1 at 80 and 120°C. This is due to the different temperature dependencies in the carbamate equilibrium constant and the electrolyte-NRTL parameters. The difference also results from a lack of data in those regions which constitute extrapolations of the model. The average heat of absorption calculated from the model matches experimental data extremely well. In addition, the model is consistent with the hydroxide concentration and pH data measured in this work.

DEA-CO_2-H_2S

Experimental data that was not regressed has been predicted very well by the mixed parameter set. Data from Lal et al (1985) at 100°C was not predicted as well as the others and tended to be overpredicted by this model. Mixed gas total partial pressure data from Bullin et al. (1996) and Lee et al. (1974) was very well predicted and the model split the data scatter. This leads to the conclusion that there were no parameters for the mixture which had any effect on the partial pressure predictions that were not already determined in the single gas systems.

MDEA-DEA-CO$_2$-H$_2$S

A method has been demonstrated for judicious selection of parameters and their values in the mixed amine systems. Unlike the single amine-mixed gas systems, the mixture parameters in an amine mixture cannot be set to arbitrary default values. Proper accounting of the interactions of the amines with carbamate, bicarbonate, carbonate, and bisulfide ions are required to form an accurate model for loadings below 0.1. Partial pressure predictions above a total acid gas loading of 0.1 matched experimental data well and appear to be independent of the mixed parameters.

The model matches experimental H$_2$S data very well without any parameter adjustments. Austgen et al. (1991) set all of the H$_2$S mixed amine parameters to values of 15 and -8. These default values result in H$_2$S partial pressures being underpredicted by a factor of ten at low loading.

CO$_2$ pressures are also predicted well above a loading of 0.1. However, at loadings below 0.1, the model consistently underpredicts partial pressures by a factor of two. This is because the parameter values chosen were not optimized to fit the current data sets. The assumption that bicarbonate interactions are similar to carbamate interactions might also be a source of error.

Austgen (1989) set all of the CO$_2$ parameters to the 15 and -8 defaults and regressed the H$_2$O (MDEAH$^+$ DEACOO$^-$) parameters to fit his mixed amine CO$_2$ data. However, his data was at high loadings so the degree that these parameters helped to fit the data is uncertain and the standard deviations on them were relatively large.

CO_2 partial pressures in MDEA solutions are greatly decreased by the addition of DEA. In addition, the high heat of absorption of DEA with CO_2 quickly increases heat of absorption of an amine mixture. As little as 2 wt% DEA in a 50 wt% amine solution will result in noticeable differences in the equilibrium partial pressures and heats of absorption with CO_2.

The method for determination of mixed amine parameters and their values is completely general. This technique can easily be applied to other amine mixtures for which VLE data might not exist. Many of the interactions noted also appear to be independent of the amine. Therefore, it is conceivable that this technique could be applied to modeling of similar alkanolamine solutions for which no VLE data exists in a purely predictive way.

Chapter 8: Conclusions and Recommendations

8.1 CONCLUSIONS

In order to better understand behavior in acid gas treating systems that are based on aqueous alkanolamine solutions an equilibrium model is needed. Therefore, the goal of this work was to obtain a thermodynamically consistent model which matches experimental VLE data in addition to predicting with confidence conditions where VLE data is non-existent or inaccurate. In the process of creating this equilibrium model many things were learned.

1) Binary alkanolamine-water systems are highly non-ideal.

Many existing equilibrium models incorrectly assume ideal behavior for the binary amine water systems. Heat of mixing was measured for MEA-H_2O, MDEA-H_2O and DEA-H_2O systems and was shown to be large. Heat of mixing is directly related to the temperature dependence of the activity coefficients, therefore the amine systems are non-ideal. Heat of mixing from largest to smallest values is MDEA>MEA>DEA.

2) Total pressure data is insufficient for proper modeling of binary amine-water systems.

Total pressure of amine-water solutions is dominated by the water vapor pressure due to the low volatility of the alkanolamines. This results in experimental data which is not sensitive to the amine activity coefficient and

therefore is poor data for creation of a model. Freezing point depression and heat of mixing data have been regressed with total pressure data to form the best models of the amine-water systems to date.

3) A simple VLE model can be used to quickly compare data.

A simple model was developed in this work and regressed upon experimental VLE data. Using the model, experimental data sets that were far from the norm were identified with minimal effort. The model works well for all of the single amine systems studied except for DEA-CO_2 and has comparable partial pressure predictions to more complex models. CO_2 partial pressures in DEA are independent of amine concentration at low loading, but the model assumes a direct dependence upon amine concentration over the entire loading range.

4) Accurate low loading predictions cannot be based upon VLE data alone.

VLE data has the greatest errors at low loadings where experimental techniques have been pushed to the lower detection limits. Therefore, pH and conductivity data were measured to supplement the VLE data.

- Conductivity is directly related to ionic concentrations and was used to determine hydroxide concentrations in unloaded amine-water solutions. Hydroxide ions are an important species below a loading of 0.001 and significantly affect VLE predictions in this range.

- pH data is accurate over the entire loading range and can be regressed simultaneously with VLE data. These data also serve as a thermodynamic check

of the model and of discrepant VLE data sets. pH data and predictions in this work also have applications in process control and laboratory work where pH can be an indirect measure of acid gas loading.

5) The electrolyte-NRTL model is an appropriate structure for representing acid gas vapor-liquid equilibria.

The model is thermodynamically consistent and its implementation in Aspen Plus™ is versatile. Predictions can be made anywhere on the continuum from pure water and amines to the mixed amine-mixed acid gas systems. One drawback is an inconsistency in Aspen Plus'™ activity coefficient reference state for Henry's Law components. The activity coefficients at infinite dilution are a function of the acid gas loading. This is unexpected since the concentration of all of the species associated with a Henry's component are defined to be zero at infinite dilution conditions. This difference mainly affects activity coefficients and calculated speciation at acid gas loadings above 0.5 and does not affect calculated partial pressures at acid gas loadings below 0.8.

6) Interactions of the amines with salts are necessary for accurate modeling of the solution thermodynamics.

Mole fraction concentrations of the amines are normally less than 15% of the total solution. Therefore, one might assume that the interactions with water are more important than with the amine. However, it is the difference between the water and amine interactions that is needed for modeling solution behavior. From that standpoint, the water parameters, amine parameters or both could be regressed.

The amine parameters, however, have a greater power to affect the model because they are further away from their reference state than is water.

7) Ionic concentrations are difficult to predict accurately from the model for CO_2 systems.

Carbonate parameters were regressed in this work, but the lack of sensitivity of the data to carbonate concentrations resulted in poorly predicted parameters. Carbamate speciation in the DEA-CO_2 system is also of great interest. Unfortunately, the equilibrium constant is not well known and must be regressed upon experimental VLE data. This results in the carbamate equilibrium constant being correlated with all of the other parameters that were simultaneously regressed. Therefore, simple comparisons of values of the carbamate equilibrium constant are not appropriate. For DEA-CO_2 models, predicted ionic concentrations, pH and partial pressures should be compared rather than model parameters.

8) Predictions for single amine-mixed acid systems can be made by combining parameters from the single amine-single acid gas systems.

No significant parameters arise in the mixed acid gas system. The only parameters that were not already included in the single gas systems involve the molecular acid gases. Since molecular acid gas concentrations are very small, these parameters have no power to affect model predictions and any reasonable default value will suffice. Partial pressure data for the MDEA-H_2S-CO_2 and DEA-H_2S-CO_2 systems are predicted well by this model. The good fit not only

confirms the above assumption but also serves to further confirm predictions for the single amine-single acid gas systems.

9) Accurate predictions for mixed amine systems cannot be made with arbitrary default values for the mixed amine parameters.

Predictions above a loading of 0.1 appear to be independent of the mixed amine parameter values. However, at acid gas loadings below 0.1, without intelligent amine mixture parameters, experimental data was underpredicted by as much as a factor of 100. Mixed amine parameters involving carbonate, carbamate, bicarbonate and bisulfide ions were found to be very important for accurate model predictions. Comparison of analogous parameters between MDEA and DEA systems leads to better choices for mixed amine parameter values. This procedure can be used for other mixed amine systems to improve low loading predictions even in the absence of mixed amine data.

8.2 RECOMMENDATIONS

8.2.1 Speciation Experiments

Activity coefficients and species concentrations are by definition correlated in the activities of the equilibrium constants. Without accurate knowledge of one of them, independent values for the pair cannot be obtained from regression of experimental data. However, with direct measurement of species concentrations this correlation can be broken and the parameters will be more accurately determined.

Titration experiments with hydroxide can be performed in the carbamate forming systems. A preloaded solution is titrated to a high pH with base. The protonated amine and bicarbonate are titrated, but the carbamate species is assumed to be unaffected. The carbamate concentration can be determined by subtracting the bicarbonate concentration from the total CO_2 loading obtained from a separate measurement.

8.2.2 pH Experiments

pH experiments were only made at temperatures below 40°C. The usefulness of the data could be expanded by taking measurements up to 100°C, which is the upper temperature limit for most pH probes. This data could subsequently be used to further refine model predictions at high temperatures where VLE data is less abundant. Because pH data is related to activity of the hydronium ion, it also suffers from correlation and is not as powerful of a regression tool as speciation data would be.

pH data is, however, a useful tool due to its direct relationship with acid gas loading. The pH of a solution could be measured directly to determine acid loading instead of taking a sample and performing a time consuming liquid analysis. pH might not be a good measure of loading in an industrial process stream where significant amounts of salts or other contaminants affect the measured pH.

8.2.3 Conductivity Experiments

The conductivity probe used in this work was rated only up to 50°C. Therefore, extracting a temperature dependence of the hydroxide concentration

was not possible within the error of the data. However, conductivity probes exist which work at temperatures up to 100°C. A new probe could be used to better determine the temperature dependence of the hydroxide concentration and therefore low loading predictions.

Experiments could also be expanded as a function of amine concentration and amine mixtures. Measurements as a function of amine concentration will allow confirmation of hydroxide predictions as the amine concentration approaches zero. Experiments in mixed amines will allow determination of the mixed amine hydroxide parameters. The assumption in this work that these parameters are not needed might also be confirmed.

8.2.4 Aspen Plus™ Activity Coefficient Normalization

The reference state for Henry's constants as implemented by Aspen Plus™ should be further studied. An independent FORTRAN code should be developed to quantify the effect this discrepancy has on high loading predictions. Once a model is constructed, parameters for the electrolyte-NRTL model will have to be re-regressed under the new framework. A conclusion might be that the error is not very significant. If the error is significant, a provision can be added stating that the model should not be used above some specified loading.

8.2.5 Regress N_2O Solubility data

Data for the physical solubility of N_2O in the amine-water solutions exists in the literature. From analogy the physical solubility of CO_2 in amine-water solutions can be obtained. In this work, only the solubility of CO_2 in water was

explicitly accounted for. Binary parameters of the model should regressed with this data to improve predictions of molecular CO_2 concentration.

8.2.6 Modeling Other Mixed Amine Systems

The procedures for obtaining good choices for the mixed amine parameters should be applied to other industrially significant mixtures such as MDEA-MEA and MDEA-DGA. Predictions might be made by simply assuming that DEA behaves like MEA and DGA and by using the identical parameter set. Of course, primary data such as equilibrium constants and physical properties of the amine to be modeled would have to be used. This theory can be tested for the MEA system for which some mixed amine data exists.

8.3 SUMMARY

Overall, a thermodynamically sound model has been constructed for the alkanolamine-acid gas systems. Partial pressure data are shown to be accurately predicted by the model. This work also represents the best prediction to date of low loading conditions due to the conductivity data utilized and the careful parameter choices made for the mixed amine systems. Model predictions have been augmented using thermodynamically related data such as heat of absorption, pH, conductivity and speciation. Standard deviations and correlation matrices are given for the parameters to help determine model accuracy and sensitivities. By combining knowledge of all aspects of the solution the model does not only predict partial pressures, but presents a complete thermodynamic picture of acid gas loaded, aqueous alkanolamine solutions.

Appendix A : Tabular Conductivity Data

Table A.1. Conductivity measurements

Temp., °C	Conductance, millimhos	Conductivity, mmho/cm	Temp., °C	Conductance, millimhos	Conductivity, mmho/cm
49 wt% MDEA #1, CO₂ ldg = 0.00018			**49 wt% MDEA #2**		
24.93	0.0519	0.0565	28.5	0.0634	0.0690
30	0.062	0.0675	30	0.0622	0.0677
35	0.0768	0.0836	35	0.0719	0.0782
38.5	0.0874	0.0951	37.5	0.0795	0.0865
39.5	0.09	0.0979	39	0.0847	0.0922
40	0.0911	0.0991	40	0.0887	0.0965
24.5 wt% MDEA			**1 wt% MDEA**		
25.71	0.214	0.233	23.5	0.1176	0.1279
30	0.245	0.267	25.5	0.118	0.1284
34	0.266	0.289	30	0.1395	0.1518
38	0.313	0.341	35	0.1582	0.1721
40	0.326	0.355	37.5	0.1698	0.1847
			39	0.1768	0.1924
			40	0.1824	0.1985
0.1M KCl in 49wt% MDEA			**0.58 wt% MDEA**		
24.65	1.834	2.00	24.29	0.101	0.110
30	1.974	2.15	26.09	0.1045	0.1137
35	2.6	2.83	30	0.1171	0.1274
40	3.04	3.31	35	0.1354	0.1473
			40.05	0.1529	0.1664
0.1M HCl in DI water			**0.1 M HCl in 49 wt% MDEA**		
23.5	38.8	42.21	23.7	0.796	0.8660
25	39.5	42.98	25	0.805	0.8758
30	44.8	48.74	30	0.884	0.9618
35	47	51.14	35	1.12	1.2186
37.5	48.5	52.77	37.5	1.238	1.3469
38.5	49	53.31	39	1.314	1.4296
39.5	49.6	53.96	40	1.37	1.4906
40	49.9	54.29			
0.1021 M KOH in DI water #1			**0.1M KOH in 49wt% MDEA**		
24	22.2	24.15	23.8	2.08	2.26
25.65	23	25.02	25	2.23	2.43
40	28.4	30.90	30	2.47	2.69
0.102 M KOH in DI water # 2			35	3.02	3.29
23.95	19.1	20.8	37.5	3.35	3.64
25	19.7	21.4	39	3.57	3.88
30	21.4	23.3	40	3.65	3.97
35	23.1	25.1			
40.15	24.7	26.9			

Cell Constant = 1.088 1/cm

Table A.2. Conductivity measurements-continued

Temp., °C	Conductance, millimhos	Conductivity, mmho/cm	Temp., °C	Conductance, millimhos	Conductivity, mmho/cm
0.1 M NaHCO₃ in DI water			0.01 M NaHCO₃ in DI water		
22.8	6.3	6.85	22.4	0.721	0.784
25	6.58	7.16	25	0.781	0.850
30	7.62	8.29	30	0.884	0.962
35	8.40	9.14	35	0.973	1.059
37.5	8.80	9.57	37.5	1.018	1.108
39	9.04	9.84	39	1.044	1.136
40	9.20	10.01	40	1.067	1.161
0.001M NaHCO₃ in DI water			0.0001 M NaHCO₃ in DI water		
22.5	0.0851	0.0926	23	0.0115	0.0125
25	0.0911	0.0991	25	0.0119	0.0129
30	0.1047	0.1139	30	0.0137	0.0149
35	0.1153	0.1254	35	0.0155	0.0169
37.5	0.1208	0.1314	37.5	0.0164	0.0178
39	0.1238	0.1347	39	0.0171	0.0186
40	0.1264	0.1375	40	0.0176	0.0191
0.1 M K₂CO₃ in DI water			0.01 M K₂CO₃ in DI water		
22.4	15.1	16.4	22.4	1.90	2.07
25	16.1	17.5	25	2.03	2.21
30	18.3	19.9	30	2.35	2.56
35	19.9	21.7	35	2.58	2.81
37.5	20.7	22.5	37.5	2.70	2.94
39	21.2	23.1	39	2.77	3.01
40	21.5	23.4	40	2.82	3.07
0.001 M K₂CO₃ in DI water			0.0001 M K₂CO₃ in DI water		
22.5	0.236	0.257	22.4	0.0242	0.0263
25	0.256	0.279	25	0.0253	0.0275
30	0.295	0.321	30	0.0302	0.0329
35	0.326	0.355	35	0.0335	0.0364
37.5	0.341	0.371	37.5	0.0349	0.0380
39	0.350	0.381	39	0.0358	0.0390
40	0.356	0.387	40	0.0363	0.0395
DI water 6/19					
22.62	0.002	0.0022			
39.92	0.0041	0.0045			
DI water 7/10					
22.2	0.0018	0.0020			
DI water 7/27					
21.94	0.00155				

Cell Constant = 1.088 1/cm

Table A.3. Conductivity measurements-continued

Temp., °C	Conductance, millimhos	Conductivity, mmho/cm	Temp., °C	Conductance, millimhos	Conductivity, mmho/cm
48.5 wt% (4.06 M) MDEA HCl ldg=1.04 (4.215 M), 0.00028 M CO2			1/10 0.406 M MDEA 0.4215 M HCl, 0.000072 M CO2		
21.8	58.7	63.9	22.5	25.4	27.6
25	59.7	65.0	25	26.8	29.2
30	67.1	73.0	30	30.5	33.2
35	75	81.6	35	33.5	36.4
37.5	79.7	86.7	37.5	35.1	38.2
39	82.6	89.9	39	35.8	39.0
40	85.1	92.6	40	36.4	39.6
1/100 0.0406 M MDEA 0.04215 M HCl			1/1000 0.004 M MDEA 0.0042 M HCl		
22.6	3.60	3.92	22.1	0.39	0.424
25	3.81	4.15	25	0.405	0.441
30	4.34	4.72	30	0.468	0.509
35	4.75	5.17	35	0.516	0.561
37.5	4.99	5.43	37.5	0.540	0.588
39	5.10	5.55	39	0.554	0.603
40	5.18	5.64	40	0.565	0.615
1/10000 0.0004 M MDEA 0.00042 M HCl					
22	0.0432	0.0470			
25	0.0480	0.0522			
30	0.0537	0.0584			
35	0.0592	0.0644			
37.5	0.0619	0.0673			
39	0.0635	0.0691			
40	0.0645	0.0702			

Cell Constant = 1.088 1/cm

Table A.4. Conductivity measurements-continued

Temp., °C	Conductance, millimhos	Conductivity, mmho/cm	Temp., °C	Conductance, millimhos	Conductivity, mmho/cm
0.1 M KCl in 29.2 wt% DEA			0.1 M K2CO3 in 29.2 wt% DEA		
22.23	4.47	4.86	22.56	5.88	6.40
25	4.83	5.26	25	6.64	7.22
30	5.47	5.95	30	7.28	7.92
35	6.11	6.65	35	8.05	8.76
38	6.73	7.32	40	9.15	9.96
40	7.05	7.67	38	8.78	9.55
29.2 wt% DEA, CO2 ldg=0.00014			36	8.45	9.19
22.56	0.261	0.284	35	8.16	8.88
25	0.290	0.316	28	6.83	7.43
30	0.329	0.358	0.1 M NaHCO3- in 29.2 wt% DEA		
35	0.376	0.409	22.17	3.03	3.30
39	0.414	0.450	24.95	3.27	3.56
40	0.428	0.466	30	3.84	4.18
34	0.370	0.403	35	4.23	4.60
32	0.348	0.379	38	4.44	4.83
29.6	0.321	0.349	40	4.52	4.92
0.1 M KOH in 29.2 wt% DEA CO2 ldg =0.0003			40.30	4.44	*4.83
22.2	5.51	5.99			
25	5.66	6.16			
30	6.79	7.39			
35	7.63	8.30			
37.5	8.12	8.83			
39	8.43	9.17			
40	8.72	9.49			

*Cell Constant = 1.088 1/cm. *Solution appeared to be losing CO_2.*

Table A.5. Conductivity measurements-continued

Temp., °C	Conductance, millimhos	Conductivity, mmho/cm	Temp., °C	Conductance, millimhos	Conductivity, mmho/cm
29 wt% (2.839 M) DEA HCl ldg= 1.013 (2.874 M) , 0.0002 M CO2			1/10 0.284 M DEA 0.287 M HCl, 0.00014 M CO2		
22.2	79.6	86.6	22.2	18.4	20.0
25	81.7	88.9	25	19.3	21.0
30	91.6	99.7	30	22.2	24.1
35	101.1	110.0	35	24.4	27.7
37.5	105.6	114.9	37.5	25.5	28.3
39	109.4	119.0	39	26.0	28.8
40	113.0	122.9	40	26.5	
1/100 0.0284 M DEA 0.0287 M HCl			1/1000 0.0028 M DEA 0.0029 M HCl		
22.3	2.28	2.48	22.5	0.232	0.252
25	2.37	2.58	25	0.256	0.279
30	2.69	2.93	30	0.292	0.318
35	2.96	3.22	35	0.321	0.349
37.5	3.10	3.37	37.5	0.335	0.364
39	3.17	3.45	39	0.343	0.373
40	3.23	3.51	40	0.350	0.381
1/10,000 0.00028 M DEA 0.00029 M HCl			1/50,000 5.68E-5 M DEA 5.74E-5 M HCl		
22.2	0.0266	0.0289	23.7	0.00818	0.00890
25	0.0282	0.0307	25	0.00838	0.00912
30	0.0331	0.0360	30	0.00975	0.0106
35	0.0365	0.0397	35	0.01081	0.0118
37.5	0.0382	0.0416	37.5	0.01134	0.0123
39	0.0391	0.0425	39	0.01162	0.0126
40	0.0399	0.0434	40	0.01178	0.0128

Cell Constant = 1.088 1/cm

Table A.6. Specific Ionic Conductivities at infinite dilution in water

	(mho-cm^3) / (cm-mol)			(mho-cm^3) / (cm-mol)	
	25°C	40°C		25°C	40°C
K^+	73.5		HCO_3^-	44.5	*57.9
Cl^-	76.4	*99.0	$CO_3^=$	138.6	
OH^-	199.1	*257	$MEAH^+$	42.2	
H^+	349.6	*444	$MDEAH^+$	*50.9	*72.2
Na^+	50.10		$DEAH^+$	*30	*40

Most of the 25°C values were taken from Atkins, P. , Physical Chemistry 3rd ed. and CRC Handbook 1st Student ed. * These values obtained by experiments and calculations in this work.

Table A.7. Specific Ionic Conductivities of ions in water, DEA and MDEA

Ion	Paired ion	Temp. °C	Concentration mol / Liter	Specific ionic conductivity (mho-cm^3)/(cm-mol)		
				Water	29.2 wt% DEA	49 wt% MDEA
K^+	Cl^-	25	0.1	63.1	25.8	9.98
K^+	Cl^-	40	0.1	82.0	37.6	16.25
Cl^-	K^+	25	0.1	65.5	26.8	10.4
Cl^-	K^+	40	0.1	85.0	39.1	16.85
OH^-	K^+	25	0.1	150.9	35.8	§ 14.3
OH^-	K^+	40	0.1	187	57.3	§ 23.5
OH^-	K^+	25	0.0		47.9	28
OH^-	K^+	40	0.0		76	51
$H+$	$Cl-$	25	0.1	351.6		
$H+$	$Cl-$	40	0.1	443.9		
$Cl-$	$H+$	25	0.1	78.4		
$Cl-$	$H+$	40	0.1	99.0		
$CO_3^=$	K^+	25	0.1		§ 19.6	
$CO_3^=$	K^+	40	0.1		§ 22.75	
$MDEAH^+$	Cl^-	25	0.1			§ 3.5
$MDEAH^+$	Cl^-	40	0.1			§ 6.3
$MDEAH^+$	Cl^-	25	0.0004	50.9		8
$MDEAH^+$	Cl^-	40	0.0004	72.2		14.4
Cl^-	$MDEAH^+$	25	0.1			§ 5.3
Cl^-	$MDEAH^+$	40	0.1			§ 8.9
$DEAH^+$	Cl^-	25	0.1		6	
$DEAH^+$	Cl^-	40	0.1		9.2	
$DEAH^+$	Cl^-	25	0.000	30	12.3	
$DEAH^+$	Cl^-	40	0.000	40	16.6	

§ *Ionic association could be occurring which reduces the measured conductivity.*

Appendix B: Tabular pH Data

Table B.1 Experimental pH data for MDEA neutralized with hydrochloric acid.

2/12/96 HCl Loading	pH	acid free MDEA wt%	Temp °C	2/12/96 Continued HCl Loading	pH	acid free MDEA wt%	Temp °C
0.0020229	11.575	48.7	approx. 22	0.052596	9.9680	47.5	
0.0040458	11.142	48.7		0.054619	9.9520	47.5	
0.0060687	10.961	48.6		0.056642	9.9360	47.5	
0.0080916	10.772	48.6		0.058665	9.9210	47.4	
0.010115	10.674	48.5		0.062710	9.8900	47.3	
0.014160	10.565	48.4		0.064733	9.8750	47.3	
0.016183	10.480	48.4		0.066756	9.8620	47.2	
0.018206	10.430	48.3		0.068779	9.8480	47.2	
0.020229	10.388	48.3		0.070802	9.8310	47.1	
0.022252	10.345	48.3		0.072825	9.8160	47.1	
0.026298	10.274	48.2		0.074848	9.8100	47.0	
0.028321	10.243	48.1		0.076871	9.7980	47.0	
0.030344	10.202	48.1		0.078894	9.7790	47.0	
0.032367	10.188	48.0		0.080917	9.7690	46.9	
0.034390	10.145	48.0		0.082939	9.7580	46.9	
0.036412	10.120	47.9		0.084962	9.7470	46.8	
0.038435	10.099	47.9		0.086985	9.7350	46.8	
0.040458	10.089	47.8		0.089008	9.7250	46.7	
0.042481	10.058	47.8		0.091031	9.7160	46.7	
0.044504	10.039	47.7		0.093054	9.7060	46.6	
0.046527	10.023	47.7		0.095077	9.6950	46.6	
0.048550	10.004	47.6		0.097100	9.6850	46.6	
				0.099123	9.6750	46.5	
				0.10115	9.6660	46.5	
				0.10317	9.6570	46.4	28

Table B.2 Experimental pH data for MDEA neutralized with hydrochloric acid.

2/16/96 HCl Loading	pH	acid free MDEA wt%	Temp °C	2/16/96 continued HCl Loading	pH	acid free MDEA wt%	Temp °C
9.9127e-05	11.851	48.8	~22°C	0.0040642	11.052	46.9	
0.00019825	11.819	48.7		0.0041633	11.042	46.9	
0.00029738	11.794	48.7		0.0042624	11.032	46.8	
0.00039651	11.753	48.6		0.0043616	11.021	46.8	
0.00059476	11.696	48.5		0.0044607	11.010	46.8	
0.00069389	11.645	48.5		0.0045598	11.006	46.7	
0.00079301	11.615	48.5		0.004659	10.995	46.7	
0.00099127	11.553	48.4		0.0047581	10.987	46.6	
0.0010904	11.520	48.3		0.0048572	10.978	46.6	
0.0011895	11.493	48.3		0.0049563	10.970	46.5	
0.0012886	11.480	48.2		0.0051546	10.956	46.4	
0.0013878	11.453	48.2		0.0052537	10.948	46.4	
0.0014869	11.428	48.1		0.0053528	10.941	46.4	
0.001586	11.404	48.1		0.005452	10.936	46.3	
0.0016851	11.382	48.0		0.0055511	10.928	46.3	
0.0017843	11.359	48.0		0.0057493	10.910	46.2	
0.0018834	11.347	47.9		0.0058485	10.904	46.1	
0.0019825	11.321	47.9		0.0059476	10.898	46.1	
0.0020817	11.308	47.8		0.0061458	10.883	46.0	
0.0021808	11.289	47.8		0.006245	10.879	46.0	
0.0022799	11.270	47.7		0.0063441	10.872	45.9	
0.002379	11.260	47.7		0.0064432	10.862	45.9	
0.0024782	11.242	47.7		0.0065424	10.857	45.8	
0.0025773	11.235	47.6		0.0066415	10.852	45.8	
0.0026764	11.220	47.6		0.0067406	10.846	45.8	
0.0027755	11.204	47.5		0.0068397	10.839	45.7	
0.0028747	11.190	47.5		0.0069389	10.832	45.7	~22°C
0.0029738	11.180	47.4					
0.0030729	11.167	47.4					
0.003172	11.152	47.3					
0.0032712	11.139	47.3					
0.0033703	11.125	47.2					
0.0034694	11.119	47.2					
0.0035686	11.100	47.2					
0.0036677	11.094	47.1					
0.0038659	11.076	47.0					
0.0039651	11.058	47.0					

Table B.3 Experimental pH data for 49 wt% MDEA titrated with a partially neutralized 49 wt% MDEA-HCl solution.

2/21/96 HCl Loading	pH	acid free MDEA wt%	Temp °C	2/21/96 HCl Loading	Continued pH	acid free MDEA wt%	Temp °C
0.01226	10.656	48.95	-22°C	0.51109	8.923	48.98	
0.01468	10.577	48.95		0.55300	8.863	48.99	
0.01710	10.524	48.95		0.60076	8.795	48.99	
0.01952	10.46	48.95		0.64405	8.732	48.99	
0.02192	10.415	48.95		0.64405	8.76	48.99	
0.02432	10.384	48.95		0.68347	8.704	49.00	
0.02909	10.324	48.95		0.71951	8.637	49.00	
0.03146	10.28	48.95		0.75260	8.574	49.00	
0.03383	10.244	48.95		0.78308	8.513	49.00	
0.03854	10.183	48.95		0.80024	8.48	49.00	
0.04088	10.176	48.95		0.82714	8.425	49.01	
0.04322	10.143	48.95		0.85212	8.372	49.01	
0.04555	10.124	48.95		0.87538	8.315	49.01	
0.04787	10.093	48.95		0.89708	8.259	49.01	
0.05249	10.054	48.95		0.90536	8.236	49.01	
0.05709	10.013	48.95		0.92514	8.178	49.01	
0.06165	9.989	48.96		0.94370	8.116	49.01	
0.07294	9.913	48.96		0.96114	8.052	49.01	
0.08406	9.849	48.96		0.96783	8.028	49.01	
0.09501	9.799	48.96		0.97013	8.021	49.01	-22°C
0.10579	9.748	48.96					
0.11641	9.704	48.96					
0.12688	9.665	48.96					
0.13719	9.634	48.96					
0.15736	9.578	48.96					
0.17695	9.525	48.96					
0.19599	9.475	48.96					
0.23250	9.391	48.97					
0.26706	9.319	48.97					
0.29982	9.257	48.97					
0.33092	9.202	48.97					
0.37471	9.128	48.98					
0.44099	9.024	48.98					

273

Table B.4 Experimental pH data for 49 wt% MDEA titrated with a partially
neutralized 49 wt% MDEA-HCl solution.

3/25/96 HCl Loading	pH	acid free MDEA wt%	Temp °C	HCl Loading	pH	acid free MDEA wt%	Temp °C
3.4479E-05	11.615	48.94					
6.8842E-05	11.596	48.94					
0.00010309	11.578	48.94					
0.00018821	11.553	48.94					
0.00027262	11.532	48.94					
0.00035633	11.438	48.94	25.53				
0.00043935	11.417	48.93					
0.00052169	11.394	48.93					
0.00060336	11.383	48.93					
0.0007647	11.336	48.93					
0.00092345	11.298	48.93	25.66				
0.00107966	11.28	48.93					
0.0012334	11.243	48.93					
0.00138472	11.209	48.92	25.66				
0.00153368	11.18	48.92					
0.00168034	11.137	48.92	25.67				
0.00182475	11.111	48.92					
0.00196695	11.086	48.92	25.68				
0.00224496	11.043	48.91					
0.00251475	11.003	48.91	25.67				
0.00277667	10.973	48.91					
0.00303107	10.953	48.90	25.67				
0.00339926	10.916	48.90	25.68				
0.00375224	10.893	48.90					
0.00420081	10.843	48.89					
0.00452177	10.817	48.89					
0.00483033	10.792	48.88	25.67				
0.00522365	10.762	48.88	25.70				
0.0055977	10.735	48.88					
0.00604026	10.709	48.87					
0.00645727	10.687	48.87	25.63				
0.00685089	10.659	48.86					
0.00715023	10.64	48.86					
0.00750643	10.62	48.85	25.60				
0.0078441	10.602	48.85					
0.00816465	10.589	48.85	25.59				
0.00846935	10.57	48.84					
0.00875935	10.558	48.84					
0.00903569	10.546	48.84	25.57				
0.00929931	10.534	48.83					
0.00955107	10.523	48.83					
0.00974447	10.518	48.83	25.60				

Table B.5 Experimental pH data for 49 wt% MDEA titrated with a partially neutralized 49 wt% MDEA-HCl solution.

3/27/96 HCl Loading	pH	acid free MDEA wt%	Temp °C	3/27/96 Continued HCl Loading	pH	acid free MDEA wt%	Temp °C
0.00015731	11.28	48.95	39.67	0.0050475	10.444	48.94	40.09
0.00034299	11.211	48.95	39.67	0.00522766	10.425	48.94	40.05
0.00046493	11.156	48.95	39.48	0.00540377	10.415	48.94	40.00
0.00061534	11.083	48.95	39.54	0.00557596	10.403	48.94	40.03
0.00076355	11.043	48.95	39.88	0.00590908	10.379	48.94	40.03
0.0009096	11	48.95	39.88	0.006228	10.357	48.94	39.97
0.00105355	10.963	48.95	39.88	0.00653362	10.336	48.94	39.98
0.00119544	10.926	48.95	39.87	0.00682674	10.316	48.94	40.03
0.00133531	10.894	48.94	39.82	0.00710812	10.299	48.94	40.05
0.0014732	10.857	48.94	40.05	0.00737844	10.283	48.94	40.12
0.00160917	10.822	48.94	40.31	0.00765109	10.273	48.94	40.25
0.00174324	10.794	48.94	40.46	0.00788845	10.261	48.94	40.03
0.00187546	10.768	48.94	40.55	0.00812926	10.252	48.94	40.03
0.00200586	10.747	48.94	40.60	0.00836131	10.242	48.94	40.02
0.00213448	10.727	48.94	40.65	0.00858506	10.231	48.94	40.18
0.00226137	10.728	48.94	40.63	0.00890606	10.217	48.94	40.03
0.00238654	10.712	48.94	40.55	0.00921073	10.203	48.94	39.95
0.00251005	10.703	48.94	40.48	0.00950027	10.188	48.94	40.10
0.00263191	10.693	48.94	40.42	0.00977578	10.176	48.94	39.99
0.00275217	10.688	48.94	40.39	0.01003826	10.163	48.94	40.12
0.00287085	10.676	48.94	40.34	0.01024769	10.156	48.94	40.10
0.00298799	10.662	48.94	40.29	0.01048856	10.149	48.94	40.09
0.00310361	10.647	48.94	40.25	0.01064317	10.144	48.94	40.20
0.00321775	10.632	48.94	40.20				
0.00333043	10.619	48.94	40.19				
0.00344169	10.606	48.94	40.17				
0.00355154	10.592	48.94	40.18				
0.00376714	10.568	48.94	40.10				
0.00387293	10.558	48.94	40.10				
0.00408065	10.538	48.94	40.02				
0.00428336	10.515	48.94	40.07				
0.00448123	10.495	48.94	40.12				
0.00467444	10.477	48.94	40.00				
0.00486314	10.46	48.94	40.00				

Table B.6 Experimental pH data for 49 wt% MDEA titrated with a partially
neutralized 49 wt% MDEA-HCl solution.

4/5/96 HCl Loading	pH	acid free MDEA wt%	Temp °C	4/5/96 continued HCl Loading	pH	acid free MDEA wt%	Temp °C
0.00150524	10.929	48.96	40.16	0.05028862	9.515	48.96	40.27
0.00298844	10.665	48.96	40.14	0.05199239	9.501	48.96	40.47
0.0044501	10.49	48.96	40.12	0.05365885	9.488	48.96	40.48
0.00589067	10.369	48.96	40.08	0.0552892	9.477	48.96	40.40
0.00731061	10.285	48.96	40.05	0.05844619	9.455	48.96	40.23
0.00871035	10.215	48.96	40.06	0.06147209	9.435	48.96	40.06
0.01009033	10.156	48.96	40.00	0.06437488	9.417	48.96	40.11
0.01145097	10.106	48.96	40.00	0.06716194	9.401	48.96	40.02
0.01279265	10.062	48.96	39.98	0.06984004	9.386	48.96	40.00
0.01411579	10.021	48.96	40.06	0.07241545	9.372	48.96	40.00
0.01542076	9.981	48.96	40.34	0.07489398	9.359	48.96	40.00
0.01670793	9.947	48.96	40.66	0.07728097	9.347	48.96	40.00
0.01797766	9.919	48.96	40.96	0.07958143	9.335	48.96	40.04
0.01923031	9.887	48.96	41.15	0.08179996	9.326	48.96	40.00
0.02046622	9.864	48.96	41.12	0.08394086	9.316	48.96	40.00
0.02168572	9.842	48.96	41.02	0.08600815	9.307	48.96	40.00
0.02288913	9.824	48.96	40.93	0.08800554	9.298	48.96	40.02
0.02407678	9.804	48.96	40.83	0.09087817	9.289	48.96	39.97
0.02524897	9.785	48.96	40.72	0.09361215	9.287	48.96	39.97
0.02640599	9.767	48.96	40.63	0.09621729	9.27	48.97	40.22
0.02754815	9.751	48.96	40.55	0.0987025	9.258	48.97	40.16
0.02867573	9.736	48.96	40.49	0.10029669	9.251	48.97	40.14
0.03088824	9.707	48.96	40.36				
0.03304566	9.682	48.96	40.25				
0.03515002	9.66	48.96	40.17				
0.03720325	9.639	48.96	40.18				
0.0392072	9.617	48.96	40.22				
0.04116362	9.597	48.96	40.20				
0.04326278	9.577	48.96	40.22				
0.04494047	9.561	48.96	40.26				
0.04676402	9.545	48.96	40.32				
0.04854628	9.529	48.96	40.29				

276

Table B.7 Experimental pH data for 29.68 wt% DEA titrated with a partially
neutralized 29.95 wt% DEA-HCl solution.

4/24/96 HCl Loading	pH	acid free DEA wt%	Temp °C	HCl Loading	pH	acid free DEA wt%	Temp °C
0	11.195	29.68	39.93				
0.00072211	11.115	29.69	39.76				
0.0008962	11.092	29.69	39.76				
0.00106784	11.073	29.70	39.76				
0.00140391	11.033	29.70	39.75				
0.00173074	11	29.71	39.69				
0.0020487	10.964	29.71	39.75				
0.00235814	10.934	29.71	39.79				
0.0026594	10.909	29.72	39.82				
0.0029528	10.882	29.72	39.89				
0.00323865	10.862	29.73	39.89				
0.00351723	10.836	29.73	40				
0.00378882	10.816	29.73	39.97				
0.00405367	10.8	29.74	39.93				
0.00456415	10.776	29.74	39.8				
0.00505052	10.75	29.75	39.84				
0.00551444	10.732	29.76	39.77				
0.00595743	10.719	29.76	39.71				
0.00638088	10.693	29.77	39.82				
0.00678605	10.666	29.77	39.83				
0.0071741	10.639	29.78	39.89				
0.00754609	10.616	29.78	40				
0.00807609	10.585	29.79	40.04				
0.00857511	10.554	29.80	40.07				
0.0090458	10.533	29.81	3.984				
0.0094905	10.507	29.81	40.01				
0.0099113	10.491	29.82	39.83				
0.01031009	10.472	29.82	39.98				
0.01068854	10.457	29.83	39.97				
0.01104818	10.442	29.83	39.86				
0.01139037	10.429	29.84	39.83				
0.01171634	10.417	29.84	39.83				
0.01202724	10.404	29.85	39.94				
0.01242006	10.389	29.85	39.88				
0.01269958	10.376	29.86	40.04				
0.0129671	10.362	29.86	40.26				
0.01322336	10.354	29.86	40.14				
0.01346907	10.346	29.87	40.05				

Table B.8 Experimental pH and conductivity data for 29.2 wt% DEA neutralized with CO_2.

8/14/96 CO2 Loading	pH	Conductivity, millimho/cm	Temp °C	8/14/96 Continued CO2 Loading	pH	Conductivity, millimho/cm	Temp °C
0.787	7.907	23.2	22.13	0.399	9.268	12.6	23.47
0.768	7.991	23.0	22.32	0.389	9.293	12.3	23.49
0.750	8.060	22.4	22.49	0.380	9.317	12.1	23.5
0.732	8.145	22.2	22.68	0.371	9.340	11.8	23.51
0.732	8.107	21.7	22.51	0.362	9.361	11.5	23.5
0.716	8.193	21.4	22.68	0.354	9.382	11.3	23.51
0.700	8.275	21.2	22.82	0.346	9.402	11.1	23.51
0.685	8.340	21.0	22.96	0.339	9.420	10.9	23.5
0.670	8.409	20.7	23.09	0.339	9.419	10.7	23.56
0.656	8.466	20.3	23.19	0.332	9.438	10.5	23.59
0.643	8.522	20.0	23.31	0.325	9.456	10.3	23.61
0.630	8.568	19.7	23.39	0.315	9.479	10.0	23.62
0.618	8.613	19.4	23.45	0.315	9.479	9.92	23.31
0.606	8.653	19.0	23.52	0.309	9.495	9.62	23.25
0.594	8.693	18.7	23.55	0.303	9.510	9.44	23.21
0.583	8.730	18.4	23.54	0.297	9.525	9.37	23.16
0.573	8.765	18.1	23.55	0.292	9.538	9.22	23.13
0.562	8.795	17.7	23.58	0.286	9.552	9.07	23.09
0.553	8.825	17.4	23.59	0.281	9.565	8.83	23.06
0.543	8.857	17.1	23.6	0.276	9.578	8.70	23.05
0.534	8.885	16.9	23.6	0.272	9.590	8.56	23.02
0.525	8.910	16.5	23.59	0.269	9.596	8.50	22.98
0.516	8.940	16.2	23.59	0.265	9.608	8.37	22.96
0.508	8.967	16.0	23.58	0.260	9.619	8.25	22.93
0.500	8.990	15.7	23.56	0.258	9.624	8.17	22.91
0.492	9.015	15.4	23.54				
0.485	9.035	15.1	23.45				
0.477	9.056	14.9	23.41				
0.470	9.077	14.7	23.38				
0.470	9.072	14.6	23.32				
0.463	9.095	14.4	23.31				
0.457	9.113	14.1	23.32				
0.450	9.131	13.9	23.33				
0.444	9.149	13.8	23.35				
0.438	9.165	13.6	23.36				
0.432	9.180	13.4	23.4				
0.426	9.195	13.3	23.42				
0.420	9.210	13.2	23.43				
0.409	9.241	12.8	23.46				

Table B.9 Experimental pH and conductivity data for 49 wt% MDEA neutralized with CO_2.

8/19/96 CO2 Loading	pH	Conductivity, millimho/cm	Temp °C	CO2 Loading	pH	Conductivity, millimho/cm	Temp °C
0.0001	11.723	0.0499	23.3				
0.0017	11.301	0.0727	23.06				
0.0032	11.082	0.1076	22.92				
0.0047	10.948	0.1426	22.82				
0.0062	10.853	0.1755	22.75				
0.0077	10.777	0.2088	22.65				
0.0091	10.73	0.238	22.54				
0.0105	10.683	0.265	22.48				
0.0119	10.634	0.296	22.46				
0.0145	10.545	0.349	22.4				
0.0171	10.485	0.400	22.36				
0.0196	10.432	0.452	22.34				
0.0220	10.391	0.492	22.36				
0.0266	10.323	0.586	22.37				
0.0308	10.265	0.668	22.36				
0.0368	10.195	0.774	22.34				
0.0421	10.144	0.862	22.32				
0.0471	10.103	0.950	22.31				
0.0516	10.07	1.024	22.29				
0.0558	10.037	1.087	22.32				
0.0597	10.011	1.154	22.35				
0.0632	9.988	1.214	22.37				
0.0659	9.972	1.260	22.4				

279

Appendix C: Activity Coefficient Equations for Electrolyte-NRTL Equation

C.1 PITZER-DEBYE-HÜCKEL

Solvent:

$$\ln \gamma_s^{pdh*} = 2 \left(\frac{1000}{M_o} \right)^{1/2} A_\phi \frac{I_x^{3/2}}{(1 + \rho I_x^{1/2})} \tag{C.1}$$

Ionic Species:

$$\ln \gamma_i^{pdh} = - \left(\frac{1000}{M_o} \right)^{1/2} A_\phi \left\{ \left(\frac{2z_i^2}{\rho} \ln (1 + \rho \, I_x^{1/2}) \right. \right.$$

$$\left. \left. + \frac{(z_i^2 I_x^{1/2} - 2 I_x^{3/2})}{(1 + \rho I_x^{1/2})} \right\} \right. \tag{C.2}$$

C.2 BORN CORRECTION

$$\ln \gamma_{i \, BORN}^{\infty} = - \left(\frac{e^2}{2kT} \right) \left(\frac{z_i^2}{r_i} \right) \left(\frac{1}{D_s} - \frac{1}{D_w} \right) \tag{C.3}$$

C.3 NONRANDOM TERMS

Molecular Species:

$$
\ln \gamma_m^{\text{NRTL}} = \frac{\sum_j X_j G_{jm} \tau_{jm}}{\sum_k X_k G_{km}}
$$

$$
+ \sum_{m'} \frac{X_{m'} G_{mm'}}{\sum_k X_k G_{km}} \left(\tau_{mm'} - \frac{\sum_k X_k G_{km'} \tau_{km'}}{\sum_k X_k G_{km'}} \right)
$$

$$
+ \sum_c \sum_{a'} \frac{X_{a'}}{\sum_{a''} X_{a''}} \frac{X_c G_{mc.a'c}}{\sum_k X_k G_{kc.a'c}} \left(\tau_{mc.a'c} - \frac{\sum_k X_k G_{kc.a'c} \tau_{kc.a'c}}{\sum_k X_k G_{kc.a'c}} \right)
$$

$$
+ \sum_a \sum_{c'} \frac{X_{c'}}{\sum_{c''} X_{c''}} \frac{X_a G_{ma.c'a}}{\sum_k X_k G_{ka.c'a}} \left(\tau_{ma.c'ca} - \frac{\sum_k X_k G_{ka.c'a} \tau_{ka.c'ca}}{\sum_k X_k G_{ka.c'a}} \right) \quad \text{(C.4)}
$$

Cations:

$$
\frac{1}{Z_c} \ln \gamma_c^{\text{NRTL}} = \sum_{a'} \frac{X_{a'}}{\sum_{a''} X_{a''}} \frac{\sum_k X_k G_{kc.a'c} \tau_{kc.a'c}}{\sum_k X_k G_{kc.a'c}}
$$

$$
+ \sum_m \frac{X_m G_{km} \tau_{km}}{\sum_k X_k G_{km}} \left(\tau_{cm} - \frac{\sum_k X_k G_{km} \tau_{km}}{\sum_k X_k G_{km}} \right)
$$

$$
+ \sum_a \sum_{c'} \frac{X_{c'}}{\sum_{c''} X_{c''}} \frac{X_a G_{ca.c'a}}{\sum_k X_k G_{ca.c'a}} \left(\tau_{ca.c'a} - \frac{\sum_k X_k G_{ka.c'a} \tau_{ka.c'a}}{\sum_k X_k G_{ka.c'a}} \right) \quad \text{(C.5)}
$$

281

Anions:

$$\frac{1}{Z_a} \ln \gamma_a^{NRTL} = \sum_{c'} \frac{X_{c'}}{\sum_{c''} X_{c''}} \frac{\sum_k X_k G_{ka.c'a} \tau_{ka.c'a}}{\sum_k X_k G_{ka.c'a}}$$

$$+ \sum_m \frac{X_m G_{km} \tau_{km}}{\sum_k X_k G_{km}} \left(\tau_{am} - \frac{\sum_k X_k G_{km} \tau_{km}}{\sum_k X_k G_{km}} \right)$$

$$+ \sum_c \sum_{a'} \frac{X_{a'}}{\sum_{a''} X_{a''}} \frac{X_c G_{ac.a'c}}{\sum_k X_k G_{ac.a'c}} \left(\tau_{ac,a'c} - \frac{\sum_k X_k G_{kc.a'c} \tau_{kc.a'c}}{\sum_k X_k G_{kc.a'c}} \right) \qquad (C.6)$$

Appendix D: Aspen Plus™ Input File for MDEA-DEA-H₂S-CO₂ System

```
TGS
TITLE 'MDEA-DEA-H2O-CO2-H2S SYSTEM'
DESCRIPTION 'FITTING PARAMETERS OF THE ELECTROLYTE-NRTL
     EQUATION FOR MDEA-DEA-H2O-CO2-H2S USING SYSOP15M'

; This file was generated under contract to the Gas Research Institute, Contract
;No. 5092-260-2495.  This file is also copyrighted, 1996 by Mark L. Posey and
;Gary T. Rochelle.  It may not be duplicated or distributed in any way without
;express written permission.  All rights are reserved.

IN-UNITS SI TEMP=C PRES='N/SQM'
RUN-CONTROL MAX-TIME = 200000

COMPONENTS H2O H2O/H3O+ H3O+/OH- OH-/ &
     MDEA/C5+/ &
     DEA C4H11NO2-1/C4+/RHNCOO-/ &
     CO2 CO2/HCO3- HCO3-/CO3-2 CO3-2/ &
     H2S H2S/HS- HS-/S-2 S-2/

HENRY-COMPS LIST1 CO2 H2S
PROPERTIES SYSOP15M CHEMISTRY=FINALMODEL &
                         HENRY-COMPS=LIST1 TRUE-COMPS=1
DATABANKS AQUEOUS

CHEMISTRY FINALMODEL
     PARAM KBASIS=MOLEFRAC ;K IS MOLE FRACTION BASED

     STOIC 1 H2O -2/ H3O+ 1/ OH- 1
     K-STOIC 1  132.899 -13445.9 -22.4773 0 ;MAUER

     STOIC 2 C5+ -1/ H2O -1/ MDEA 1/ H3O+ 1
     K-STOIC 2  -56.2 -4044.8 7.848 0 ;POSEY

     STOIC 3 C4+ -1/ H2O -1/ DEA 1/ H3O+ 1
     K-STOIC 3  -9.4 -6457 0.81 0 ;POSEY

     STOIC 4 RHNCOO- -1/ H2O -1/ DEA 1/ HCO3- 1
     K-STOIC 4  0.2616 -2585 0 0 ;Posey 10.4

     STOIC 5 CO2 -1/ H2O -2/ H3O+ 1/ HCO3- 1
     K-STOIC 5  231.465 -12092.1 -36.78160 ;EDWARDS ET AL.
```

283

STOIC 6 HCO3- -1/ H2O -1/ H3O+ 1/ CO3-2 1
K-STOIC 6 216.049 -12431.7 -35.4819 0 ;EDWARDS ET AL.

STOIC 7 H2S -1/ H2O -1/ H3O+ 1/ HS- 1
K-STOIC 7 214.582 -12995.4 -33.54710 ;EDWARDS ET AL.

STOIC 8 HS- -1/ H2O -1/ H3O+ 1/ S-2 1
K-STOIC 8 -32.0 -3338.0 0 0 ;GIGGENBACH ET AL

; PURE MOLECULAR PHYSICAL PROPERTIES
PROP-DATA
    IN-UNITS SI

; HENRY'S CONSTANT FOR ACID GASES IN H2O
    PROP-LIST HENRY
    BPVAL CO2 H2O 110.034525 -6789.04 -11.4519 -0.010454 273 500
;POSEY
    BPVAL H2S H2O 18.1937 -2808.5 2.5629 -0.01868 273 423
;LEE&MATHER 1977

    COMP-LIST H2O CO2
    CVAL VLBROC 1 1 0.0464 0.0956
    COMP-LIST H2O H2S
    CVAL VLBROC 1 1 0.0464 0.0887

; DIELECTRIC CONSTANT OF MDEA, MEASURED BY MARCIA
;MIDDLETON AT THE UNIVERSITY OF TEXAS
; DIELECTRIC CONSTANT OF DEA, FROM IKADA ET AL., BULL. INST.
;CHEM. RES., KYOTO UNIV., VOL46. NO5, 1968
    PROP-LIST CPDIEC
    PVAL MDEA 24.76 8989.31 273.15
    PVAL DEA 28.01 9277.0 273.15

; VAPOR PRESSURES
; H2O TAKEN FROM THE DIPPR DATA BANKS
; DEA TAKEN FROM THE DIPPR DATA BANKS
; MDEA INITIALLY TAKEN FROM DATA OF UNION CARBIDE AND
;DOW WEIGHTED EQUALLY - FITTED BY DMA
    PROP-LIST PLXANT
    PVAL H2O 7.255D1 -7.2067D3 0 0 -7.1385D0 4.0460D-6 2.0 273 650
    PVAL MDEA 26.137 -7.5885D3 0 0 0 0 393 513 ;POSEY/AUSTGEN
    PVAL C5+ -.1D36 0 0 0 0 0 0 0 .2D4
    PVAL DEA 2.8601D2 -2.036D4 0 0 -4.0422D1 3.2378D-2 1.0 301.15 542.04
    PVAL C4+ -.1D36 0 0 0 0 0 0 0 .2D4
    PVAL RHNCOO- -.1D36 0 0 0 0 0 0 0 .2D4

; CHARGE - ION TYPE - MOLECULAR WEIGHT
    PROP-LIST CHARGE/IONTYP/MW
    PVAL C5+ +1D0/ +1D0/ 120.17
    PVAL C4+ +1D0/ +1D0/ 106.144
    PVAL RHNCOO- -1D0/ 3D0/ 148.14

; IDEAL GAS HEAT CAPACITY OF UNKNOWN IONS
    PROP-LIST CPIG
    PVAL C5+ .208D5 0 0 0 0 0 0 .2D4 .1D36 .1D36 .1D36
    PVAL C4+ .208D5 0 0 0 0 0 0 .2D4 .1D36 .1D36 .1D36
    PVAL RHNCOO- .208D5 0 0 0 0 0 0 .2D4 .1D36 .1D36 .1D36

    PROP-LIST MW/TC/PC/VC/ZC/OMEGA/TB
    PVAL MDEA 119.16/677.79/3.8761D+6/0.39300/0.192/1.2418/520.35
    PVAL DEA 105.136/715.00/3.2700D+6/0.34900/0.192/1.0463/542.04

    PROP-LIST DHFORM/DGFORM
    PVAL MDEA -3.9688D+8/-2.1408D+8
    PVAL DEA -3.9688D+8/-2.1408D+8

; MDEA FROM XIAO PENG
    PROP-LIST CPIG
    PVAL MDEA 4.91723D4 5.59457D2 -3.13382D-1 1.10180D-4 &
        0 0 0 0.2D4 0.1D36 0.1D36 0.1D36
    PROP-LIST CPIGDP
    PVAL DEA 6.8900D+4 4.5680D+5 1.8500D+2 8.0920D-1 0 100 900

; DELTA H VAPOR - LIQUID FOR WATSON MODEL
    PROP-LIST DHVLWT
    PVAL MDEA 6.18132D7 293.15 0.38 0 0

; DIPPR PARAMETERS
    PROP-LIST DHVLDP
    PVAL MDEA 1.0340D+8 3.3300D-1 0 0 0 301.15 542.04
    PVAL DEA 1.0340D+8 3.3300D-1 0 0 0 301.15 542.04

    COMP-LIST DEA
    CVAL THRSWT 1 3 1 /
            4 1 /
            7 1

```
; MOLECULE-MOLECULE INTERACTION PARAMETERS
; OF THE ELEC-NRTL MODEL
    PROP-LIST        GMELCA / GMELCB / GMELCM
    BPVAL H2O CO2    10.064  /-3268.135/ 0.20 ;INSERT SOUR
    BPVAL CO2 H2O    10.064  /-3268.135/ 0.20 ;INSERT SOUR
    BPVAL H2O H2S    -3.674  / 1155.9  / 0.20 ;INSERT SOUR
    BPVAL H2S H2O    -3.674  / 1155.9  / 0.20 ;INSERT SOUR
    BPVAL CO2 H2S     0.0    /  0.0    / 0.20
    BPVAL H2S CO2     0.0    /  0.0    / 0.20


    BPVAL H2O MDEA    9.473  /-1902.4  / 0.20 ;POSEY
    BPVAL MDEA H2O   -2.173  / -147.4  / 0.20 ;POSEY
    BPVAL MDEA CO2    0.0    /  0.0    / 0.20
    BPVAL CO2 MDEA    0.0    /  0.0    / 0.20
    BPVAL MDEA H2S    0.0    /  0.0    / 0.20
    BPVAL H2S MDEA    0.0    /  0.0    / 0.20


    BPVAL H2O DEA     4.172  /  175.1  / 0.20 ;POSEY
    BPVAL DEA H2O    -1.579  / -546.4  / 0.20 ;POSEY
    BPVAL DEA CO2     0.0    /  0.0    / 0.20
    BPVAL CO2 DEA     0.0    /  0.0    / 0.20
    BPVAL DEA H2S     0.0    /  0.0    / 0.20
    BPVAL H2S DEA     0.0    /  0.0    / 0.20


    BPVAL MDEA DEA    0.0    /  0.0    / 0.20
    BPVAL DEA MDEA    0.0    /  0.0    / 0.20

; MOLECULE-ION PAIR INTERACTION PARAMETERS OF THE
; ELECTROLYTE- NRTL MODEL
    PROP-LIST              GMELCC / GMELCD / GMELCN

; H2O
    PPVAL  H2O (H3O+ OH-)      8  / 0 / 0.2
    PPVAL  (H3O+ OH-) H2O     -4  / 0 / 0.2

; H2O-MDEA
    PPVAL  H2O (C5+ OH-)       8   / 0 / 0.2
    PPVAL  (C5+ OH-) H2O      -5.6 / 0 / 0.2 ;MDEA 7.13/6.5
    PPVAL  MDEA (C5+ OH-)     15   / 0 / 0.1
    PPVAL  (C5+ OH-) MDEA     -8   / 0 / 0.1
    PPVAL  MDEA (H3O+ OH-)    15   / 0 / 0.1
    PPVAL  (H3O+ OH-) MDEA    -8   / 0 / 0.1

; H2O-DEA
    PPVAL  H2O (C4+ OH-)       8    / 0 / 0.2
    PPVAL  (C4+ OH-) H2O      -5.75 / 0 / 0.2 ;DEA 10.4/6.3
    PPVAL  DEA (C4+ OH-)      15    / 0 / 0.1
```

```
PPVAL (C4+ OH-) DEA        -8    /  0  /  0.1
PPVAL DEA (H3O+ OH-)       15    /  0  /  0.1
PPVAL (H3O+ OH-) DEA       -8    /  0  /  0.1

; H2O-CO2
PPVAL H2O (H3O+ HCO3-)      8    /  0  /  0.2
PPVAL (H3O+ HCO3-) H2O     -4    /  0  /  0.2
PPVAL H2O (H3O+ CO3-2)      8    /  0  /  0.2
PPVAL (H3O+ CO3-2) H2O     -4    /  0  /  0.2
PPVAL CO2 (H3O+ HCO3-)     15    /  0  /  0.1
PPVAL (H3O+ HCO3-) CO2     -8    /  0  /  0.1
PPVAL CO2 (H3O+ CO3-2)     15    /  0  /  0.1
PPVAL (H3O+ CO3-2) CO2     -8    /  0  /  0.1
PPVAL CO2 (H3O+ OH-)       15    /  0  /  0.1
PPVAL (H3O+ OH-) CO2       -8    /  0  /  0.1

; H2O-H2S
PPVAL H2O (H3O+ HS-)        8    /  0  /  0.2
PPVAL (H3O+ HS-) H2O       -4    /  0  /  0.2
PPVAL H2O (H3O+ S-2)        8    /  0  /  0.2
PPVAL (H3O+ S-2) H2O       -4    /  0  /  0.2
PPVAL H2S (H3O+ HS-)       15    /  0  /  0.1
PPVAL (H3O+ HS-) H2S       -8    /  0  /  0.1
PPVAL H2S (H3O+ S-2)       15    /  0  /  0.1
PPVAL (H3O+ S-2) H2S       -8    /  0  /  0.1
PPVAL H2S (H3O+ OH-)       15    /  0  /  0.1
PPVAL (H3O+ OH-) H2S       -8    /  0  /  0.1

; MDEA-CO2
PPVAL H2O (C5+ HCO3-)    7.503  /   0  /  0.2 ;MDEA-CO2 7.13
PPVAL (C5+ HCO3-) H2O   -5.837  /  695 /  0.2 ;MDEA-CO2 7.13
PPVAL H2O (C5+ CO3-2)       8   /   0  /  0.2
PPVAL (C5+ CO3-2) H2O      -4   /   0  /  0.2
PPVAL MDEA (C5+ HCO3-)     15   /   0  /  0.1
PPVAL (C5+ HCO3-) MDEA   0.839  / -2067 / 0.1 ;MDEA-CO2 7.13
PPVAL MDEA (C5+ CO3-2)     15   /   0  /  0.1
PPVAL (C5+ CO3-2) MDEA     -8   / 1873 /  0.1 ;MDEA-CO2 7.13
PPVAL MDEA (H3O+ HCO3-)    15   /   0  /  0.1
PPVAL (H3O+ HCO3-) MDEA    -8   /   0  /  0.1
PPVAL MDEA (H3O+ CO3-2)    15   /   0  /  0.1
PPVAL (H3O+ CO3-2) MDEA    -8   /   0  /  0.1
PPVAL CO2 (C5+ HCO3-)      15   /   0  /  0.1
PPVAL (C5+ HCO3-) CO2      -8   /   0  /  0.1
PPVAL CO2 (C5+ CO3-2)      15   /   0  /  0.1
PPVAL (C5+ CO3-2) CO2      -8   /   0  /  0.1
PPVAL CO2 (C5+ OH-)        15   /   0  /  0.1
PPVAL (C5+ OH-) CO2        -8   /   0  /  0.1
```

```
; MDEA-H2S
    PPVAL H2O (C5+ HS-)      5.00  /  0   /  0.2 ;MDEA-H2S 6.5
    PPVAL (C5+ HS-) H2O     -2.625 / 64.87 / 0.2 ;MDEA-H2S 6.5
    PPVAL H2O (C5+ S-2)        8   /  0   /  0.2
    PPVAL (C5+ S-2) H2O       -4   /  0   /  0.2
    PPVAL MDEA (C5+ HS-)      15   /  0   /  0.1
    PPVAL (C5+ HS-) MDEA     0.0416 / -1436 / 0.1 ;MDEA-H2S 6.5
    PPVAL MDEA (C5+ S-2)      15   /  0   /  0.1
    PPVAL (C5+ S-2) MDEA      -8   /  0   /  0.1
    PPVAL MDEA (H3O+ HS-)     15   /  0   /  0.1
    PPVAL (H3O+ HS-) MDEA     -8   /  0   /  0.1
    PPVAL MDEA (H3O+ S-2)     15   /  0   /  0.1
    PPVAL (H3O+ S-2) MDEA     -8   /  0   /  0.1
    PPVAL H2S (C5+ HS-)       15   /  0   /  0.1
    PPVAL (C5+ HS-) H2S       -8   /  0   /  0.1
    PPVAL H2S (C5+ S-2)       15   /  0   /  0.1
    PPVAL (C5+ S-2) H2S       -8   /  0   /  0.1
    PPVAL H2S (C5+ OH-)       15   /  0   /  0.1
    PPVAL (C5+ OH-) H2S       -8   /  0   /  0.1

; MDEA-CO2-H2S
    PPVAL CO2 (C5+ HS-)       15   /  0   /  0.1
    PPVAL (C5+ HS-) CO2       -8   /  0   /  0.1
    PPVAL CO2 (C5+ S-2)       15   /  0   /  0.1
    PPVAL (C5+ S-2) CO2       -8   /  0   /  0.1
    PPVAL H2S (C5+ HCO3-)     15   /  0   /  0.1
    PPVAL (C5+ HCO3-) H2S     -8   /  0   /  0.1
    PPVAL H2S (C5+ CO3-2)     15   /  0   /  0.1
    PPVAL (C5+ CO3-2) H2S     -8   /  0   /  0.1

; DEA-CO2
    PPVAL H2O (C4+ HCO3-)     2.46  /  0    /  0.2 ;DEA 10.4
    PPVAL (C4+ HCO3-) H2O    -5.408 / 1182  /  0.2 ;DEA 10.4
    PPVAL H2O (C4+ CO3-2)      8   /  0    /  0.2
    PPVAL (C4+ CO3-2) H2O     -4   /  0    /  0.2
    PPVAL H2O (C4+ RHNCOO-)  11.799 /  0   /  0.2 ;DEA 10.4
    PPVAL (C4+ RHNCOO-) H2O  -6.898 /  0   /  0.2 ;DEA 10.4
    PPVAL H2O (H3O+ RHNCOO-)   8   /  0    /  0.2
    PPVAL (H3O+ RHNCOO-) H2O  -4   /  0    /  0.2
    PPVAL DEA (C4+ HCO3-)     15   /  0    /  0.1
    PPVAL (C4+ HCO3-) DEA    4.865 / -3432 /  0.1 ;DEA 10.4
    PPVAL DEA (C4+ CO3-2)     15   /  0    /  0.1
    PPVAL (C4+ CO3-2) DEA     -8   / 747   /  0.1 ;DEA 10.4
    PPVAL DEA (C4+ RHNCOO-)   15   /  0    /  0.1
    PPVAL (C4+ RHNCOO-) DEA   -8   /  0    /  0.1
    PPVAL DEA (H3O+ HCO3-)    15   /  0    /  0.1
```

288

```
PPVAL (H3O+ HCO3-) DEA        -8    /  0  /  0.1
PPVAL DEA (H3O+ CO3-2)        15    /  0  /  0.1
PPVAL (H3O+ CO3-2) DEA        -8    /  0  /  0.1
PPVAL DEA (H3O+ RHNCOO-)      15    /  0  /  0.1
PPVAL (H3O+ RHNCOO-) DEA      -8    /  0  /  0.1
PPVAL CO2 (C4+ HCO3-)         15    /  0  /  0.1
PPVAL (C4+ HCO3-) CO2         -8    /  0  /  0.1
PPVAL CO2 (C4+ CO3-2)         15    /  0  /  0.1
PPVAL (C4+ CO3-2) CO2         -8    /  0  /  0.1
PPVAL CO2 (C4+ RHNCOO-)       15    /  0  /  0.1
PPVAL (C4+ RHNCOO-) CO2       -8    /  0  /  0.1
PPVAL CO2 (C4+ OH-)           15    /  0  /  0.1
PPVAL (C4+ OH-) CO2           -8    /  0  /  0.1
PPVAL CO2 (H3O+ RHNCOO-)      15    /  0  /  0.1
PPVAL (H3O+ RHNCOO-) CO2      -8    /  0  /  0.1

; DEA-H2S
PPVAL H2O (C4+ HS-)        7.766 /  0  /  0.2 ;DEA-H2S 6.3
PPVAL (C4+ HS-) H2O       -3.328 /-185 /  0.2 ;DEA-H2S 6.3
PPVAL H2O (C4+ S-2)           8  /  0  /  0.2
PPVAL (C4+ S-2) H2O          -4  /  0  /  0.2
PPVAL DEA (C4+ HS-)          15  /  0  /  0.1
PPVAL (C4+ HS-) DEA      -4.132 /-399 /  0.1 ;DEA-H2S 6.3
PPVAL DEA (C4+ S-2)          15  /  0  /  0.1
PPVAL (C4+ S-2) DEA          -8  /  0  /  0.1
PPVAL DEA (H3O+ HS-)         15  /  0  /  0.1
PPVAL (H3O+ HS-) DEA         -8  /  0  /  0.1
PPVAL DEA (H3O+ S-2)         15  /  0  /  0.1
PPVAL (H3O+ S-2) DEA         -8  /  0  /  0.1
PPVAL H2S (C4+ HS-)          15  /  0  /  0.1
PPVAL (C4+ HS-) H2S          -8  /  0  /  0.1
PPVAL H2S (C4+ S-2)          15  /  0  /  0.1
PPVAL (C4+ S-2) H2S          -8  /  0  /  0.1
PPVAL H2S (C4+ OH-)          15  /  0  /  0.1
PPVAL (C4+ OH-) H2S          -8  /  0  /  0.1

; DEA-CO2-H2S
PPVAL CO2 (C4+ HS-)          15  /  0  /  0.1
PPVAL (C4+ HS-) CO2          -8  /  0  /  0.1
PPVAL CO2 (C4+ S-2)          15  /  0  /  0.1
PPVAL (C4+ S-2) CO2          -8  /  0  /  0.1
PPVAL H2S (C4+ HCO3-)        15  /  0  /  0.1
PPVAL (C4+ HCO3-) H2S        -8  /  0  /  0.1
PPVAL H2S (C4+ CO3-2)        15  /  0  /  0.1
PPVAL (C4+ CO3-2) H2S        -8  /  0  /  0.1
PPVAL H2S (C4+ RHNCOO-)      15  /  0  /  0.1
PPVAL (C4+ RHNCOO-) H2S      -8  /  0  /  0.1
```

```
        PPVAL  H2S (H3O+ RHNCOO-)    15  /  0  /  0.1
        PPVAL  (H3O+ RHNCOO-) H2S    -8  /  0  /  0.1

; MDEA-DEA
        PPVAL  MDEA (C4+ OH-)        15  /  0  /  0.1
        PPVAL  (C4+ OH-) MDEA        -8  /  0  /  0.1
        PPVAL  DEA (C5+ OH-)         15  /  0  /  0.1
        PPVAL  (C5+ OH-) DEA         -8  /  0  /  0.1

; MDEA-DEA-CO2
        PPVAL  H2O (C5+ RHNCOO-)     11.8  /  0     /  0.2
        PPVAL  (C5+ RHNCOO-) H2O     -6.9  /  0     /  0.2
        PPVAL  MDEA (C5+ RHNCOO-)    15   /  0     /  0.1
        PPVAL  (C5+ RHNCOO-) MDEA    2.8  / -2727  /  0.1
        PPVAL  MDEA (C4+ HCO3-)      15   /  0     /  0.1
        PPVAL  (C4+ HCO3-) MDEA      2.8  / -2727  /  0.1
        PPVAL  MDEA (C4+ CO3-2)      15   /  0     /  0.1
        PPVAL  (C4+ CO3-2) MDEA      -8   /  747   /  0.1
        PPVAL  MDEA (C4+ RHNCOO-)    15   /  0     /  0.1
        PPVAL  (C4+ RHNCOO-) MDEA    2.8  / -2727  /  0.1
        PPVAL  MDEA (H3O+ RHNCOO-)   15   /  0     /  0.1
        PPVAL  (H3O+ RHNCOO-) MDEA   -8   /  0     /  0.1
        PPVAL  DEA (C5+ HCO3-)       15   /  0     /  0.1
        PPVAL  (C5+ HCO3-) DEA       2.8  / -2727  /  0.1
        PPVAL  DEA (C5+ CO3-2)       15   /  0     /  0.1
        PPVAL  (C5+ CO3-2) DEA       -8   /  747   /  0.1
        PPVAL  DEA (C5+ RHNCOO-)     15   /  0     /  0.1
        PPVAL  (C5+ RHNCOO-) DEA     2.8  / -2727  /  0.1
        PPVAL  CO2 (C5+ RHNCOO-)     15   /  0     /  0.1
        PPVAL  (C5+ RHNCOO-) CO2     -8   /  0     /  0.1

; MDEA-DEA-H2S
        PPVAL  MDEA (C4+ HS-)        15    /  0      /  0.1
        PPVAL  (C4+ HS-) MDEA        -1.73 / 1026.7 /  0.1
        PPVAL  MDEA (C4+ S-2)        15    /  0      /  0.1
        PPVAL  (C4+ S-2) MDEA        -8    /  0      /  0.1
        PPVAL  DEA (C5+ HS-)         15    /  0      /  0.1
        PPVAL  (C5+ HS-) DEA         -1.73 / 1026.7 /  0.1
        PPVAL  DEA (C5+ S-2)         15    /  0      /  0.1
        PPVAL  (C5+ S-2) DEA         -8    /  0      /  0.1

; MDEA-DEA-CO2-H2S
        PPVAL  H2S (C5+ RHNCOO-)     15  /  0  /  0.1
        PPVAL  (C5+ RHNCOO-) H2S     -8  /  0  /  0.1
```

; CO2-H2S
      PPVAL CO2 (H3O+ HS-)   15 / 0 / 0.1
      PPVAL (H3O+ HS-) CO2   -8 / 0 / 0.1
      PPVAL CO2 (H3O+ S-2)   15 / 0 / 0.1
      PPVAL (H3O+ S-2) CO2   -8 / 0 / 0.1
      PPVAL H2S (H3O+ HCO3-)   15 / 0 / 0.1
      PPVAL (H3O+ HCO3-) H2S   -8 / 0 / 0.1
      PPVAL H2S (H3O+ CO3-2)   15 / 0 / 0.1
      PPVAL (H3O+ CO3-2) H2S   -8 / 0 / 0.1

; SET SALT-SALT BINARY INTERACTION PARAMETERS TO DEFAULT
;OF 0. This includes CO2 salts with H2S salts.

PROP-SET PROP1 MOLEFRAC PHASE=L COMPS=MDEA C5+ DEA C4+ &
                              H2O OH- H3O+
PROP-SET PROP2 MOLEFRAC PHASE=L COMPS=H2S HS- S-2 CO2 &
                              HCO3- CO3-2 RHNCOO-
PROP-SET PROP3 GAMMA PHASE=L COMPS=MDEA C5+ DEA C4+ &
                              H2O OH- H3O+
PROP-SET PROP4 GAMMA PHASE=L COMPS=H2S HS- S-2 CO2 &
                              HCO3- CO3-2 RHNCOO-
PROP-SET PROP5 PRES
PROP-SET PROP6 MOLEFRAC PHASE=V COMPS=H2S CO2 H2O

;Example TGS table format

PROP-TABLE TABLE1 FLASHCURVE
   MOLE-FLOW H2O 0.8658 / MDEA 0.1046 / DEA 0.0296 / H2S 0.001342
; H2S Loading = 0.01
   STATE   TEMP=40 VFRAC=0.001
   VARY   MOLEFRAC COMP=CO2
   RANGE   LIST=0.000092 0.000105 0.000118 0.000131 0.000263 0.000394 &
            0.000525 0.000657 0.000788 0.000919 0.001050 0.001182 &
            0.001313 0.001970 0.002626 0.003283 0.003939 0.004596 &
            0.005252 0.005909 0.006565 0.007222 0.007878 0.008535 &
            0.009191 0.009848 0.010504 0.011160 0.011817 0.012474 &
            0.013130 0.019695 0.026260 0.032825 0.039390 0.045955 &
            0.052520 0.059085 0.065650 0.072215 0.078780 0.085345 &
            0.091910 0.098475 0.105040 0.111605 0.118170 0.124735
   TABULATE '40/10 WT% 40C, 0.01 H2S' PROPERTIES=PROP1 PROP2 &
                              PROP3 PROP4 PROP5 PROP6

References

Aspen Technology, Inc. *ASPEN PLUS™ Data Regression Manual*; Aspen Technology: Cambridge, MA, **1985**.

Aspen Plus™ Reference Manual - Volume 2, Physical Property Methods and Models, Aspen Plus Release 9, Aspen Technology, Inc., **1994**.

Astarita, G., Savage, D., Bisio, A., Gas Treating with Chemical Solvents, John Wiley & Sons, New York, **1983**.

Atkins, P., Physical Chemistry, Third Edition, W. H. Freeman and Company, **1986**.

Atwood, K., Arnold, M., Kindrick, R., Equilibria for the System of Ethanolamines - Hydrogen Sulfide - Water, *Ind. Eng. Chem.*, **1957**, 49(9), 1439-1444.

Austgen, D. M. A Model of Vapor-Liquid Equilibria for Acid Gas-Alkanolamine-Water Systems. Ph.D. Dissertation, The University of Texas at Austin, Austin, TX, **1989**.

Austgen, D. M.; Rochelle, G. T.; Peng, X.; and Chen, C-C. Model of Vapor-Liquid Equilibria for Aqueous Acid Gas-Alkanolamine Systems using the Electrolyte-NRTL Equation. *Ind. Eng. Chem. Res.*, **1989**, 28(7), 1060.

Austgen, D. M.; Rochelle, G. T.; Chen, C. C. A Model of Vapor-Liquid Equilibria for Aqueous Acid Gas-Alkanolamine Systems. 2. Representation of H_2S and CO_2 Solubility in Aqueous Mixtures of MDEA with MEA and DEA. *Ind. Eng. Chem. Res.*, **1991**, 30, 543.

Beutier, D. and Renon, H., Representation of NH_3-H_2S-H_2O, NH_3-CO_2-H_2O, and NH_3-SO_2-H_2O Vapor-Liquid Equilibria, *Ind. Eng. Chem. Process Des. Dev.*, **1978**, 17, 220-230.

Bhairi, A., Experimental Equilibrium Between Acid Gases and Ethanolamine solutions, Ph.D. Dissertation, Oklahoma State University, Stillwater, OK **1984**.

Bullin, J., Davison, R., Rogers, W., The Collection of VLE Data for Acid Gas-Alkanolamine Systems Using Fourier Transform Infrared Spectroscopy, Final Report, Gas Research Institute Contract No. 5091-260-2312, May **1996**.

292

Buslaeva, M., Tsvetkov, V., Markova, V., Kaimin, I., Themochemical Study of the Donor Capacity of Ethanolamine in Solutions, *Koord. Khim. (Soviet Journal of Coordination Chemistry)*, **1983**, 9, 752-754.

Chakravarty, S., Absorption of carbon dioxide in aqueous blends of diethanolamine and methyldiethanolamine, M.S. Thesis, University of Texas at Austin, December, **1992**.

Chakravarty, T., Solubility Calculations For Acid Gases in Amine Blends, Ph.D. Dissertation, Clarkson College, Potsdam, NY, **1985**.

Chan, H., Danckwerts, P., Equilibrium of MEA and DEA with Bicarbonate and Carbamate, *Chem. Eng. Sci.*, **1981**, 36, 229.

Chang, H-T. Thermodynamic Parameters for Predicting Acid Gas Solubility in Aqueous Alkanolamine Solutions. M.S. Thesis, The University of Texas at Austin, TX, **1992**.

Chang, H.-T.; Posey, M.; Rochelle, G. T. Thermodynamics of Alkanolamine-Water Solutions from Freezing Point Measurements. *Ind. Eng. Chem. Res.* **1993**, 32, 2324.

Chen, C.-C. and Evans, L. B. A Local Composition Model for the Excess Gibbs Energy of Aqueous Electrolyte Systems, *AIChE J.*, **1986**, 32 (3), 444-454.

Chen, C.-C., Britt, H. I., Boston, J. F., Evans, L. B. Extension and Application of the Pitzer Equation for Vapor-Liquid Equilibrium of Aqueous Electrolyte Systems with Molecular Solutes. *AIChE J.*, **1979**, 25 (5), 820.

Chen, C.-C., Britt, H. I., Boston, J. F., Evans, L. B. Local Composition Model for Excess Gibbs Energy of Electrolyte Systems, Part I: Single Solvent, Single Completely Dissociated Electrolyte Systems, *AIChE J.*, **1982**, 28 (4), 588-596.

Clarke, E. and Glew, D., Aqueous Nonelectrolyte Solutions. Part VIII. Deuterium and Hydrogen Sulfides Solubilities in Deuterium Oxide and Water, *Can. J. Chem.*, **1971**, 49, 691-698.

CRC Handbook of Chemistry and Physics, 42nd edition, CRC Press, Inc., Boca Raton, FL, **1961**.

CRC Handbook of Chemistry and Physics, 1st Student Edition, CRC Press, Inc., Boca Raton, FL, **1988**.

Daubert, T. E. and Danner, R. P. Data Compilation Tables of Properties of Pure Compounds; *Design Institute for Physical Property Data*; American Institute of Chemical Engineers, New York, NY, **1985**.

293

Daubert, T. E. and Hutchison, G. Vapor Pressure of 18 Pure Industrial Chemicals, American Institute of Chemical Engineers Symposium Series, Vol. 86, No. 279, New York, NY, **1990**.

Daubert, T. E., Goren, V., Jalowka, J. Vapor Pressure of 22 Pure Industrial Chemicals, American Institute of Chemical Engineers Symposium Series, Vol. 83, No. 256, New York, NY, **1987**.

Deshmukh, R. and Mather, A., A mathematical model for equilibrium solubility of hydrogen sulfide and carbon dioxide in aqueous alkanolamine solutions, *Chem. Eng. Sci.*, **1981**, 36, 355-362.

Dow Chemical Company. *The Alkanolamines Handbook.* Company technical literature, **1988**.

Edwards, T. et al., Thermodynamics of aqueous solutions containing volatile weak electrolytes, *AIChE J.*, **1975**, 21, 248-259.

Edwards, T., Maurer, G., Newman, J., Prausnitz, J., Vapor-liquid equilibria in multicomponent aqueous solutions of volatile weak electrolytes, *AIChE J.*, **1978**, 24, 966-976.

Ellis, A., The Effect of Pressure on the First Dissociation Constant of "Carbonic Acid.", *J. Chem. Soc.*, **1959**, 3689-3699.

Gow, A. S. Calculation of Vapor-Liquid Equilibria from Infinite-Dilution Excess Enthalpy Data Using the Wilson or NRTL Equation, *Ind. Eng. Chem. Res.*, **1993**, 32, 3150-3161.

Haji-Sulaiman, M., Aroua, M., Pervez, M., Equilibrium concentration profiles of species in CO_2-alkanolamine-water systems, *Gas. Sep. Purif.*, **1996**, 10, 13-18.

Hanks, R. W., Gupta, A. C., Christensen, J. J. Calculation of Isothermal Vapor-Liquid Equilibrium Data for Binary Mixtures from Heats of Mixing, *Ind. Eng. Chem. Fundam.*, **1971**, 10, 504-509.

Hanks, R. W., Tan, R. L., Christensen, J. J. Limits of the Simultaneous Correlation of g^E and h^E Data by the NRTL, LEMF and Wilson's Equations, *Thermochimica Acta*, **1978a**, 23, 41-55.

Hanks, R. W., Tan, R. L., Christensen, J. J. The Prediction of High Temperature Vapor-Liquid Equilibria from Lower Temperature Heat of Mixing Data, *Thermochimica Acta*, **1978b**, 27, 9-18.

Harned, H. and Davis, R., The Ionization Constant of Carbonic Acid in Water and the Solubility of Carbon Dioxide in Water and Aqueous Salt Solutions from 0 to 50°C, *J. Am. Chem. Soc.*, **1943**, 65, 2030-2037.

Harned, H. S.; Owen, B. B. The Physical Chemistry of Electrolyte Solutions 2nd ed.; Reinhold: New York, NY, 1950.

Ho, B. and Eguren, R., Amoco Production Company, Solubility of acidic gases in aqueous DEA and MDEA solutions, Presented at the 1988 Spring National Meeting of the American Institute of Chemical Engineers, March 6-10, **1988**.

Huang, S. and Ng, H.-J., DB Robinson Research Ltd., GPA Project 911, Solubility of H_2S and CO_2 in Alkanolamines, Gas Processors Association Report, September **1995**.

Huang, S., DB Robinson Research Ltd., GRI Project 1121.002, contract # 5092-260-2343, Gas Research Institute progress report, July-September **1993**.

International Critical Tables, Vol. 6, **1930**.

Jensen, M., Jorgensen, E., Faurholt, C., Reactions Between Carbon Dioxide and Amino Alcohols I. Monoethanolamine and Diethanolamine, *J. Chem. Eng. Data*, **1954**, 25, 118.

Jou, F-Y., Mather, A., Otto, F., Solubility of H_2S and CO_2 in aqueous methyldiethanolamine solutions, *Ind. Eng. Chem. Process Des. Dev.*, **1982**, 21, 539-544.

Jou, F-Y., Carroll, J., Mather, A., Otto, F., Solubility of Carbon Dioxide and Hydrogen Sulfide in a 35 wt% Aqueous Solution of Methyldiethanolamine, *Can. J. Chem. Eng.* **1993a**, 71, 264-268.

Jou, F-Y., Carroll, J., Mather, A., Otto, F., Solubility of Mixtures of Hydrogen Sulfide and Carbon Dioxide in Aqueous N-Methyldiethanolamine Solutions, *J. Chem. Eng. Data*, **1993b**, 38, 75-77.

Jou, F-Y., Otto, F., Mather, A., Vapor-liquid equilibrium of carbon dioxide in aqueous mixtures of monoethanolamine and methyldiethanolamine, *Ind. Eng. Chem. Res.* **1994**, 33, 2002-2005.

Kennard, M. and Meisen, A., "Solubility of Carbon Dioxide in Aqueous Diethanolamine Solutions at Elevated Temperatures and pressures", *J. Chem. and Eng. Data*, **1984**, 29, 309.

Kensell, W., The M. W. Kellogg Company, Letter with graphs comparing MDEA heat capacity data from several sources, June 11, **1996**.

Kent, R. and Eisenberg, B., Better data for amine treating, *Hydrocarbon Proc.*, **1976**, 55, 87-90.

Kim, J-H., Dobrogowska, C., and Hepler, L. Thermodynamics of Ionization of Aqueous Alkanolamines, *Can. J. Chem.*, **1987**, 65, 1726-1728.

Kozintseva, T., Geochemical Investigations, ed. by N. Khitarov, **1965**, 121-134.

Kuwairi, B. S., "Vapor Pressures of Selected Pure Materials and Mixtures". Ph.D. Dissertation, Oklahoma State University, Stillwater, OK, **1983**.

Lal, D., Otto, F., Mather, A., The Solubility of H_2S and CO_2 in a Diethanolamine Solution at Low Partial Pressures, *Can J. Chem. Eng.*, **1985**, 63, 681-685.

Lawson, J. and Garst, A., Gas Sweetening Data: Equilibrium Solubility of Hydrogen Sulfide and Carbon Dioxide in Aqueous Monoethanolamine and Aqueous Diethanolamine Solutions, *J. Chem. Eng. Data*, **1976**, 21(1), 20-30.

Lee, J., Otto, F., Mather, A., Solubility of Carbon Dioxide in Aqueous Diethanolamine Solutions at High Pressures, *J. Chem. and Eng. Data*, **1972**, 17(1), 465.

Lee, J., Otto, F., Mather, A., Solubility of Hydrogen Sulfide in Aqueous Diethanolamine Solutions at High Pressures, *J. Chem. and Eng. Data*, **1973a**, 18(1), 71-73.

Lee, J., Otto, F., Mather, A., Partial Pressures of Hydrogen Sulfide over Aqueous Diethanolamine Solutions, *J. Chem. and Eng. Data*, **1973b**, 18(4), 420.

Lee, J., Otto, F., Mather, A., The Solubility of Mixtures of Carbon Dioxide and Hydrogen Sulfide in Aqueous Diethanolamine Solutions, *Can. J. Chem. Eng.*, **1974**, 52, 125.

Lee, J. and Mather, A., Solubility of Hydrogen Sulfide in Water, *Berichte der Bunsen-Gesellschaft*, **1977**, 81, 1020-1023.

Lee, L., Thermodynamic Models for Natural Gas Sweetening Units, Gas Research Institute **1992** annual report, contract no. 5091-260-2288.

Lee, L., Thermodynamic Models for Natural Gas Sweetening Units, Gas Research Institute **1994** annual report, contract no. 5091-260-2288.

Li, M-H and Shen, K-P, Solubility of Hydrogen Sulfide in Aqueous Mixtures of Monoethanolamine with N-Methyldiethanolamine, *J. Chem. Eng. Data*, **1993**, 38, 105-108.

Licht, S. and Weiland, R., Density and physical solubility of CO_2 in partially loaded solutions of MEA, DEA, and MDEA, Presented at AIChE **1989** Spring National Meeting, Paper No. 57f, Houston, TX.

MacGregor, R. and Mather, A., Equilibrium Solubility of H_2S and CO_2 and Their Mixtures in a Mixed Solvent, *Can. J. Chem. Eng.*, **1991**, 69, 1357-1366.

Mason, J. W. and Dodge, B. F., *Trans. Am. Inst. Chem. Engr.*, **1936**, 32, 27-47.

McDonald, R. A., Shrader, S. A., Stull, D. R. Vapor Pressures and Freezing Points of 30 Organics, *J. Chem. Eng. Data*, **1959**, 4, 311-313.

Merkley, K., Christensen, J., Izatt, R., Enthalpies of Absorption of Carbon Dioxide in Aqueous Methyldiethanolamine Solutions, *Thermochimica Acta*, **1987**, 121, 437-446.

Mock, B., Evans, L. B., Chen, C.-C. Thermodynamic Representation of Phase Equilibria of Mixed-Solvent Electrolyte Systems, *AIChE J.*, **1986**, 32, 1655.

Mshewa, M. Carbon Dioxide Desorption/Absorption with Aqueous Mixtures of Methyldiethanolamine and Diethanolamine at 40 to 120°C. Ph.D. Dissertation, University of Texas at Austin, Austin, TX, **1995**.

Nath, A. and Bender, E. Isothermal Vapor-Liquid Equilibria of Binary and Ternary Mixtures Containing Alcohol, Alkanolamine, and Water with a New Static Device, *J. Chem. Eng. Data.*, **1983**, 28, 370-375.

Oscarson, J., Van Dam, R., Christensen, J., Izatt, R., Enthalpies of Absorption of Carbon Dioxide in Aqueous Diethanolamine Solutions, *Thermochimica Acta*, **1989a**, 146, 107-114.

Oscarson, J., Van Dam, R., Christensen, J., Izatt, R., Enthalpies of Absorption of Hydrogen Sulfide in Aqueous Diethanolamine Solutions, *Thermochimica Acta*, **1989b**, 154, 89-95.

Oscarson, J., Van Dam, R., Izatt, R., Enthalpies of Absorption of Hydrogen Sulfide in Aqueous Methyldiethanolamine Solutions, *Thermochimica Acta*, **1990**, 170, 235-241.

Peng, X. SINOPEC Bejing Design Institute, Private communication while Peng was visiting at ASPEN Technology, Inc., **1988**.

Perry, R. and Green, D. eds. Perry's Chemical Engineers' Handbook. Sixth Edition. McGraw-Hill, New York, NY, **1984**.

297

Pitzer, K. S. Electrolytes. From Dilute Solutions to Fused Salts. *J. Am. Chem. Soc.*, **1980**, 102, 2902.

Posey, M. and Rochelle, G. T.   A Nonrandom Two-Liquid Model for Alkanolamine-Water Systems.   Presented at the 44th Canadian Chemical Engineering Conference, Calgary, Alberta, Oct. 2-5, **1994**.

Posey, M., Tapperson, K. and Rochelle, G. T.   A Simple Model for Prediction of Acid Gas Solubilities in Alkanolamines, Gas Separation & Purification, **1996**, 10, 181-186.

Prausnitz, J. M., Lichtenthaler, R. N., Azevedo, E. G.   <u>Molecular Thermodynamics of Fluid-Phase Equilibria</u>, Second Edition, Prentice-Hall, Englewood Cliffs, New Jersey, **1986**.

Reid, R., Prausnitz, R., Sherwood, T., The Properties of Gases and Liquids, 3rd ed., McGraw-Hill Book Co., New York, **1977**.

Renon, H. and Prausnitz, J. M. Local Compositions in Thermodynamic Excess Functions for Liquid Mixtures, *AIChE J.*, **1968**, 14, 135.

Sandall, O.C., U.C. Santa Barbara, **1993** GRI Annual Report, Gas Research Institute contract #5092-260-2345, Chicago, Illinois.

Selleck, F., Carmichael, L., Sage, B., Phase Behavior in the Hydrogen Sulfide-Water System, *Ind. Eng. Chem.*, **1952**, 44, 2219-2226.

Shen, K.-P. and Li, M.-H., Solubility of carbon dioxide in aqueous mixtures of monoethanolamine with methyldiethanolamine, *J. Chem. Eng. Data*, **1992**, 37, 96-100.

Snijder, E., te Riele, M., Versteeg, G., van Swaaij, W., Diffusion Coefficients of Several Aqueous Alkanolamine Solutions, *J. Chem. Eng. Data*, **1993**, 38, 475-480.

Soave, G., Equilibrium Constants for Modified Redlich-Kwong Equation of State, *Chem. Eng. Sci.*, **1972**, 27, 1196-1203.

Stewart, P. and Munjal, P., Solubility of Carbon Dioxide in Pure Water, Synthetic Sea Water, and Synthetic Sea Water Concentrates at -5°C to 25°C and 10 to 45 atm Pressure, *J. Chem. Eng. Data*, **1970**, 15, 67-71.

Texaco Chemical, Letter providing in-house data for MDEA, DGA, DEA and MEA for use in regressions and not to be tabulated, **1989**.

Thomas, W. and Furzer, I., Diffusion measurements in liquids by the Gouy method, *Chem. Eng. Sci.*, **1962**, 17, 115-120.

Touhara, H., Okazaki, S., Okino, F., Tanaka, H., Ikari, K., Nakanishi, K., Thermodynamic Properties of Aqueous Mixtures of Hydrophilic Compounds 2. Aminoethanol and its Methyl Derivatives. *J. Chem. Thermodynamics*, **1982**, 14, 145-156.

Versteeg, G. and van Swaaij, W., Solubility and diffusivity of Acid gases (CO_2, N_2O) in Aqueous Alkanolamine Solutions, *J. Chem. Eng. Data*, **1988**, 33, 29-34.

Weiland, R., Chakravarty, T. and Mather, A., Solubility of carbon dioxide and hydrogen sulfide in aqueous alkanolamines, *Ind. Eng.Chem. Res.*, **1993**, 32, 1419-1430. Also see corrections *Ind. Eng.Chem. Res.*, **1995**, 34, 3173.

Weiland, R., Dingman, J., Browning, G., Cronin, D., Physical and Transport Properties of CO_2 Loaded Amines, Presented at AIChE **1994** Spring National Meeting, Paper No. 64a, Atlanta, GA.

Weiland, R., Heat Capacity of Aqueous MEA, DEA, MDEA and MDEA-Based Blends Partially Loaded with CO_2, Presented at AIChE **1996** Spring National Meeting, Paper No. 105b, New Orleans, LA.

Wiebe, R. and Gaddy, V., The Solubility in Water of Carbon Dioxide at 50, 75, and 100°C, at Pressures to 700 atmospheres, *Am. Chem. Soc. Jour.*, **1939**, 61, 315-318.

Wright, R., and Maass, O., The Electrical Conductivity of Aqueous Solutions of Hydrogen Sulphide and the State of the Dissolved Gas, *Can. J. Res.*, **1932**, 6, 588-595.

Xu, S., Qing, S., Zhen, Z., Zhang, C., Carroll, J. Vapor pressure measurements of aqueous N-methyldiethanolamine solutions. *Fluid Phase Equilibria*, **1991**, 67, 197-201.

YSI Incorporated, Instruction Manual for YSI Model 32 Conductance Meter, Yellow Springs Instrument Co. Inc., Yellow Springs, OH, **1989**.

Zelvenskii, Y., The Solubility of Carbon Dioxide in Water under Pressure, *J. Chem. Ind.* (U.S.S.R.), **1937**, 14, 1250-1257.

Ziaee, S. Polymer-Polymer Interactions Via Analog Calorimetry. Ph.D. Dissertation, The University of Texas at Austin, Austin, TX, **1995**.

Vita

Mark Leon Posey was born in Corpus Christi, Texas, U.S.A. on July 17, 1969. His parents are Linda Bess Posey and Ralph Leon Posey. Mark graduated from Pflugerville High School in Pflugerville, Texas in May 1987. He entered The University of Texas at Austin in September 1987 as a Chemical Engineering major. In September 1988, Mark entered the Cooperative Education Program with the National Aeronautics and Space Administration in Houston, Texas. Mark worked a total of one year and five months, in alternating semesters, for the Johnson Space Center. Mark graduated with a B.S. in Chemical Engineering on May 23, 1992 and entered the doctoral chemical engineering program in September 1992, also at the University of Texas at Austin.

Mark has authored papers published in Industrial Engineering Chemistry Research in 1993 and Gas Separation & Purification in 1996. His work has been presented at national and international chemical engineering conferences and locally for the Separations Research Program at UT.

Employment has been accepted with Phillips Petroleum Company in Bartlesville, Oklahoma in the Process Support Group.

Permanent address: 12007 Cherie Drive, Austin, Texas 78758.

This dissertation was typed by the author.